Lecture Notes in Electrical Engineering 489

Klimis Ntalianis · Anca Croitoru
Editors

Applied Physics, System Science and Computers II

Proceedings of the 2nd International Conference on Applied Physics, System Science and Computers (APSAC2017), September 27–29, 2017, Dubrovnik, Croatia

Springer

Lecture Notes in Electrical Engineering

Volume 489

**** Indexing: The books of this series are submitted to ISI Proceedings, EI-Compendex, SCOPUS, MetaPress, Springerlink ****

Lecture Notes in Electrical Engineering (LNEE) is a book series which reports the latest research and developments in Electrical Engineering, namely:

- Communication, Networks, and Information Theory
- Computer Engineering
- Signal, Image, Speech and Information Processing
- Circuits and Systems
- Bioengineering
- Engineering

The audience for the books in LNEE consists of advanced level students, researchers, and industry professionals working at the forefront of their fields. Much like Springer's other Lecture Notes series, LNEE will be distributed through Springer's print and electronic publishing channels.

For general information about this series, comments or suggestions, please use the contact address under "service for this series".

To submit a proposal or request further information, please contact the appropriate Springer Publishing Editors:

Asia:

China, *Jessie Guo, Assistant Editor* (jessie.guo@springer.com) (Engineering)

India, *Swati Meherishi, Senior Editor* (swati.meherishi@springer.com) (Engineering)

Japan, *Takeyuki Yonezawa, Editorial Director* (takeyuki.yonezawa@springer.com)
(Physical Sciences & Engineering)

South Korea, *Smith (Ahram) Chae, Associate Editor* (smith.chae@springer.com)
(Physical Sciences & Engineering)

Southeast Asia, *Ramesh Premnath, Editor* (ramesh.premnath@springer.com)
(Electrical Engineering)

South Asia, *Aninda Bose, Editor* (aninda.bose@springer.com) (Electrical Engineering)

Europe:

Leontina Di Cecco, Editor (Leontina.dicecco@springer.com)
(Applied Sciences and Engineering; Bio-Inspired Robotics, Medical Robotics, Bioengineering; Computational Methods & Models in Science, Medicine and Technology; Soft Computing; Philosophy of Modern Science and Technologies; Mechanical Engineering; Ocean and Naval Engineering; Water Management & Technology)

(christoph.baumann@springer.com)
(Heat and Mass Transfer, Signal Processing and Telecommunications, and Solid and Fluid Mechanics, and Engineering Materials)

North America:

Michael Luby, Editor (michael.luby@springer.com) (Mechanics; Materials)

More information about this series at http://www.springer.com/series/7818

Klimis Ntalianis · Anca Croitoru
Editors

Applied Physics, System Science and Computers II

Proceedings of the 2nd International Conference on Applied Physics, System Science and Computers (APSAC2017), September 27–29, 2017, Dubrovnik, Croatia

Springer

Editors
Klimis Ntalianis
Department of Business Administration
University of West Attica
Athens, Greece

Anca Croitoru
Faculty of Mathematics
Al.I. Cuza University
Iasi, Romania

ISSN 1876-1100 ISSN 1876-1119 (electronic)
Lecture Notes in Electrical Engineering
ISBN 978-3-319-75604-2 ISBN 978-3-319-75605-9 (eBook)
https://doi.org/10.1007/978-3-319-75605-9

Library of Congress Control Number: 2017939605

Printed on acid-free paper

This Springer imprint is published by the registered company Springer International Publishing AG
part of Springer Nature
The registered company address is: Gewerbestrasse 11, 6330 Cham, Switzerland

Contents

Applied Physics

Mechanism of Film Boiling Elimination During Quenching in Mineral Oils Caused by Oligomeric Additives

Petro Lohvynenko[1,4(✉)], Anatolii Moskalenko[2], Nikolai Kobasko[3], Larisa Karsim[1], and Sergii Riabov[1]

[1] Institute of Macromolecular Chemistry of NASU, Kyiv, Ukraine
petmol@ukr.net
[2] Institute of Engineering, Thermophysics of NASU, Kyiv, Ukraine
an.moskalenko@gmail.com
[3] Intensive Technologies Ltd., Kyiv, Ukraine
nkobasko@gmail.com
[4] Barkor – Oil Ltd., Kyiv, Ukraine

Abstract. Previously, it has been shown by authors [1–3] that the addition of a special additives, for example PIB (polyisobutylene oligomer), creates an insulating layer on the surface of steel parts during quenching in mineral oils that eliminates film boiling without affecting physical properties of the oil. Insulating layer decreases initial heat flux density which becomes less than critical one. In current paper, the detailed investigations are provided concerning the mechanism of film boiling elimination or its cardinal decreasing due to presence a small amount of PIB in mineral oil. Experiments were made using Inconel 600 probe (10 mm in diameter and 30 mm long) which was quenched from 810 °C in I-8A, I-12A and I-20A oils. Effect of viscosity and molecular weight of PIB was investigated by authors. By elimination film boiling during quenching, it is possible to govern intensity of cooling and provide uniformity of hardening process. A phenomenon of eliminating film boiling due to presence a small amount of PIB in mineral oil is called EFB effect which has an important practical use.

Keywords: PIB additives · Film boiling elimination · Mechanism
Uniformity · EFB effect

1 Introduction

It is well known that absence of film boiling, especially local film boiling, provides uniform cooling and decreases distortion [1–3]. According to existing approach, researches are trying to decrease duration of film boiling process by special additives affecting surface tension, viscosity, etc. Nobody paid attention to absolutely different approach consisting in creating an insulating layer on the surface of quenched steel parts. Such approach was proposed by authors [1] and is revolutionary because it affects duration of film boiling more effectively as compared with existing methods. The aim of current investigation is a study of the mechanism of film boiling elimination

K. Ntalianis and A. Croitoru (Eds.): APSAC 2017, LNEE 489, pp. 3–10, 2019.
https://doi.org/10.1007/978-3-319-75605-9_1

due to small addition of PIB (polyisobutylene oligomer) to I-8A, I-12A and I-20A mineral oils.

2 Experimental Investigations

2.1 Effect of PIB 2400 on Film Boiling Elimination (FBE Effect)

Figure 1 provides cooling curves and cooling rates [4] for solutions of PIB 2400 in different mineral oils at 50 °C. Mineral I-20A oil was investigated at different concentrations:1–0; 2–0.5; 3–1.0; 4–1.5; 5–2.0; 6–3.0 (see Fig. 1a); mineral oil I-12A at concentrations 1–0; 2–0.5; 3–1.0; 4–1.5; 5–2.0; 6–3.5 (see Fig. 1b) and mineral oil I-8A at concentrations 1–0; 2–0.5; 3–1.0; 4–2.0; 5–3.5; 6–10.0; 7–14.0 (see Fig. 1c). Some exact data are provided in Table 1.

It has been established by experiments that PIB 2400 can eliminate completely film boiling in mineral oil I-20A, however cannot eliminate completely film boiling in mineral oils I-12A and I-8A. Authors explain such behavior by decreasing critical heat flux densities of I-12A and I-8A oils. It means that small addition of PIB 2400 to I-20A oil provides FBE effect for 100% and for oils I-20A and I- 8A maximum for 80% – 90%. Authors explain such behavior by decreasing critical heat flux densities of I-12A and I-8A oils. It should be underlined that film boiling can be eliminated also at higher concentration of PIB 680 in I-20A oil (see Fig. 2).

Maximal cooling rates V_t^{max} and duration of film boiling obtained for PIB 2400 and PIB 680 solutions in oil I 20A at 50 °C are shown in Fig. 3. Since it was impossible to explain decreasing or elimination film boiling during testing of small (10 x 30 mm) Inconel 600 probe in mineral oils by changing tension or viscosity (see Table 2), author came to conclusion that PIB addition creates thin coating on the surface of probe which decreases initial heat flux density and by this way decreases film boiling process or eliminate it completely [1–5]. This idea is a good hypothesis for further investigations of authors.

2.2 Effect of Molecular Weight of PIB on Duration of Film Boiling

It has been established by authors that exists a critical molecular weight of PIB which provides FBE effect. No effect at all when molecular weight of PIB is less than critical one (see Fig. 4 and Table 3).

To make final conclusion on mechanism of elimination film boiling process, one should do more thorough experiments with different additives.

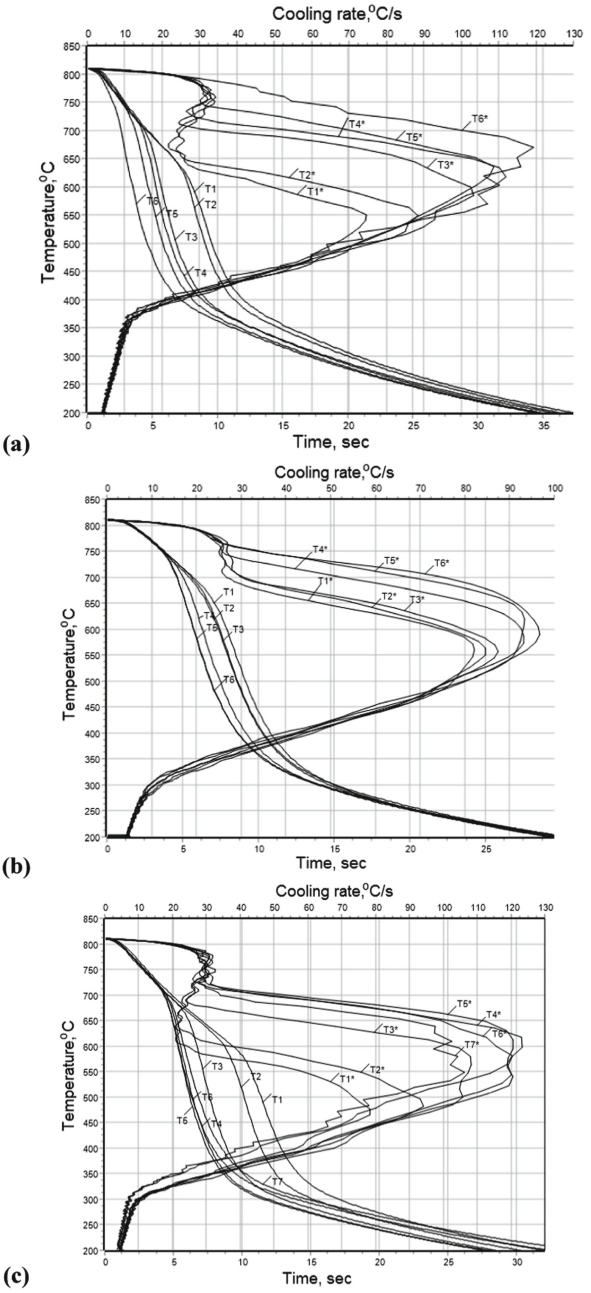

Fig. 1. Cooling curves and cooling rates for solutions of PIB 2400 in different mineral oils at 50 °C: (a), I-20A oil, concentrations 1–0; 2–0.5; 3–1.0; 4–1.5; 5–2.0; 6–3.0; (b), I-12A oil, concentrations 1–0; 2–0.5; 3–1.0; 4–1.5; 5–2.0; 6–3.5; (c), I = 8A, concentrations %wt 1–0; 2–0.5; 3–1.0; 4–2.0; 5–3.5; 6–10.0; 7–14.0.

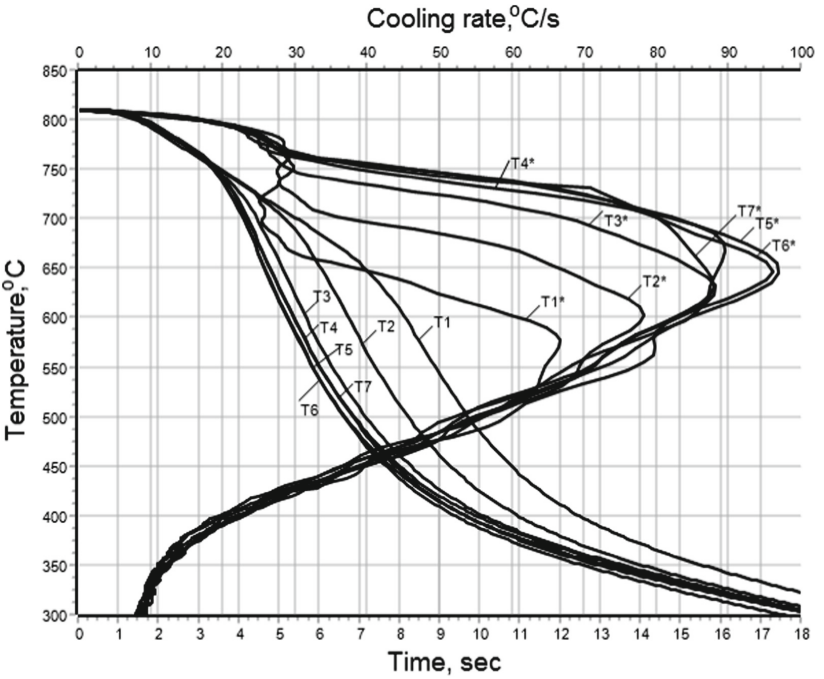

Fig. 2. Cooling curves and cooling rates for PIB 680 solutions in I-20 Oil at 50 °C and different concentrations, % wt.: 1-0.0; 2–3.0; 3–5.0; 4–7.0; 5–10.0; 6-12.5; 7–19.0.

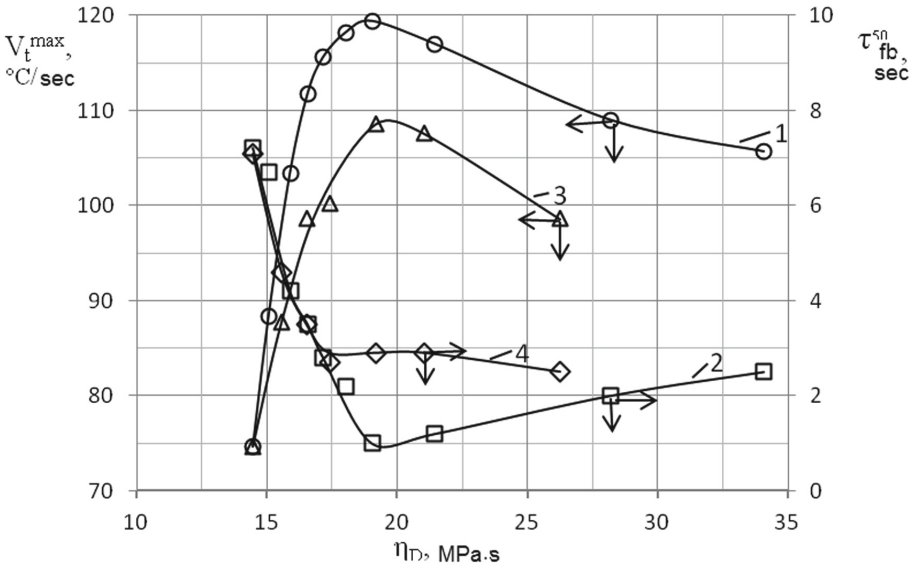

Fig. 3. Maximal cooling rates V_t^{max} (curve 1 and curve 3) and duration of film boiling (curve 2 and curve 4) for PIB 2400 (1, 2) and PIB 680 (3, 4) solutions in oil I-20A at 50 °C versus viscosity η_D.

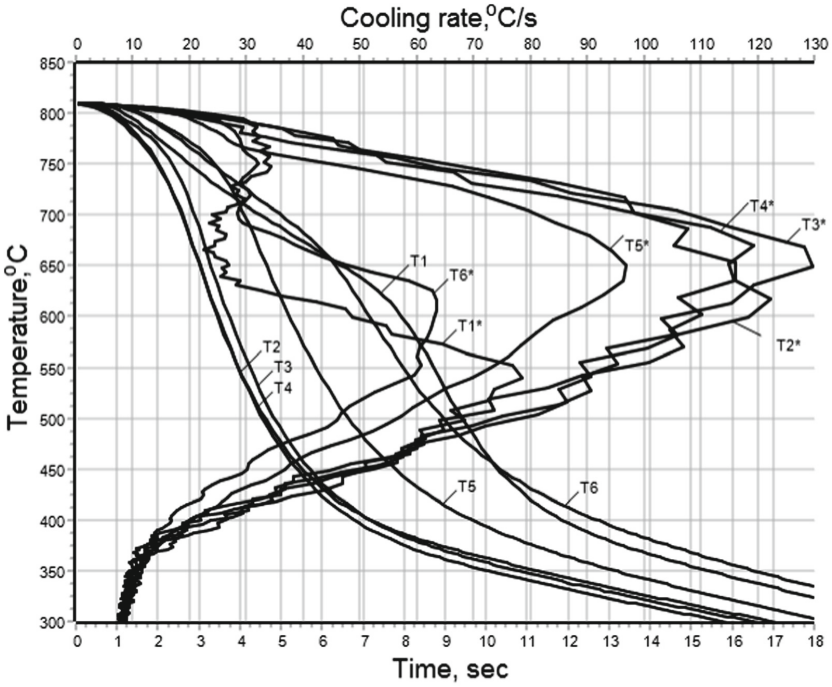

Fig. 4. Cooling curves and cooling rates for different solutions in oil I-20A: for oil I-20A (1), for 7% PIB 950 solution in oil I-20 (2), for 5% PIB 1300 solution in oil I-20 (3), for 3% PIB 2400 (4), for 10% PIB 680 solution in oil I-20 (5), and solution of 40% I-40 oil in I-20 oil (6).

Table 1. Cooling curve and cooling rate data obtained during testing of Inconel 600 probe (10 mm in diameter and 30 mm long) in solutions of oligomer PIB 2400 in oil I-20A at 50 °C

№	Data	Designation	Concentration, % vt.					
			0.0	0.5	1.0	1.5	2.0	3.0
1	Cooling time from 810 °C to 600 °C in sec.	τ_{600}	8.1	7.8	5.7	5.3	4.7	3.5
2	Cooling time from 810 °C to 400 °C in sec.	τ_{400}	12.0	11.3	9.2	8.8	8.1	7.2
3	Cooling time from 810 °C to 200 °C in sec.	τ_{200}	37.3	36.3	34.7	35.7	34.5	34.7
4	Maximal cooling rate in °C/s	V_t^{max}	74.7	88.4	103.4	111.8	108.8	119.4
5	Core temperature of probe at maximum cooling rate, °C	$T_з^{Vt\ max}$	551	550	584	617	635	669
6	Cooling rate in °C/s when core temperature is 300 °C	$V_t^{T=300}$	8.6	8.2	8.0	7.7	8.1	8.3

Table 2. Viscosity η_D of oligomeric solutions in mineral oils at 50 °C (η_D, MPa·s; Dr = 729 s^{-1})

PIB 2400													
I - 20A	Concentration. C. % wt.												
	0.0	0.5	1.0	1.5	2.0	2.5	3.0	4.5	5.0	7.5	10.0		
	14.48	15.08	15.90	16.58	17.17	18.04	19.04	21.45	22.68	28.20	34.07		
I- 12A	Concentration. C. % wt.												
	0.0	0.5	1.0	1.5	2.0	3.5	5.0	7.5	9.0	10.0	12.5	14.5	15.0
	9.47	9.84	10.39	10.84	11.21	12.98	15.03	18.52	21.18	23.14	28.61	33.57	35.66
I -8A	Concentration. C. % wt.												
	0.0	0.5	1.0	1.5	2.0	3.5	5.0	10.0	14.0	15.0	16.0	19.0	21.5
	5.10	5.36	5.60	5.92	6.19	7.01	8.06	13.12	18.36	20.13	21.95	28.47	34.79
PIB 1300													
I - 20A	Concentration. C. % wt.												
	0.0		3.0		5.0		7.5		10.0		12.5		
	14.48		16.94		18.97		21.50		24.64		28.15		
PIB 950													
I - 20A	Concentration. C. % wt.												
	0.0	3.0		4.3		5.0		7.0		7.5		10.0	16.0
	14.48	16.26		17.26		17.63		19.04		19.54		21.77	28.01
PIB 680													
I- 20A	Concentration. C. % wt.												
	0.0	3.0		5.0		7.0		10.0		12.5		19.0	
	14.48	15.58		16.53		17.40		19.18		21.04		26.24	

Table 3. Cooling curves characteristics for oil I-20A (1), for 7% PIB 950 solution in oil I-20 (2), for 5% PIB 1300 solution in oil I-20 (3), for 3% PIB 2400 (4), for 10% PIB 680 solution in oil I-20 at 50 °C (5), and solution of 40% I-40 oil in in I-20 oil (6).

Data	Designation	Quenchants					
		1	2	3	4	5	6
Cooling time from 810 °C to 600 °C. s.	τ_{600}	8.1	3.5	3.7	3.4	5.2	7.6
Cooling time from 810 °C to 400 °C. s.	τ_{400}	12.0	7.2	7.2	6.8	9.7	13.4
Cooling time from 810 °C to 200 °C. s.	τ_{200}	37.3	34.7	34.3	33.4	34.7	38.6
Maximum cooling rate. °C/s	V_t^{max}	74.7	119.4	129.8	122.4	96.8	65.8
Temperature at maximum cooling rate. °C	$T_з^{Vtmax}$	551	669	649	617	650	574
Cooling rate at 300 °C. °C/c	$V_t^{T=300}$	8.0	8.3	8.3	7.0	8.5	8.4

3 Discussion

The approach of authors has a great practical importance because elimination of film and local film boiling results in decreasing distortion of steel parts after quenching. Especially, this problem is very important for bearing industry where elimination distortion can bring the huge benefits. To investigate carefully these processes, it is

better to use Liscic/Petrofer probe [6] with three thermocouples instrumented in it. Also, critical heat flux densities and heat transfer coefficients should be carefully investigated to make possible controlling and governing quenching processes. For example, it was shown [5] that complete cooling during batch quenching in polymers of inverse solubility can lead to big distortion because dissolving of polymeric layer resulting in non – uniform cooling and martensitic transformations. To run technology correctly, one should deal with HTCs allowing make proper interruption to avoid big distortions. Thus, careful investigation of insulating layers will result in decreasing distortion and bring great benefits for industry.

4 Conclusions

1. Low addition (3%) of PIB 2400 into mineral oil I-20A eliminates completely film boiling during quenching which is called FBE effect.
2. Addition of PIB 2400 into I-8A and I-12A oils decreases film boiling process for 80% and 90% accordingly that is explained by lower critical heat flux densities of I-8A and I-12A oils.
3. Oligomeric solutions in mineral oils, in contrast to water polymer solutions, do not follow the viscosity criteria.
4. There is a critical molecular weight of PIB below of which FBE effect doesn't take place.
5. Mechanism and FBE effect is explained by formation an insulating layer on the metallic surface. It decreases initial heat flux density and makes it lesser than the first critical heat flux density [7].
6. The FBE effect opens the great opportunity to optimize investigations on designing and content of the new oil quenchants for heat treatment of metals.

References

1. Kobasko, N.I.: Real and effective heat transfer coefficients (HTCs) used for computer simulation of transient nucleate boiling processes during quenching. Mater. Perform. Charact. **1**(1), 1–20 (2012)
2. Lohvynenko, P.N., Moskalenko, A.A., Kobasko, N.I., Karsim, L.O., Riabov, S.V.: Experimental investigation of effect of polyisobutilene additives to mineral oil on cooling characteristics. Mater. Perform. Charact. **5**(1), 1–13 (2016)
3. Kobasko, N.I., Moskalenko, A.A., Lohvynenko, P.N., Karsim, L.O., Riabov, S.V.: An effect of PIB additive to mineral oil resulting in elimination of film boiling during steel parts quenching. EUREKA: Phys. Eng. **3**, 17–24 (2016)
4. ISO 9950 :1995(E): Industrial quenching oils – Determination of cooling characteristics – Nickel – alloy probe test method.- Geneva: International Organization for Standardization, 9p. (1995)
5. Kobasko, N.I.: Cooling intensity of inverse solubility polyalkylene glykol polymers and some results of investigations focused on minimizing distortion of metal components. EUREKA: Phys. Eng. **1**, 55–62 (2017)

6. Liscic, B.: Measurement and recording of quenching intensity in workshop conditions based on temperature gradients. Mater. Perform. Charact. **5**(1), 202–219 (2016). https://doi.org/10.1520/mpc20160007. ISSN 2165–3992
7. Kobasko, N.I., Moskalenko, A.A., Lohvynenko, P.N., Dobryvechir, V.V.: Maximizing critical and reducing initial heat flux densities to eliminate any film boiling and minimize distortion during quenching. EUREKA: Phys. Eng. **4**(10), 33–41 (2017). https://doi.org/10.21303/2461-4262.2017.00366

Comparison of E-mode GaN HEMT Using Different Gate Oxide Stack Approach

Edward Yi Chang[1,2,3(✉)], Chia-Hsun Wu[1], Yueh-Chin Lin[1], Ping-Cheng Han[3], Yu-Xiang Huang[4], Quang Ho Luc[1], Jian-You Chen[1], and Yu-Hsuan Ho[5]

[1] Department of Materials Science and Engineering, National Chiao Tung University, 1001 Ta Hsueh Road, Hsinchu 30010, Taiwan
edc@mail.nctu.edu.tw
[2] Department of Electronic Engineering, National Chiao Tung University, Hsinchu, Taiwan
[3] International College of Semiconductor Technology, National Chiao Tung University, Hsinchu, Taiwan
[4] Institute of Photonic System, National Chiao Tung University, Hsinchu, Taiwan
[5] Institute of Lighting and Energy Photonics, National Chiao Tung University, Hsinchu, Taiwan

Abstract. In this study, three different types of gate recessed E-mode GaN MIS-HEMTs were fabricated by different gate oxide stack techniques. The gate oxide stacks were designed with different oxide potential barrier, resulting in the device with different threshold voltages. Each device performance was evaluated, compared and discussed. The proposed device with charge trap gate stack showed the best device performance with high threshold voltage and high maximum drain current density in this work.

Keywords: GaN · Enhancement-mode · MIS-HEMTs · Gate oxide Potential barrier

1 Introduction

Gallium nitride (GaN) materials have been widely used for power electronic applications because of its wide bandgap (3.4 eV), high saturation velocity (2.5×10^7cm/s), and large breakdown electrical field (3.3 MV/cm). Enhancement-mode (E-mode) GaN high-electron- mobility transistors (HEMTs) have been widely investigated recently for electric vehicle applications due to the simplicity of the circuit design and safety issues. [1]. Several approaches have been demonstrated to achieve E-mode GaN HEMTs in the past, such as recessed-gate [2], p-type GaN [3], and fluorine implantation [4]. To effectively suppress ON-state gate leakage current and increase gate swing, E-mode devices have been fabricated by combining recessed-gate and MIS (metal-insulator-gate) approaches [5, 6]. Those approaches increase the potential barrier underneath the device gate region to positively shift the threshold voltage. Even though these approaches can achieve the device with E-mode operation, the device performance still

K. Ntalianis and A. Croitoru (Eds.): APSAC 2017, LNEE 489, pp. 11–17, 2019.
https://doi.org/10.1007/978-3-319-75605-9_2

cannot satisfy real power device applications, such as high threshold voltage (>3 V), low ON-resistance and large gate swing.

In this work, we compared the device performance of three types of gate recessed E-mode GaN MIS-HEMTs with different gate oxide stack techniques. Device A with the high interface quality composite high-k dielectric as the gate oxide. Device B with fluorine doped gate dielectric. Device C with a novel charge trap gate oxide stack.

2 Device Fabrication

The epitaxial structure of the devices was grown by metal-organic chemical vapor deposition (MOCVD) on Si (111) substrate. It consisted of a 1-μm thick GaN buffer layer and a 25-nm-thick $Al_{0.22}Ga_{0.78}N$ barrier layer with a 3-nm undoped GaN cap layer on the top of the structure. The device fabrication started with ohmic contact formation with alloyed Ti/Al/Ni/Au metal stack. Mesa isolation using inductively coupled plasma (ICP) etching was employed to define the active region of the device. For device passivation, in-situ nitrogen plasma treatment was performed using PECVD machine, followed by the deposition of a 50-nm PECVD SiNx layer as the passivation layer. The nitride etch and gate recess were performed by low power ICP-RIE system, the remaining barrier thickness was about 7 nm. The gate oxide deposition was performed by three different methods as shown in Fig. 1. For Device A, the composite La_2O_3/HfO_2 was deposited by the molecular beam deposition (MBD) system at 200 °C at a pressure of 10^{-7} Torr. Post-deposition annealing (PDA) at 600 °C was performed to improve the oxide film quality. For Device B, 15 nm Al_2O_3 was deposited by ALD system. After gate window was opened, fluorine ions were directly implanted into the gate region by Varian E500HP ion implanter. The implantation energy and ion dose were 10 keV and $1x10^{12}$ cm^{-2}, respectively. A post–implantation annealing at 400 °C was performed in N_2 ambient. For Device C, 6 nm Al_2O_3/3 nm $HfON/Hf_{0.5}Zr_{0.5}O_2$ was deposited by ALD system. A post–deposition annealing (PDA) at 400 °C was performed in N_2 ambient. Ni/Au was deposited by electron beam evaporation as the gate metal, subsequently. The gate length of all devices was 2 μm, and the gate-to-source and gate-to-drain distances were 3 μm and 15 μm, respectively.

3 Result and Discussion

Figure 2 shows the schematic band diagram with different gate oxide techniques. Due to the fact that $LaHfO_x$ has low energy bandgap (5–6 eV) and high dielectric constant (–23), Device A shows the lowest oxide potential barrier, resulting in the GaN conduction band edge close to the Fermi level at the AlGaN/GaN interface, causing to a small threshold voltage for Device A. Device B with the fluorine doped Al_2O_3 gate oxide layer shows the higher oxide potential barrier than Device A, which was caused by the negatively charged fluorine ions implanted into Al_2O_3. The previous report suggested fluorine ions incorporated into Al_2O_3 could effectively increase the oxide potential barrier due to the negative charge fluorine ions [7].

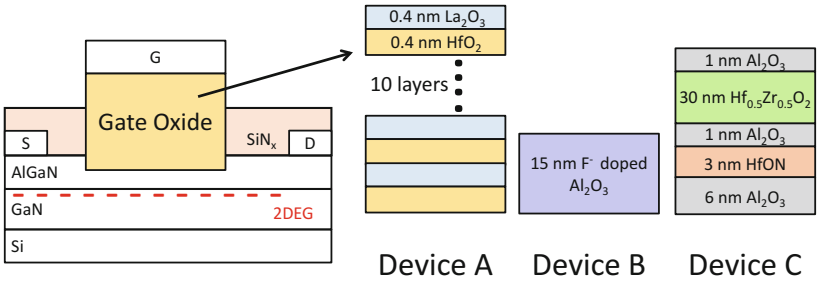

Fig. 1. Schematic cross section of the fabricated E-mode GaN MIS-HEMT with three different gate oxide stacks. (Device A with 10 layers of La_2O_3 (0.4-nm)/HfO_2 (0.4-nm) composite gate insulator. Device B with fluorine doped Al_2O_3. Device C with a novel charge trap gate oxide stack.

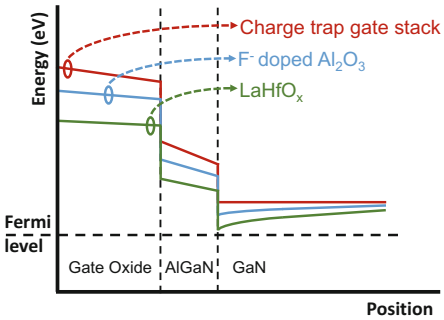

Fig. 2. Schematic band diagram of fabricated device with three different gate oxide stacks.

The V_{th} for fluorinated MOS-HEMTs can be expressed as

$$V_{th} = \frac{\Phi_b}{q} - \frac{\Delta E_c}{q} - \frac{\Phi_f}{q} - \frac{qt_{AlGaN}}{\varepsilon_{\text{AlGan}}} Q_{\text{AlGaN/GaN}} - q\varphi(F) - \frac{qt_{ox}}{\varepsilon_{ox}} \left[Q_{\text{AlGaN/GaN}} + Q_{\text{Al}_2\text{O}_3/\text{AlGaN}} + Q(F) \right] - \frac{q\overline{n_{\text{ox}}}}{2\varepsilon_{ox}} t_{ox}^2 \quad (1)$$

Φ_b : the metal barrier height for Ni on Al_2O_3
ΔE_c : the conduction band offset between Al_2O_3 and GaN
Φ_f : the conduction band distance from the Fermi-level in GaN
$q\varphi(F)$: a constant band bending only dependent on density of fluorine charge and distribution, but independent of the gate oxide thickness.
$\overline{n_{\text{ox}}}$: the average oxide bulk charge (per unit volume)
$\varepsilon_{\text{AlGaN}}$: the permittivity of: the permittivity of Al_2O_3
t_{AlGaN} : the thickness of AlGaN, t_{ox}: the thickness of Al_2O_3
$Q_{\text{AlGaN/GaN}}$: interface charge density at the Al_2O_3/AlGaN interface

$Q_{Al_2O_3/AlGaN}$: interface charge density at AlGaN/GaN-channel interface
$Q(F)$: a fluorine equivalent interface charge (per area) located at the AlGaN/Al_2O_3 interface calculated by integration of the fluorine negative charge in the bulk GaN and AlGaN.

The formula (1) suggests the negative charge fluorine ions can compensate the positive oxide charge to increase the threshold voltage [8]. It's consistent with the fact that amount of negative charge in the gate oxide stack increase the oxide potential barrier and thus increase threshold voltage. Device C has a novel charge trap gate oxide stack to trap more electrons into the gate oxide stack. After initialization process (applied a high gate voltage at gate electrode to make electron inject into the gate oxide layer), a lot of electrons are trapped in the gate oxide stack, obtaining the much higher potential barrier. As a result, the E-mode GaN MIS-HEMT has a high threshold voltage.

The *I-V* characteristics of Devices A, B and C are shown in the Figs. 3, 4, and 5, respectively. It indicates the trend of threshold voltage increase is consistent with the prediction. The device performances of Device A, B, and C are shown in Figs. 3, 4, and 5, and the results are summarized in Table 1.

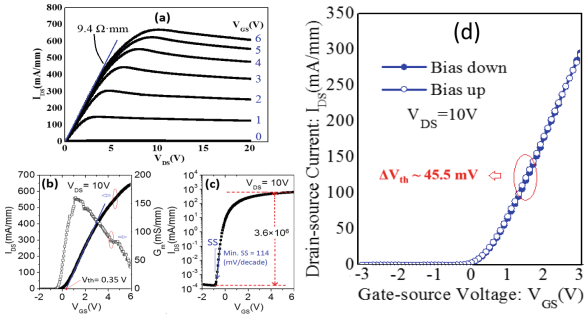

Fig. 3. *I-V* characteristics of Device A with 8-nm LaHfOx gate insulator: (a) I_{DS}-V_{DS} curve, (b) transfer curve curves in linear scale and (c) in the log scale, and (d) I_{DS} -V_{GS} curve by up and down sweep measurements.

Device A shows the lowest hysteresis of threshold voltage (ΔV_{th}) due to the excellent interface quality of $LaHfO_x$ film. All devices show good ON/OFF ratio $>10^7$. It demonstrates the potential for power application because of its low static power consumption. Besides, all devices show low ON-resistance (<11 Ω·mm) and high maximum drain current density (>600 mA/mm). It indicates the channel mobility does not suffer from severe degradation caused by gate recess or fluorine doping. Device C shows the best device performance of high threshold voltage (+4.4 V) with high current density (770 mA/mm). This is attributed that the charge trap gate stack largely increases the potential barrier due to the electron trapping in the gate stack structure. Figure 6 shows the transfer characteristics of Device C before and after initialization. After initializing, more electrons trapped into the gate oxide stack, achieving device from negative threshold voltage to positive threshold voltage. Besides, the current

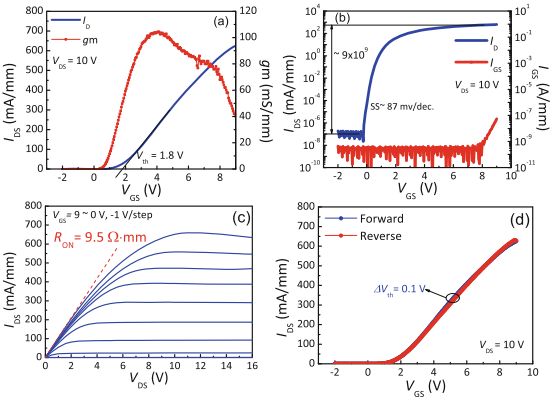

Fig. 4. *I-V* characteristics of Device B with fluorine doped gate insulator: (a) transfer curve curves in linear scale and (b) in the log scale, (c) I_{DS}-V_{DS} curve, and (d) I_{DS} -V_{GS} curve by up and down sweep measurements.

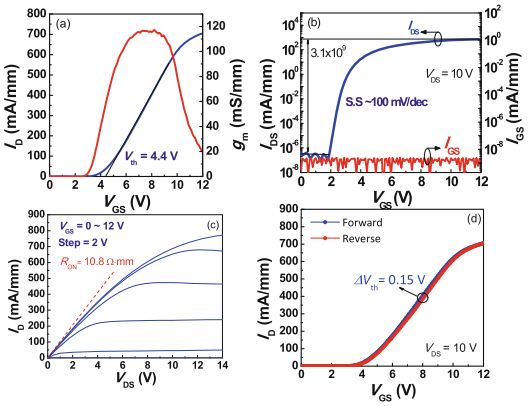

Fig. 5. *I-V* characteristics of Device C with charge trap gate stack: (a) transfer curve curves in linear scale and (b) in the log scale, (c) I_{DS}-V_{DS} curve, and (d) I_{DS} -V_{GS} curve by up and down sweep measurements.

density before and after initialization is nearly the same. In contrast, Device B with fluorine doping could achieve higher threshold voltage, but fluorine doping causes the current density reduction due to the mobility degradation. Device A with high-k gate dielectric has low threshold voltage. It cannot achieve high threshold voltage without the deep recess depth, thus, it results in large current degradation.

Table 1. Comparison of the DC characteristics of fabricated E-mode GaN MIS-HEMT.

	Device A	Device B	Device C
Gate oxide	$LaHfO_x$	F^- doped Al_2O_3	Charge trap gate stack
$I_{D,MAX}$ (mA/mm)	648	675	770
$G_{m,MAX}$ (mS/mm)	165	106	116
V_{th}(V)	0.35	1.8	4.4
R_{on}(Ω·mm)	9.4	9.5	10.0
Subthreshold Swing(mV/decade)	114	87	100
I_{on}/I_{off} ratio	3.6×10^7	9×10^9	3.1×10^9
Hysteresis(mV)	45.5	100	150

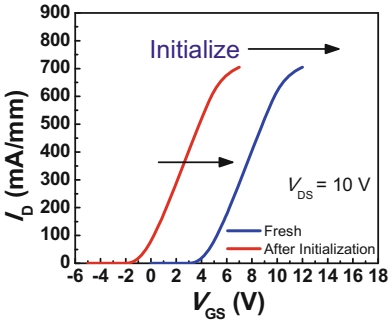

Fig. 6. Transfer characteristics of Device C before and after initialization.

4 Conclusion

In this work, three gate recessed E-mode GaN MIS-HEMTs were fabricated by different gate oxide stack techniques. Because the gate oxide stacks have different oxide potential barriers, the device performances were different. The device with charge trap gate stack shows the best device performance with high threshold voltage and maximum drain current density in this work. Thus, the proposed E-mode GaN MIS-HEMTs with charge trap gate stack is a promising architecture for future GaN power electronic applications.

References

1. Imada, T., Kanamura, M., Kikkawa, T.: Enhancement-mode GaN MIS-HEMTs for power supplies. In: Proceedings of the International Power Electronics Conference (IPEC), pp. 1027–1033, June 2010
2. Oka, T., Nozawa, T.: AlGaN/GaN recessed MIS-gate HFET with high-threshold-voltage normally-off operation for power electronics applications. IEEE Electron Device Lett. **29**, 668–670 (2008)

3. Uemoto, Y., Hikita, M., Ueno, H., Matsuo, H., Ishida, H., Yanagihara, M., Ueda, D.: A Normally-off AlGaN/GaN Transistor with R on A= 2.6 mΩcm 2 and BV ds= 640V using conductivity modulation. In: Proceedings of the International Electron Devices Meeting, 2006. IEDM'06, pp. 1–4. IEEE, December 2006
4. Tang, Z., Jiang, Q., Lu, Y., Huang, S., Yang, S., Tang, X., Chen, K.J.: 600-V Normally Off SiN_x/AlGaN/GaN MIS-HEMT With large gate swing and low current collaps. IEEE Electron Device Lett. **34**(11), 1373–1375 (2013)
5. Lin, S., Wang, M., Sang, F., Tao, M., Wen, C.P., Xie, B., Yu, M., Wang, J., Hao, Y., Wu, W., Xu, Jun, Cheng, K., Shen, B.: A GaN HEMT structure allowing self-terminated, plasma-free etching for high-uniformity, high-mobility enhancement-mode devices. IEEE Electron Device Lett. **37**, 377–380 (2016)
6. Shi, Y., Huang, S., Bao, Q., Wang, X., Wei, K., Jiang, H., Li, J., Zhao, C., Li, S., Zhou, Y., Gao, H., Sun, Q., Yang, H., Zhang, J., Chen, W., Zhou, Q., Zhang, B., Liu, X.: Normally OFF GaN-on-Si MIS-HEMTs fabricated with LPCVD-SiN x passivation and high-temperature gate recess. IEEE Trans. Electron Devices **63**, 614–619 (2016)
7. Wang, Y.-H., Liang, Yung C., Samudra, G.S., Huang, H., Huang, B.-J., Huang, S.-H., Chang, T.-F., Huang, C.-F., Kuo, W.-H., Lo, G.-Q.: 6.5 V high threshold voltage AlGaN/GaN power metal-insulator-semiconductor high electron mobility transistor using multilayer fluorinated gate stack. IEEE Electron Device Lett. **36**, 381–383 (2015)
8. Zhang, Y., Sun, M., Joglekar, S.J., Fujishima, T., Palacios, T.: Threshold voltage control by gate oxide thickness in fluorinated GaN metal-oxide-semiconductor high-electron-mobility transistors. Applied Physics Lett. **103**, 033524 (2013)

Physical Parameterization in MRI

Alexey Protopopov[1,2(✉)]

[1] Moscow Institute of Physics and Technology,
Institutskiy Street, 9, 141701 Moscow District, Dolgoprudniy, Russia
proto.alex@hotmail.com
[2] Federal Scientific Clinical Center for Gematology, Oncology,
and Immunology, GSP-7, Samora Mashel Street, 1, 117997 Moscow, Russia

Abstract. Gradient recalled echo (GRE) sequences are nowadays routinely used in clinical applications of magnetic resonance imaging (MRI). Contrast of GRE images is determined by several different physical mechanisms, like proton density, T_2 relaxation time, gradients of magnetic field, and spatial heterogeneities of spin-spin interaction. Although the combined effect of all these parameters is of great value for physicians, it is possible that their separate mapping may reveal new features, that are masked in traditional GRE images. Separate mapping of physical parameters, contributing to contrast of GRE images, is called the parameterization, and has not been entirely solved by now. The present publication reports on development of the necessary tools for the solution. Finally, results obtained on volunteers are presented.

Keywords: Gradient recalled echo (GRE) · Relaxation function
Least squares · Magnetic gradients

1 Introduction

A common parameter used to describe the rate of spin-spin relaxation in the presence of local magnetic field gradients is the T_2^* time, which is calculated by fitting a monoexponent over the relaxation curve. While nowadays it is commonly considered to be an evolution of the T_2 decay (first described in [1]), its original purpose was to describe the width of the relaxation spectrum [2], and the parameter was not directly related to relaxation speed. However, subsequent theoretical research showed that the behavior of spin-spin relaxation is more complex than a monoexponent, and structural characteristics of biological tissues are encoded in the shape of relaxation curve rather than in a single parameter T_2^* [3–9]. Furthermore, the difference between the shape of a monoexponential curve and the relaxation curve of a voxel affected by local magnetic field gradients and T_2 heterogeneities meant that T_2^* is a surrogate parameter without any significant physical meaning. Several attempts have been made to introduce a more accurate relaxation model [10, 11], but none of them were able to provide an example of how well the new model fits the experimental data. In light of the aforementioned, this report introduces the concept of the 4th dimension in MRI – the relaxation curve shape. As three Cartesian coordinates x, y, z determine position of the voxel in the body, the 4th coordinate determines its structure. Based on the tissue model, it is

K. Ntalianis and A. Croitoru (Eds.): APSAC 2017, LNEE 489, pp. 18–24, 2019.
https://doi.org/10.1007/978-3-319-75605-9_3

possible to define the unique relaxation curve shape in each voxel with various numerical parameters, which characterize the tissue structure. For practical implementation of this concept, the four basic components are needed:

- analytical 3D model of relaxation process;
- non-iterative multi-point algorithm with clamping (MPC) for determining the analytical form of relaxation function;
- approximation function, valid for the entire time range: from zero to infinity;
- branching algorithm of spatial averaging of relaxation signals;
- resolution-preserving composite colour imaging (RPCC).

2 Methods

The work on a 3D relaxation model, first presented in [12] and later expanded in [13], gives the following formula for gradient recalled echo (GRE) signal:

$$S(t) = S_0 \cdot e^{-t/T_2 + \beta t^2} \cdot R_{p_x}(\alpha_x t) \cdot R_{p_y}(\alpha_y t) \cdot R_{p_z}(\alpha_y t), \tag{1}$$

where function $R(t)$ accounts for all possible gradients:

$$R_p(x) = \frac{1}{x}\int_0^x \cos(pu)e^{-u^2}du. \tag{2}$$

Here $\alpha_{x,y,z}$ and $p_{x,y,z}$ are the coefficients describing the magnetic field gradients, and β is the coefficient responsible for the T_2 heterogeneities. By applying a Taylor expansion to approximate (1) at low t, we can turn the formula into

$$S(t) = S_0 \cdot \exp\left[-t/T_2 + \left(\beta^2 - \alpha^2\right)t^2\right], \tag{3}$$

which can be fitted to a curve non-iteratively with the help of the least squares condition. Due to the use of a Taylor expansion, this method works only at low t, so the experimental points are assigned dynamic statistical weights based on their distance from the start of the time coordinate, so that only the appropriate points are used in the fitting. This method is named «Multiple Point Algorithm with Clamping» or MPC.

But in order to calculate parameters such as $T_{1/e}$, which is the time it takes for the signal to decrease by a factor of e, one would need an approximation function that provides an adequate fit across the entire range of t: from zero to infinity. This Full Range Approximation (FRA) would also need to be analytical, since it will need to be calculated for each individual pixel of the image. Furthermore, the function in question would need to have physical meaning and not contradict reality. Finally, it must not contradict the polynomial exponent used for fitting in [12] around zero, as well as pass through the first and last points of the experimental curve. The main purpose of this last condition is to make the approximation easier to compute. The following function fulfills all of these requirements:

$$S(t) \approx \exp[a - bt - w(e^{-\varepsilon t} - 1 + \varepsilon t)]. \tag{4}$$

Parameters a, b and c are provided by the MPC algorithm, while w and ε are derived from them in order to match the function with the experimental curve.

Due to its non-linear nature, this system is best solved using an iterative method. At the first step, we take the last experimental point at t_m and assume that $\varepsilon t_m \gg 1$ and $e^{-\varepsilon t_m} \approx 0$, which produces

$$\varepsilon^{(0)} = \frac{2ct_m}{y_m - bt_m - a}. \tag{5}$$

This value is not precise enough to be used for plotting the curve, but it can be used to produce the first set of parameters using the following general formula:

$$\begin{cases} w^{(n+1)} = \frac{-z_m}{e^{-\varepsilon^{(n)} t_m} - 1 + \varepsilon^{(n)} t_m}; \\ \varepsilon^{(n+1)} = \sqrt{\frac{-2c}{w^{(n+1)}}}, \end{cases} \tag{6}$$

where n is the number of the current iteration. This operation can be repeated an unlimited number of times, however the number of iterations typically stays below 10 in practice. Figure 1 shows an example of the full-range approximation being fitted over an experimental curve.

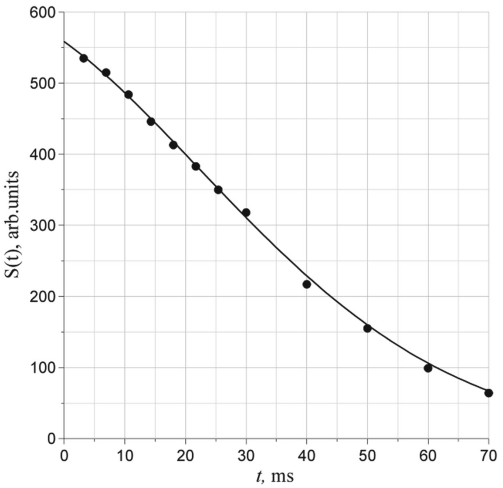

Fig. 1. Solid line – FRA, points – experimental data.

The methods described above require the signal-to-noise ratio (SNR) to be above a certain value. Specifically, the MPC algorithm produces reliable results only at SNR >60. While this is achievable with sequences of sufficiently long duration, many patient related applications do not allow such luxury. For example, due to significant

displacement of internal organs during the breathing cycle, imaging of the abdominal region must often be with the patient holding breath, which limits the duration of the sequence to ~20 s. In other words, the signal quality required for MPC may not always be provided by the sequence. This can be rectified by introducing a branching method of spatial averaging. The difference between a standard spatial averaging algorithm and an averaging algorithm with branching is simple: the former uses the same area around the central pixel for each echo time, while the latter dynamically adjusts the area depending on the amplitude of the signal – assuming that the level of noise would be the same for each echo, a stronger signal would have a better SNR and would therefore require a smaller averaging area. This way, the averaging area seems to branch out as illustrated on Fig. 2, which gives this algorithm its name.

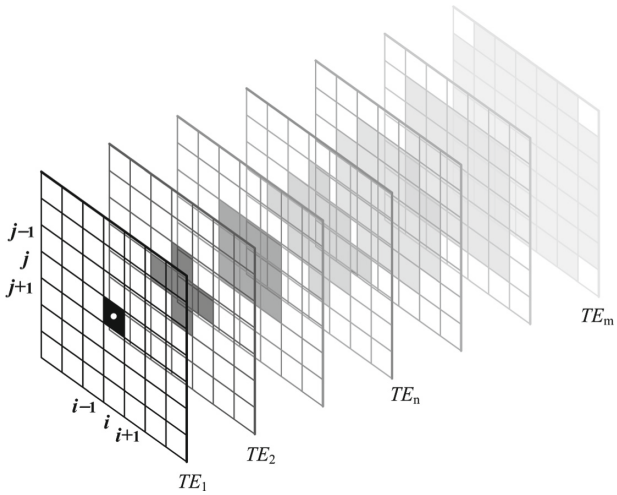

Fig. 2. Concept of branching averaging. Pixels used for the averaging calculation are shown in black. The decrease in signal amplitude with subsequent TEs is depicted by the opacity of each layer of the image.

In addition to branching, adjustment of statistical weights of the pixels used in averaging was implemented in this work. The weight of the central pixel would be set by the operator in the range between one and zero, and the weights of all surrounding pixels would be adjusted automatically. For example, with the averaging area encompassing four pixels arranged around a central pixel, the statistic weights of the pixels would need to comply with the following equation:

$$4\beta + \alpha = 1, \tag{7}$$

where α is the weight of the central pixel, and β is the individual weight of every surrounding pixel. This way, if $\alpha = 1$, all pixels but the central one are ignored, and no averaging is performed. Conversely, with $\alpha = 0.2$, all pixels have the same statistic weight.

Yet despite the implementation of the branching, this averaging algorithm reduces the resolution of the calculated parameter map. To offset that, the Resolution Preserving Colour Compounds (RPCC) were used. The concept of this method is simple. The intensity of a colour pixel is typically split between three channels: red, green and blue. It can be presented as

$$\vec{P}_{i,j} = 256(\, r_{i,j} \quad g_{i,j} \quad b_{i,j}\,), \tag{8}$$

where i and j are the coordinates, the parameters r, g and b vary between zero and one, and 256 is the maximum commonly used brightness value. MRI images are generally presented as grayscale images, which have the same intensity in all three channels:

$$\vec{P}_{i,j} = a_{i,j}(\, 1 \quad 1 \quad 1\,) \tag{9}$$

What the RPCC does, is take the value of the parameter map $u_{i,j}$, and substitute it into one of the channels of the original MRI image, while the data from the original image is substituted into another channel:

$$\vec{P}_{i,j} = a_{i,j}(\, 1 \quad u_{i,j}/u_{\max} \quad 1\,), \tag{10}$$

where $u_{\max}$ is the maximum value across the entire parameter map. This way, the parameter map is displayed as a variation of colour, while at the same time maintaining the resolution of the original MRI image. Thus, the RPCC allows the use of spatial averaging to calculate the parameter map without sacrificing the resolution of the image.

A method similar to the one presented in this article was described in [14]. However, there the original image and the parameter map were assigned to separate channels:

$$\vec{P}_{i,j} = (\, a_{i,j} \quad u_{i,j} \quad 0\,) \tag{11}$$

3 Results

The sequence used for the experiments performed in this article was a standard Siemens gradient recalled echo sequence (GRE). Twelve separate echoes were acquired with each sequence, with echo times ranging between 2.6 ms and 70 ms. Scans of the head were taken using a standard birdcage coil, while the abdomen and hips were imaged using a standard flexible body coil. Figure 3 shows the results. It is immediately apparent, that the T_2 and $T_{0.5}$. For example, the liver in the abdominal images is darker than the surrounding tissues on the $T_{0.5}$ map, while on the T_2 map it is brighter. Furthermore, the gradient colourmap noticeably highlights the borders between different organs, where changes in susceptibilities between different organs create magnetic field gradients.

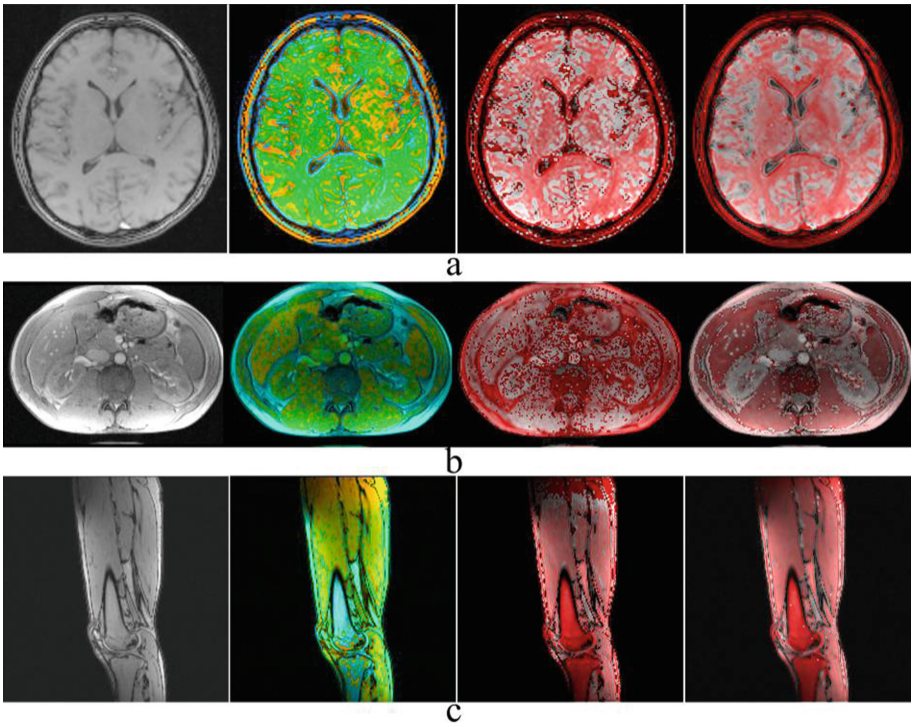

Fig. 3. The rows of colour images correspond to: (a) brain, (b) abdomen, (c) hip. In each row, the first image is the original GRE image, followed by the maps of T_2, $T_{0.5}$ and, finally, a colourmap of gradients created using RPCC.

4 Discussion

The concept of the 4th dimension splits every original GRE image into a series of maps, showing spatial distribution of physically meaningful parameters, like T_2, average gradients, $T_{0.5}$, or others. Thus, from pure intensity rendering in conventional GRE imaging, we come to mapping of physical parameters relevant to specific clinical applications, such as BOLD. In addition, the gradient map reveals many details not present in the original image. It is also important to note, that all of these maps were acquired using a single sequence. On one hand, this means a reduction in time required for the scan, since the GRE sequence can be considered one of the faster sequences used in MRI. On the other hand, this also reduces the overall exposure of the patient to RF radiation. Both of these qualities are valuable when the subject needs to undergo a long examination involving many sequences. Finally, while this article presents T_2, $T_{0.5}$ and gradient maps as results, many more parameters can be derived from the shape of the relaxation curve, including, but not limited to total volume under the curve, decay rate and spin density. It is entirely possible, that with further study one could establish a correlation between these parameters and various pathological conditions.

5 Conclusion

It may be theorized that, in clinical applications, the concept of the 4^{th} dimension in GRE imaging could improve classification of tissues and detection of tumors, as well as speed up the examination process and reduce overall exposure to radiation.

References

1. Bloch, F.: Nuclear induction. Phys. Rev. **70**(7–8), 460–474 (1946)
2. Bloembergen, N., Purcell, E.M., Pound, R.V.: Relaxation effects in nuclear magnetic resonance absorption. Phys. Rev. **73**(7), 679–712 (1948)
3. Yablonskiy, D.A., Haacke, E.M.: Theory of NMR signal behavior in magnetically inhomogeneous tissues – the static dephasing regime. Magn. Reson. Med. **32**(6), 749–763 (1994)
4. Sukstanskii, A.L., Yablonskiy, D.A.: Gaussian approximation in the theory of MR signal formation in the presence of structure-specific magnetic field inhomogeneities. J. Magn. Res. **163**, 236–247 (2003)
5. Sukstanskii, A.L., Yablonskiy, D.A.: Gaussian approximation in the theory of MR signal formation in the presence of structure-specific magnetic field inhomogeneities. Effects of impermeable susceptibility inclusions. J. Magn. Res. **167**, 56–67 (2004)
6. Kiselev, V.G.: Effect of magnetic field gradients induced by microvasculature on NMR measurements of molecular self-diffusion in biological tissues. J. Magn. Res. **170**, 228–235 (2004)
7. Dickson, J.D., Ash, T.W.J., Williams, G.B., Sukstanskii, A.L., Ansorge, R.E., Yablonskiy, D.A.: Quantitative phenomenological model of the BOLD contrast mechanism. J. Magn. Res. **212**, 17–25 (2011)
8. Knight, M.J., Kauppinen, R.A.: Diffusion-mediated nuclear spin phase decoherence in cylindrically porous materials. J. Magn. Res. **269**, 1–12 (2016)
9. Wharton, S., Bowtell, R.: Fiber orientation-dependent white matter contrast in gradient echo MRI. Proc. Natl. Acad. Sci. U.S.A. **109**, 18559–18564 (2012). https://doi.org/10.1073/pnas.1211075109
10. Fernandez-Seara, M.A., Wehrli, F.W.: Postprocessing technique to correct for background gradients in image-based R_2^* measurements. Magn. Reson. Med. **44**, 358–366 (2000)
11. Dahnke, H., Schaeffter, T.: Limits of detection of SPIO at 3.0T using T_2^* relaxometry. Magn. Reson. Med. **53**, 1202–1206 (2005)
12. Protopopov, A.: Relaxation model and mapping of magnetic field gradients in MRI. Appl. Magn. Reson. **48**, 255–274 (2017)
13. Protopopov, A.: Structural analysis of relaxation curves in MRI. Appl. Magn. Reson. **48**, 1–12 (2017)
14. Valdés Hernández, M.C., Royle, N.A., Jackson, M.R., et al.: Color fusion of magnetic resonance images improves intracranial volume measurement in studies of aging. Open J. Radiol. **2**, 1–9 (2012)

A Choosing of the Disperse Sample for Investigation of Magnetic Properties of the Disperse Phase Particles. Noticing of Volume Fraction Limiting

A. A. Sandulyak(✉), D. A. Sandulyak, V. A. Ershova, A. V. Sandulyak, and M. N. Polismakova

Moscow Technological University, 20 Stromynka Street, Moscow, Russian Federation
anna.sandulyak@mail.ru

Abstract. The paper provides a thorough analysis of existing and obtained experimental dependences of magnetic susceptibility of the disperse samples containing a disperse phase of magnetite particles on the concentration of this phase. We proved a possibility of obtaining the information on the particles magnetic susceptibility using the data of the initial section (nearly linear) of such dependence at the range of volume fraction up to 0.2. We considered a possibility of accuracy increase of such information for narrowed range of volume fraction (it is up to 0.02–0.05 that is usually recommended). At this range concentration dependences follow a self-consistent linear trend.

Keywords: Disperse phase of medium · Ferroparticles · Magnetite
Volume fraction · Criterion value · Field intensity · Magnetic susceptibility

1 Introduction

Dispersed phase of various technological and natural media often features some ferroparticles that possess ferro- and ferromagnetic properties. It is imperative to obtain the data on magnetic susceptibility χ such particles, in particular, in solving many applied scientific tasks of magnetophoresis and/or magnetic control, especially in analysis criteria magnetic capture of such particles [1–3].

An approach to obtaining such χ data for the given purpose could be based on data of the susceptibility $\langle\chi\rangle$ of the disperse sample (in particular, suspension, colloid, powder) containing such particles. In this case data of the susceptibility $\langle\chi\rangle$ could be obtained by using ponderomotive Faraday method (it is enough having a small volume of sample), data of the susceptibility χ - by using a necessary relation:

$$\chi = \langle\chi\rangle/\gamma, \tag{1}$$

where γ – volume fraction (concentration) of ferroparticles in sample. We should mention specially, that the relation (1) is true only under condition of sufficient mutual

K. Ntalianis and A. Croitoru (Eds.): APSAC 2017, LNEE 489, pp. 25–32, 2019.
https://doi.org/10.1007/978-3-319-75605-9_4

Table 1. Proportionality coefficient k_H of the dependences in Fig. 1b, c for their linear approximation case according to (3).

№	H, kA/m	Values k_H	
		with $\gamma \leq 0.25$	with $\gamma \leq 0.035$
1	90	1.968	1.603
2	150	1.579	1.286
3	190	1.506	1.136
4	220	1.119	0.963
5	270	0.964	0.749
6	340	0.771	0.618
7	365	0.806	0.599
8	420	0.619	0.541
9	550	0.522	0.469
10	650	0.497	0.376
11	730	0.459	0.369
12	780	0.453	0.388

distancing of the ferroparticles in the test specimen (when we virtually exclude any mutual magnetic impact), i.e. with relatively small values of the volume fraction γ.

The issue of allowable value of $\gamma = [\gamma]$ (allowable for this calculation of χ) should be admitted as controversial. Thus, alongside with the somewhat standard concept of rigid limitation of γ to $\gamma = [\gamma] = 0.02–0.05 \cong 0.035$ (it was mentioned at researches undertaken by Kondorskiy E.I., Dikanskiy Y.I. and systematized at [4]), there are noteworthy values of the so-called demagnetising factor of the disperse (grain) medium sample [5], that are almost zero with $\gamma \leq 0.2–0.25$. Since this factor can be justly considered as an 'indicator' of magnetic interaction of ferroparticles in the disperse sample, we cannot exclude a possibility of a radically different conceptual assumption of a less rigid limitation of γ: to $\gamma = [\gamma] = 0.2–0.25$.

The most objective data to solve this debatable issue would be the data of direct experiments on γ impact on $\langle\chi\rangle$, at that values $\gamma = [\gamma]$ are assumed to be the criterion value of γ, which restrict the directly proportional relation of $\langle\chi\rangle$ with γ.

Largely, this problem was essentially considered as far back as in papers [4, 6] by systematization the concentration dependences of $\langle\chi\rangle$ for powders and colloids with a disperse phase of the magnetite particles, which are obtained by a Kondorskiy E.I., Bibik E.E., Chekanov V.V., Grebnev S.K. et al. As exemplified by these dependences (for various ranges of γ with the general range of 0.1–0.85 and for selected different values of H at range from 25 to 520 kA/m), these researches [4, 6] demonstrated that those concentration dependences $\langle\chi\rangle$, which cover quite wide ranges of γ (no limited by values up to $\gamma = [\gamma] = 0.25$), are far from being directly proportional. They are approximated by a power function:

$$\langle\chi\rangle \sim \gamma^n \tag{2}$$

with a degree of n = 1.1–1.3. Therefore, they are inapplicable for solution of the given task to define values χ with the use of the explicitly stated relation (1).

At the researches [4, 6] which was made at the range of γ – from γ = 0,065 to γ = 0.2–0.25 (disperse phase is magnetite) dependences $\langle\chi\rangle$ (γ) is near to linear at logarithmic coordinates (Fig. 1a); average value of degree n really equals $n \cong 1.1$ (by the results of processing the data in MS Excel). So, these dependences at this range of γ [4, 6] are near to linear ($n \cong 1$). This could easily be verified by illustration of these dependences at simple (nonlogarithmic) coordinates (Fig. 1b, c).

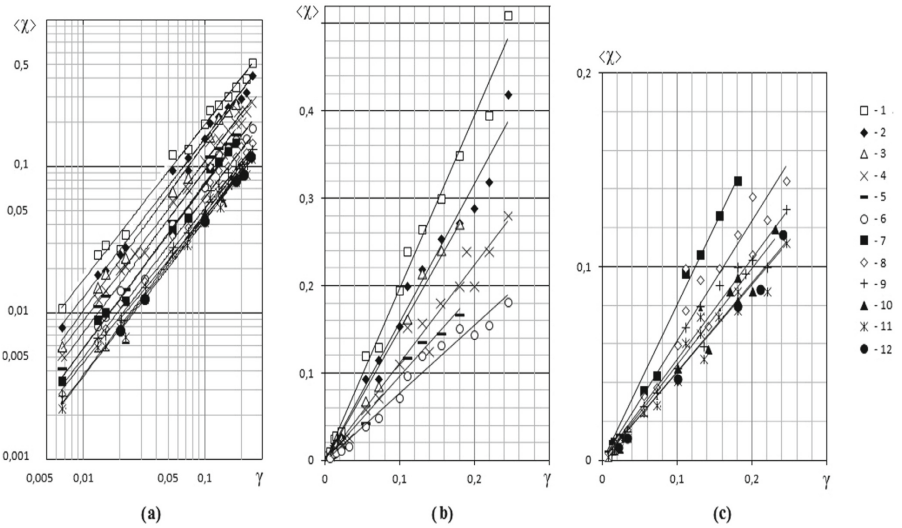

Fig. 1. Magnetic susceptibility of the disperse medium $\langle\chi\rangle$ [4, 6] depending on the γ volume fraction of the disperse phase (magnetite) at various values of field intensity H; 1 – H = 90 kA/m, 2 – 150, 3 – 190, 4 – 220, 5 – 270, 6 – 340, 7 – 365, 8 – 420, 9 – 550, 10 – 650, 11 – 730, 12 – 780; (a) at logarithmic coordinates, (b), (c) – the same at simple (nonlogarithmic) coordinates.

These data point to the possibility of limitation γ-values (in the case using $\langle\chi\rangle$ data for obtaining χ data by (1)) by value $\gamma \leq [\gamma]$ = 0.2–0.25 at least. Corresponding experimental data (for extended range of γ) are essential for detection visible change from linear dependence $\langle\chi\rangle$ (γ) to nonlinear.

2 Detection of «Kink» in a Characteristic Curve $\langle\chi\rangle$ (γ) of Disperse Sample by Experimental Method

Conclusion about possible criterion value of γ ($\gamma = [\gamma]$ = 0.2–0.25) could be proved by special researches (Fig. 2). It is necessary to mix define mass of dispersed phase (magnetite) with milled sand to obtain one or another γ value, taking into account mass of mix, its volume in sample and density of particle's material. Test loose sample is

situated at the tank with near spheric shape (its diameter is 5 mm) between spheric pole pieces at Faraday balance to obtain data of magnetic susceptibility $\langle\chi\rangle$ of sample [7].

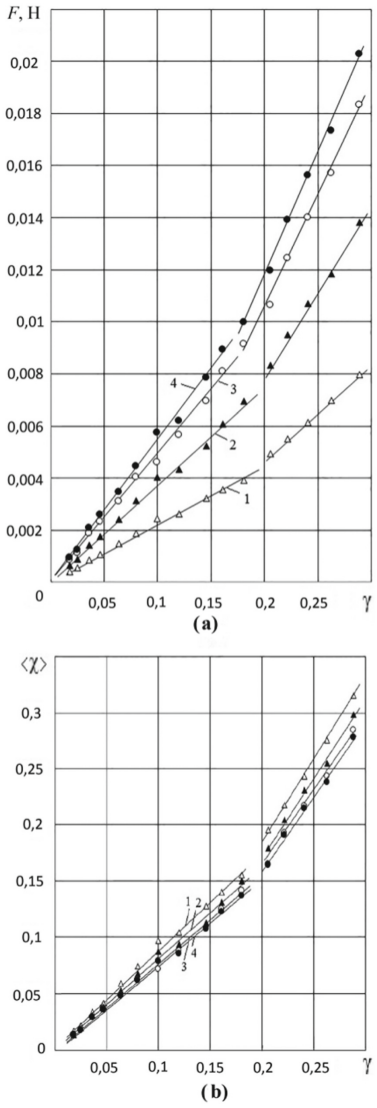

Fig. 2. Influence volume fraction γ of magnetite disperse phase on parameters: (a) ponderomotive force F which acts on spheric sample (at nonuniform magnetic field of Faraday balance); (b) magnetic susceptibility $\langle\chi\rangle$ of the disperse medium; average field intensity H values at sample positioning: 1 – H = 84 kA/m, 2 – 113, 3 – 133, 4 – 141.

Results of measuring a ponderomotive force F and following determination of magnetic susceptibility $\langle\chi\rangle$ of sample are shown in Fig. 2 at the range of magnetite volume fraction up to $\gamma \cong 0.3$ and field intensity H = 84–141 kA/m. It is clear that the linear character of dependences between F (and $\langle\chi\rangle$) and γ at the selected range of H is keeped while $\gamma \cong 0.2$. Estimated by (1) magnetic susceptibility values of test magnetite particles are χ = 0.9–0.8 (by using data $\langle\chi\rangle$ and $\gamma < 0.2$).

Thus, acceptable value of γ could equals $\gamma = [\gamma] = 0.2$ (for estimating χ by (1)). It agrees with the result that is obtained by analysis data [4, 6] on Fig. 1b, c.

Having these results (Fig. 1b, c) detailed analysis of this vast range of dependences $\langle\chi\rangle$ (γ) is interesting for both ranges: obtained extended range of $\gamma \leq 0.2$ and recommended mentioned earlier rather narrowed range of $\gamma \leq 0.02$–0.05.

3 The Analysis of Dependences Between Magnetic Susceptibility and Concentration of Disperse Sample for Extended Acceptable Range of γ

One more confirmation to possibility of using data $\langle\chi\rangle$ (besides Fig. 1b, c) at the range of $\gamma \leq 0.2$–0.25 to obtain χ data by (1) is the artificial linear generalization family of dependences $\langle\chi\rangle(\gamma)$ (Fig. 3). This generalization is made in specially created coordinates and it is a result of the data approximation as a direct proportional relationship (in particular, in MS Excel) by using data of Fig. 1b, c:

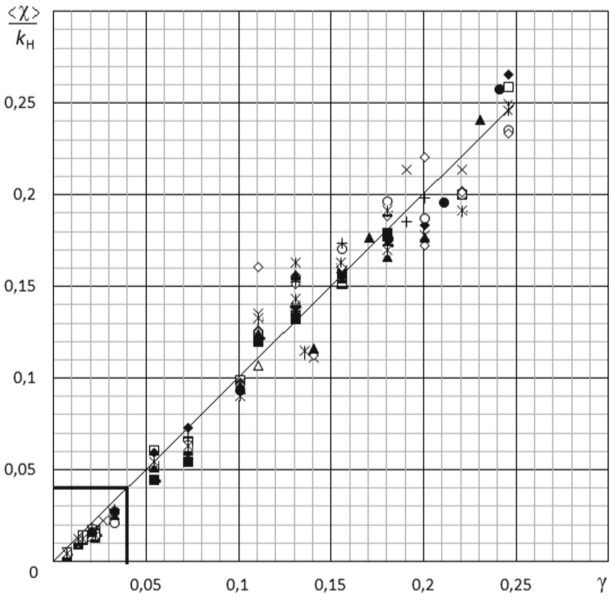

Fig. 3. Generalization of data in Fig. 1b, c for the range $\gamma \leq 0.25$: approximation with the use of coefficient k_H values for $\gamma \leq 0.25$ (Table) correlates to the bisector of the right angle of the chosen coordinates system.

$$\langle\chi\rangle = k_H \times \gamma, \tag{3}$$

then defining particular values (for some dependences with inherent for them field intensity H value) of the proportionality coefficient k_H (Table, $\gamma \leq 0.25$) that enters formula (3); k_H values are necessary for obtaining such parameter (by ordinate in Fig. 3) of generalization as relation $\langle\chi\rangle/k_H$.

As expected, this generalization dependence between $\langle\chi\rangle/k_H$ and γ (Fig. 3) obeys the right angle bisector for the chosen generalization coordinates in the range studied $\gamma = 0.065$–0.25 (Fig. 1b, c). Thus, we can conclude about the eligibility of artificial linearization of dependences of $\langle\chi\rangle$ on γ in the range $\gamma \leq 0.2$–0.25 and, therefore, now the substantiated conclusion on the data $\langle\chi\rangle$ belonging to the range of $\gamma \leq 0.2$–0.25 can really be used for acquiring the calculated data χ by (1).

4 The Analysis of Concentration Dependences of Disperse Sample for a Narrowed Range of γ

A vast data array (Fig. 1b, c) allow to analyse dependences not only for extended acceptable range of γ ($\gamma \leq 0.2$–0.25), but for a narrowed range of γ ($\gamma \leq 0.035$) mentioned earlier. The issue of allowable value range of γ, where dependence $\langle\chi\rangle(\gamma)$ is near to linear, is still controversial.

If we employ the corresponding data of $\langle\chi\rangle$ which belong to the range of γ 0.035 in Fig. 1b, c or in Fig. 3 (limited by heave lines area), then their linear generalization as it was done the one performed before with the use of values k_H (Table, $\gamma \leq 0.25$) – does not yield the desired result. Thus, Fig. 4a clearly illustrates that the approximation of data $\langle\chi\rangle$ (dashed line) does not correlate to the right angle bisector of

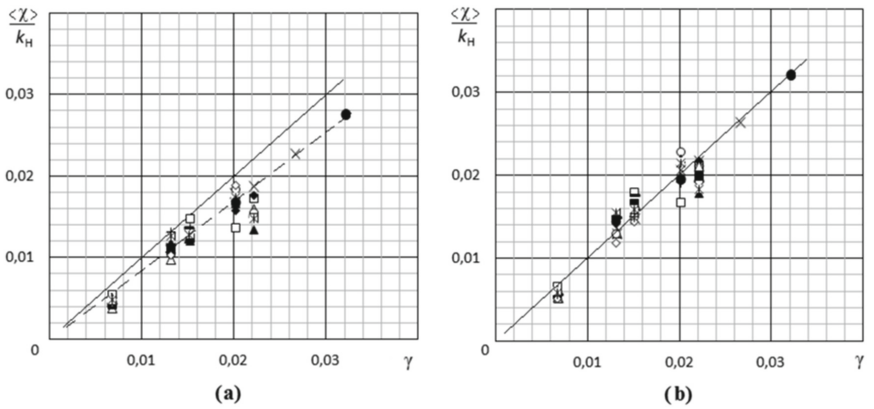

Fig. 4. Generalisation of data in Fig. 1b, c for the range $\gamma \leq 0.035$ (limited by heavy lines area in Fig. 3): approximation with the use of coefficient k_H values (Table 1) for $\gamma \leq 0.25$ (a) - does not correlate to the right angle bisector of the chosen coordinates system; the same for $\gamma \leq 0.035$ (b) correlates to the right angle bisector of the chosen coordinates system.

the chosen system of coordinates (solid line). It means that linear concentration dependences $\langle\chi\rangle$ obtained at $\gamma \leq 0.035$ differ from the same linear dependences of $\langle\chi\rangle$ received at $\gamma \leq 0.25$. Values of the coefficient k_H verify this fact.

Previous values of the proportionality coefficient k_H (Table, $\gamma \leq 0.25$) are not quite applied to the range of $\gamma \leq 0.035$. They are defined separately by the afore-described procedure based on the data of $\langle\chi\rangle$ which belong to this narrowed range of γ. In this case k_H (Table, $\gamma \leq 0.035$) differ from the previous values of coefficient k_H (Table, $\gamma \leq 0.25$) on average by 18%.

The respective generalization of the data $\langle\chi\rangle$ belonging to the narrowed range of γ with the account for the newly acquired values of coefficient k_H are given in Fig. 4b. The approximation of the results of this generalisation corresponds to the bisector of the right angle of the chosen coordinate system.

Thus both variants may be acceptable (for obtaining magnetic susceptibility data χ of ferroparticles by expression (1)): the first – range of $\gamma \leq 0.2$, the second – range of $\gamma \leq 0.02$–0.05 (as more accurate result).

5 Conclusion

It was identified that it is enough having the values of magnetic susceptibility $\langle\chi\rangle$ of disperse sample with ferroparticles to obtain values of magnetic susceptibility χ of its particles (particularly, in solving many scientific-applied tasks of magnetic control or magnetophoresis such particles). It is important that the values of volume fraction (concentration) γ would be low. Question of criterion value of γ (it is still a discussion question) is considered. This value is up to $\gamma = 0.02$–0.05 (this is evaluated data existing for a long time; for the magnetite samples) and even is up to $\gamma = 0.2$–0.25 (circumstantial evidence – by determining a demagnetization factor of disperse samples).

Results of experiments with powder sample at range of volume fraction $\gamma \leq 0.3$ (for disperse phase - magnetite) show that linear part of relation $\langle\chi\rangle$ (γ) ends on $\gamma \cong 0.2$. This value is a criterion value of γ.

It is shown that determined linear dependence between $\langle\chi\rangle$ and γ (γ is up to 0.2) is verified by another generalized array data. However, at lower values of γ ($\gamma \leq 0.02$–0.05) «individual» linear relation between $\langle\chi\rangle$ and γ is noticed. This relation is a bit different from previous (values of proportional coefficients are different from each other at average 18%). This fact means that there is a possibility for obtaining more accurate values of χ.

Acknowledgements. The research is conducted with financial support from RFFI within the frameworks of research project № 16-38-60034 mol_a_dk and from Russian Federation Ministry of Education and Science № 9.9626.2017.

References

1. Sandulyak, A.A., Polismakova, M.N., Ershov, D.V., Sandulyak, A.V., Ershova, V.A., Sandulyak, D.A.: Functional extrapolation of the mass-operational characteristic of magnetophoresis as a basis for a precision method of monitoring ferroparticles. Measur. Tech. **53**(8), 914–918 (2010)
2. Sandulyak, A.A., Sandulyak, A.V., Ershova, V.A., Polismakova, M.N., Sandulyak, D.A.: Use of the magnetic test-filter for magnetic control of ferroimpurities of fuels, oils, and other liquids (phenomenological and physical models). J. Magn. Magn. Mater. **426**, 714–720 (2017)
3. Sandulyak, A.A., Sandulyak, D.A., Ablaeva, A.E., Sandulyak, A.V.: A phenomenological model of experimental and computational control of ferrous impurities in foodstuffs. In: Proceedings of the International Conference on Advances in Environmental and Agricultural Science, Dubai, pp. 135–138 (2015). ISBN 978-1-61804-270-5, ISSN 2227-4359
4. Sandulyak, A.V.: Magnetic and filtration purification of liquids and gases, Chemistry, Moscow, 133 p. (1988)
5. Mattei, J.-L., Le Floc'h, M.: Percolative behaviour and demagnetizing effects in disordered heterostructures. J. Magn. Magn. Mater. **257**, 335–345 (2003)
6. Sandulyak, A.V.: Magnetic susceptibility of particles capable of magnetic deposition. Magn. hydrodyn. **3**, 14–18 (1986)
7. Sandulyak, A.A., Sandulyak, A.V., Polismakova, M.N., Kiselev, D.O., Sandulyak, D.A.: An approach for choosing positioning of small volume sample at instantiation ponderomotive Faraday method in determining its magnetic susceptibility. Russ. Technol. J. **2**, 57–69 (2017)

Simulation of the Inflow to a Well Equipped with a Vertical Slot Filter

Vladimir Astafev(✉) and Vasilina Podyacheva

Samara State Technical University, Molodogvardeyskaya Street, 144,
443100 Samara, Russia
Vladimir.Astafev@mail.ru

Abstract. To ensure the necessary flow rates of wells equipped with an anti-sand filter, it is necessary to evaluate the throughput of the filter. In this paper we are considering one of its most common designs – a vertical-slotted filter. For the case of a single slit periodically repeating over the pipe, an expression for the determination of the skin factor was obtained by V. P. Pilatovsky. In order to identify the best filtering scheme for the arrangement of the slots in the vertical-slit filter, in this work a universal dependence for determining the value of the additional filtering resistance that appears in the bottomhole zone of the well has been considered.

Keywords: Borehole · Filtration · Vertical-slit filter · Skin factor

1 Introduction

At present, the one of the most common complicating factors under extraction of reservoir fluid is the increased content of mechanical impurities in the extracted products. In the event that the source of mechanical impurities is the formation itself, the technical method of preventing an increased content of suspended particles in the extracted production has become widespread [1]. Among the technical methods the most widespread is the installation of different types of filters in the production interval of wells. The essence of the method is based on creating on the path of migration particles a screen-barrier.

To date, the oil industry offers a huge variety of filter designs designed for various conditions of implementation. Among them, the following basic designs of filters can be distinguished [2]: carcass-core (ringed), vertical-slotted, wire and perforated. It is believed that the slot filter is the most versatile design and can be used in installations of any manufacturers, which is its undoubted advantage [3]. But we must not forget about the importance of the wells filters for efficient sand cut-off - this is the filter's throughput for providing the necessary well flow rates.

A study of fluid filtration to a well equipped with a vertical slit filter was carried out by V. P. Pilatovsky, who in his paper [4] gave an expression for the skin factor (the value of the additional filtering resistance that appears in the bottomhole zone of the well due to the presence of a filter element in it). Solution of Pilatovsky was obtained only for the case of a single gap periodically repeating over the tube body. The authors of this work have generalized the method of Pilatovsky to the case of a group

K. Ntalianis and A. Croitoru (Eds.): APSAC 2017, LNEE 489, pp. 33–38, 2019.
https://doi.org/10.1007/978-3-319-75605-9_5

arrangement of gaps, that is, a group of two or more slits, which also repeats periodically. Taking into account the fact that in reality the width of the gap (on average 0.15–3 mm) is much shorter than its length (on average 40–80 mm), even in the case of the chess arrangement of the slots (groups of slits), the inflow problem to a well equipped with such a filter, Can also be solved in a flat setting, since in the central part of the slit the flow will be flat-radial.

2 Statement of the Problem

Consider the process of filtration of a viscous incompressible fluid to a vertical well equipped with a slot filter (Fig. 1).

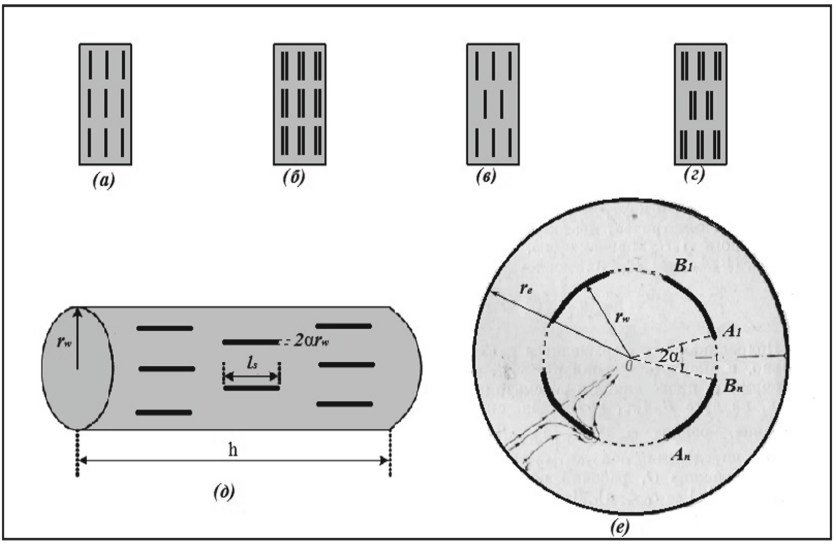

Fig. 1. The scheme of a vertical slit filter (a, c – single arrangement of slits, b, d – group arrangement of slits, i, f – geometric characteristics of the filter)

Taking into account that the height of the vertical slits l_s significantly exceeds its width $2\alpha\, r_w$, the filtration process in the middle plane of the gap will be considered in a plane setting (Fig. 1e). In this case, the potential $\varphi(x, y)$ of the plane-radial filtration of a viscous incompressible fluid in an isotropic homogeneous medium satisfies the equation $\Delta\varphi = 0$. The filtration rate $\boldsymbol{V}(x, y)$ and the pressure $P(x, y)$ are expressed through the potential $\varphi(x, y)$ as $\boldsymbol{V} = grad\varphi$, $P = \mu\varphi/k$, where μ is the fluid viscosity and k is the permeability of fluid reservoir [5–7].

The well itself will be modeled by a point source with a source power Q, and a slot filter - by a circle of radius r_w with permeable (B_nA_1,…) and impermeable (A_1B_1,…) walls. In this case, the boundary conditions for the potential $\varphi(x, y)$ can be written as

$$P|_{r=re} = P_e, 2\pi rhV_r(r,\theta)|_{r\to 0} = Q, V_r|_{A1B1,\ldots} = 0 \quad (1)$$

were, h is the oil-saturated thickness, and n is the number of rows of slits along the vertical axis.

3 The Case of a Single Arrangement of Slits

To solve the problem described by Eq. (1), it is convenient to use the complex variables $z = x+iy = re^{i\theta}$. In this case, the complex-conjugate velocity $V_x - iV_y = (V_r - iV_\theta)\, e^{-i\theta}$ is expressed in terms of the complex potential $W(z) = \varphi(x,y) + i\psi(x,y)$ as

$$V_x - iV_y = dW/dz \quad (2)$$

In the case, when n slits with a solution angle 2α in the slot filter are placed evenly (Fig. 1e), the centers of the slits will be located at the points $z_k = r_w exp(ik\theta_n)$, where $k = 0,1,2,\ldots, n-1$, $x_n = 2\pi/n$, and the angle θ for the k-th slot will change in the range $-\alpha + k\theta_n < \theta < \alpha + k\theta_n$. In this case the complex potential $W(z)$ can be written in the following form [4]:

$$dW/dz = (A/z)(z^n + r_w^n)/\sqrt{(z^n - z_0^n)(z^n - \bar{z}_0^n)}, \quad (3)$$

where $z_0 = r_w exp(i\theta)$.

Boundary values at the points $z = r_w exp(i\theta)$, located on a circle of radius r_w, will be:

$$V_r - iV_\theta = (A\sqrt{2}/a)\cos(n\theta/2)/\sqrt{\cos n\theta - \cos n\alpha}. \quad (4)$$

This means that for filter points that fall on the line of slits, (that is $\alpha + k\theta_n < \theta < \alpha + k\theta_n$, $k = 0,1,\ldots, n-1$), the value of $cos(n\theta) - cos(n\alpha)$ will be positive, and for points falling on the line of the impermeable filter wall, ($\alpha + k\theta_n < \theta < -\alpha + (k+1)\theta_n$, $k = 0,1,\ldots, n-1$), this value will be negative.

Therefore $V_r - iV_\theta$ on the slit line will be real, and on the line of the impermeable filter wall - imaginary. In other words, $V_r \neq 0$, $V_\theta = 0$ on the slits, and $V_r = 0$, $V_\theta \neq 0$ on the impermeable wall.

For large distance from the filter (when $|z| \gg a$) we can write $dW/dz \simeq A/z$. On the other hand, the case $|z| \gg a$ corresponds to the motion of an incompressible fluid unperturbed by the filter, for which $dW/dz = -Q/2\pi hz$, where Q is the flow rate of the fluid, h is the thickness of the formation, that is, $A = -Q/2\pi h$.

To satisfy the remaining boundary conditions, we write the potential $W(z)$ as

$$W(z) = Aln(z/r_w) + B + AF(z) \quad (5)$$

where $F(z) = \int_{r_w}^{z} \left((\xi^n + r_w^n)/\sqrt{(\xi^n - z_0^n)(\xi^n - \bar{z}_0^n)} - 1\right) d\xi/\xi$

Since the pressure at any point is expressed as $P(z) = -(\mu/k)ReW(z)$, the pressure P_e on the line $z_e = r_e exp(i\theta)$ will be $P_e = -(\mu/k)Re\{Aln(r_e exp(i\theta)) + B + A\Phi(z_e)\}$.

Hence, the pressure distribution in the reservoir can be written in the following form:

$$P(z) = P_e + (Q\mu/2\pi kh)[\ln(z/r_e) + \mathrm{Re}\{F(z) - F(\infty)\}] \tag{6}$$

As follows from (6), the pressure at the points of the gap does not change and is equal to the pressure in the well P_w. As a result, we obtain

$$Q = 2\pi khP_e/\mu - P_w/(\ln(r_e/a) + \mathrm{Re}F(\infty)) \tag{7}$$

Formula (7) is the Dupuy formula for a well with a filtration current deviating from the radial flow due to the presence of a slot filter. The magnitude of the deviation is the perforation skin factor of the well, that is:

$$S = \mathrm{Re}F(\infty) = (1/n)\int_0^\infty \left((e^x + 1)/\sqrt{e^{2x} - 2e^x\cos(n\alpha) + 1} - 1\right)dx \tag{8}$$

The value of the perforating skin factor S can be expressed in the following form [4, 8]:

$$S = \mathrm{Re}F(\infty) - (2/n)\ln\,\sin(n\alpha/2) \tag{9}$$

4 The Case of a Group Arrangement of Slits

Let us generalize the solution obtained for the case of a single periodically recurring slit to the case of a group of several slots periodically repeating along the surface of the casing. An example of such a slit element is shown on Fig. 2 (a group of three slots, three times repeated along the surface of the tube).

Similarly to Eq. (3), in this case the complex potential *W(z)* can be written in the following form:

$$dW/dz = (A/z)(z^{3n} + r_w^{3n})/\sqrt{(z^n - z_1^n)(z^n - \bar{z}_1^n)(z^n - z_2^n)(z^n - \bar{z}_2^n)(z^n - z_3^n)(z^n - \bar{z}_3^n)} \tag{10}$$

where $z_1 = r_w\,exp(i\alpha_1)$, $z_2 = r_w\,exp(i\alpha_2)$, $z_3 = r_w\,exp(i\alpha_3)$.

Consequently, for the potential *W(z)* written in the form (11), the quantity $V_r - iV_\theta$ will be real on the line of slits and imaginary on the line of an impenetrable wall.

For the case of a group arrangement of slits the value of the perforating skin factor S can be expressed in the following form

$$S = 2/n\int_0^\infty \left((t^2 + 1/4)/\sqrt{(t^2 + k_1^2)(t^2 + k_2^2)(t^2 + k_3^2)} - 1/\sqrt{1 + t^2}\right)dt \tag{12}$$

where $k_1 = sin(n\alpha_1/2)$, $k_2 = sin(n\alpha_2/2)$, $k_3 = sin(n\alpha_3/2)$.

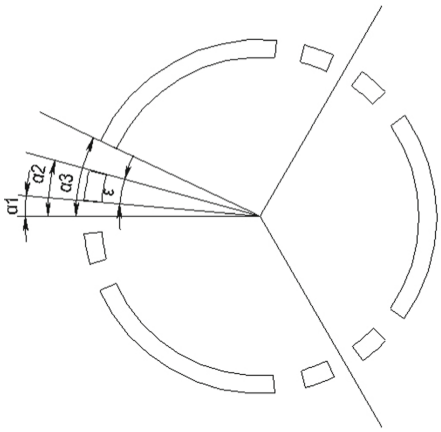

Fig. 2. A group of three slots, three times repeated along the surface of the pipe.

As in the case of a single arrangement of slits, the potential *W(z)* for a group arrangement of slits has the same expression $W(z) = Aln(z/r_w) + B+AF(z)$, where

$$F(z) = \int_{r_w}^{z} \left(\frac{(\xi^{3n} + r_w^{3n})/}{\sqrt{(\xi^n - z_1^n)(\xi^n - \bar{z}_1^n)(\xi^n - z_2^n)(\xi^n - \bar{z}_2^n)(\xi^n - z_3^n)(\xi^n - \bar{z}_3^n)} - 1} \right) d\xi/\xi \tag{13}$$

5 Conclusion

The problem posed before the authors about the derivation of the dependencies describing the inflow to the slot filter, periodically repeating holes in which can be located both singly and in groups of slots, was successfully performed.

The correctness of the obtained dependence is confirmed by a comparison of the results on the calculation of the skin factor with the results obtained by the method described in the work of V. P. Pilatovsky for the case of a single slit periodically recur through the body of a pipe.

References

1. Kamaletdinov, R.S., Lazarev, A.B.: Review of existing methods of combating mechanical impurities. Eng. Pract. **2**, 6–13 (2010)
2. Petukhov, A.A.: Mathematical models of fluid flows to borehole filters. North-Caucasian State Technical University, Stavropol, Russia. Thesis for degree by Candidate of Physical and Mathematical Sciences (2006)

3. Khuzhin, M.R.: Improving the efficiency of wells of a complicated fund (on the example of Western Siberia deposits). Institute for Transport of Energy Resources, Ufa, Russia Thesis for scientific degree by Candidate of Technical Sciences (2015)
4. Pilatovsky, V.P.: Fundamentals of Thin Layer Hydromechanics. Nedra, Moscow (1966)
5. Barenblatt, G.I., Entov, V.M., Rygyk, V.M.: Movement of Liquids and Gases in Natural Formations. Nedra, Moscow (1984)
6. Basniev, K.S., Kochin, I.N., Maksimov, V.M.: Underground Hydromechanics. Nedra, Moscow (1993)
7. Basniev, K.S., Dmitriev, N.M., Rosenberg, G.D.: Oil and Gas Hydromechanics. Institute for Computer Research, Moscow-Izhevsk (2005)
8. Furui, K.A.: Comprehensive Skin Factor Model for Well Completions Based on Finite Element Simulations. The university of Texas. Austin. Thesis of the requirements for the degree of Ph.D. (2004)

Errors of Approximation with Polynomial Splines of the Fifth Order

I. G. Burova(✉) and A. G. Doronina

St. Petersburg State University,
7/9 Universitetskaya nab., St. Petersburg 199034, Russia
i.g.burova@spbu.ru

Abstract. This paper is a continuation of a series of papers devoted to the construction and investigation of the properties of integro-differential polynomial splines of the fifth order. It is supposed that values of function in grid nodes and values of integrals over intervals are known. Solving the system of linear algebraic equations, we find basic splines. An approximation of the function in this paper is constructed on every grid interval separately using values of the function in two adjacent grid nodes and the values of three integrals over intervals, and basic splines.

We call this approximation an integro-differential spline and we call these basic splines integro-differential basic splines. The properties of interpolation with integro-differential polynomial basic splines are investigated. A comparison of the properties of integro-differential approximations for a different choice of integrals is presented. A comparison of the integro-differential approximation with approximation using polynomial splines of the Lagrangian type is made. Numerical examples are presented.

Keywords: Integro-differential splines · Approximation

1 Introduction

A variety of splines with different properties are used in calculations in many engineering projects [1, 3]. Among them are analysis-suitable T-splines of arbitrary degree, which are useful for modeling cracks in plane problems, and for the solution of boundary-value problems, cubic, bicubic and biquadratic B-splines, trigonometric, orthogonal splines. These splines are applied to the construction of curves and surfaces, to the designing of ship hulls, to the transformation of a sound signal's frequency and to many others [1–13].

This paper is a continuation of the series of papers devoted to the construction and investigation of the properties of integro-differential polynomial splines of the fifth order [7, 14, 15]. In this paper we discuss the construction of polynomial splines which use three integrals over subintervals in addition to the values of the function in the nodes. As in previous papers, we construct the approximation separately for each subinterval. As usual, local spline approximation uses values of the approximated function and, sometimes, values of its derivatives.

K. Ntalianis and A. Croitoru (Eds.): APSAC 2017, LNEE 489, pp. 39–46, 2019.
https://doi.org/10.1007/978-3-319-75605-9_6

2 Approximation of the Function

Suppose that *n, m* are natural numbers, while *a, b, c, d, h* are real numbers, *h = (b-a)/n*. Let the function $u(x)$ be such that $u \in C^5[a-3h, b]$. We have the grid of interpolation nodes x_i such that $x_{-k} = a - kh, k = 3, 2, 1, x_0 = a, x_{i+1} = x_i + h, i = 0, \ldots, n, x_n = b$.

Suppose that $u(x_i), i = 0, 1, \ldots, n$ and $\int_{x_{i-1}}^{x_i} u(\xi)d\xi, \int_{x_{i-2}}^{x_i} u(\xi)d\xi, \int_{x_{i-3}}^{x_i} u(\xi)d\xi, i = 0, \ldots, n$ are known. We denote $\tilde{\tilde{u}}(x)$ as an approximation of function *u(x)* in interval $[x_i, x_{i+1}] \subset [a, b]$:

$$\tilde{\tilde{u}}(x) = u(x_i)w_i(x) + u(x_{i+1})w_{i+1}(x) + \int_{x_{i-1}}^{x_i} u(\xi)d\xi w_i^{<-1,0>}(x) + \int_{x_{i-2}}^{x_i} u(\xi)d\xi\, w_i^{<-2,0>}(x) + \int_{x_{i-3}}^{x_i} u(\xi)d\xi\, w_i^{<-3,0>}(x).$$

We obtain basic splines $w_i(x)$, $w_{i+1}(x)$, $w_i^{<-1,0>}(x), w_i^{<-2,0>}(x), w_i^{<-3,0>}(x)$ from system: $\tilde{\tilde{u}}(x) \equiv u(x), \quad u(x) = x^{i-1}, \quad i = 1, 2, 3, 4, 5$.

If $x = x_i + th, \quad t \in [0, 1]$, then the basic splines can be written in the form:

$$w_i(x_i + th) = \frac{(1-t)(125t^3 + 577t^2 + 736t + 222)}{222}, w_{i+1}(x_i + th) = \frac{t(12 + 33t + 24t^2 + 5t^3)}{74},$$

$$w_i^{<-1,0>}(x_i + th) = \frac{t(t-1)(155t^2 + 603t + 516)}{148h}, w_i^{<-2,0>}(x_i + th) = \frac{t(1-t)(55t^2 + 171t + 90)}{148h},$$

$$w_i^{<-3,0>}(x_i + th) = \frac{t(t-1)(85t^2 + 197t + 92)}{1332h}.$$

We can also construct the approximation in this form:

$$V(x) = u(x_i)\omega_i(x) + u(x_{i+1})\omega_{i+1}(x) + \int_{x_{i-1}}^{x_i} u(\xi)d\xi\, \omega_i^{<-1,0>}(x) + \int_{x_{i-2}}^{x_{i-1}} u(\xi)d\xi\, \omega_i^{<-2,-1>}(x) + \int_{x_{i-3}}^{x_{i-2}} u(\xi)d\xi\, \omega_i^{<-3,-2>}(x), x \in [x_i, x_{i+1}]. \quad (1)$$

We obtain basic splines $\omega_{i,0}(x)$, $\omega_{i+1,0}(x), \omega_i^{<s,s+1>}(x), s = -1, -2, -3$, from the system:

$$V(x) = u(x), \quad u(x) = x^{j-1}, \quad i = 1, 2, 3, 4, 5. \quad (2)$$

If $x = x_i + th, \quad t \in [0,1]$, then the basic splines can be written in the following form:

$$\omega_i(x_i + th) = \frac{(1-t)(125t^3 + 577t^2 + 736t + 222)}{222},$$
$$\omega_{i+1}(x_i + th) = \frac{t(12 + 33t + 24t^2 + 5t^3)}{74},$$

$$\omega_i^{<-1,0>}(x_i + th) = \frac{t(t-1)(985t^2 + 4085t + 3926)}{1332h},$$
$$\omega_i^{<-2,-1>}(x_i + th) = -\frac{t(t-1)(205t^2 + 671t + 359)}{666h},$$

$$\omega_i^{<-3,-2>}(x_i + th) = \frac{t(t-1)(85t^2 + 197t + 92)}{1332h}.$$

Our aim is to determine if $V(x) = \tilde{\tilde{u}}(x)$.

Lemma 1. Let function $u \in C^5[a - 3h, b]$. The next statement is valid:

$$V(x) = \tilde{\tilde{u}}(x), \quad x \in [x_i, x_{i+1}], \quad i = 0, 1, \ldots, n-1.$$

Proof. It can be shown that the next relations are valid:

$$I_1 = w_i^{<-1,0>}(x_i + th) + w_i^{<-2,0>}(x_i + th) + w_i^{<-3,0>}(x_i + th) = \omega_i^{<-1,0>}(x_i + th),$$

$$I_2 = w_i^{<-2,0>}(x_i + th) + w_i^{<-3,0>}(x_i + th) = \omega_i^{<-2,-1>}(x_i + th),$$

$$I_3 = w_i^{<-3,0>}(x_i + th) = \omega_i^{<-3,-2>}(x_i + th).$$

Therefore, we obtain:

$$\tilde{\tilde{u}}(x_i + th) = u(x_i)\omega_{i,0}(x) + u(x_{i+1})\omega_{i+1,0}(x) + \int_{x_{i-1}}^{x_i} u(\xi)d\xi\, I_1 + \int_{x_{i-2}}^{x_{i-1}} u(\xi)d\xi\, I_2$$
$$+ \int_{x_{i-3}}^{x_{i-2}} u(\xi)d\xi\, I_3 = u(x_i)\omega_{i,0}(x) + u(x_{i+1})\omega_{i+1,0}(x) + \int_{x_{i-1}}^{x_i} u(\xi)d\xi\, \omega_i^{<-1,0>}(x_i + th)$$
$$+ \int_{x_{i-2}}^{x_{i-1}} u(\xi)d\xi\, \omega_j^{<-2,-1>}(x_j + th) + \int_{x_{i-3}}^{x_{i-2}} u(\xi)d\xi\, \omega_i^{<-3,-2>}(x_i + th) = V(x_i + th).$$

The proof is complete.

Lemma 2. Let the function be such that $u \in C^5[a-3h, b]$. The next statements are valid:

$$(1)\quad V(x_i) = u(x_i), \quad (2)\quad V(x_{i+1}) = u(x_{i+1}), \quad (3)\quad \int\limits_{x_{i-1}}^{x_i} V(x)dx = \int\limits_{x_{i-1}}^{x_i} u(x)dx,$$

$$(4)\quad \int\limits_{x_{i-2}}^{x_{i-1}} V(x)dx = \int\limits_{x_{i-2}}^{x_{i-1}} u(x)dx, \quad (5)\quad \int\limits_{x_{i-3}}^{x_{i-2}} V(x)dx = \int\limits_{x_{i-3}}^{x_{i-2}} u(x)dx.$$

Proof. Firstly, let us notice that statements (1)–(2) follow from the next relations:

$$\omega_i(x_i) = 1, \omega_i(x_{i+1}) = 0, \omega_{i+1}(x_i) = 0, \omega_{i+1}(x_{i+1}) = 1, \omega_i^{<-1,0>}(x_i) = 0,$$

$$\omega_i^{<-1,0>}(x_{i+1}) = 0, \omega_i^{<-2,-1>}(x_i) = 0, \omega_i^{<-2,-1>}(x_{i+1}) = 0, \omega_i^{<-3,-2>}(x_i) = 0,$$

$$\omega_i^{<-3,-2>}(x_{i+1}) = 0.$$

Similarly, statements (3)–(5) follow from the next relations:

$$\int_{x_{i-1}}^{x_i} \omega_i(x)dx = 0, \int_{x_{i-1}}^{x_i} \omega_{i+1,0}(x)dx = 0, \int_{x_{i-1}}^{x_i} \omega_i^{<-1,0>}(x)dx = 1, \int_{x_{i-1}}^{x_i} \omega_i^{<-2,-1>}(x)dx = 0,$$

$$\int_{x_{i-1}}^{x_i} \omega_i^{<-3,-2>}(x)dx = 0.$$

$$\int_{x_{i-2}}^{x_{i-1}} \omega_i(x)dx = 0, \int_{x_{i-2}}^{x_{i-1}} \omega_{i+1,0}(x)dx = 0, \int_{x_{i-2}}^{x_{i-1}} \omega_i^{<-1,0>}(x)dx = 0,$$
$$\int_{x_{i-2}}^{x_{i-1}} \omega_i^{<-2,-1>}(x)dx = 1,$$

$$\int_{x_{i-2}}^{x_{i-1}} \omega_i^{<-3,-2>}(x)dx = 0, \int_{x_{i-3}}^{x_{i-2}} \omega_i(x)dx = 0, \int_{x_{i-3}}^{x_{i-2}} \omega_{i+1,0}(x)dx = 0,$$
$$\int\limits_{x_{i-3}}^{x_{i-2}} \omega_i^{<-1,0>}(x)dx = 0,$$

$$\int\limits_{x_{i-3}}^{x_{i-2}} \omega_i^{<-2,-1>}(x)dx = 0, \int\limits_{x_{i-3}}^{x_{i-2}} \omega_i^{<-3,-2>}(x)dx = 1.$$

The proof is complete.

Now we can find the points $\zeta_1, \zeta_2, \zeta_3$ such that

$$u(\zeta_1)h = \int_{x_{i-1}}^{x_i} u(\xi)d\xi, \zeta_1 \epsilon [x_{i-1}, x_i], u(\zeta_2)h = \int_{x_{i-2}}^{x_{i-1}} u(\xi)d\xi, \zeta_2 \epsilon [x_{i-2}, x_{i-1}],$$

$$u(\zeta_3)h = \int_{i-3}^{x_{i-2}} u(\xi)d\xi, \zeta_3 \epsilon [x_{i-3}, x_{i-2}].$$

We can construct approximation $\tilde{u}(x)$, $x \in [x_j, x_{j+1}]$, in the form:

$$\tilde{u}(x) = u(x_j)\omega_{j,0}(x) + u(x_{j+1})\omega_{j+1,0}(x) + u(\zeta_1)h\omega_j^{\langle -1,0\rangle}(x) + u(\zeta_2)h\omega_j^{\langle -2,-1\rangle}(x) + u(\zeta_3)h\omega_j^{\langle -3,-2\rangle}(x).$$

The interpolation of the Lagrange type with nodes $\zeta_1, \zeta_2, \zeta_3, \zeta_4 = x_j, \zeta_5 = x_{j+1}$, has the form

$$\tilde{U}(x) = \sum_{i=1}^{5} u(\zeta_i)W(x)/((x - \zeta_i)W'(\zeta_i)), x \in [x_j, x_{j+1}], \tag{3}$$

where $W(x) = (x - \zeta_1)(x - \zeta_2)(x - \zeta_3)(x - \zeta_4)(x - \zeta_5)$.

The remainder term of the Lagrange interpolation (3) is as follows:

$$U^{(5)}(\eta)(x - x_j)(x - x_{j+1})(x - \zeta_1)(x - \zeta_2)(x - \zeta_3)/5!, \eta \epsilon [x_{j-3}, x_{j+1}].$$

Table 1 shows actual errors of approximation of functions constructed with formula (1) and theoretical errors of approximation of functions constructed with formula (3) when $[a, b] = [-1, 1], h = 0.1$. Calculations were done in Maple with Digits = 15.

Table 1. Actual errors $max_{t\in[0,1]}|V - u|$ constructed with formula (1) and theoretical errors of approximation (3)

u(x)	Actual errors	Theoretical errors
$\sin(3x)\cos(5x)$	$0.26 \cdot 10^{-2}$	$0.139 \cdot 10^{-1}$
$x^5/5!$	$0.18 \cdot 10^{-6}$	$0.85 \cdot 10^{-6}$
$1/(1 + 25x^2)$	$0.25 \cdot 10^{-1}$	0.27

3 Comparison with Lagrange Type Splines

Suppose we know the values of function $u \in C^5[a - 3h, b]$ in the points x_i. We consider the interpolation with Lagrange type splines

$$W(x) = u(x_j)\omega_j(x) + u(x_{j+1})\omega_{j+1}(x) + u(x_{j-1})\omega_{j-1}(x) + u(x_{j-2})\omega_{j-2}(x) + u(x_{j-3})\omega_{j-3}(x), x \in [x_j, x_{j+1}] \tag{4}$$

It can be found that $\omega_{j+1}(x) = (x-x_j)(x-x_{j-1})(x-x_{j-2})(x-x_{j-3})/Z_{j+1}$,

$$Z_{j+1} = (x_{j+1}-x_j)(x_{j+1}-x_{j-1})(x_{j-1}-x_{j-2})(x_{j+1}-x_{j-3}),$$

$$\omega_j(x) = (x-x_{j+1})(x-x_{j-1})(x-x_{j-2})(x-x_{j-3})/Z_j,$$

$$Z_j = (x_j-x_{j+1})(x_j-x_{j-1})(x_j-x_{j-2})(x_j-x_{j-3}),$$

$$\omega_{j-1}(x) = (x-x_{j+1})(x-x_j)(x-x_{j-2})(x-x_{j-3})/Z_{j-1},$$

$$Z_{j-1} = (x_{j-1}-x_{j+1})(x_{j-1}-x_j)(x_{j+1}-x_{j-2})(x_{j+1}-x_{j-3}),$$

$$\omega_{j-2}(x) = (x-x_{j+1})(x-x_j)(x-x_{j-1})(x-x_{j-3})/Z_{j-2},$$

$$Z_{j-2} = (x_{j-2}-x_{j+1})(x_{j-2}-x_j)(x_{j-2}-x_{j-1})(x_{j-2}-x_{j-3}),$$

$$\omega_{j-3}(x) = (x-x_{j+1})(x-x_j)(x-x_{j-1})(x-x_{j-2})/Z_{j-3},$$

$$Z_{j-3} = (x_{j-3}-x_{j+1})(x_{j-3}-x_j)(x_{j-3}-x_{j-1})(x_{j-3}-x_{j-2}).$$

Lemma 3. Suppose $u \in C^5[a-3h, b]$. There is a point $\eta \in [x_{j-3}, x_{j+1}]$, such that

$$u(x) - W(x) = \frac{u^{(5)}(\eta)}{5!} (x-x_j)(x-x_{j+1})(x-x_{j-1})(x-x_{j-2})(x-x_{j-3}), x \in [x_j, x_{j+1}].$$

Proof. The points x_{j-i}, $i = -1, 0, 1, 2, 3$ are the points of interpolation. Using the formula of the remainder term of Lagrange interpolation we obtain the formula.

Corollary. If $M = \max\limits_{x\in[a-3h,b]} |u^{(5)}(x)|$ and we put $x = x_j + th, \quad t \in [0,1]$, then

$$|W(x_j+th) - u(x_j+th)| \le 3.63Mh^5/5!$$

Proof. Obviously,

$$|W(x_j+th) - u(x_j+th)| \le Mh^5|t(t-1)(t+1)(t+2)(t+3)|/5!$$

It can be obtained, that
$max_{t\in[0,1]}|t(t-1)(t+1)(t+2)(t+3)| = 3.63$,
when $t \approx 0.6444$.
The proof is complete.

Table 2 shows actual and theoretical errors of approximation of functions constructed with formula (4) when $[a,b] = [-1,1], \quad h = 0.1$. Calculations were done in Maple with *Digits* = 15.

Table 2. Actual and theoretical errors $max_{t\in[0,1]}|V-u|$ of approximation constructed with formula (4)

$u(x)$	Actual errors	Theoretical errors
$\sin(3x)\cos(5x)$	$0.45 \cdot 10^{-2}$	$0.139 \cdot 10^{-1}$
$x^5/5!$	$0.30259 \cdot 10^{-6}$	$0.30262 \cdot 10^{-6}$
$1/(1+25x^2)$	$0.34 \cdot 10^{-1}$	$0.95 \cdot 10^{-1}$

4 Conclusion

Here we investigated approximation using the values of integrals of the function over the subintervals immediately to the left of this subinterval. If the values of the integral of the function are unknown, we will use quadrature formulae with the fifth order of approximation.

References

1. Casquero, H., Liu, L., Zhang, Y., Reali, A., Gomez, H.: Isogeometric collocation using analysis-suitable T-splines of arbitrary degree. Comput. Methods Appl. Mech. Eng. **301**, 164–186 (2016)
2. Doganalp, S., Selvi, H.Z.: Local geoid determination in strip area projects by using polynomials, least-squares collocation and radial basis functions. Meas. J. Int. Meas. Confederation **73**, 429–438 (2015)
3. Habib, S.H., Belaidi, I.: Extended isogeometric analysis using analysis-suitable T-splines for plane crack problems. Mechanika **23**(1), 11–17 (2017)
4. Jahangiry, H.A., Tavakkoli, S.M.: An isogeometrical approach to structural level set topology optimization. Comput. Methods Appl. Mech. Eng. **319**, 240–257 (2017)
5. Abbas, M., Majid, A.A., Awang, M.N.H., Ali, J.: Shape-preserving rational bi-cubic spline for monotone surface data. WSEAS Trans. Math. **11**(7), 644–657 (2012)
6. Abdul Karim, S.A., Mohd Rosli, M.A., Mohd Mustafa, M.I.: Cubic spline interpolation for petroleum engineering data. Appl. Math. Sci. **8**(102), 5083–5098 (2014)
7. Burova, I.: On integro-differential splines construction, advances in applied and pure mathematics. In: Proceedings of the 7th International Conference on Finite Differences, Finite Elements, Finite Volumes, Boundary Elements (F-and-B 2014), Gdansk, Poland, 15–17 May, pp. 57–61 (2014)
8. Saini, S., Mishra, H.K.: A new quartic B-spline method for third-order self-adjoint singularly perturbed boundary value problems. Appl. Math. Sci. **9**(8), 399–408 (2015)
9. Sarfraz, M.: Generating outlines of generic shapes by mining feature points. WSEAS Trans. Syst. **13**, 584–595 (2014)
10. Sarfraz, M., Al-Dabbous, N.: Curve representation for outlines of planar images using multilevel coordinate search. WSEAS Trans. Comput. **12**(2), 62–73 (2013)
11. Skala, V.: Fast interpolation and approximation of scattered multidimensional and dynamic data using radial basis functions. WSEAS Trans. Math. **12**(5), 501–511 (2013)
12. Zamani, M.: A new, robust and applied model for approximation of huge data. WSEAS Trans. Math. **12**(6), 727–735 (2013)

13. Zhuang, X., Mastorakis, N.E.: A model of virtual carrier immigration in digital images for region segmentation. WSEAS Trans. Comput. **14**, 708–718 (2015)
14. Burova, I.G., Doronina, A.G.: On approximations by polynomial and nonpolynomial integro-differential splines. Appl. Math. Sci. **10**(13–16), 735–745 (2016)
15. Burova, I.G., Poluyanov, S.V.: On approximations by polynomial and trigonometrical integro- differential splines. Int. J. Math. Models Methods Appl. Sci. **10**, 190–199 (2016)

Type of Substance as a New Physical Quantity

Milan Perkovac[1(✉)], Stipe Kutleša[2], Josip Zdenković[3], and Branko Balon[4]

[1] University of Applied Sciences, Vrbik 8, 10000 Zagreb, Croatia
milan@drivesc.com
[2] Institute of Philosophy, Ulica grada Vukovara 54, 10000 Zagreb, Croatia
stipekutlesal@gmail.com
[3] Schrack Technik d.o.o., Zavrtnica 17, 10000 Zagreb, Croatia
josip.zdenkovic@schrack.hr
[4] First Technical School TESLA, Klaićeva 7, 10000 Zagreb, Croatia
branko.balon@gmail.com

Abstract. The International System of Units (SI) is founded on 7 SI base units (meter, kilogram, second, ampere, kelvin, mole, candela) for 7 base quantities (length, mass, time, electric current, thermodynamic temperature, amount of substance, luminous intensity) assumed to be mutually independent. There is a need for a new quantity that describes the quality or type of the substance. The processing and introduction of this quantity is investigated. The method of the maximum possible atomic number of elements in *Mendeleev's Periodic Table* was used. Here is a proposal of the 8th base quantity called *type of substance* and its unit boscovich, B. This quantity cannot be derived from 7 existing quantities and therefore should be introduced as a separate new one. It is also explained why the unit boscovich for type of substance is suggested.

Keywords: Boscovich · Quantity · SI units · Soddy · Structural constant

1 Introduction

A quantity is a physical property of a phenomenon, body, or substance that can be quantified by measurement. Some quantities are obvious, clearly defined, highly needed and widely used in everyday life; for example, length, mass, time, thermodynamic temperature. Some other quantities are not so frequent; for example, electric current, amount of substance, or luminous intensity. There is a need for some quantities, but they have not been established; for example, for smell, for taste or for flair. It has been noted that there are other quantities that are not included in the existing base quantities. These new quantities can become useful in life or science in the future. One of them is represented in this article called the *type of substance*, with new unit (boscovich, B). The *measurement* is a method for determining *quantity*, *capacity*, or *dimension*.

M. Perkovac—Author's discovery of structural constant s_0 allowed the creation of this article. Namely, the structural constant $s_0 = 8.278\ 692\ 517$ led to the knowledge of the *maximum atomic number*, $Z_{max} = 2\ s_0^2 = 137.073\ 4996$, [1] and Eq. (42) in [2]. This is the basis for recognizing existence and determining the capacity of quantity which we have called the *type of substance*.

K. Ntalianis and A. Croitoru (Eds.): APSAC 2017, LNEE 489, pp. 47–55, 2019.
https://doi.org/10.1007/978-3-319-75605-9_7

All systems of measurement use *units* whose amounts have been arbitrarily set and agreed upon by a group of people. The steps needed to introduce the new quantity and unit will be processed here.

2 The Substance; Properties, Capacity, Dimension and Unit

2.1 The Form of Description of Physical Properties of the Substance

Let's focus here on the physical properties of the substance. The substance is the real physical matter of which a person or thing consists. The substance here means:

(1) A vacuum (a space empty of matter, which has no substance),
(2) A particle (electron, proton, neutron),
(3) An element (a basic substance that can't be simplified; hydrogen, oxygen, etc.),
(4) An atom (the smallest unit of an element, having all the characteristics of that element and consisting of a very small and dense central nucleus containing protons and neutrons, surrounded by one or more shells of orbiting electrons; atoms remain undivided in chemical reactions except for the donation, acceptance, or exchange of valence electrons),
(5) A nuclide (which may be isotopic nuclides, with the same atomic number *Z*, isobaric nuclides, with the same mass number *M* or isotonic nuclides, with the same difference between the mass number and the atomic number, *M-Z*),
(6) A molecule (which has no more properties of its constituent atomic parts),
(7) A compound (a molecule that contains more than one element), and
(8) An ion (it is an element, atom, nuclide, molecule or compound, in which the total number of electrons is not equal to the total number of protons, giving the element, atom or molecule a net positive or negative electrical charge).

So we determined the quantity called the *Type of substance*, and marked it with *S*, in honor to English radiochemist Frederick Soddy (1877–1956), discoverer of isotopic nuclides.

The physical properties of this quantity are described by means of three parts. The first part, a *proton part*, contains the number of protons in the nucleus (*Z*, or p). In the second part, a *neutron part*, there is the number of neutrons in the nucleus (n). The third part, a *part belonging to electrons*, contains the number of electrons in the atomic shell (e).

2.2 Capacity of the Quantity the *Type of Substance*

To determine the capacity of the quantity (it is to determine the largest amount or number that can be held or contained) we need to find out the highest possible atomic number in the Periodic Table of Elements. According to the research [2–5], the highest atomic number Z_{max} is $2\ s_0^2$, where s_0 is the structural constant of the atom, it is $s_0 = 8.278\ 692\ 517$, and $Z_{max} = 137.0735$ is related to the fact that no element can form if its electron travels in the first orbit faster than the speed of light.

Table 1. The unit boscovich, B, in relation to the other initial and derived constants.

Quantity	Symbol	Formula	Value	Unit
6 initial fundamental constants: s_0, c, e, m, m_p, π				
Structural constant	s_0	$\sqrt{\sigma Z}$[a]	8.278 692 517 066 260	1
Speed of light; vacuum	c	c	299 792 458	m/s
Elementary charge	e	e	$1.602\ 176\ 6208 \times 10^{-19}$	A·s
Electron mass	m	m	$9.109\ 383\ 56 \times 10^{-31}$	kg
Proton mass	m_p	m_p	$1.672\ 621\ 898 \times 10^{-27}$	kg
Archimedes constant[b]	π	$\arccos(-1)$[b]	3.141 592 653 589 793	1
15 (without e 14) constants derived from previous 6: $\mathbf{B}, \alpha^{-1}, \alpha, \mu_0, R_K, A_0, K_0, e/A_0, K_J, e, R_\infty, a_0, \mu_B, \mu_N$				
Boscovich (unit)[c]	B	$1/(2\ s_0^2)$	0.007 295 356 163 7514	1
Inverse fine-structure constant	α^{-1}	1/B	137.073 499 584 258	1
Fine-structure const.	α	$1/(2\ s_0^2)$	1	B
Magnetic constant	μ_0	$4\pi \times 10^{-7}$	$12.566\ 370\ 614\ 35 \times 10^{-7}$	H/m
Electric constant	ε_0	$1/(4\pi \times 10^{-7} c^2)$	$8.854\ 187\ 817\ 62 \times 10^{-12}$	F/m
von Klitzing constant	R_K	$\mu_0 c s_0^2$	$2.581\ 987\ 123\ 285 \times 10^{4}$	Ω
Action constant[d]	A_0	$\mu_0 c e^2 s_0^2$	$6.627\ 883\ 290\ 24 \times 10^{-34}$	J·s
Conversion constant	K_0	$1/(2\mu_0 c e s_0^2)$	$1.208\ 663\ 875\ 508 \times 10^{14}$	Hz/V
Ratio $\frac{e}{A_0}$	$\frac{e}{A_0} = 2K_0$	$1/(\mu_0 c e s_0^2)$	$2.417\ 327\ 751\ 017 \times 10^{14}$	Hz/V
Josephson constant	$K_J = 4K_0$	$2/(\mu_0 c e s_0^2)$	$4.834\ 655\ 502\ 034 \times 10^{14}$	Hz/V
Elementary charge	e	$\sqrt{2\alpha A_0/\mu_0 c} = e$	$1.602\ 176\ 6208 \times 10^{-19}$	A·s
Rydberg constant	R_∞	$m/(8\mu_0 e^2 s_0^6)$	$1.096\ 472\ 748\ 403\ 35 \times 10^{7}$	1/m
Bohr radius	a_0	$\mu_0 e^2 s_0^4/(\pi m)$	$5.294\ 668\ 730\ 599 \times 10^{-11}$	m
Bohr magneton	μ_B	$\frac{\mu_0 c e^3 s_0^2}{4\pi m}$	$9.276\ 547\ 861\ 521 \times 10^{-24}$	A·m^2
Nuclear magneton	μ_N	$\frac{\mu_0 c e^3 s_0^2}{4\pi m_p}$	$5.052\ 165\ 865\ 121 \times 10^{-27}$	A·m^2

a. Here σ is the *structural coefficient* of transmission (Lecher's) line representing the electromagnetic oscillator in an atom, and Z is *atomic number* [6–9] (do not replace the *structural coefficient* with the *structural constant*; those are two related but different things; $\sigma = s_0^2/Z$).

b. This formula is derived in [10].

c. As Planck's h is intended to be used to determine the unit of kg, here too, another constant (the structural constant s_0) is used to determine the unit boscovich (B).

d. All calculations are made with the condition that Planck's $h = A_0$. In this case all differences (otherwise maximal ±0.082%) compared to 2014 CODATA disappear [5].

If we include 1000 positions for the neutrons within the neutron part, then the capacity of the *type of substance* is 1000 × Zmax.

If we additionally include 1000 more positions for the electrons within the part belonging to the electrons, then the capacity of *type of substance* is 1000 × 1000 Zmax = 137 073 499.584 257 positions. By incorporating molecules and compounds, this number may be higher. With the now known more than 3180 nuclides, it can be said that quantity *Type of substance* is about 0.0023 percent filled.

2.3 A Dimension and Unit of the Quantity the *Type of Substance*

A dimension of the *type of substance* is one (it is therefore dimensionless quantity).

The choice of unit as usual can be arbitrarily made. For the unit it is convenient to choose $1/Z_{\max}$. In that case, namely, this unit represents the *distance* of two neighboring atoms in the Periodic Table of Elements. That unit we call boscovich, B, in honor to Roger Joseph Boscovich [Croatian: Ruđer Josip Bošković, born 18 May 1711 in Dubrovnik, Republic of Ragusa (modern-day Croatia) – died 13 February 1787 in Milan, Duchy of Milan (modern-day Italy)]. He was a precursor of atomistic science in the eighteenth century. Here is 1 B = $1/Z_{\max}$ = 1/137.073 499 584 = 7.295 356 × 10^{-3}. This is actually a *fine-structure constant*, i.e., the unit B = α (see Table 1).

According to the above, the calculation of a Soddy's number is made from the following formula:

$$\frac{S}{\mathrm{B}} = \frac{\mathrm{p}}{1} + \frac{\mathrm{n}}{1\,000} + \frac{\mathrm{e}}{1\,000\,000} = \frac{\mathrm{e} + 1000\,\mathrm{n} + 1\,000\,000\,\mathrm{p}}{1\,000\,000}, \tag{1}$$

S is here *Soddy's number*, B is a unit boscovich, p is the number of protons in the nucleus of atoms (known as atomic number *Z*), n is the number of neutrons in the nucleus of atoms, e is the number of electrons in the atomic shell.

How the unit boscovich fits with other units and constants can be seen in Table 1.

2.4 A Few Examples

Each of the more than 137 million positions of the Type of substance is calculated using Eq. (1) and they are shown in Fig. 1 and Table 2. The Fig. 1 shows all the elements and their nuclides, while Table 2 contains *Soddy's numbers* for some elements, nuclides, molecules, and compounds.

In this way it can be counted with Type of substance as with any other measurable quantity.

The *type of substance* thus becomes a new physical quantity with the unit boscovich. For now this unit is only a proposal (see Table 3). We suggest accepting it.

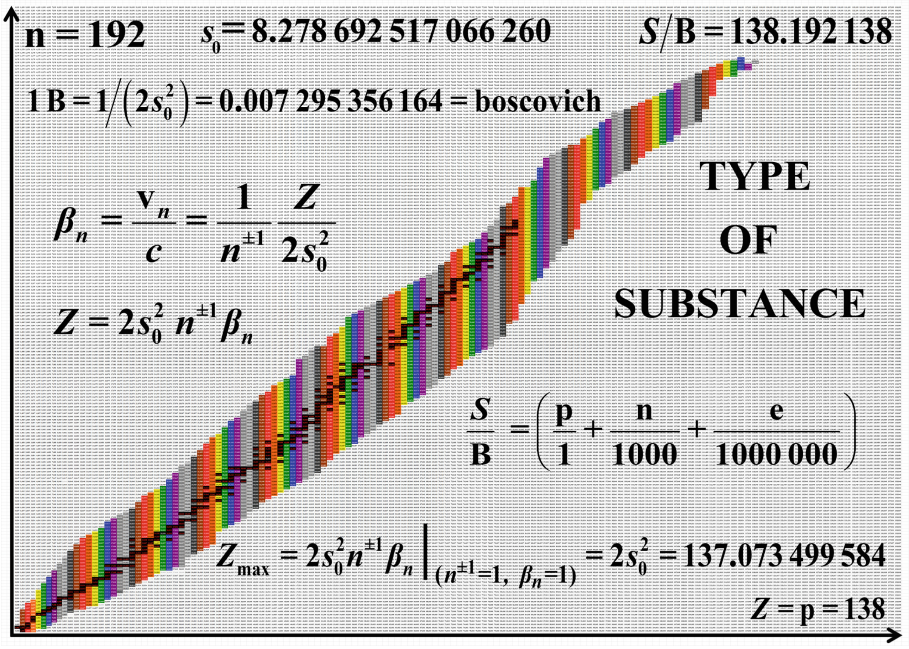

Fig. 1. The *type of substance* shown for the case of all known (3 180, all colored) nuclides. Soddy's number of substances *S* is calculated by Eq. (1), depending on the number of protons p (abscissa) and the number of neutrons n as well as on the number of electrons e. Then (divided by boskovich unit B), enter *S*/B in a place corresponding to the number of neutrons (ordinates). Colored black positions represent stable nuclides. All the others are unstable (http://periodictable.com/Isotopes/001.1/index.html, https://en.wikipedia.org/wiki/Table_of_nuclides).

Table 2. The Soddy's number *S* for several elements, nuclides and compounds. Each atom, nuclide, molecule or compound, as complex as it may be, can thus be processed and displayed unique Soddy's number *S* or *S*/B ratio as shown in this Table (1 B = 0.007 295 356 163 7514).

Substance	Unit	p	n	e	*S*/B	*S*
		1	1	1	B	1
Vacuum[a]	^{0}Va	0	0	0	0.000 000	0.000 000 000
Electron	^{0}e	0	0	1	0.000 001	7.295356×10^{-9}
Proton	^{1}p	1	0	0	1.000 000	0.007 295 356
Neutron	^{1}n	0	1	0	0.001 000	0.000 007 295
Hydrogen (protium)	^{1}H	1	0	1	1.000 001	0.007 295 363
Hydrogen (deuterium)	^{2}H	1	1	1	1.001 001	0.007 302 658
Hydrogen (tritium)	^{3}H	1	2	1	1.002 001	0.007 309 954
Thulium	^{169}Tm	69	100	69	69.100 069	0.504 109 614
Gold	^{197}Au	79	118	79	79.118 079	0.577 194 565
Oganesson	^{293}Og	118	175	118	118.175 118	0.862 129 575

(*continued*)

Table 2. (*continued*)

Substance	Unit	p	n	e	*S*/B	*S*
		1	1	1	B	1
Oganesson (triple ionized)	^{293}Og	118	175	115	118.175 115	0.862 129 553
The largest atoms (theoretical)	^{325}Xx	137	188	137	137.188 137	1.000 836 321
Water, H_2O,	^{1}H2	2	0	2	10.008 010	0.073 011 997
	^{16}O	8	8	8		
Sulfuric acid, H_2SO_4	^{1}H2	2	0	2	50.050 050	0.365 132 940
	^{34}S	16	18	16		
	^{16}O4	32	32	32		
Butane, $C_4H_{10,}$	^{12}C4	24	24	24	34.024 034	0.248 217 446
	^{1}H10	10	0	10		
Ethyl alcohol, C_2H_6O	^{6}C2	12	12	12	26.020 026	0.189 825 357
	^{1}H6	6	0	6		
	^{16}O	8	8	8		
Glucose, $C_6H_{12}O$	^{12}C6	36	36	36	56.044 056	0.408 861 349
	^{1}H12	12	0	12		
	^{16}O	8	8	8		
Sucrose, $C_{12}H_{22}O_{11}$	^{12}C12	72	72	72	182.160 182	1.328 923 406
	^{1}H22	22	0	22		
	^{16}O11	88	88	88		
Carbamic acid, NH_2COOH	^{15}N	7	8	7	32.033 032	0.233 692 377
	^{1}H2	2	0	2		
	^{12}C	6	6	6		
	^{16}O	8	8	8		
	^{18}O	8	10	8		
	^{2}H	1	1	1		

a. A vacuum does not have its official abbreviated tag, so, Va, here is an occasional shortcut (mass number is up to the left).

Table 3. The proposal of SI base units with an added new unit, boscovich (B).

Quantity	Sign	Dimension	Unit name	Unit symbol
Length	*l*	L	meter	m
Mass	*m*	M	kilogram	kg
Time	*t*	T	second	s
Electric current	*I*	I	ampere	A
Thermodynamic temperature	*T*	Θ	kelvin	K
Luminous intensity	I_v	J	candela	cd
Amount of substance	*n*	N	mole	mol
Type of substance	*S*	N	boscovich	B

3 Here's Why the Name 'Boscovich' Was Suggested for the Unit

It is well known that in his *A Theory of Natural Philosophy* (or *Theory*) Boscovich first came up with the idea that all natural phenomena can be described by one law of force [11]. This law is depicted by the famous Boscovich's curve (*curva Boscovichiana*). This is actually the first unification of all forces, i.e., interactions in nature so that the contemporary physics program of unification of four fundamental interactions (gravitation, weak, electromagnetic, strong) has not yet been achieved. Boscovich considered this to be achieved, and called that "my new world". In analogy with Copernicus and *Copernican turn*, some scientist later talked about *Boscovich's turn* [12]. If curves relating to interactions among nucleons, atoms, molecules and the like are compared to Boscovich's curve in today's science then a striking resemblance is observed [13].

By allowing more repulsive areas of asymptotic repulsive force in its curve, Boscovich presented one of the basic ideas of contemporary physics of elemental particles, i.e., he gave the first model of the "quark confinement" (*Theoria*, No 518). This fact is pointed out by American physicist Phillip Rinard [14].

The basic elements of the substance, according to Boscovich's understanding, are simple, non-dimensional, indivisible, non-extensible, discrete material (physical) points that represent the center of force - the idea of the fields, Michael Faraday accepted directly from Boscovich [15]. These Boscovich's "atoms" cannot be identified with the atoms of today's science but rather with quarks, as Nobel Prize- winner Leon Lederman has emphasized [16]. Boscovich's "atoms" are not mere mathematical points but rather the material, physical points endowed with power of inertia and of Boscovich's attractive and repulsive forces.

From such non-dimensional material points (Latin, *puncta materiae*), more complex material structures are built. Boscovich speaks about the particle hierarchy and calls them the particles of the first, second, third, fourth, fifth… orders which in nowadays physics of elementary particles correspond to nucleons (protons and neutrons), atoms, molecules and even more complex material structures. Thus, the idea of the order or type of substance is for the first time mentioned in Boscovich's theory of forces and structure of matter. Particle properties are conditioned by their structure. This idea was later stressed by chemists J. J. Bercelius, A. M. Butler and A. Crum Brown in the 19th century.

Let's just mention that Boscovich's theory has anticipated some later results of science such as the idea of quantization and the Bohr's model of atom with discrete paths, elements of theory of relativity, elements of the fractal theory, Big Bang Theory, [17], etc.

Because of all that, and because of the fact that Boscovich measured the length of the arc of the meridian between Rome and Rimini, which generally contributed to the measurements, we suggest that the unit of the physical quantity *type of substance* be called "boscovich" in honor of Roger Joseph Boscovich [18].

4 Conclusion

The knowledge of the atoms' properties in particular the determination of the maximum atomic number is used here to form new physical quantity, called the Type of substance. It has been shown that only one constant should be sufficient for the whole procedure, it is the structural constant of the atom s_0. This constant is theoretically defined and accurately calculated in previously published our articles. The new quantity includes vacuum, particles, elements, atoms, nuclides, molecule, compounds and ions; therefore, all known matter.

Proposed and defined unit of Type of substance is 'boscovich', in honor to precursor of atomistic theory Roger Joseph Boscovich. The amount of 'boscovich' is $1/(2s_0^2)$. The sign of new quantity is S, in honor to radiochemist Frederick Soddy. Numerous examples show the functioning of quantity S and its unit B.

The eighth basic unit is thus ready to occupy its place beside the existing seven.

The article also emphasizes that the 14 constants are derived from the six initial constants. By introducing the *structural constant* even 12 constants become redundant. Since the boscovich unit is also based on the *structural constant* this means that it also belongs to redundant constants, but also that it is well-grounded.

Acknowledgements. Once again, we thank Ms. Srebrenka Ursić and Mr. Damir Vuk for very useful discussions and advices that helped us very much.

Mr. Davor Pavuna has been intensively involved in supporting the project, advocating for its realization and disseminating project information through its contacts.

Mr. Krunomir Dvorski helped with his suggestions that conceptually, besides the protons and neutrons, Soddy's number also include electrons.

Mrs. Dubravka Brandić kindly helped with the language advice.

Great thanks to Schrack Technik d.o.o. for recognizing this scientific initiative.

References

1. Perkovac, M.: Model of an atom by analogy with the transmission line. J. Mod. Phys. **4**, 899–903 (2013)
2. Perkovac, M.: Determination of the structural constant of the atom. J. Appl. Math. Phys. **2**, 11–21 (2014)
3. Perkovac, M.: Maxwell's equations as the basis for model of atoms. J. Appl. Math. Phys. **2**, 235–251 (2014)
4. Perkovac, M.: The structural constant of an atom as the basis of some known physical constants. In: Proceedings of the International Conference on Applied Physics, Simulation and Computers (APSAC 2015), pp. 92–102 (2015)
5. Perkovac, M.: Planck's h and structural constant s_0. J. Mod. Phys. **8**, 425–438 (2017)
6. Perkovac, M.: Quantization in classical electrodynamics. Phys. Essays **15**, 41–60 (2002)
7. Perkovac, M.: Absorption and emission of radiation by an atomic oscillator. Phys. Essays **16**, 162–173 (2003)
8. Perkovac, M.: Statistical test of Duane-Hunts's law and its comparison with an alternative law (2010). https://arxiv.org/abs/1010.6083

9. Perkovac, M.: Maxwell's equations for nanotechnology. In: Proceedings of the 35th International Convention MIPRO, Opatija, 21–25 May 2012, pp. 429–436. IEEE Xplore, 16 July 2012
10. Perkovac, M.: Measurement of mathematical constant π and Physical Quantity *Pi*. J. Appl. Math. Phys. **4**, 1899–1905 (2016)
11. Boscovich, R.J.: A Theory of Natural Philosophy. The M.I.T. Press, Cambridge and London (1966)
12. Filipović, V.: Ruđer Bošković and his significance for contemporary science and philosophy of nature. Tesla **8**, 29–31 (1961)
13. Ullmaier, H.: Puncta, particulae et phaenomena. Roger Joseph Boscovich und seine Naturphilosophie. Wehrhahn Verlag, Hannover-Laatzen (2005)
14. Rinard, M.P.: Quarks and boscovich. Am. J. Phys. **44**(7), 704–705 (1976)
15. Faraday, M.: A Speculation touching electric conduction and the nature of matter. Philos. Mag. J. Sci. **24**, 136–144 (1844). 3rd series
16. Lederman, L., Teresi, D.: The God Particle. If the Universe is Answer, What is the Quation? Dell Publishing, New York City (1993)
17. Kutleša, S.: Filozofija Ruđera Boškovića. KruZak, Zagreb (2012)
18. Perkovac, M.: Measurement of type of substance based on protons, neutrons and electrons in the substance. Asian Journal of Phys. Chem. Sci. **4**(4), 1–8 (2017). Article no. AJOPACS.37863, ISSN: 2456-7779

Spectroscopy of Colorants for Fine Art in Visual and Near Infrared Spectrum

Denis Jurečić[1(✉)], Vilko Žiljak[1,2], Lidija Tepeš Golubić[2], and Jana Žiljak Gršić[1,2]

[1] Faculty of Graphic Arts, University of Zagreb, Getaldiceva 2, 10000 Zagreb, Croatia
minerva.graphica.d.o.o@zg.t-com.hr, vilko@ziljak.hr, jana@tvz.hr

[2] Zagreb University of Applied Sciences, Vrbik 8, 10000 Zagreb, Croatia
lidija75@yahoo.com

Abstract. We are studying inks through information of their absorption spectra. Data are measured continuously in visual and near infrared region. New color hues are achieved by different colors mixtures, but their appearance properties are respected in both spectral domains. Measured spectra of dyes are key information for identification of twins, for at least two dyes, that obtain equal spectrograms in visual, but different in near infrared region. New colors are prepared for ceramic application with "metallic-gold" ink This article presents light colors in the visual spectrum, and which have high absorption values in near infrared spectrum. Dyes with the addition of metallic gold, significantly changes the direction of research on the development of the twin colors and dyes.

This paper presents innovative solutions for tints intended for creating double images, double information, creating intimate and hidden invisible artworks with colorants for ceramics. This is an advance in safety and proving the authenticity of artwork. At the exhibition, and at a conference, the visitors can observe ceramic exhibits with new developed of the dual infrared camera.

Keywords: VZ spectroscopy · Hidden picture · Twin colorant
Infrared art

1 Introduction

"Infrared colorants" have found their application on documents, valuables and packaging [1]. The application has been extended to "security print" on clothes of army linen [2]. The new technology of hiding the information as well as the development of double image on polymer food packaging has been introduced [3].

Dyes for art painting, oil on canvas, offer a great diversity of colors. Each dye has their own absorption values in near infrared spectrum (NIR) [4]. This property is used by painters Nada Žiljak and Dijana Nazor for creating a personal art duality on canvas. The dual image is being observed through two cameras: Visual V and Z camera with selection, blockage, light on 1000 nm in near infrared spectrum. Each camera presents us with its own image.

K. Ntalianis and A. Croitoru (Eds.): APSAC 2017, LNEE 489, pp. 56–62, 2019.
https://doi.org/10.1007/978-3-319-75605-9_8

The INFRAREDESIGN® (IRD) theory and application with two cameras or two security cameras which are placed either in the streets or in banks as for extended night observation [5]. Visual spectrum (RGB red, green and yellow), marked as V, is determined by wave lengths from 400 to 750 nm [6]. Near infrared spectrum is observed in its initial area in the range of 750 to 1000 nm. This area is divided into two parts. The first part, marked as Z1, is transitive area from visual to infrared spectrum which we separate because it is a mixture that we purposely block. Cameras, for the observation of effects of infrared design® print project, are adjusted to the area Z2 (850 to 1000 nm) at 1000 nm (Z) [7]. Colorants are studied as digital information in order to develop new algorithms for managing inks, toners and printing colorants in the reproduction of visual information of two spectral areas [8]. Researches are directed to the creation of double visual information, double image in the same place and which are independently registered with visual and infrared cameras. The security IRD print is also tested at large printing editions in offset technology on newspaper paper. We also make efforts o extend considerably the safety technology to fine arts scene, theatre scenography and packaging of pharmaceutical products for example.

2 Measured Visual and NIR Values of Ceramic Dyes

In the paper we studied spectrum, covering the wavelength from 400 to 900 nm.

The spectrogram of light absorption in V-visual and Z-near infrared region for liquid, thick dyes of series for art ceramic has been measured. The spectrogram measurements have been performed with the Projectina [9] in steps of 5 nm.

The tones of new, unexplored colors are being achieved by mutual mixing of different dyes but also by respecting their properties of appearing in two spectra. The dual image information has been put on the ceramic background.

The colors for art painting have been recorded with a ZRGB camera in the visual RGB spectrum and in NIR-Z spectrum with a blockage at 1000 nm. First nine colors are pure colors from manufacturer. Green, red, silver, white and blue. Colors black, gold, cyan, yellow and mixture of cyan and black colorant are in the second line.

Silver color is visually almost white (the third in the first line). It absorbs strongly NIR light. Its Z value is equal to dark grey carbon color. The same effect of "inversely

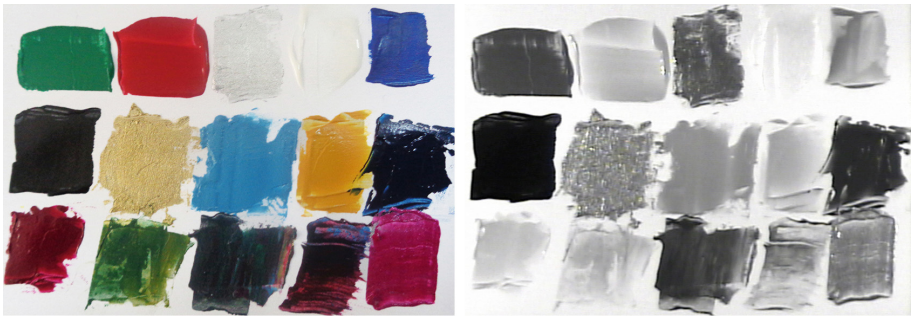

Fig. 1. A photograph of ceramic dyes in visual and NIR-Z spectrum

response" is achieved with "silver colorants" for screen printing. Colors with gold and silver metallic qualities are ideal for safety graphic. They act unexpectedly in infrared visual area. The printer can secure himself from forging of his tradecraft works by adding such colorants.

The mixture of various colorants from the first and second line are in the third line. Each colorant is carefully observed in two spectrums in order to achieve controlled double response in V and Z spectrum according to the idea of the artist (Table 1).

Table 1. Numerical values of 9 dyes

Colour	L*a*b	Z
Dark green 068	41, −30, 12	71
Cherry red 125	38, 56, 36	29
Met. silver 782	78, 0, 3	77
White 070	81, 0, 3,	5
Ultramar. 055	30, 16, −53	55
Black 073	8, 2, 0	96
met. gold 784	70, 5, 39	50
Cyan 056	47, −14, −29	50
Yellow 021	62, 22, 6	50

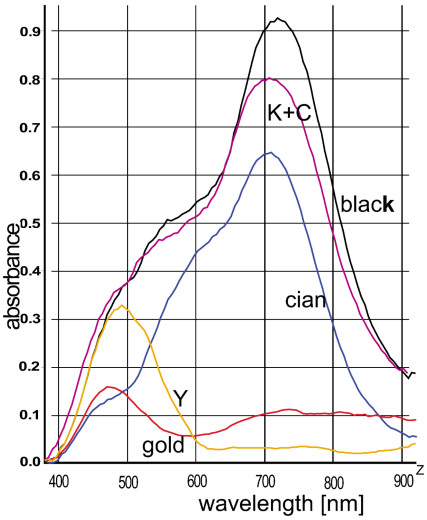

Fig. 2. Spectra of dyes in the second line of Fig. 1.

The first color in the third line is a mixture of yellow and red. This color absorbs poorly in Z spectrum because it is composed from the colorants of the same Z characteristics. The second color (green) in the third line is the mixture of yellow and cyan which also absorb poorly in Z spectrum. That green color is of the same hue color (in V) as is the green color in the first line. But their possibility of absorption near infrared spectrum is quite different. They are "twins of green hue" color: the same in visual but different in NIR spectrum. The fifth color in the third line consists of red and gold. Such hue of red color has positive value and it is a twin to the red color from the first line.

We have performed spectral analysis of dyes for art ceramics. Absorption spectra measured in continuity from 400 to 1000 nm for dyes that are being applied to painting ceramic objects have been shown in this paper.

Visual V and NIR (Z) absorption spectrum of ceramic inks were measured in range of 400 to 900 nm [9]. Spectral area for twin colorants are observed through three bands: visual (V), transitive Z1 and Z2. The spectrograms from the second line of colorants in Fig. 1 are given in Fig. 2. Those are black, golden, blue and yellow colors. The fifth color is the mixture of cyan (50%) with added (50%) of black color (BK).

The yellow ink has the maximum absorption of radiation at 480 nm. The absorption of gold ink has two maxima, at 470 and at 730 nm. The blue color has a maximum at 600 nm. The black dye has a maximum at 720 nm and from all the dyes it absorbs NIR the most in Z wave length.

3 Infrared Painting with Ceramic Dyes

Inventive movement "infrared painting" uses the knowledge of the light absorption quality of the colorants for art ceramics. The painter mixes colorants in order to create double images on ceramic for two different light blockade. The ultimate intimacy, extreme message, hidden information or extreme eroticism will not be seen by the naked eye (Fig. 3).

Fig. 3. V. Painting on a ceramic plate, photograph in visual and Z spectrum

The color absorption was performed by measuring with Projectina PAG B50 No 664620913 that have 25 filters with blockages from 225 to 1000 nm [9]. We have experimentally selected blockages to make a continuous motion translation film of ceramic drawing and Z drawings at 385, 455, 515, 590, 645, 715, 780, 830, 850 and 1000 nm. By combining digital records and related images, an animation film was created and it is placed on the author web address [10] (Figs. 4 and 5).

Security cameras with blockage of NIR light have been set up at the exhibition. The double state of the image has been recorded with two cameras. The first camera has been set to a visual (V) – RGB (red green blue) mode. The second camera records in the near infrared spectrum (Z – NIR) with a blockade at 1000 nm (Fig. 6).

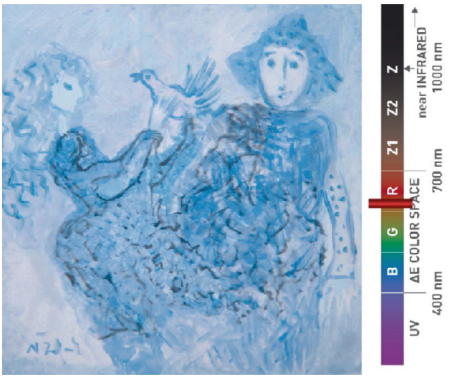

Fig. 4. Painting with a blockage at 630 nm address: http://jana.ziljak.hr/AnimacijaFigure4.mp4

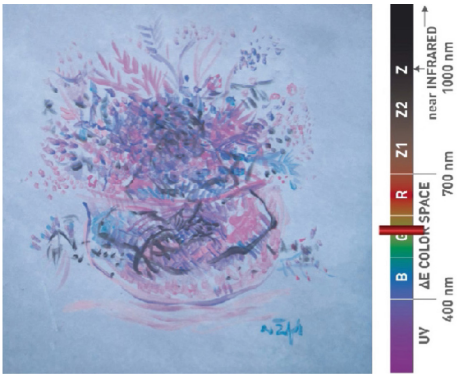

Fig. 5. Painting with a blockage at 580 nm http://jana.ziljak.hr/AnimacijaFigure5.mp4

Fig. 6. V. Gallery SV. I. Zelina, Plates on the wall in two V and Z spectra

4 Discussion on Art and Science

Artist Nada Žiljak mixes colors according to the idea of creating double painting "infrared painting". She categorizes the colors according to their response in NIR spectrum. Value Z is being added to each dye and that is information on light absorption at 1000 nm.

Fine arts reach out to new ways of experiencing colors and mixing dyes. Painters, graphic designers and artists in the multimedia field are aware of the possibility of using light properties outside the range of naked human eye, and thereby creating new painting. That new "INFRARED painting" art has been expanded to dyeing ceramics. The artist uses spectroscopy, something that is totally new to the painters. That is a tool for achieving hidden, double, invisible image. They are using "Z glasses", custom

developed for painters and graphic designers, that enable them to simultaneously look at the state of artistic work in the infrared spectrum and to look at the painting intended for naked eye. Never until now could the artist better create what is in their imagination, by hiding their intimate artistic work into some other image. They are using light properties, properties of dye material and the way that has opened them a new way of expressing.

Art ceramic dyes use colors for achieving special effects. In their collection you can find colors named "gold" and "silver". Graphics with those colors cannot be reproduced for paper book monographic editions, with only C, M, Y, K dyes.

New ceramic artworks containing infrared paintings mode are exhibited at the St. Ivan Zelina Gallery, where annual international contemporary ceramics exhibition takes place. Infrared paintings are applied on pottery, vases and plates. The visitors of the exhibition are looking at the ceramic works through infrared cameras.

5 Conclusion

We need spectroscopy to create twin dyes with different default Z values. New painting, imaging, weaving, drawing with individualization of the authenticity of artistic work have been opened. Infrared painting with ceramic dyes is the painting of connecting two images for separate observation in the visual and infrared light. Research on metallic dyes is being continued in the direction of mixing those colors with other dyes. The goal is to acquire a sorted data base on light absorption in two independent light regions and to define dualities of colors and dyes for them. The artists will be able to manage the dyes and with a goal of creating a personal new dual painting. To conclude: the innovative solutions are mixing of colorants for ceramics with the intention of creating double image, double information and hidden intimate fine art painting.

References

1. Pogarcic, I., Agic, A., Matas, M.: Evaluation of the colorant twins for the neutral grey spectra in infrared graphic procedure. Tehnicki vjesnik **23**(6), 1659–1664 (2016). https://doi.org/10.17559/tv-20150303132036. ISSN 1330-3651, ISSN 1848-6339. Hrcak ID: 169526
2. Stanimirovic, I.Z., Vujic, Z.J., Stanic Loknar, N.: Marking of the camouflage uniform for visual and near infrared spectrum. Tech. Technol. Educ. Manag. **8**(3), 920–926 (2013). ISSN 1840-1503
3. Friscic, M., Medugorac, O., Tepeš, L., Jurecic, D.: Invisible information on the transparent polymer food packaging with Infra V/Z technology. Tech. Technol. Educ. Manag. **8**(4), 1512–1519 (2013). ISSN 1840-1503, e-ISSN 1986-809X
4. Ziljak, J., Golubic, T.L., Jurecic, D., Ziljak, V.: Hidden infrared graphics on a painted canvas. Int. J. Appl. Phys. **2**, 18–23 (2017). www.iaras.org/iaras/filedownloads/ijap/2017/015-0003(2017).pdf. ISSN: 2367-9034
5. Pap, K., Ziljak, I., Vujic, Z.J.: Image reproduction for near infrared spectrum and the infraredesign theory. J. Imaging Sci. Technol. **54**(1), 10502-1–10502-9 (2010)

6. Ziljak, V., Agic, D., Rajendrakumar, A.: Broadening INFRARED technology on cotton fabric coloration with double information ability in visual and infrared spectra. Tech. Technol. Educ. Manag. **11**(1), 3–10 (2016). ISSN 1840-1503, e-ISSN 1986-809X
7. Ziljak, V., Pap, K., Ziljak-Stanimirovic, I., Ziljak Vujic, J.: Managing dual color properties with the Z-parameter in the visual and NIR spectrum. Infrared Phys. Technol. **55**(4), 326–336 (2012). https://doi.org/10.1016/j.infrared.2012.02.009
8. Grsic, Z.J.: Near infrared spektroskopy in print tehnology. Polytech. Des. **5**(1), 32–36 (2017). https://doi.org/10.19279/tvz.pd.2017-5-1-05
9. Projectina Docucenter 4500. Switzerland. http://forensictechnology.com/projectina/
10. Animation. http://jana.ziljak.hr/AnimacijaFigure4.mp4, http://jana.ziljak.hr/AnimacijaFigure5.mp4

An Ultrasound Technique for the Characterization of the Acoustic Emission of Reinforced Concrete Beam

N. A. Lamberti[1(✉)], M. La Mura[1], C. Guarnaccia[2], G. Rizzano[2], C. Chisari[3], Joseph Quartieri[2], and N. E. Mastorakis[4]

[1] Dipartimento d'Ingegneria Industriale, University of Salerno, via Giovanni Paolo II, Fisciano, Italy
{nlamberti, mlamura}@unisa.it
[2] Department of Civil Engineering, University of Salerno, via Giovanni Paolo II, Fisciano, Italy
{cguarnaccia, g.rizzano, quartieri}@unisa.it
[3] Department of Civil and Environmental Engineering, Imperial College London, London SW7 2AZ, UK
corrado.chisari@gmail.com
[4] Department of Electrical Engineering and Computer Science, Hellenic Naval Academy, Piraeus, Greece
mastor@snd.edu.gr

Abstract. Among the various non-destructive techniques for health monitoring in structures, the Acoustic Emission (AE) is well known in scientific literature. Ultrasonic waves emitted by the creation and propagation of cracks in concrete or Reinforced Concrete specimens are usually collected by means of ultrasonic sensors. The signals must be treated in front-end readout process with preamplifiers and filters, to be able to set a proper trigger level and to cut the background noise (belonging to different frequency ranges). In addition, the post processing of the data is important to "clean up" the dataset, removing fake events, and to extract the proper information, useful for structure damage assessment. In this paper, the authors present the experimental set up and the transducers used to acquire the AE signals recorded during a four-point bending test on a RC beam. The ad hoc realized amplifier and filtering circuit used in the test are also described. Then, an example of an AE signal is also reported, in terms of frequency spectrum analysis and noise filtering.

Keywords: Acoustic Emission · Piezoelectric Sensor · Filters Amplifiers

1 Introduction

The Acoustic Emission analysis is a well-known non-destructive test for structures (see for example [1, 2]). The study of ultrasonic waves produced by Reinforced Concrete (RC) specimen under load, is extremely interesting to understand damaging and breaking behaviour [3, 4]. For this purpose, the need for an efficient read out electronics

K. Ntalianis and A. Croitoru (Eds.): APSAC 2017, LNEE 489, pp. 63–68, 2019.
https://doi.org/10.1007/978-3-319-75605-9_9

and off line data processing is evident. AE signals, in fact, are usually of a small amplitude. For this reason, it is extremely important to properly match the frequency range of the events with the bandwidth of the sensors. In addition, a preamplifier and filtering circuit is needed, both to improve the signal/noise ratio and to remove background noise from low frequency signals (both mechanical and electrical).

In this paper, the authors present the sensors used in a four-point bending test performed at the University of Salerno. In [5], the authors presented the results of the test under the civil engineering point of view, underlining several parameters that allow to evaluate the damage in the specimen. The aim of this paper, is to present the electronic approach, in terms of readout electronics, pre-amplification filtering circuits and post processing procedures, that led to the data collection and analysis.

2 Four Points Bending Test

A four-point bending test on a reinforced concrete beam was performed at the Laboratory of Materials and Structures of the Department of Civil Engineering of the University of Salerno (Fig. 1).

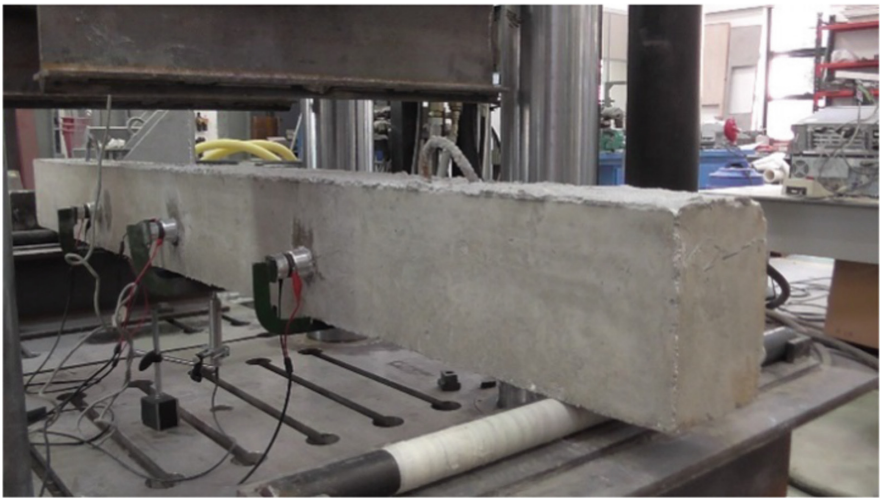

Fig. 1. Picture of the experimental set up.

In order to measure the Acoustic Emission (AE) and to match the AE frequency, two kinds of Ultrasonic Transducers were used: the lower frequency transducer is a classical Langevin transducer (LT) (see Fig. 2(a)) with a resonance frequency of about 40 kHz; in order to measure the higher AE frequency, the ultrasonic transducer (HFT) shown in Fig. 2(b) was used. To characterize both transducers we measured their electrical input impedance Z_i; in Fig. 3, the amplitude of the LT Z_I is shown evidencing its resonance frequency at 43.4 kHz.

Fig. 2. (a) Picture of the classical Langevin transducer (LT) and (b) of the high frequency ultrasonic transducer (HFT) used.

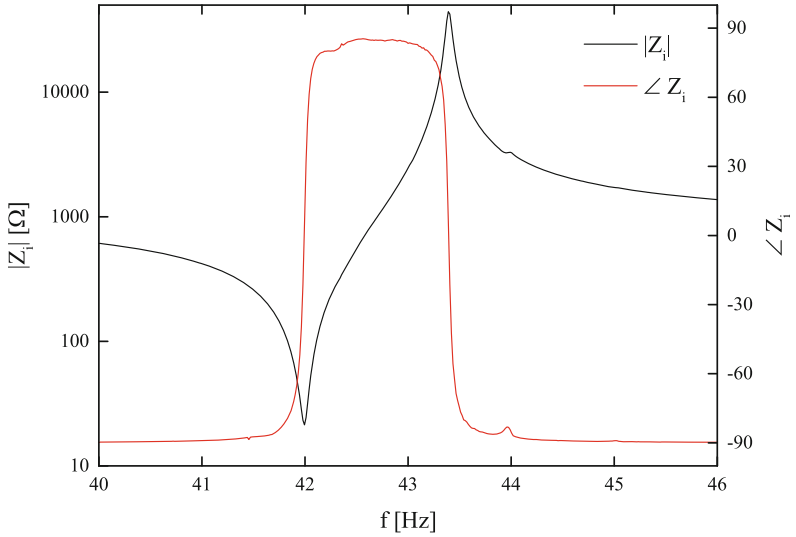

Fig. 3. Amplitude ($|Z_i|$) and phase ($<Z_i$) of the electrical input impedance of the Langevin transducer.

The HFT is composed by a thick piezoelectric disk (t_D = 10 mm) with a diameter d_D = 25 mm glued to a aluminum disk with the same diameter and a thickness t_s = 12 mm. In Fig. 4 the electrical input impedance of the HFT is reported; as it can be seen, there are many resonance frequencies around 200 kHz, a frequency of interest for the application. The purpose of the aluminum disk in front of the PZT emitting surface is to acoustically match the piezoceramic disk to concrete [6].

In Fig. 5 the four-point bending test on a reinforced concrete beam, performed at the Laboratory of Materials and Structures of the Department of Civil Engineering of the University of Salerno is shown. The simply supported, 150 × 200 mm^2 cross-section beam with length equal to 2000 mm, was loaded in two points 625 mm far

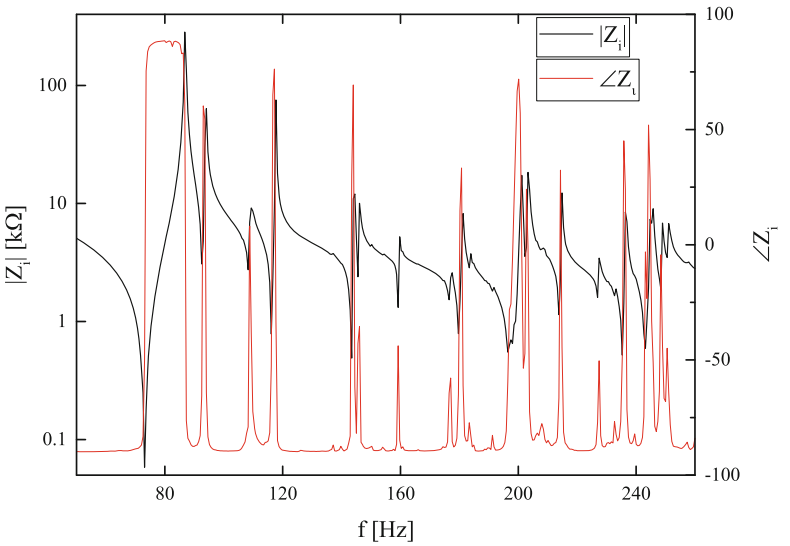

Fig. 4. Amplitude ($|Z_i|$) and phase ($<Z_i$) of the electrical input impedance of the high frequency ultrasonic transducer (HFT) in Fig. 2(b).

from the supports by means of a stiff steel beam transferring the load from a hydraulic jack. The load was applied in displacement control, according to a protocol involving preliminary increasing cycles and then a ramp until failure. The total force F transferred by the hydraulic jack and the displacement at mid-span were recorded by the central unit; the analytical values of first-cracking and ultimate loads are F_{cr} = 10.05 kN and F_u = 91.97 kN respectively. To measure the beam acoustic emission, we used three Langevin transducers (LT) and one high frequency transducer (HFT). In Fig. 5 the positions of the Langevin transducers on the beam are evidenced by circles named 1, 2 and 3 while the HF transducer position is reported with the circle named 4. A picture of the experimental set up is shown in Fig. 1.

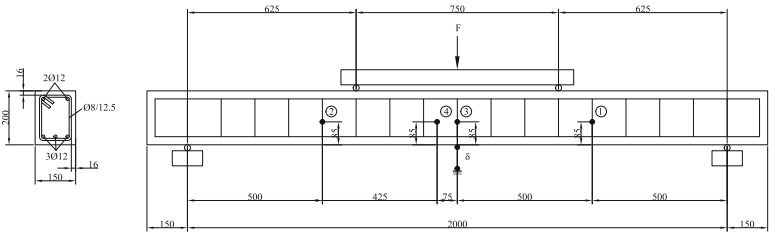

Fig. 5. Sketch of the RC beam under test with sensors positions (circles).

In order to amplify the signal received by all transducers we designed and realized an amplifier whose circuit is shown in Fig. 6(a). The circuit is a voltage amplifier and it was repeated four times in order to amplify all the transducer signals and to enhance the

signal to noise ratio (SNR). The amplifier gain can be adjusted from 10 to 100, but we used the 10 gain in order to avoid saturation at high AE. The voltage amplifier in Fig. 6 (a) is followed by the high pass filter (HPF) in Fig. 6(b), needed to avoid both electric and mechanical low frequency noise. The cascade of the amplifier and the HPF shows a −3 dB bandwidth between 2.5 kHz and 140 kHz with a gain of 38.

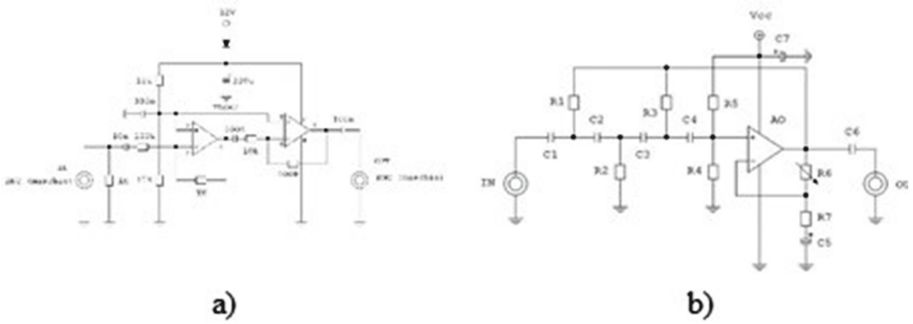

Fig. 6. Schematic of the (a) voltage amplifier, (b) High Pass Filter HPF.

The circuit amplifying the HF transducer output is not provided with the HPF because the high frequency limit is less than the transducer resonance. In order to measure the AE we connected the transducers amplifiers' output to the four channels of a Lecroy "Waverunner 104 MXI" digital oscilloscope; we recorded, for each transducer 1213 AE events, each composed by 5002 points. In order to process the measurements, we developed a "Matlab" script that, first of all, filters the signals according to their amplitude. The filtering amplitude can be selected according to acquired signals, in the

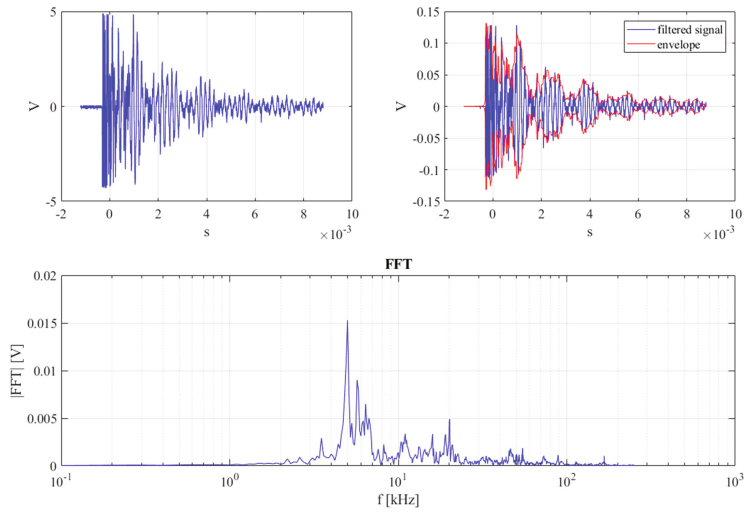

Fig. 7. The acquired AE signal.

present case we selected a filtering amplitude of 50 mV. In this way the 1213 events were reduced to 910. The next steps were the cancellation of the signal offset, about 48 mV in our case, and the cancellation of noise overlapping the signal in the amplifier band. This last step is performed by using an adjustable noise threshold; the threshold value was selected at 150 mV. Finally, the last step, before computing the AE quantities of interest was the elimination the elimination of the gain factor for the LT (38) and for the HFT (10). As an example of the AE first steps process, in the Fig. 7 is reported an AE signal (a) as acquired by the oscilloscope at the output of the Langevin transducer, (b) after the filtration and the envelope, in red, and (c) the FFT of the filtered signal.

3 Conclusions and Future Work

Two considerations can be done on the results shown: the first one is the analysis of the sensors sensitivity in order to select the transducer with highest performance. The other is that the analysis of the recorded AEs is crucial in order to study the RC specimen response under load and its durability and resistance. Future steps of this work will be the optimization of the data acquisition process and the physical analysis of the frequencies activated during the test.

References

1. Ohtsu, M., Uchida, M., Okamoto, T., Yuyama, S.: Damage assessment of reinforced concrete beams qualified by acoustic emission. ACI St. J. **99**(4), 411–417 (2002)
2. NDIS-2421, Recommended Practice for In-Situ Monitoring of Concrete Structures by Acoustic Emission, Japanese Society for Non-Destructive Inspection (2000)
3. Iturrioz, I., Lacidogna, G., Carpinteri, A.: Acoustic emission detection in concrete specimens: experimental analysis and lattice model simulations. Int. J. Damage Mech. **23**(3), 327–358 (2014)
4. Benedetti, M.D., Loreto, G., Matta, F., Nanni, A.: Acoustic emission historic index and frequency spectrum of reinforced concrete under accelerated corrosion. J. Mater. Civ. Eng. **26** (9), 1–8 (2014)
5. Chisari, C., Guarnaccia, C., Lamberti, N., Piluso, V., Quartieri, J., Rizzano, G.: Acoustic emissions analysis of a four-point bending test on a reinforced concrete beam. In: Proceedings of the CSCC 2017 conference, Crete Island, Greece (2017)
6. Lamberti, N.A., Caliano, G., Iula, A., Pappalardo, M.: A new approach for the design of ultrasonotherapy transducers. IEEE Trans. Ultrason. Ferroelectr. Freq. Control **44**(1), 77–84 (1997)

Prediction of Airport Acoustical Noise by Deterministic Decomposition and Seasonal ARIMA Techniques

Claudio Guarnaccia[1(✉)], Carmine Tepedino[1], Nikos E. Mastorakis[2], Stavros D. Kaminaris[3], and Joseph Quartieri[1]

[1] Department of Civil Engineering, University of Salerno, via Giovanni Paolo II, Fisciano, Italy
{cguarnaccia, ctepedino, quartieri}@unisa.it
[2] Department of Electrical Engineering and Computer Science, Hellenic Naval Academy, Piraeus, Greece
mastor@snd.edu.gr
[3] Department of Electrical Engineering, Piraeus University of Applied Sciences, Aigaleo, Greece
skamin@teipir.gr

Abstract. In this paper a time series of hourly equivalent noise levels acquired near the international airport of Nice, France, is analysed. Two different techniques are proposed to model and forecast the time series: deterministic decomposition and seasonal autoregressive moving average. The two models are defined and fitted on the calibration dataset. Subsequently, the developed models are tested comparing their forecasts with 25 noise level data not used in the calibration phase. A detailed error analysis, by means of statistics and metrics, will be presented to test the models performances.

Keywords: Time series analysis · Acoustical noise prediction
Seasonal ARIMA modelling · Deterministic decomposition modelling
Airport pollution

1 Introduction

The great need for long range travelling is leading to a general improvement of the airplanes traffic, both on regional and international scale [1]. Even if the flag companies try to adopt a small number of hubs in each country, many other companies are increasing their destinations, in order to connect as much places as possible, both for business or touristic purposes.

An important externality of air traffic and airports is the acoustical noise. It is obvious that an airplane is a strong source of acoustical noise, due to the turbines, to the aero-dynamical noise, to the acceleration or the breaking during the take-off and landing phases, to the contact tyre-pavement, etc. (see for instance [2, 3]). The authors proposed many methods to assess and predict the noise produced by transportation means, mainly trains [4, 5] and road traffic [6–13]. Regarding airport noise, in [14], a non-homogeneous Poisson model is applied, in order to evaluate the probability of

K. Ntalianis and A. Croitoru (Eds.): APSAC 2017, LNEE 489, pp. 69–75, 2019.
https://doi.org/10.1007/978-3-319-75605-9_10

exceedance of a given noise threshold. In this paper, a different approach is presented. According to the models presented in [15–17], the Time Series Analysis (TSA) approach is adopted. In particular, two models are calibrated on a field measurement dataset. This dataset includes 249 hourly equivalent levels, measured in proximity of the airport of Nice (France), during the Christmas period of 2000: 224 data will be used for the calibration and the last 25 for the validation.

2 Methods

Time Series Analysis is a technique largely adopted in many contexts of the Applied Physics and of the Engineering: it is very common that variables of interest are collected sequentially in time. In this work, the analyzed time series is composed by observations of acoustic equivalent levels, equispaced in time. Two different models are proposed to describe and predict the series.

The first model is of the deterministic decomposition typology (DD-TSA); therefore, the estimation of a future value is computed by the combination of the trend, i.e. long term measurements behaviour, multiplied by a seasonal factor, i.e. a correction due to the specific periodic pattern. The lag that maximizes the autocorrelation is expected to be the periodicity of the series. In the data considered in this paper, the authors expect a lag of 24 h. Detailed description of the adopted model can be found in [15, 18].

The second model is of the Seasonal ARIMA typologies. Since the observed acoustical level dataset highlights strong seasonal tendencies, a good choice can be the adoption of seasonal autoregressive models (SARIMA). In general, the SARIMA linear polynomials are stochastic seasonal models built to analyse and predict a time series under study. The Seasonal ARIMA implemented here is embedded with a periodicity of 24 h ($s = 24$), and does not include coefficients of autoregression. Therefore, the chosen model is a SARIMA $(0,1,1) \times (0,1,1)_{24}$. More on the model description can be found in [18] and, more in general, in [19].

In order to estimate the models accuracy, the statistical features of the difference between actual data and forecasted value (residuals) will be studied. In addition, quantitative metrics of error will be used, such as the "Mean Percentage Error" (MPE) and "Coefficient of Variation of the Error" (CVE), according to the formulas presented in [15]. A measurement of model performance can be obtained also by "Mean Absolute Scaled Error" (MASE) [20], that is basically the comparison of the model predictions with a "naïve" model. In this paper, the "naïve" model is the value measured in the series k periods before the period t, assuming that the period t can replicate the observed value at time t-k [21].

3 Models Calibration and Residuals Analysis

The dataset adopted in the calibration is made of 224 hourly equivalent levels registered in proximity of the airport of Nice (France), during the Christmas period of 2000. The statistical characterization of the analysed data are reported in [18].

The most used technique to quantitatively check the performances of a forecasting model is the analysis of residuals. A positive residual will exploit an underestimation performed by the model, while a negative one will mean that the model is overestimating the actual value.

Briefly recalling what has been said in [18], when the abrupt change in the mean occurs, the SARIMA model takes about one day (24 periods) to adapt itself following the new slope of the data. On the contrary, DD-TSA model has constant coefficients and its prediction goes in the middle of the data, overestimating in the first part of the series and underestimating when the rise of the noise levels occurs. This explanation is confirmed by the difference in the MPE (Table 1), that is lower for the SARIMA model. In fact, since MPE is a percentage error, when a model gives a wrong prediction in the periods with higher values of the series, this error metric is lower.

Table 1. MPE, CVE and MASE (error metrics) values calculated in the calibration phase, for the two different models.

Model	MPE	CVE	MASE
DD-TSA	−1.559	0.118	0.750
SARIMA	−0.102	0.128	0.795

Figure 1 reports the frequencies histograms (1a and 1c) and the Q-Q plots (1b and 1d), respectively for the DD-TSA and the SARIMA models. All these plots prove the good overall performances of the models, in particular confirming the normal distribution of the residuals.

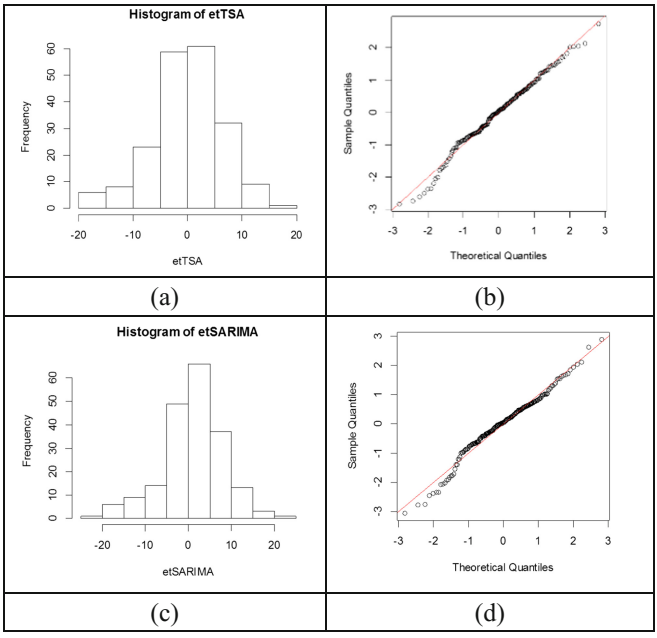

Fig. 1. Residuals of the DD-TSA (up) and SARIMA (down) models applied to the 224 calibration data: (a)-(c) are the histograms; (b)-(d) are the normal probability plot that describe the error behaviour compared to a normal distribution.

4 Forecasting

In order to verify the forecasting capacity of the proposed models, it was decided to carry out a validation phase using different data than those used for the calibration phase. In particular, noise emission levels were forecasted within 25 h immediately following those used for the construction of the models. The hours used for validation are from the beginning of 31 December 2000 to the first hour of 1 January 2001.

In Table 2 there are summary statistics of the validation period; the average value of about 53 dBA is comparable with that measured in the calibration period. The standard deviation of about 12 dBA is high, confirming that the observed signal is very variable in the considered range. The indexes of skewness and kurtosis suggest that the data is normally distributed.

Table 2. Summary of statistic main parameters of the 25 h of the validation data set.

	Mean [dBA]	Std.Dev. [dBA]	Median [dBA]	Min [dBA]	Max [dBA]	Skew	Kurt
Validation 25 Data	52.55	11.80	56.6	32.2	68.0	−0.53	−1.23

In Fig. 2 there is a comparison between the measured acoustical levels and the levels in the same periods forecasted by the two proposed models. In particular for the SARIMA is possible to observe both the one step ahead prediction (blue dotted line) and the same model using a 25 h forecast horizon (green dash-dot line).

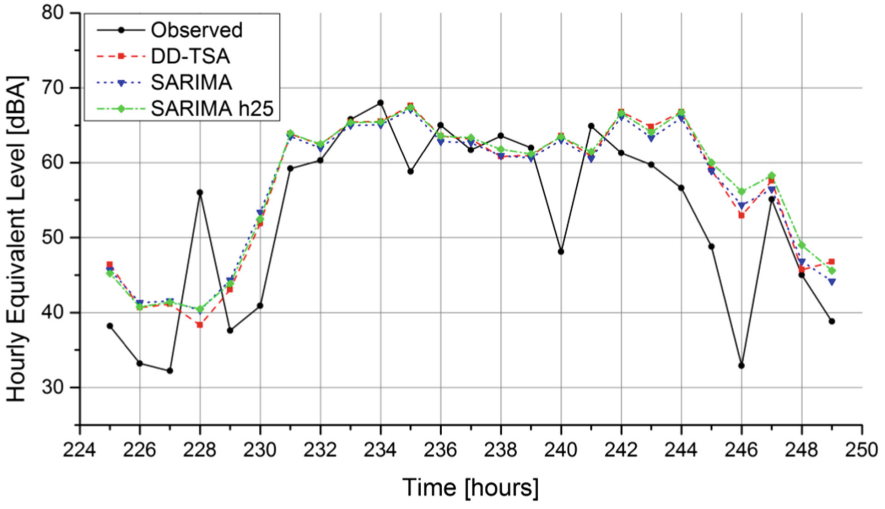

Fig. 2. Comparison between the observed 25 validation data and the levels in the same periods forecasted by the proposed models.

Table 3 shows the statistics of the forecasting errors: the general trend of the series is correctly reproduced by the proposed models, but in a few hours the variation of the levels is too fast to have low forecasting errors compared to the average measured value. The indexes of skewness and kurtosis suggest that the errors can be considered normally distributed.

Table 3. Summary statistics of the errors distribution evaluated on the validation dataset using the two proposed models.

Model	Mean [dBA]	Std.Dev. [dBA]	Median [dBA]	Min [dBA]	Max [dBA]	Skew	Kurt
DD-TSA	−4.24	7.45	−5.12	−20.01	17.67	0.56	1.24
SARIMA	−4.10	7.40	−4.33	−21.42	15.70	0.18	0.72
SARIMA h25	−4.66	7.41	−4.72	−23.25	15.53	0.15	2.21

The proposed error metrics, shown in Table 4, suggest that the SARIMA model may be preferred because it offers a slightly lower overall forecast error.

Table 4. MPE, CVE and MASE (error metrics) values calculated in the validation phase for the two different models.

Model	MPE	CVE	MASE
DD-TSA	−10.709	0.164	0.972
SARIMA	−10.611	0.162	0.954
SARIMA h25	−11.657	0.167	0.990

5 Conclusions

In this paper a time series analysis of acoustical noise measured near the international airport of Nice, France, has been performed. The aim of this research is to develop a model able to predict the hourly equivalent level. The complete dataset was split in a calibration series composed by 224 hourly levels, used to estimate parameters and coefficients of the models. The last part of dataset was preserved for a validation phase: 25 measurements were compared to the forecasts made by the models.

Two different methods have been implemented: deterministic decomposition (DD-TSA) and seasonal autoregressive moving average (SARIMA). The DD-TSA model has a large forecast horizon, while the SARIMA model was applied one step ahead and also with a forecast horizon of 25 h. The good performances of the two models were confirmed both in the calibration and in the validation phase. In the latter case, the SARIMA model showed a slightly lower error due to the short forecast horizon. Also the computed error metrics supported the conclusions given above. Finally, it can be concluded that, according to the dataset used in this application, if a large forecast horizon is needed, a DD-TSA model should be preferred, otherwise the proposed SARIMA model can provide a slightly better one step ahead prediction.

References

1. Air Passenger Market Analysis 2015, International Air Transport Association (IATA) (2016)
2. Schlenker, W., Reed Walker, W.: Airports, Air Pollution, and Contemporaneous Health, National Bureau of Economic Research (NBER), Working Paper No. 17684 (2011)
3. Genescà, M., Romeu, J., Arcos, R., Martin, S.: Measurement of aircraft noise in a high background noise environment using a microphone array. Transp. Res. Part D **18**, 70–77 (2013)
4. Quartieri, J., Troisi, A., Guarnaccia, C., Lenza, T.L.L., D'Agostino, P., D'Ambrosio, S., Iannone, G.: Application of a predictive acoustical software for modelling low speed train noise in an Urban environment. WSEAS Trans. Syst. **8**(6), 673–682 (2009). ISSN: 1109-2777
5. Quartieri, J., Troisi, A., Guarnaccia, C., Lenza, T.L.L., D'Agostino, P., D'Ambrosio, S., Iannone, G.: An acoustical study of high speed train transits. WSEAS Trans. Syst. **8**(4), 481–490 (2009). ISSN: 1109-2777
6. Guarnaccia, C.: Advanced tools for traffic noise modelling and prediction. WSEAS Trans. Syst. **12**(2), 121–130 (2013)
7. Guarnaccia, C., Lenza, T.L.L., Mastorakis, N.E., Quartieri, J.: A comparison between traffic noise experimental data and predictive models results. Int. J. Mech. **5**(4), 379–386 (2011). ISSN: 1998-4448
8. Guarnaccia, C.: Analysis of traffic noise in a road intersection configuration. WSEAS Trans. Syst. **9**(8), 865–874 (2010). ISSN: 1109-2777
9. Iannone, G., Guarnaccia, C., Quartieri, J.: Speed distribution influence in road traffic noise prediction. Environ. Eng. Manag. J. **12**(3), 493–501 (2013)
10. Guarnaccia, C., Quartieri, J.: Analysis of road traffic noise propagation. Int. J. Math. Models Methods Appl. Sci. **6**(8), 926–933 (2012)
11. Guarnaccia, C., Quartieri, J., Tepedino, C., Rodrigues, E.R.: A time series analysis and a non-homogeneous Poisson model with multiple change-points applied to acoustic data. Appl. Acoust. **114**, 203–212 (2016)
12. Guarnaccia, C., Quartieri, J., Mastorakis, N.E., Tepedino, C.: Environmental noise level threshold surpassing analysis by non-homogeneous Poisson model with informative and non-informative prior distributions. Int. J. Mech. **10**, 14–22 (2016)
13. Guarnaccia, C., Quartieri, J., Barrios, J.M., Rodrigues, E.R.: Modelling environmental noise exceedances using non-homogenous poisson processes. J. Acoust. Soc. Am. **136**, 1631–1639 (2014). https://doi.org/10.1121/1.4895662
14. Guarnaccia, C., Quartieri, J., Tepedino, C., Rodrigues, E.R.: An analysis of airport noise data using a non-homogeneous Poisson model with a change-point. Appl. Acoust. **91**, 33–39 (2015)
15. Guarnaccia, C., Quartieri, J., Mastorakis, N.E., Tepedino, C.: Development and application of a time series predictive model to acoustical noise levels. WSEAS Trans. Syst. **13**, 745–756 (2014)
16. Guarnaccia, C., Quartieri, J., Rodrigues, E.R., Tepedino, C.: Acoustical noise analysis and prediction by means of multiple seasonality time series model. Int. J. Math. Models Methods Appl. Sci. **8**, 384–393 (2014)
17. Guarnaccia, C., Quartieri, J., Tepedino, C.: Integration of ARIMA and software models for wind speed forecast and noise map prediction in a wind farm. Int. J. Math. Models Methods Appl. Sci. **10**, 259–269 (2016)

18. Guarnaccia, C., Quartieri, J., Tepedino, C.: Deterministic decomposition and seasonal ARIMA time series models applied to airport noise forecasting. In: Proceedings of the 2017 International Conference on Applied Mathematics and Computer Science, AIP Conf Proc, vol. 1836, pp. 1–7 (2017)
19. Cryer, P.D., Chan, K.: Time Series Analysis, with Applications in R, 2nd Edn. Springer (2008)
20. Franses, P.H.: A note on the mean absolute scaled error. Int. J. Forecast. **32**, 20–22 (2016)
21. Hyndman, R.J., Athanasopoulos, G.: Forecasting: Principles and Practice. OTexts (2013)

Express Registration of Partial Discharges in Gas-Insulated Switchgear

Alexandra Khalyasmaa[1(✉)], Stanislav Eroshenko[1], Egor Maryshko[2], and Alexandr Ovsiannikov[2]

[1] Ural Federal University Named After the First President of Russia B. N. Yeltsin, Mira Street, 19, 620002 Ekaterinburg, Russia
lkhalysmaa@mail.ru
[2] Novosibirsk State Technical University, Prospekt K. Marksa Street 20, 630073 Novosibirsk, Russia

Abstract. The paper presents the methodology of express partial discharge registration in gas-insulated switchgear without its decommissioning and internal intervention. Within the framework of the research the algorithm for calculating the number and location of partial discharge sensors was developed, based on the design features of the gas-insulated switchgear and the time-of-flight (wave) methodology of locating the focus of partial discharges, allowing for a minimum number of sensors to monitor all gas-insulated compartments.

Keywords: Gas-insulated switchgear · Partial discharge
Technical diagnostics

1 Introduction

Nowadays in modern power engineering gas-insulated equipment is increasingly being used for new construction and renovation: switchgear, high-voltage switches, current and voltage transformers, gas-insulated transmission lines, power transformers [1]. The equipment with SF_6 insulation is highly reliability, has compact dimensions, low fire risks, environmental safety and other benefits.

However, the tests that are carried out during the manufacturing and installation of the gas-insulated switchgear do not give the possibility to identify all the existing defects, as a result, some of the defects remain hidden and develop only after commissioning. According to statistics, more than 30% of all failures in gas-insulated switchgear are caused by hidden and operational defects. Therefore, reliable detection of the defects is the only way to prevent power equipment failures.

The control of the intensity of the partial discharges in gas-insulated switchgear is carried out mainly at the stage of commissioning tests and much less often - during the periods of scheduled maintenance. Taking into account the service life of the switchgear and repair intervals, the probability of missing the defect development stage remains considerable. A comprehensive solution to the problem of preventing gas-insulated switchgear failures could be continuous monitoring, however, the high cost of the monitoring systems justifies their installation only in exceptional cases.

K. Ntalianis and A. Croitoru (Eds.): APSAC 2017, LNEE 489, pp. 76–82, 2019.
https://doi.org/10.1007/978-3-319-75605-9_11

For these reasons, the development of low-cost, effective and non-destructive diagnostic methods for partial discharge identification in gas-insulated switchgear is of crucial importance.

2 Express-Diagnostics of Gas-Insulated Switchgear

Currently, the most common methods for registration of partial discharges in gas-insulated switchgear include taking out of service for repair and diagnostics or the installation of a real-time stationary partial discharge monitoring system. Both options presuppose significant financial costs [2]. For these reasons, the development and implementation of new non-destructive control methods of the gas-insulated switchgear are of great importance. Based on the analysis of national and foreign practical experience, the following key steps of the diagnostics were identified:

- analysis of main design solutions of the switchgear;
- selection of the type and location of partial discharge sensors;
- providing measures against external and internal interference;
- identification of partial discharge source location;
- identification of possible causes of partial discharge effect occurrence;
- determination of the danger rate of the partial discharges;
- providing recommendations for further actions.

2.1 Gas-Insulated Switchgear

Before starting the diagnostics, when analyzing the design of the switchgear, special attention is paid to the following aspects [3]:

- the type of the switchgear assembly;
- constructive design of separate modules connection of gas-insulated switchgear;
- the presence of radio-transparent windows in the shell of the switchgear;
- the presence of inputs “cable - SF_6”;
- the presence of air-gas-insulated inputs with condenser type insulation;
- the presence of built-in sensors of partial discharges (inductive, capacitive, electromagnetic).

2.2 Partial Discharge Sensors Selection and Allocation

Based on the analysis of design features of the gas-insulated switchgear under consideration, types of sensors and a list of places suitable for partial discharge registration are selected [4]:

- built-in capacitive partial discharge sensors;
- high-frequency current transformers (HCTT) on the grounding conductors of cables’ shields, grounding of cones of cable glands or testing air-gas-insulated inputs;
- add-on electromagnetic sensors on dielectric windows;

- add-on electromagnetic high-voltage or ultra-high-voltage sensors on dielectric belts at the junctions of modules;
- acoustic sensors on the surface of the switchgear shell.

The calculation of the optimal number of partial discharge sensors, which is necessary for effective control of the entire internal volume of the gas-insulated switchgear, is carried out according to the following expression:

$$D_{PD} = 3 \cdot N_{inp} + T_{GIS} \cdot N_{bus} \quad (1)$$

where N_{inp} – the number of gas-insulated switchgear inputs; N_{bus} – the amount of switching points of gas-insulated switchgear buses; T_{GIS} – gas-insulated switchgear design (for single-phase – 3, for three-phase – 1).

The proposed approach requires 3–4 times smaller number of partial discharge sensors, than in case of each gas-insulated switchgear compartment control.

2.3 External and Internal Interference Reduction Methods

The problem of transmitted signal protection from induced interference is solved using a developed fiber optic channel, the functional diagram of which is shown in Fig. 1. The fiber optic channel includes the following elements [5]:

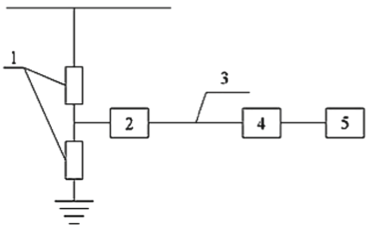

Fig. 1. Fiber-optical measuring channel: *1*-sensor, *2*-transmitter, *3*-fiber-optic link, *4*-receiver, *5*-recording device

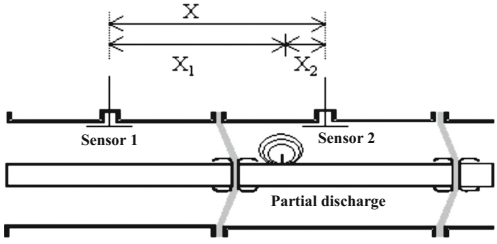

Fig. 2. Identification of the distance between the sensor and partial discharge source in gas-insulated switchgear

- transmitter that converts the electrical signal at the output of the discharge sensor;
- signal transmission channel - fiber-optic communication line;
- receiver - a device, that converts an optical signal into an electrical signal.

2.4 Partial Discharge Source Identification

Firstly, it is necessary to identify whether the source of the partial discharge is inside the object under consideration or outside it. When performing express diagnostics, the switchgear is not taken out of the operation, therefore, it is not an isolated object and it

is connected to other substation equipment by means of cable links or by means of busbars via air-gas-insulated inputs.

The second step is to determine the location of the partial discharge source inside the switchgear. It is made on the basis of time tag comparison of the signals, arriving to separate sensors of the metering circuit (Fig. 2).

The distance X between the sensors is calculated from the design drawings of the switchgear. Then the distance between the partial discharge source and the first sensor is calculated according to the following equation:

$$X_1 = [X - (X_1 - X_2)]/2 = [X + c \cdot \Delta T]/2 \quad (2)$$

where X – the distance between the first and the second sensor, X_1 – the distance between the partial discharge source and the first sensor, X_2 – the distance between the partial discharge source and the second sensor, c – electromagnetic wave propagation speed c = 0,3 m/ns, ΔT– the difference between the time tags of the sensors.

2.5 Determination of Possible Causes of Partial Discharge and the Danger Level for the Subsequent Operation

Depending on the location of the partial discharge source, it is possible to determine the potential causes of its occurrence, as described in Table 1.

Table 1. Partial discharge causes

Partial discharge source	Defect description
Located in the junction of the compartments of gas-insulated switchgear	A typical source of partial discharges are microcavities or microcracks in support insulators separating the compartments of gas-insulated switchgear
Located near the module, containing a current or voltage transformer	The potential source of the partial discharge is the damaged insulation of the current or voltage transformer
Located near the cable or overhead wire input	The potential source of the partial discharge is the end of the input “cable - SF_6 gas” or the input “air - SF_6 gas”
Located near the busbar module, which does not contain any additional equipment	Potential source of partial discharge is free metal particles

3 Case Study

The validation of the developed method of express registration of partial discharges is carried out on the basis of diagnostics of the technical state of a 220 kV SF_6 switchgear at 220 kV Substation Vlasikha in Barnaul, Russia. Measurements for partial discharges identification was carried out using high-frequency current transformers RFCT-4

manufactured by Dimrus and a digital oscilloscope Tektronix DPO3014. The following measurements were made:

- synchronous measurement of the signals from different points of sensors connection on the cable entry;
- synchronous measurement of signals on the grounding of the cones of the three phases of the "cable-SF_6" inputs;
- synchronous measurement of signals on the grounding of the cones of all cable inputs, separately for each phase.

The identification of the source of the signal within the diagnosed object was determined using a time-of-flight (wave) method. The results are shown in Table 2.

Table 2. First negative peak parameters

Channel	Peak recording time, ns	Signal arrival delay relative to the time of the first registration, ns	Signal amplitude, mV
1	129592,8	0,4	26,78
2	129592,4	0	28,19
3	129737,6	145,2	3,23
4	129660,0	67,6	2,76

The calculation of the signal travel time and the distance from the source of partial discharge to the sensor 2 is carried out according to (3):

$$T_2 = [L/c + \Delta T]/2,\ X_2 = [L + c \cdot \Delta T]/2 \tag{3}$$

The propagation velocity of the signal was assumed to be equal to the speed of light c = 299792458 m/s. On the basis of the design documentation, the distance between the sensors of the 1st and 2nd channels was determined, where the signal from the partial discharge source was initially detected L = 18 m. The running time to the second channel sensor was T2 = 28 ns, which corresponds to a distance of 8,4 m.

The most accurately recorded signal (Fig. 3) in terms of the amplitude and the shape corresponds to the oscillogram obtained for the defect model "current conductor protrusion - shell of the switchgear", combined with dielectric particles in the discharge gap (Fig. 4). The cause of the protrusion appearance on the conductor can be the low quality of surfacing of the current conductor during production or the damage, obtained during installation of the switchgear. Dielectric particles inside the pressurized shell of the switchgear compartment is usually a metal dust, that appeared inside the shell during installation works. Such dust is usually concentrated around the increased electric field strength. The apparent charge of partial discharges calculated from the oscillogram is 4.98 pC. The following conclusions can be drawn:

- The source of partial discharge is a small protrusion on the current conductor, possibly with the presence of free dielectric particles in the discharge gap.

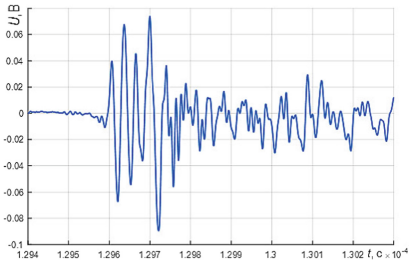

Fig. 3. Oscillogram of the signal registered inside the switchgear

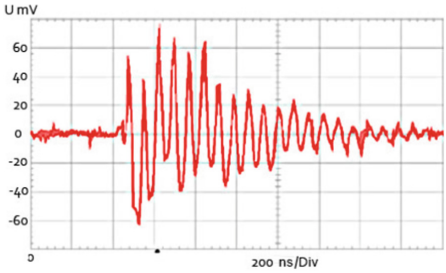

Fig. 4. Signal template of the defect "protrusion on current conductor gas-insulated switchgear shell" plus dielectric particles

- The apparent charge of the partial discharge does not exceed 5 pC and in accordance with [6] does not exceed the marginal level for the equipment.
- The equipment is in a good technical state, further operation is possible.

4 Conclusion

Diagnostics or monitoring of the technical state of gas-insulated switchgear requires the control of the pressure of SF_6 gas and its properties, as well as the detection and assessment of the number of defects on the basis of partial discharge intensity records. Most of the types of partial discharge analysis are carried out in the framework of commissioning tests at the installation site of the switchgear, and the installation of continuous monitoring systems requires additional capital investment.

Within the framework of this study, a device for transmitting a signal over a fiber-optic link has been developed, providing protection against induced interference and galvanic isolation of recording equipment and the object under consideration. To clean the signal from low-frequency interference, a high-pass filter is proposed and tested based on a section of a coaxial cable. An algorithm has been developed for calculating the optimum number of partial discharge sensors for the rapid diagnostics of the gas-insulated switchgear.

New methods of simulating the partial discharge for calibrating the registration system are proposed. In practice, the possibility of using the developed method of express registration of partial discharges in the switchgear is verified.

References

1. Report of CIGRE WG 23.10. SF6 and the Global Atmosphere. Electra, No. 164, pp. 121–132 (1996)
2. Arakelian, V.G.: Diagnostics for the condition of SF6 equipment based on physico-chemical parameters. IEEE Electr. Insul. Mag. **17**(2), 42–51 (2001)

3. Van Brunt, R.J.: Stochastic properties of partial-discharge phenomena [Текст]. IEEE Trans. Electr. Insul. **26**, 902–948 (1991)
4. Arshansky, I.S.: The development of SF6-insulated test-sets for GIS dielectric tests. In: Proceedings of 9th International Symposium on High Voltage Engineering, Graz, Austria, Report 5276 (1995)
5. Halkiadis, I.S.: A high-voltage low-cost wide-band fiber optic transmission system with improved linearity [Текст]. Electric Power Systems Research, No. 37, pp. 121–128 (1996)
6. National Standard GOST 1516.3-96. Alternating current power equipment 1–750 kV. Insulation requirements (1996)

Computers

Risk Factors for the Occurrence of Traumatic Vacuum Phenomenon After Chest Compression for Patients with Cardiac Arrest

Youichi Yanagawa(✉), Kouhei Ishikawa, Hiroki Nagasawa, Ikuto Takeuchi, Suguru Kato, Kei Jitsuiki, Takashi Iso, Toshihiko Yoshizawa, Hiromichi Ohsaka, and Kazuhiko Omori

Department of Acute Critical Care Medicine, Juntendo Shizuoka Hospital, 1129 Nagaoka, Izunokuni, Shizuoka 410-2295, Japan
yyanaga@juntendo.ac.jp

Abstract. We retrospectively investigated the risk factors for the occurrence of traumatic vacuum phenomenon (TVP) after chest compression for patients with cardiopulmonary arrest (CPA) using computed tomography (CT). A medical chart review was performed for all patients with out-of-hospital endogenous CPA. The subjects were divided into two groups: TVP + group and the TVP – group. 110 patients were enrolled as subjects. TVP was observed in 33. The rates of witness collapse and rib fracture were significantly higher in the TVP + group than in the TVP – group. The duration from the commencement of CPR by emergency medical technicians to the CT examination in the TVP + group was significantly longer than in the TVP – group. Accordingly, among patients with out-of-hospital CPA, witness collapse, rib fracture and a longer duration from the commencement of cardiopulmonary resuscitation (CPR) by EMTs to the CT examination were risk factors for TVP.

Keywords: Traumatic vacuum phenomenon · Cardiopulmonary arrest
Chest compression · Rib fracture

1 Introduction

Chest compressions for patients with cardiopulmonary arrest (CPA) are recommended at a rate of 100–120/min with adequate compression depth (5–6 cm) because the blood flow is created primarily by increasing the intrathoracic pressure and directly compressing the heart, which in turn results in critical blood flow and oxygen delivery to the heart and brain [1, 2]. The 2015 Guideline recommends pushing harder than the 2010 Guideline (at least 5 cm) [2].

In the human body, if an enclosed tissue space is allowed to expand as a rebound phenomenon after an external impact, the volume within the enclosed space increases. With this expanding volume, the pressure within the space decreases, resulting in the solubility of the gas in the enclosed space also decreasing. This decreased solubility allows a gas to leave a solution. The combination of a reduced nitrogen solubility and

K. Ntalianis and A. Croitoru (Eds.): APSAC 2017, LNEE 489, pp. 85–91, 2019.
https://doi.org/10.1007/978-3-319-75605-9_12

the minimal metabolism of nitrogen by the body mainly accounts for the formation of gas, known as vacuum phenomenon (VP) [3].

Chest compression can also cause rib fractures [4–7]. VP is observed at locations that experience a traumatic impact; therefore, an analysis of traumatic VP (TVP) may be useful for determining the mechanism underlying an injury [8]. However, there have been no reports investigating the occurrence of TVP induced by chest compressions. Accordingly, we retrospectively investigated whether or not TVP occurred due to chest compression; if TVP did occur, we evaluated the risk factors for the occurrence of TVP after chest compression for patients with CPA using computed tomography (CT).

2 Methods

This retrospective study protocol was approved by the review board of Juntendo Shizuoka Hospital. The Department of Acute Critical Care Medicine is located in Shizuoka Hospital, a 552-bed hospital of Juntendo University in the Izu Peninsula in Shizuoka Prefecture (near Tokyo). Our hospital has helicopter landing pads and an emergency medical system utilizing physician-staffed emergency helicopters in Eastern Shizuoka Prefecture and serves a population of approximately 1,000,000.

From February 2016 to March 2017, a medical chart review was retrospectively performed for all patients with out-of-hospital endogenous CPA who were treated by our department staff. The exclusion criteria included CPA in the hospital, exogenous CPA (trauma, hanging, suffocation, or poisoning), and a lack of a CT examination. In our study, a CT examination and biochemical analysis for blood were routinely performed if a patient was not in the terminal stage of cancer unless informed consent could not be obtained.

The subjects were divided into two groups: the TVP + group, which included patients who had TVP identified by CT, and the TVP – group, which included patients who did not have TVP. TVP was defined as linear or oval radiolucency in the tissue corresponding to gas where it was not normally located (Figs. 1, 2 and 3) and was excluded when CT revealed pneumothorax.

The characteristics of the patients (age, sex, witness collapse, bystander cardiopulmonary resuscitation [CPR], initial rhythm at scene, value of base excess on arrival, method of transportation [air or ground ambulance], duration from commencement of CPR by emergency medical technicians [EMTs] to the CT examination, rib fracture, return of spontaneous circulation, and the survival rate) were analyzed between the TVP + and TVP – groups. CT was performed immediately after ceasing resuscitation or obtaining stable circulation at our department. Accordingly, the duration from the commencement of CPR by the EMTs to the CT examination represented the duration of CPR executed by professional medical workers.

Both the chi-squared test and the non-paired Student's t-test were used for the statistical analyses. P values of <0.05 were considered to be statistically significant.

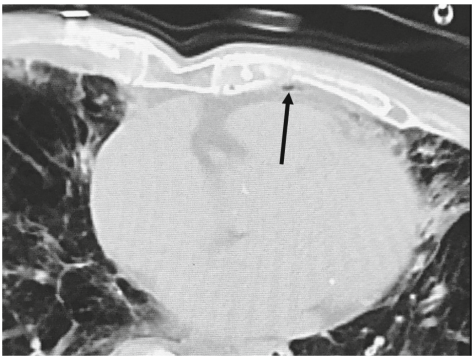

Fig. 1. Traumatic vacuum phenomena in the anterior mediastinum. Gas density can be seen in the anterior mediastinum (black arrow).

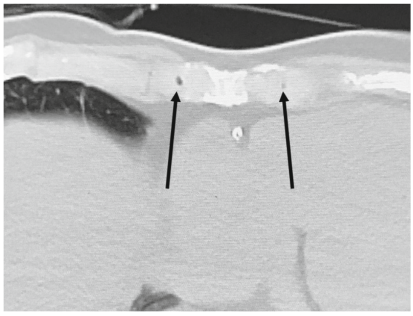

Fig. 2. Traumatic vacuum phenomena in the costal cartilage. Gas density can be seen in the costal cartilage (black arrow).

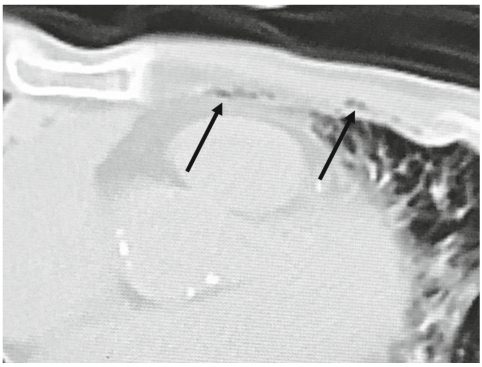

Fig. 3. Traumatic vacuum phenomena in the anterior mediastinum and near a fractured rib. Gas density can be seen in the anterior mediastinum (left black arrow) and near a fractured rib (right black arrow).

3 Results

During the investigation period, a total of 196 patients with CPA were treated by the staff of our department. Among these patients, seven were inpatients who suddenly collapsed. Another 62 had exogenous CPA induced by trauma, hanging, or poisoning. Another 17 did not undergo CT. After excluding these 86 patients, 110 remained and were enrolled as subjects in the present study.

The results of the analyses between the TVP + and TVP – groups are summarized in Table 1. TVP was observed in 33 subjects. The average age, gender, rates of bystander CPR, initial rhythm, method of transport, return of circulation, value of base excess, and the survival ratio were not significantly different between the groups. The rate of witness collapse and rib fracture were significantly higher in the TVP + group than in the TVP – group. The duration from the commencement of CPR by the EMTs to the CT examination in the TVP + group was significantly longer than in the TVP – group.

Table 1. The results of the analyses between the vacuum phenomena (TVP) + and – groups

Variables	TVP + (n = 33)	TVP – (n = 76)	p-value
Age (years)	68.8 ± 2.4	72.6 ± 1.9	n.s.
Sex (male/female)	26/7	48/28	n.s.
Witness collapse (yes/no)	27/46	40/36	0.01
Bystander chest compression (yes/no)	13/20	38/38	n.s.
Initial rhythm at scene			n.s.
Asystole	24	43	
Pulseless electrical activity	5	22	
Ventricular fibrillation	4	11	
Method of transport (air/ground ambulance)	8/25	23/53	n.s.
Duration of basic life support by EMTs (min)	56.6 ± 1.9	48.8 ± 1.8	0.01
Rib fracture (yes/no)	29/4	49/27	<0.01
Return of circulation (yes/no)	4/26	20/56	n.s.
Base excess (mmol/L)	–21.7 ± 1.2	–18.7 ± 1.1	n.s.
Survival rate (%)	1/32 (3.1%)	1/75 (1.3%)	n.s.

EMTs: emergency medical technicians; n.s.: not significant

The rate of witness collapse and rib fracture were significantly higher in the TVP + group than in the TVP – group.

Traumatic vacuum phenomena was found mainly in the anterior portion of the thoracic gage directly affected by chest compressions (Table 2).

Table 2. Location and number of traumatic vacuum phenomena

Location	Number
Anterior mediastinum	12
Costal cartilage	9
Rib (fracture)	7
Anterior chest wall	6
Sterno-clavicular joint	3

4 Discussion

This is the first report to demonstrate that, among patients with out-of-hospital CPA, TVP could be inducible by chest compression, and witness collapse, rib fracture, and a longer duration from commencement of CPR by the EMT to the CT examination were factors for TVP.

Clinically, the differentiation of subcutaneous emphysema from vacuum phenomenon is important. Subcutaneous emphysema can be produced by a number of diseases, such as injury to the trachea, bronchus, lung, esophagus, and gastroenterocolon; positive pressure gas-related injury; and iatrogenic conditions such as pneumoperitoneum, soft tissue injury, or infection [8–12]. Among these disease, lung injury is a common cause of subcutaneous emphysema and pneumothorax. In some patients with pleural adhesion, lung injury causes only isolated subcutaneous emphysema without pneumothorax. However, in this study, 33/110 (30%) had TVP, an extremely high frequency if all of the patients had pleural adhesion. In addition, we did not count the number of TVP cases in which the patients had pneumothorax. Accordingly, the possibility of subcutaneous emphysema or pneumomediastinum from lung injury was low.

The existence of rib fracture and a longer duration from the commencement of CPR by EMTs to the CT examination may have been because the risk of TVP increases with the number and strength of chest compressions, as these are a traumatic insult. Of note, however: the existence of chest compressions executed by a bystander did not markedly affect the occurrence of the TVP. This might be because the duration of chest compressions by bystanders was shorter than that of compressions executed by professional health workers (data not shown). The quality of chest compressions may also be related to the risk of TVP. The quality of CPR executed by EMTs is presumed to be adequate, based on training and experience, compared with a lay person [8, 13]. This difference in CPR quality between bystanders and professional health workers may have resulted in a greater occurrence of TVP induced by chest compressions delivered by professional health workers. However, witness collapse was associated with an increased risk of the TVP, possibly because the professional health workers pushed down on the chest more aggressively than usual because such patients still had a chance of surviving and achieving social rehabilitation compared with non-witnessed collapse.

The present study is associated with several limitations, including its retrospective design and the small number of patients in the study population. Future prospective studies involving a larger number of patients are therefore needed to further examine this issue.

5 Conclusion

The present study showed that, among patients with out-of-hospital CPA, TVP can be inducible by chest compressions, and witness collapse, rib fracture, and a longer duration from commencement of CPR by the EMT to the CT examination were factors for TVP.

Acknowledgments. This work received funding from Ministry of Education, Culture, Sports, Science and Technology (MEXT)-Supported Program for the Strategic Research Foundation at Private Universities, 2015–2019. The title is [The constitution of total researching system for comprehensive disaster, medical management, corresponding to wide-scale disaster].
Conflict of Interest Statement. We obtained financial support from Pfizer Corporation.

References

1. Travers, A.H., Perkins, G.D., Berg, R.A., Castren, M., Considine, J., Escalante, R., Gazmuri, R.J., Koster, R.W., Lim, S.H., Nation, K.J., Olasveengen, T.M., Sakamoto, T., Sayre, M.R., Sierra, A., Smyth, M.A., Stanton, D., Vaillancourt, C.: Basic life support chapter collaborators. Part 3: adult basic life support and automated external defibrillation: 2015 international consensus on cardiopulmonary resuscitation and emergency cardiovascular care science with treatment recommendations. Circulation **132**(16 Suppl. 1), S51–S83 (2015)
2. American Heart Association: Highlights of the 2015 American Heart Association Guidelines update for CPR and ECC (2015)
3. Koga, Y., Fujita, M., Yagi, T., Nakahara, T., Miyauchi, T., Kaneda, K., Kawamura, Y., Oda, Y., Tsuruta, R.: Effects of mechanical chest compression device with a load-distributing band on post-resuscitation injuries identified by post-mortem computed tomography. Resuscitation **96**, 226–231 (2015)
4. Hoke, R.S., Chamberlain, D.: Skeletal chest injuries secondary to cardiopulmonary resuscitation. Resuscitation **63**, 327–338 (2004)
5. Oberladstaetter, D., Braun, P., Freund, M.C., Rabl, W., Paal, P., Baubin, M.: Autopsy is more sensitive than computed tomography in detection of LUCAS-CPR related non-dislocated chest fractures. Resuscitation **83**, e89–e90 (2012)
6. Lederer, W., Mair, D., Rabl, W., Baubin, M.: Frequency of rib and sternum fractures associated with out-of-hospital cardiopulmonary resuscitation is underestimated by conventional chest X-ray. Resuscitation **60**, 157–162 (2004)
7. Ohsaka, H., Ishikawa, K., Jitsuiki, K., Yanagawa, Y.: Factors affecting difficulty in extubation after initial successful resuscitation in cardiopulmonary arrest patients. J. Emerg. Trauma Shock **9**, 88–89 (2016)
8. Jeavons, R.P., Dowen, D., Rushton, P.R., Chambers, S., O'Brien, S.: Management of significant and widespread, acute subcutaneous emphysema: should we manage surgically or conservatively? J. Emerg. Med. **46**, 21–27 (2014)
9. Lin, L.W., Wu, C.C., Chong, L.W., Lin, A.C.: Periampullary diverticulum perforation following endoscopic retrograde cholangiopancreatography (ERCP); a case report. Emergency (Tehran) **3**, 78–80 (2015)
10. Parmaksızoglu, F., Koprulu, A.S., Unal, M.B.: Massive subcutaneous emphysema and pneumomediastineum after finger subtotal amputation with barotrauma. J. Emerg. Med. **41**, e79–e82 (2011)

11. Chang, C.Y., Cheng, S.L., Chang, S.C.: Conservative treatment of severe tracheal laceration after endotracheal intubation. Respir. Care **56**, 861–862 (2011)
12. Verelst, W., Verbrugghe, W., Lammens, M., Snoeckx, A., Jorens, P.G.: Ventilation-induced massive lethal air embolism and subcutaneous emphysema in a patient with a lung cavern. Respir. Care **60**, e6–e10 (2015)
13. Kajino, K., Kitamura, T., Iwami, T., Daya, M., Ong, M.E., Nishiyama, C., Sakai, T., Tanigawa-Sugihara, K., Hayashida, S., Nishiuchi, T., Hayashi, Y., Hiraide, A., Shimazu, T.: Impact of the number of on-scene emergency life-saving technicians and outcomes from out-of-hospital cardiac arrest in Osaka City. Resuscitation **85**, 59–64 (2014)

Security and Performance of a Textual Substitution Compression Method Applied to Images

Bruno Carpentieri(✉)

Dipartimento di Informatica, Università di Salerno, 84084 Fisciano, SA, Italy
bc@dia.unisa.it

Abstract. This paper discusses the performances and security of a textual substitution compression algorithm applied to images. This algorithm derives from the blending of the Lempel-Ziv compression methods and the Vector Quantization compression approach: it is called Adaptive Vector Quantization (AVQ). We review the performance and the security of AVQ and present new testing results on a specific set of medical images: the baropodometric images.

Keywords: Data compression · Textual substitution algorithms

1 Introduction

The lossless compression schemes known as Lempel-Ziv algorithms belongs to the class of "textual substitution compression methods" and are also known as "dictionary methods".

The basic idea is to replace part of the current input (this is the "textual substitution") with a pointer into a history buffer or a dictionary. The buffer or the dictionary are dynamic in the sense that their content is updated at each coding step and it is input dependent.

These encoders produce good compression rates with good decompression speed.

Another widely used family of compression methods in the class of dictionary encoders is the one known as Vector Quantizers. These encoders are meant for multidimensional data and are generally lossy (i.e., the decoded output won't be a perfect reconstruction of the original input) and static (i.e., a dictionary is constructed off–line and transmitted along with the encoded data).

In this paper we discuss and analyze a blending of the Vector Quantization ideas with the dynamic nature of Lempel-Ziv methods and review the AVQ compression algorithm. Moreover here we also present new testing results on a specific set of medical images: the baropodometric images.

2 Two-Dimensional Textual Substitution Methods

Two-dimensional (i.e. images) applications of textual substitution methods have been widely studied in the past.

K. Ntalianis and A. Croitoru (Eds.): APSAC 2017, LNEE 489, pp. 92–97, 2019.
https://doi.org/10.1007/978-3-319-75605-9_13

At the beginning a linearization strategy was applied to the images, to then encode the resulting mono-dimensional vector by using standard, textual substitution, one dimensional, methods [1].

Storer in [2] suggested the possibility of using dynamic dictionary methods in combination with Vector Quantization for lossless and lossy compression of bi-dimensional data.

The AVQ algorithm of Constantinescu and Storer [3] pioneered this approach by showing that it has a number of advantages with respect to current state-of-the art algorithms such as JPEG. This algorithm has been improved and applied to new types of data in [4–7].

2.1 The AVQ Compression Algorithm

The coding process in AVQ proceeds in a way that is similar to the classical textual substitution paradigm (see [2]). We define as *Growing Border* the set of locations in the input image that have not been coded yet and that are closest to the already coded locations. A Growing Point is any not yet coded point where a match may take place. Generally we assume that the growing points come from the growing border and that they are located in corners.

The data structure that stores the growing points is called the *Growing Points Pool*.

A *Growing Method* is a set of rules that is used to identify the next growing point that will be processed. There are many different ways to implement the growing method (see [4]).

At each step the AVQ algorithm selects a growing point *gp* of the input image. The encoder uses a *Match Method* to decide which block *b* of a local dictionary *D* is the best match for the sub-block anchored in *gp* of the same shape as *b*. The match method chooses the largest block for which the distortion from the original block (namely the mean squared error) is less or equal to a threshold *T*.

The threshold *T* could be fixed for the whole image, or dynamically adjusted to the image content: higher for smooth areas, lower for zones with large variance (as in the presence of sharp edges).

When the encoding process starts, the local dictionary *D* contains one entry for each possible pixel value; during the encoding process *D* is updated by using a *Dictionary Update Method*, possibly preceded by a *Deletion Method*.

Figure 1 presents a baropodometric image (left) and its covering by using elements of the dictionary (right). To show the covering the dictionary elements in the figure are shown in false colors and not with their real pixel values. The figure outlines the behaviour of the algorithm: the covering has started at the center of the image and then has spread in a circular way (the *circular* growing heuristic was used). Larger blocks correspond to areas of constant values in the image, smaller blocks correspond to "active" areas in the image.

2.2 Secure Transmission of Compressed Images

Data Compression is motivated by the economic and logistic needs to save space in storage media and to save bandwidth in communication. Today the main application of

Fig. 1. An AVQ covering of a monopodalic baropodometric image.

data compression techniques is data transmission. Without an efficient usage of the data compression techniques we would not have digital television, cellular phones, satellite communication and all the other applications in which digital data transmission is involved.

This implies that there are often strong security requirements for the transmission of compressed data. Digital watermarking techniques are an efficient approach for ensuring security, content authentication and copyright protection [8, 9]. By means of such techniques, the input data (i.e., compressed images) might become a sort of information carrier which can be used for delivering important data [10].

In [5] we have considered the security of AVQ compressed images by using watermarks. The key idea is to embed the watermark in one or more blocks of the dictionary by using a standard watermarking algorithm. The encoder therefore knows which are the watermarked the blocks and when the compression algorithm uses these blocks it will do, only for these blocks, a lossless encoding. All the blocks containing a watermark in the dictionary are therefore marked and they shall be used with high priority. With this method the watermark is spread all over the image and the robustness and the security of this approach is very effective.

3 Compressing Baropodometric Images

The baropodometric images: are images obtained through a medical examination that allows to evaluate the quality of the ground support of the feet.

The test provides information on the pressures that are exchanged between the foot resting surface and the ground and it evaluates in depth the way the subject walks. The analysis is carried out using a baropodometric pad. There are both static and dynamic analysis. Static analysis is performed by a 4-s test at mono and bipodal standing. This study allows to quantitatively evaluate defects in support, overload areas, and to determine the percentage of body weight distribution on the lower limbs and to check the weight shift and loading times.

Dynamic analysis evaluates the progresses of the footprints during the steps by examining the percentage distribution of the support and load surface between the two footprints and between the front and the forefoot. The defects of the support can be evaluated and they are visualized a series of graphs showing the progress of the significant parameters during the walking such as the supporting surface, the laterality and the speed of the advancement of the pressure barriers and the vertical component of the pushing force of the foot on the platform.

The images of the dataset are therefore both monopodal and bipodal.

3.1 AVQ Compression of Baropodometric Images

The AVQ compression algorithm was tested on a dataset of ten images: five monopodalic and five bipodalic. For all the tests a variable dictionary size (between 29 and 215) was chosen with a match heuristic MSE (see [5]) with value 20.0.

AVQ was tested in lossy mode and the quality parameter was set to “high”. The output of the compression process was presented to a panel of doctors that acknowledged that the quality was good enough for baropodometric analysis.

Table 1 shows the compression results obtained on monopodalic images, Table 2 the results on bipodalic images.

Table 1. AVQ compression of monopodalic images.

File name	Input size	Output size	Compression ratio
3.bmp	37.251 bytes	7.918 bytes	4,7045
4.bmp	39.953 bytes	7.686 bytes	5,1981
9.bmp	32.032 bytes	8.020 bytes	3,9940
10.bmp	27.479 bytes	7.065 bytes	3,8894
11.bmp	33.792 bytes	8.333 bytes	4,0552

These results are comparable with the results obtained by standard lossless compression algorithms such as *gzip* and *bzip* that obtain on the same images compression ratios ranging from 2 to 4.

Table 2. AVQ compression of bipodalic images.

File name	Input size	Output size	Compression ratio
0.bmp	12.452 bytes	3.689 bytes	3,3754
1.bmp	14.339 bytes	4.366 bytes	3,2842
2.bmp	16.072 bytes	4.802 bytes	3,3469
5.bmp	12.598 bytes	3.890 bytes	3,2385
6.bmp	12.130 bytes	3.871 bytes	3,1335

The compression ratio depends also on the image size, for example the compression results are very good for the image 4.bmp that is the larger image in the monopodalic test set.

Bipodalic images are smaller therefore the AVQ algorithm performs better on monopodalic images.

4 Conclusions and Future Work

In this paper we have discussed the performance and security of the AVQ compression algorithm.

For the security of the transmission of AVQ compressed images we have shown that AVQ can exploit the performances of a classic watermarking algorithm when this algorithm is applied to dictionary blocks because in this case AVQ spreads the watermark all over the compressed image.

We have then presented an AVQ compression test on a specific set of medical images: the baropodometric images. The results of this test are encouraging because they show that AVQ, even in lossy mode, produces an efficient output that can be used by doctors for the analysis of both monopodalic and bipodalic baropodometric images.

Future work includes a deeper test of the AVQ performances on medical images and also the compression of a wider test set of baropodometric images that shall be compressed as an image sequence, letting the AVQ dictionary grow without initializing it every time we code a new baropodometric image.

Acknowledgements. We would like to thank our students Leo and Lomasto for carrying on the preliminary tests on the AVQ compression of baropodometric images.

References

1. Lempel, A., Ziv, J.: Compression of two-dimensional images. In: Galil, Z., Apostolico, A. (eds.) Combinatorial Algorithms of Words. NATO ASI Series, vol. 12. Springer, Heidelberg (1985)
2. Storer, J.A.: Data Compression: Methods an Theory. Computer Science Press, New York (1988)
3. Constantinescu, C., Storer, J.A.: Improved techniques for single-pass adaptive vector quantization. Proc. IEEE **82**(6), 933–939 (1994)

4. Carpentieri, B.: Image compression via textual substitution. WSEAS Trans. Inf. Sci. Appl. **6** (5), 768–777 (2009)
5. Pizzolante, R., Carpentieri, B., Castiglione, A., De Maio, G.: The AVQ algorithm: watermarking and compression performances. In: Proceedings of the 3rd IEEE International Conference on Intelligent Networking and Collaborative Systems (INCoS). IEEE Press (2011)
6. Pizzolante, R., Carpentieri, B.: Lossless, low-complexity, compression of three-dimensional volumetric medical images via linear prediction. In: 18th International Conference on Digital Signal Processing (DSP) (2013)
7. Pizzolante, R., Carpentieri, B., De Agostino, S.: Adaptive vector quantization for lossy compression of image sequences. Algorithms **10**(2), 51 (2017)
8. Albano, P., Bruno, A., Carpentieri, B., Castiglione, A., Castiglione, A., Palmieri, F., Pizzolante, R., Yim, K., You, I.: Secure and distributed video surveillance via portable devices. J. Ambient Intell. Humaniz. Comput. **5**(2), 205–213 (2014)
9. Albano, P., Bruno, A., Carpentieri, B., Castiglione, A., Castiglione, A., Palmieri, F., Pizzolante, R., Yim, K., You I.: A Secure distributed video surveillance system based on portable devices. In: Quirchmayr, G., Basl, J., You, I., Xu, L., Weippl, E. (eds.) Multidisciplinary Research and Practice for Information Systems. CD-ARES. LNCS, vol. 7465. Springer, Heidelberg (2012)
10. Pizzolante, R., Carpentieri, B., Castiglione, A., Castiglione, A., Palmieri, F.: Text compression and encryption through smart devices for mobile communication. In: 7th International Conference on Innovative Mobile and Internet Services in Ubiquitous Computing, IMIS 2013 (2013)

A Solution of the Mastermind Board Game in Scratch Suitable for Algorithmic Thinking Development

Tomas Hornik(✉), Petr Coufal, Michal Musilek, and Stepan Hubalovsky

University of Hradec Kralove, Hradec Kralove, Czech Republic
{tomas.hornik, petr.coufal, michal.musilek, stepan.hubalovsky}@uhk.cz

Abstract. The article is a case study of a specific problem - popular board game Mastermind and its solution in Scratch, visual online programming language. Emphasis is put on the educational perspective both in the logic behind the solution itself and on the way the problem can be presented to elementary school pupils. The article is focused on logical explanation of the solution and on work with several specific programming elements, like IF-ELSE conditions, data structures and simple bug hunting feature. The difficulty is suitable for elementary school pupils as a complex task meant for superior individuals or a group of pupils. It was successfully tested as a small scale preliminary study conducted on pupils aged between 11 and 14 at an extracurricular group.

Keywords: Algorithmic thinking · Algorithm development · Education
Elementary school · Mastermind game solution · Programming
Scratch

1 Introduction

The teaching of algorithm development and programming is no longer a domain of highly specialized and technically oriented high schools and universities, but progressively appears at elementary schools as well [11]. There were some attempts on children programming languages as far back as in 1960s, for example KAREL or LOGO [1]. Both of them are still used, albeit in a limited extent. Text based programming languages are in education being at least accompanied (if not replaced) by visual languages, such as Blockly, Scratch, Snap!, KODU, LEGO Mindstorms NXT-G, and many others. All these languages are very robust and can be used for creation of complex codes. Following chapters deal with a solution of board game Mastermind in Scratch, which goes beyond re-creating the game, because it also includes an algorithm by means of which the computer can solve every game of the original Mastermind (six colors, four positions) in maximally ten rounds.

K. Ntalianis and A. Croitoru (Eds.): APSAC 2017, LNEE 489, pp. 98–104, 2019.
https://doi.org/10.1007/978-3-319-75605-9_14

2 Problem Formulation

Mastermind is a commercial logical board game for two players that develops logical thinking. One player hides a secret code (combination of colors on certain positions), while the other one is trying to find it out. Every guess is evaluated by black and white pegs indicating how close it was. The detailed explanation of the rules including examples exceeds the scope of the paper and can be found for example on official website of Pressman, one of the manufacturers producing the game [2].

Even though the game was invented in early 1970s, it is still an attractive topic for mathematicians. There are variations of the game with more colors or positions used in order to make the game more difficult and the game was even proved to be NP Complete problem. [3, 4] New solutions trying to minimize the number of necessary rounds are still being introduced. Donald Knuth proved it is possible to solve the game in five or less rounds [4]. Temporel and Kovacs created a heuristic hill climbing algorithm, that induces new potential guesses with minimum computation [5].

However, all these solutions are not suitable for educational purposes and neither are the more difficult variants of the game. This paper deals with the original version consisting of six colors and four positions, where multiple use of the same color is allowed but empty spots are not. Solution presented in following chapter is slow regarding the average and maximal number of rounds, but it is very straightforward.

3 Program Solution

All the aforementioned solutions require deeper understanding of mathematics and an ability of advanced abstract thinking. Following solution is intended for pupils at elementary schools in the age of 12 to 15. Pupils at this age are already able to think in abstract terms [6], however this ability is not yet fully developed. The program itself is rather complex for an elementary pupil, but it is relatively easy to explain.

The solution was implemented in Scratch 2.0 online. When working with Scratch, it is necessary to keep in mind certain aspects of the language, as for variables. There are just general variable and a simple list. Another trait connected with Scratch is its realization in Flash. Even though Flash is still a rather robust tool on computers, utter absence of native support on Android and iOS phones and tables makes it “obsolete” for this particular group of users. Although it may seem superficial, the inability to use pupils own mobile phones and tablets is something, that should be taken into consideration when speaking of the education process. [7] This deficiency is only temporary and the problem will be addressed by Scratch 3.0 based on HTML-5 [8].

3.1 Algorithm Division

Compartmentalization of a given problem is one of the first steps necessary for the algorithm development in any programming language. This skill is also easily transferable into every day life, since everyone is dealing with more or less complex problems on a daily basis. The algorithm itself can be very roughly divided into following steps/categories:

(1) Decision of how to store the data (selection and naming of basic variables, creation and naming of necessary lists)
(2) Preparation of a new game (erasing all the lists, setting all the variables on their default value, random generation of a new hidden code and initial guess)
(3) Creation of universal evaluation custom block (a process called after every guess that tells the number of black and white pegs according to the guess and decides victory or defeat)
(4) Enumeration of all the possible decisions (based on two rows of guesses and their evaluation by black and white pegs)
(5) Addressing of exceptions (one specific combination of black and white pegs and the possibility of having 3 or even 4 same colors)
(6) Addition of graphics (background and colored dots representing guesses)
(7) Final Calculations (counting number of games and average rounds within them) (Fig. 1).

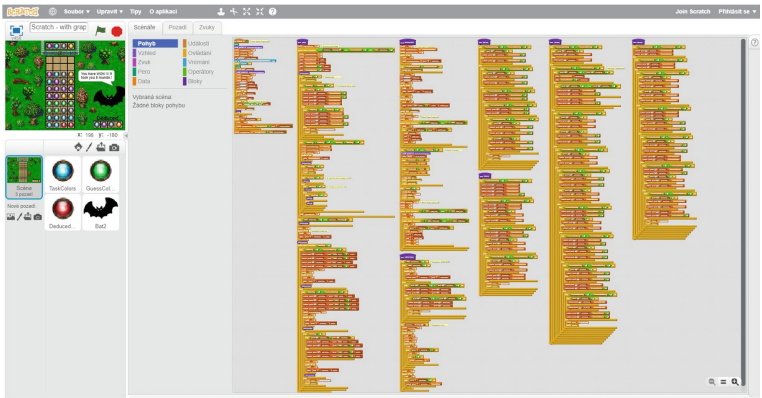

Fig. 1. Overall length of the final program created in Scratch.

3.2 Data Structures and Conditions

The program contains seven lists and sixteen variables - for standard game calculations, round calculations, exception handling, error notification, graphical representation and auxiliaries utilized in computations throughout the whole code. From the point of view of pupils, this is a lot of different and confusing numbers, but every variable and list has specific purpose. In spite of full implementation of global and local variable system in Scratch, it was avoided and all the variables are global.

The flow of the program is controlled by four basic structures - loops with counter, repeat-until loops, IF conditions and IF-ELSE conditions. The difference between IF and IF-ELSE conditions is relatively simple, yet the pupils have hard time deciding which one of these they should use under given circumstances.

The decisions in guessing colors and their order use following logic - the solver inputs two dots of one color and two dots of different color. Six colors are represented by numbers from 1 to 6, so the first line is 1122. If this line has at least one hit (either

white or black), the solver inputs four dots with only color 1 and from there he or she decides what is in the hidden task. If the first row from the guess has zero white and zero black pegs, the two colors are eliminated and second line made of just one of the two colors is skipped. The process is repeated three times. Despite having some exceptions, the logic behind the solution is simple enough to be fully understood by the pupils after the first explanation. All the possible combinations are shown below.

Table 1. Possible combinations of a two line guess. Second line made of only one color can be evaluated with black pegs only and the decision making starts from there. Black pegs are B, white pegs are W and the number of them is written before the letter (two black pegs = 2B).

2nd line	Possible combinations with the first line								
0B	1B0W	0B1W	2B0W	0B2W	1B1W				
1B	1B0W	1B1W	2B0W	0B1W	0B2W	0B3W	2B1W	1B2W	3B0W
2B	2B0W	0B2W	1B1W	3B0W	0B3W	1B2W	2B1W		
3B	3B0W	2B0W	1B2W	1B1W					

Nesting of IF-ELSE blocks is in this case far superior to basic IF conditions not only because when the correct option is found the unnecessary code section is skipped, but also because if the correct option is not found, the ending section can terminate the program and write an error message. This error message can be changed in context of the place where it happened within the program and thus it can make bug hunting process (=tracing errors within the program [9]) much easier.

3.3 Weaknesses of the Algorithm

In contrast with solutions of other authors (see Sect. 2) this algorithm lacks the robustness and takes a lot of guesses. Where other complex solutions get close to four rounds per average game and maximum number of rounds is five (see Sect. 2), this solution takes seven rounds in average and in the most unfavorable case it is ten rounds. Nevertheless, the algorithm still manages to beat the game every time.

Another weakness lies in its inability to adapt to more difficult Mastermind versions. Addition of more colors, more positions or reduction of maximum rounds before defeat causes the algorithm to fail and the algorithm does not work.

3.4 Graphical Representation of the Game

Implementation of graphical elements into the program is relatively simple if the pupils understand the program they wrote. This teaches them that readability and logical layout of the program really is important. It also shows how boring computation can be relatively easily turned into a full scale game given just a few simple sprites. When they see with their own eyes the difference (see Fig. 2) and how difficult it is to create the code part of the program, they can realize that games are equal part of graphics and coding.

Fig. 2. Side by side comparison of the game. Graphical visualization is on the right side, whereas hidden graphics with most of the variables and lists shown is on the left side.

4 Stressed Educative Elements of the Solution

The aforementioned solution is a project suitable as the final program presented at the end of a course. While creating a project of such a complexity pupils have to demonstrate deeper understanding of all the programming principles they had been learning throughout the given course as well as the ability to merge them within a single program. The teacher can give the pupils advice during any of the stages; however, it is advisable to show how should the solution work on an exemplary game. This way all the pupils can work towards the same goal and can help one another.

The first step in the development of the algorithm was for pupils to segment the whole task into several more or less independent sub-tasks. This skill is the most important one for pupils' every day life. Teaching of programming presents an opportunity to show students basic principles of compartmentalization and its impact on efficiency. It also teaches sequential thinking - finding the beginning and moving from there in premediated manner.

Although the program can be created as a single procedure, the resulting outcome is not legible and it is apt to take advantage of the possibility to create Custom Blocks. The Custom Blocks are almost necessary for the Evaluation procedure, but they are also beneficial for making the program well arranged. For the same purpose it is also good to insist on employment of comments.

The solution of the game needs 7,05 rounds in average to win the game, but the logic behind it is very easy to explain and presents interesting opportunities for teaching of algorithm development. Even though the amount of possible decisions needed to finish the game is very limited (see Table 1) pupils must enumerate all of them, otherwise the program does not work (or at least not always). This forces the pupils to think from different points of view. The pupils have a strong tendency to create a solution functional for the problem only within current circumstances. In other words - if it works now, it will work every time. The necessity to consider all the possible circumstances (like different values stored in variables) is not taken into account and the given section of code is perceived as unwaveringly correct.

Same problem also creates an opportunity to show the pupils how to implement basic bug-hunting tool. After the pupils find out on their own how difficult it is to

search for bugs in the whole program, they appreciate something, that would tell them exactly in which section of the program the problem occurs (see Sect. 3.2).

When a pupil reaches fully functional algorithm, he or she can add an option to "re-play" the game as many times in a row as the user wants. This allows to test the solution exhaustively by simply letting it repeat itself several hundred or even thousand times. Such a loop requires enormous amount of time in Scratch's standard mode, but there is an option called Turbo Mode, which "runs the project extremely fast, having minimal to no wait between blocks." [10].

Faster pupils can also implement round counter and calculation for maximal and minimal length of a round occurring during the long reiterative run of the program. Based on these numbers they can also add calculation for average round length. Since the Mastermind Game is a complex problem (as stated in Sect. 2), the pupils are welcome to try and create their own solution, after they successfully finish this one. From this point of view, the creation of a new program is more of a brain teaser than purely algorithmic problem and as such, possibly only the gifted pupils can do so.

Scratch also proved to be robust enough for implementation of far more complex solutions for the Mastermind game created for example by Knuth or Temporel and Kovacs. These solutions can be shown to pupils in order to prove that even though different solutions may lead in the end to the same results, but the path itself can be entirely different in approach, complexity, demands put on the computer and given programming language as well as in the overall efficiency of the final program.

Acknowledgments. The paper has been supported by Specific Research Project of Faculty of Science, University of Hradec Kralove, 2017 and by Specific Research Project of Faculty of Education University of Hradec Kralove, 2017.

References

1. Musílek, M.: Kapitoly z dějin informatiky. Gaudeamus, Hradec Kralove (2011). ISBN: 978-80-7435-129-7
2. Mastermind Rules. http://www.pressmantoy.com/game-rules/Mastermind_rules.pdf
3. Stuckman, J., Zhang, G.Q.: Mastermind is NP-Complete (2006)
4. Goodritch, M.T.: On the algorithmic complexity of the Mastermind game with black-peg results. Inf. Process. Lett. **109**, 675–678 (2009)
5. Temporel, A., Kovacs, T.: A heuristic hill climbing algorithm for Mastermind. In: Proceedings of the 2003 UK Workshop on Computational Intelligence, UKCI 2003, Bristol, United Kingdom, pp. 189–196 (2003)
6. Kohoutek, R.: Kognitivní vývoj dětí a školní vzdělávání. In: Pedagogická orientace 2008, vol. 18, no. 3, pp. 3–22 (2008). ISSN: 1805-9511
7. Rossing, J.P., Miller, W.M., Cecil, A.K., Stamper, S.E.: iLearning: the future of higher education? Student perceptions on learning with mobile tablets. J. Scholarsh. Teach. Learn. **12**(2), 1–26 (2012). ISSN: 1527-9316
8. Scratch 3.0. In: Scratch Wiki (2017). https://wiki.scratch.mit.edu/wiki/Scratch_3.0. Accessed 17 June 2017
9. Ganesh, S.G.: Joy of Programming: Bug Hunt (2017). http://opensourceforu.com/2011/03/joy-of-programming-bug-hunt/. Accessed 17 June 2017

10. Hidden Features: Turbo Mode. In: Scratch Wiki (2017). https://wiki.scratch.mit.edu/wiki/Hidden_Features#Turbo_Mode. Accessed 13 June 2017
11. Milková, E., Petránek, K.: Programming courses reflecting students' aptitude testing and implementing learning style preferences research results. Int. J. Math. Comput. Simul. **10**, 218–225 (2016). ISSN: 2074-1316

The Development of KarelNXT Robot as a Simulation of xKarel Programming Language

Petr Coufal(✉), Tomas Hornik, Stepan Hubalovsky, and Michal Musilek

University of Hradec Kralove, Hradec Kralove, Czech Republic
{petr.coufal, tomas.hornik, stepan.hubalovsky, michal.musilek}@uhk.cz

Abstract. The article is dealing with programming of a robot KarelNXT made from a LEGO construction set. The idea comes from xKarel programming language, which is a traditional programming language utilizing a virtual robot only shown on a screen. The virtual xKarel programming language was extended by its implementation in LEGO Mindstorm NXT-G integrated development environment. Real robots built from LEGO construction sets use additional sensors in order to make possible building of a robot with equal functions to the robot in xKarel programming language. KarelNXT robot built from LEGO construction set is using the control unit in NXT version. In the article we mention the description of individual robot movement instructions.

Keywords: xKarel · NXT · KarelNXT · LEGO · Robot · Instruction Command

1 Introduction

Specific programming languages are addressed in teaching of programming and when shifting to robotics it is necessary to change both the programming language and integrated development environment, which can be very confusing for the elementary school pupils. To make it easier it is convenient to harness the programming similarities. Initial simulation of a robot's movement positively affects the students' experience and makes the work with real robots less problematic [1, 2].

Therefore, we interconnect the programming language xKarel with the robotic construction set LEGO Mindstorms NXT. The aim is to build a robot from LEGO construction set using the NXT control unit that is according to our research [3] one of the most widespread units in teaching of programming at elementary and secondary schools in the Czech Republic. Complementary sensors are utilized by our robot KarelNXT in such a way it meets requirements of the robot Karel from xKarel.

K. Ntalianis and A. Croitoru (Eds.): APSAC 2017, LNEE 489, pp. 105–111, 2019.
https://doi.org/10.1007/978-3-319-75605-9_15

2 Construction of KarelNXT Robot According to xKarel

For proper construction of KarelNXT robot from LEGO Mindstorms NXT construction set it is necessary to understand the way in which robot Karel is moving in xKarel program. Based on the knowledge the requirements for both robot's construction and features are set so that it corresponds to reality. In the control program a set of instructions is created to make the robot controls analogous to xKarel.

2.1 Programming Language xKarel

According to experts in programming xKarel program is a programming language (programming game) suitable for teaching of structured programming. The program is created in ANSI C++ using FLTK library. It is available at Microsoft Windows®, UNIX® and MacOS® platforms and localized into Czech and English languages [4].

The aforementioned program consists of two windows. The first of them is a room where robot Karel moves on square fields. The second window represents a catalogue designated for running the instructions and defining or editing procedures (Fig. 1).

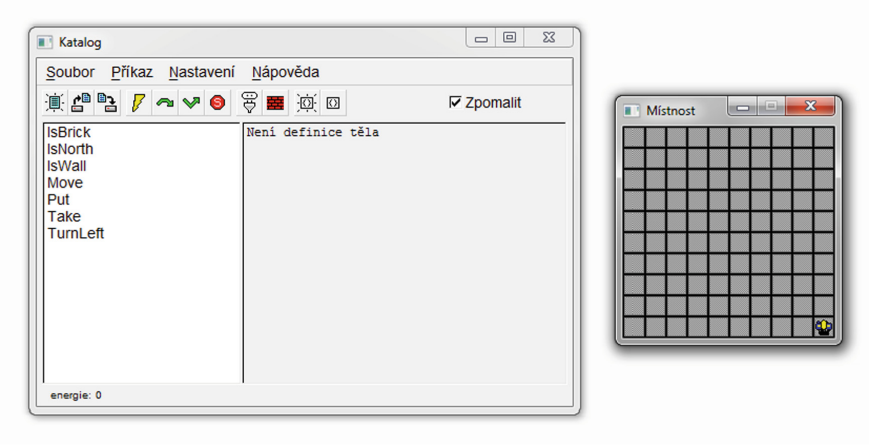

Fig. 1. xKarel development environment

Robot Karel is situated in a room where it is moving by means of instructions provided by a user. The commands for the robot are formed by the instructions in the menu and the user can gradually edit and broaden it. Having executed the program, the user selects the basic instructions Move, Put, Take and TurnLeft as well as three conditions IsNorth, IsWall and IsBrick. For creation of additional instructions (Procedure) it is possible to use aforementioned basic instructions and conditions or the cycle While and While Not [4].

Basic instructions are indivisible instructions that robot Karel comprehends automatically and other instructions are constructed from them.

Move: robot Karel moves one square forwards in direction it is heading. If it is situated in front of the wall, the error appears. Put: robot Karel puts down a brick where it is standing. In case of exceeding the maximal bricks quantity on a square, an error occurs. Take: robot Karel lifts the brick of the occupied position. When the brick is not in the field, the error emerges. TurnLeft: robot Karel turns left 90°.

The conditions are to be used for better robot control. With the help of conditions, we can separate the instructions that are and are not to be conducted. IsNorth condition is tracking robot's Karel heading northwards, if the heading is correct the instruction sequence is executed. IsWall condition is considered to be true when robot Karel is standing directly in front of the wall. In such a situation the robot cannot make any other step forwards, otherwise it would hit the wall. IsBrick, the third condition, is true if robot Karel is standing on a square where the brick is located. The conditions can be improved by using Else instruction which helps the user to conduct the instruction sequence if the condition is not fulfilled.

In loops we use `While Condition {`the sequence of instructions executed when the condition is fulfilled`}` or `While Not Condition {`the instruction sequence for not fulfilling the condition`}`.

2.2 Construction and Programming of KarelNXT Robot

Robot model built from LEGO® construction set has to meet the following requirements in a way it responds robot's Karel behavior in xKarel program: Sensor detecting the wall in front of the robot; sensor detecting the brick in a square where the robot is standing; sensor determining the cardinal points; robot is able to turn 90° on the spot; robot is able to inform about potential error on its screen; robot is able both to pick and put the bricks together.

The space representing the room for robot's movement is essential for meeting the given requirements. The criteria are as follows: The room is divided into square fields; the room includes walls and the room contains bricks.

Based on aforementioned requirements KarelNXT robot model was built and room for its movements was designed (Fig. 2).

Robot Construction. KarelNXT robot is built from LEGO® construction set using NXT control unit. The construction includes parts from 9797 and 9695 educational kits. In addition, there is the compass sensor, the color sensor and the cardboard brick feeder. Crawler delta type bottom part of the chassis enables it to turn in any direction on the spot. The third engine with the help of the rubber wheel placed on the cardboard brick feeder entrance serves as a tool for collecting and piecing the bricks together. Above the robot's engines there is an NXT control unit. The positioning helps the user to read on-screen information as well as easily manipulate and launch the robot. Another undeniable advantage is the easy availability of all robot's ports. In the raised platform above the control unit the compass sensor used for determining the North can be found. Another sensor is placed in the front-lower part of the robot right in between the engines. The sensor in question is an ultrasonic sensor for the distance measuring used for detection of the walls in the room. In the lower part of the robot, in front of the cardboard brick feeder entrance, is the color sensor functioning as a brick detector.

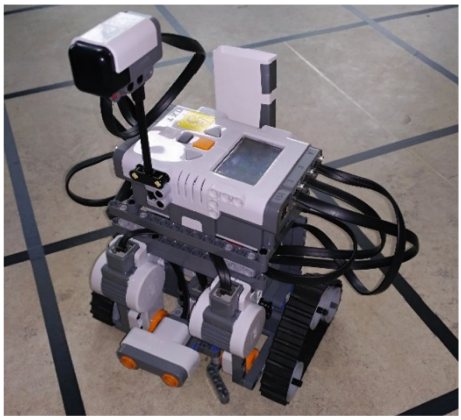

Fig. 2. KarelNXT robot construction

For accuracy control of the robot's position a gyroscope sensor is often used. Not even that guarantees exact 90° turning of the robot as stated by Dave Riske [5] in case of robot Karel from EV3 construction set.

Room Construction. Considering the size of the robot a room was created with the help of the duck tape on light straight pad. Length of the square field side is 30 cm. Blocks are built in a way they represent the walls in the room. The bricks are made up of hard wood and painted red. The amount of the bricks on a single square is limited by one brick.

The Compass Sensor. The compass sensor represents an additional sensor for LEGO Mindstorms NXT construction set from HiTechnic company, functioning for robotic models navigation. Digital compass operates with 1° azimuth accuracy, representing values from 0° to 359°, which enables its own definition of the four cardinal points for a room in any direction. Sensor is restoring given value 100 times per second. Compass sensor is susceptible to interfering magnetic field of the engines. Therefore, it is located in a raised spot in the robot's construction.

The Color Sensor. In other words, this is an optical sensor making the color detection of the scan surface much easier. Sensor is able to distinguish six colors (red, blue, green, yellow, red and white) marking them with numbers or selected color range. The sensor is located in the robot construction for recognizing red bricks situated on a square in front of the robot.

Ultrasonic Sensor. This sensor is based on the sonar principle and serves for distance measurement in 0–250 cm or 0–100 inches range with ±3 cm accuracy. The measurement accuracy is influenced by the size, surface, material and the shape of the object which reflects the wave motion back to the sensor. For more accurate distance measurement the EOPD sensor can be used. [6] The ultrasonic sensor has been found appropriate enough for both robot's KarelNXT construction and its requirements.

Robot's Program. KarelNXT robot is programmed in the LEGO MINDSTORMS NXT 2.0 program that is a part of the construction set. It is a case of iconographic programming language in which to each active component of the robot the program block is assigned. In the program block the user can set particular parameters of the active robot component. Both simplicity and easy orientation in the program enable its using when teaching in primary schools.

Program makes possible the creating of individual program blocks used during program making for KarelNXT robot. In fact, the program block is a subprogram important for setting the final robot operating program.

Simple instructions: *Move, Put, Take and TurnLeft*

Move block is testing right from the beginning whether there is a wall in front of the robot or not. If there is no obstacle, the robot moves one square field forwards, whereas after detecting of the wall there is an audio signal and on the robot's display there appears warning sign "Error, there is a wall.", and the robot stops moving.

Put block is testing if there is a brick on a square. When there is no brick, the robot puts the brick in the field, otherwise it causes Error message.

Take block is taking into consideration whether there is a brick on a square or not. If there is a brick on a square, the robot lifts it up, otherwise it writers Error.

TurnLeft block is answering for robot's moving in 90° left on the spot.

Conditions: *IsNorth, IsWall, IsBrick*

XKarel language syntax offers three conditions altogether used also for KarelNXT robot with the help of program blocks. Given program blocks are functioning as follows:

IsNorth program block compares the obtained value from the compass sensor with defined North range (absolute reading 85–95). If the detected value falls within the defined range, the robot is heading north and the first part of the program is being executed. In the opposite situation it is the second part of the program's turn.

IsWall program block determines whether a wall is or is not situated in front of the robot. When the distance of the obstacle in front of the robot measured by the ultrasonic sensor is lesser than 20 cm, the program block assesses such a situation as a wall obstacle and the first part of the program is executed. After detecting of the distance larger than 20 cm there starts the second part of the program for this is a signal meaning there is no wall in front of the robot.

IsBrick program block finds out if there is a brick on a square under the robot. Using the colour sensor it compares the colour of the objects located under the robot. When the red color is detected, the brick is under the robot and the first part of the program starts. When a brick is not on a square under the robot, the second part of the program is executed.

Both the first and the second part of the program is defined by the user in each condition from the program-block menu.

Cycles. For better robot control are used cycles operating with aforementioned defined conditions.

While condition and *While not condition*

In the first case order sequence is being repeatedly executed for the duration of condition validity whereas during the second one the sequence is being executed as long as the condition is not valid. To make the work with the program more transparent and easier six program block cycles were created:

WhileIsNorth block controls robot's heading to the north, *WhileIsWall* block controls if there is a wall in front of the robot and *WhileIsBrick* block controls the position of a brick on a square under the robot. *WhileNotIsNorth, WhileNotIsWall* and *WhileNotIsBrick* are program blocks functioning as a negation of corresponding program blocks.

Other program blocks

With the help of all aforementioned program blocks the user is able to create a program for KarelNXT robot as it would be in xKarel programming language. In LEGO Mindstorms NXT 2.0 is not possible to insert one program block to another, which means there is no recursive calling as in xKarel program. Now and then this is found to be a disadvantage.

3 Conclusion

Building both KarelNXT robot and its control program block enables us to interconnect computer programming teaching with real model robot programming teaching. KarelNXT robot is built from LEGO construction set using additional compass sensor and cardboard for brick feeder. The robot is commanded with given program blocks designed according to xKarel programming language syntax. Within LEGO Mindstorms NXT 2.0 program a set of program blocks Move, Put, Take, TurnLeft, IsNorth, IsWall, IsBrick, WhileIsNorth, WhileNotIs North, WhileIsWall, WhileNotIsWall, WhileIsBrick, WhileNotIsBrick was created. Further program blocks are being made by the students during robot programming teaching. We also plan to focus on research and comparison of teaching of programming both in xKarel language and KarelNXT robot.

Acknowledgement. The paper has been supported by Specific Research Project of Faculty of Science, University of Hradec Kralove, 2017 and by Specific Research Project of Faculty of Education University of Hradec Kralove, 2017.

References

1. Klassner, F., Kearney, S.: An evaluation of simulation in LEGO mindstorms robot programming coursework, Las Vegas, CSREA Press, pp. 3–9 (2016). ISBN: 1-60132-435-9
2. Slangen, L., Van Keulen, H., Gravemeijer, K.: What pupils can learn from working with robotic direct manipulation environments. Int. J. Technol. Des. Educ. **21**, 449–469 (2011)
3. Coufal, P.: Robotics in Education. Diploma thesis, University of Hradec Kralove (2016)
4. XKarel: Praha, Robot Karel Implementation (2017). http://xkarel.sourceforge.net/eng/. Accessed 20 June 2017

5. Building Karel the Robot: Invaluable Learning Experience for Students, Carson City, Dave Riske (2017). https://nclab.com/building-karel-robot-LEGO/. Accessed 20 June 2017
6. EOPD – How to measure distance. In: HiTechnic Blog. Miami: HiTechnic Products (2010). http://www.hitechnic.com/blog/eopd-sensor/eopd-how-to-measure-distance/. Accessed 20 June 2017

Development of Polytechnic Creativity of Primary School Pupils

Marie Hubálovská(✉), Martin Bartoň, Jan Janouch, and Pavel Krejčí

University of Hradec Kralove, Hradec Kralove, Czech Republic
{marie.hubalovska, martin.barton, jan.janouch, pavel.krejci}@uhk.cz

Abstract. The article deals with the technical literacy and implementation of the Industry 4.0 at elementary schools. It deals with the importance of construction kit in development of children's technical thinking. The article presents the results of research taken at elementary schools in the Hradec Králové Region. The research is dealing with the problematic of teaching the subject "Polytechnic creation" and is dealing with the use of construction kits during that subject.

Keywords: Technical literacy · Primary school · Building kits
Pedagogical research · Polytechnic creation

1 Introduction

We live in times of so called "The Fourth Industrial Revolution" [1]. The technique is developing at tremendous speed. The words digitalization or automation appear in almost every sphere of our lives. A billion people are connected by mobile devices. Access to information and knowledge is unlimited. The Fourth Industrial Revolution is characterized by the development of artificial intelligence, robotics, 3D printing, nanotechnology, biotechnology, material science, energy storage and quantum computing [2]. People have higher needs for quality of life. They quickly became accustomed to the comfort that technology brings them. In developed society, a preschool child can control a computer, tablet, smart phone, and other technical facilities of today. On the other hand, there is still a lack of technically educated people [3]. Education has to respond to this current trend. The priority of primary education is to attract interest in the pupils and to motivate them to study these technological disciplines [4].

2 Theoretical Background

2.1 Technical Literacy

It is necessary, in today's world of ever-evolving techniques and computer science, to understand these disciplines. With the increasing complexity of machines and information technology, it is very important to improve our technical literacy. The term of technical literacy has become more and more used in recent years. Some authors tend

K. Ntalianis and A. Croitoru (Eds.): APSAC 2017, LNEE 489, pp. 112–117, 2019.
https://doi.org/10.1007/978-3-319-75605-9_16

to be more general in defining this term, for example [5], who defines technical literacy as "Eligibility to use technical knowledge and information in everyday life or work. This literacy is gained through technical or polytechnic education." Other authors [6] emphasize that: "the definition of technical literacy should include a knowledge, skill and attitude component." The author Dyrenfurth defines technical literacy as "A summary of competences, including awareness of key processes in the technology, the ability to handle technical devices, ability to develop our own technical knowledge, skills and habits, ability to use and evaluate technical information" [6]. The areas of technical literacy are defined by Pecina [7]. According to his view, it is important for pupils to understand the meaning and characteristics of traditional and modern materials and the importance of energy and natural resources. The most important aspects of technical literacy include: the basic orientation in the various branches of technology, knowledge of the history of the technology, knowledge of the nature, functions and construction of the technical object, knowledge of the used technologies and materials, ecological, economical, aesthetical and security information, knowledge and ability to handle information stored in electronic form and more. This includes spatial imagination and basic logical thinking [8].

Some author emphasized, that pupils should have not only technical and technological knowledge, it is also important to have the necessary manual skills [7]. In addition to these areas, it is important to develop technical thinking and creativity among pupils. It is necessary to form a relationship between children and polytechnics, from the earliest age.

In recent years, education is trying to promote technological subjects at primary schools. Pupils visit companies, workshops, technology and informatics high schools. It is step into the right direction, but the level of supports is still not high enough. At the second level of primary schools, it is necessary to increase the number of lessons which are focused on technics and workshops. It is necessary to connect technology and informatics, to focus on the basics of technology, informatics and robotics.

One of the possible ways to increase the level of technical literacy in primary schools, is to use the building blocks. Depending on the type of building kit, pupils can practice compliance with the plan, or use their imagination to build whatever they want. While working with construction kits, they will also improve their gentle hand motoricity. On the electro-technical kits, pupils can try the theory and experiments, which they know from their physics classes to better understand and memorize it. On other kits, they will learn the basics of programming and robotics [8].

The development of polytechnic thinking and creativity is supported by the Industry 4.0 which is characterized by the unprecedented development of automation and digitization of production. Detailed information can be found e.g. in [9, 10]. The Industry 4.0 brings to labor market fast changes. New branches will need employees who are able to learn new things, to improvise, who are able to be creative and who are flexible. People, who are able to solve problems in a comprehensive way, control people management and are able of critical thinking, will be needed.

Education has to react to these changes. Neumajer [10] pointed out the reality of the current era: "children and young people are surrounded by digital technology every time". Most of children are naturally familiar with tablets, smartphones or social networks [11]. Our job, the task of the educators, is to guide and point them into the right

direction. So they would not only play games or watch movies on these devices, but they would discover that there are numbers of useful applications that can help them in their personal development. It is no longer enough for primary schools to teach only the subjects like computer science or and work activities separately. This system has to be interconnected and thoroughly developed to ensure that traditional technical subjects will not disappear, but that innovative polytechnic subjects are going to be developed.

2.2 Construction/Building Kits

Construction kits are a very effective way to improve creativity and technical thinking. In the kindergarten, children have a lot of space to play and work with construction sets. Children in kindergarten build, on daily basis, their own products or they work on joint projects. Playing with building kits can be spontaneous, without any supervision, or it can be controlled by a teacher, who can influence and direct that play into a certain direction for a particular purpose. Through building kits, children can, for example develop perception, memory, imagination, thinking, spatial orientation or perceptually motoric area [12]. Using the kit, the child discovers and begins to understand the basic principles of mechanics and discovers elementary laws of physics. The kit has not only a wide use in kindergartens, but it also has a place at primary schools. In primary schools it is once more important for the development of technical thinking and it can be used to demonstrate the basic principles and rules of mathematics, physics, mechanics, statics, electricity, informatics and robotics. The most commonly used kits are wooden blocks, mosaics, Lego, Merkur, Seva, Cheva.

3 Research

The research was carried out at elementary schools in the Hradec Králové Region in the Czech Republic. The research dealt with the development of polytechnic thinking in primary school students. We focused on the subject Polytechnic creation and found out whether the teachers are trying to improve the technical thinking of their pupils by using construction kits. The research was carried out at the first level of primary school (1^{st} class–5^{th} class) and at the second level of primary school (6^{th} class–9^{th} class).

3.1 Questionnaire Survey Among Teachers from the First to the Fifth Class of Primary School

This research was carried out in January 2017 among teachers who teach the subject Polytechnic creation from the first to the fifth class of primary school. The content of this subject is: working with tiny material, constructional activities, growing works and food preparation. The document “Framework educational program for primary schools” determines the weekly hourly allowance of 5 h of work from the first to fifth class of primary school. There is, in each grade, one hour of working activities taught weekly. When compared to the number of hours of working activities taught in pre-school education, we assumed that there are not enough hours of working activities taught at primary school. However, this is only a presumption that was verified with the

primary school teachers. 238 schools were addressed by the questionnaire surve. We received 99 questionnaires from the first grade of primary school and 51 from the second grade of primary schools.

The questions as well as the response of questionnaire survey are stated in the Tables 1, 2 and 3:

Table 1. The response the questionnaire question No 1.

Do you think whether the work activities for pupils is?	The number of answers:	In %
Unimportant	0	0
Less important	2	2
Important	50	50
Very important	39	39
As important as Czech language, mathematics,…	9	9

Table 2. The response the questionnaire question No 2.

Do you think that one hour of work activities weekly is enough?	The number of answers:	In %
Definitely yes	0	0
Rather yes	2	2
It is not enough	50	50
It is definitely not enough	48	48

Table 3. The response the questionnaire question No 3.

Do you use construction kits during work activities?	The number of answers:	In %
No	15	15
Yes – not very often	64	64
Yes – very often	21	21

The results of the question No 4 "What kind of construction kits do you use during work activities?" are Merkur (41 answears), Lego (37), Seva (25), Cheva (15). Construction kits like the Variant, Geomag, various mosaics, wood cubes and electrotechnics were mentioned as well, but less often.

3.2 Questionnaire Survey Among Teachers from the Sixth to the Ninth Class of Primary School

The content of the subject Polytechnic creation on the second grade of primary school (from sixth to ninth class) is based on the theoretical and practical knowledge which can be used by pupils in their everyday life and during the selection of their future profession. The subject Polytechnic creation is divided into eight areas: Working with technical materials, Design and construction, Gardening and breeding, Operation and

maintenance of household, Food preparation, Working with laboratory technology, Usage of digital technology, World of work. The areas are chosen by schools according to their educational intentions and their school equipment.

The questions as well as the response of questionnaire survey are stated in the Tables 4 and 5:

Table 4. The response the questionnaire question No 1.

Do you think that one hour of work activities taught weekly is sufficient?	Number of answers	In %
Definitely yes	0	0
Rather yes	2	2
It is not sufficient	50	50
It is definitely not sufficient	48	48

Table 5. The response the questionnaire question No 2.

The subject "Man and his world" is divided into 8 optional areas which are taught 3 h per week. Write into the table the number of hours for each area and year as they are taught at your school.	The number of hours				
	6^{th} class	7^{th} class	8^{th} class	9^{th} class	Total
Work with technical materials	35	25	22	20	102
Design and construction	8	12	10	11	41
Growing and breeding	29	15	11	11	66
Household operation and maintenance	10	19	19	21	69
Food preparation	15	31	18	12	76
Work with laboratory equipment	6	3	16	16	41
Usage of digital technology	12	18	14	17	61
World of work	6	6	18	30	60

4 Conclusion

The research carried out among teachers in primary schools in the Hradec Králové region confirmed our assumption: both first grade and second grade primary school teachers agree that there are not enough hours in education program for the subject Polytechnic creation [4]. Teachers of both grades answered identically and agreed that the subject Polytechnic creation is very important for pupil's development. Interesting information were found out from the survey that teachers use construction kits when teaching. The construction activities are neglected and underestimated in the both grades. Only 21% of first grade teachers use construction kits during the subject Polytechnic creation. At the second grade, the areas Design and construction, together with the area Work with laboratory equipment are taught the least. As has been mentioned - new disciplines will need employees with the ability to learn new things, improvise, be flexible and be creative [9]. Based our opinion, one way how to improve pupils' creativity and develop both critical

and creative thinking is through the work with the construction kits. Under this concept we understand construction kits from the simplest ones to the ones that integrate the knowledge of electricity, mechanics, informatics and cybernetics. It is necessary to teach pupils how to look at the problem in a comprehensive way and how to use all the knowledge and skills in problem solution. Education has to implement requirements of the "Fourth Industrial Revolution".

Acknowledgement. The paper has been supported by Specific Research Project of Faculty of Education University of Hradec Kralove, 2017.

References

1. Holanová, T.: Nová průmyslová revoluce. Nezaspěte nástup Práce 4.0. Aktuálně.cz, 29 July 2015. Accessed 20 Sep 2015
2. Schwab, K.: The Fourth Industrial Revolution: what it means, how to respond. https://www.weforum.org/agenda/2016/01/the-fourth-industrial-revolution-what-it-means-and-how-to-respond/. Accessed 20 June 2017
3. Read, R.: Lack of technical education produces a 'lost generation,' Oregon business leaders warn. http://www.oregonlive.com/education/index.ssf/2015/01/lack_of_technical_education_pr.html. Accessed 20 June 2017
4. Rámcový vzdělávací program pro základní vzdělávání (2017). http://www.nuv.cz/uploads/RVP_ZV_2016.pdf. Accessed 20 Apr 2017
5. Nádvorníková, H.: Polytechnické činnosti v předškolním vzdělávání. Raabe, Praha (2015). ISBN 978-80-7496-194-6
6. Kropáč, J., Kubíček, Z., Chráska, M., Havelka, M.: Didaktika technických předmětů. Univerzita Palackého, Olomouc (2004). ISBN 80-244-0848-1
7. Pecina, P.: Tvořivost ve vzdělávání žáků. Masarykova univerzita, Brno (2008). ISBN 978-80-210-4551-4
8. Roučová, E.: Vnímání pojmu technická gramotnost u studentů učitelství pro primární školu a učitelů na primární škole. J. Technol. Inf. Educ. (Časopis pro technickou a informační výchovu) **5**(3), 35–43 (2013). https://jtie.upol.cz/pdfs/jti/2013/03/06.pdf. ISSN 1803-537X
9. Národní iniciativa průmysl 4.0. Praha. http://kzps.cz/wp-content/uploads/2016/02/kzps-cr.pdf. Accessed 25 May 2017
10. Neumajer, O.: Průmysl 4.0 do každé školy. Praha. http://clanky.rvp.cz/clanek/c/Z/21119/prumysl-4.0-do-kazde-skoly.html/. Accessed 25 May 2017
11. Kudrna, D.: Průmysl 4.0 – Vzdělávání 4.0. Praha. https://medium.com/edtech-kisk/pr%C5%AFmysl-4-0-vzd%C4%9Bl%C3%A1v%C3%A1n%C3%AD-4-0-d3ee334cb287. Accessed 25 May 2017
12. Koťátková, S.: Hry v mateřské škole v teorii a praxi. Grada (2005). ISBN 80-247-0852-3

Distribution and Validation of Meteorological Data for the Air Traffic Management Systems

Ondrej Marik(✉) and Roman Marik

Faculty of Electrical Engineering and Informatics, University of Pardubice, Studentska 95, 532 10 Pardubice, Czech Republic
ondrej.marik@hotmail.com, roman.marik@hotmail.com

Abstract. The main aim of this article is to introduce you our research project which is focused on processing, validation and distribution of meteorological data for the air traffic management systems. We would like to suggest to reader the direction of our research project and present a new perspective on meteorological data processing and distribution for the industries with a high degree of dependency on weather. Usually research projects are focused on data collection in one central datacenter to do the data analysis and simulations but when we think globally, we think is better to have independent localities who talk to each other. And that is what we would like to research, and what we would like to present to reader. We are focusing especially on the air traffic industry where the need for current meteorological data is must. As a result, we would like to develop software solution which will be able to use decentralized and solid architecture for data exchange and analysis without high dependency on central datacenters.

Keywords: Meteorological · Data · Distribution · Validation · ATM
Air traffic

1 Introduction

The main aim of this article is the introduction of research project with codename TEVI. The project is focused on realization of innovative approach for the processing and distribution of meteorological data for the air traffic management where the need for quality and accurate data information is a must.

Currently the project is still in research and prototyping phase so the presented data can change during time but we still think it is a good idea to present you what we know now, what we found out and how we would like to solve the problems. Also, we are going to publish all results and experiences after the project will be finished and certified so the reader can easily track progress and good or bad approaches we tried because we believe there is a huge space for improvement how to manage and use such a data in nowadays world.

For the rest of this article we will use model situation of the Czech Republic and our pilot project with the Army of the Czech Republic (ACR) where we would like to deploy our system for the distribution of data into air traffic management system (ATMS) and other systems for support of air traffic management. We would like to

K. Ntalianis and A. Croitoru (Eds.): APSAC 2017, LNEE 489, pp. 118–126, 2019.
https://doi.org/10.1007/978-3-319-75605-9_17

deploy it on all active airbases ACR have and at two datacenters where ACR has supporting systems and services and training center.

2 Current Situation and Working Procedures

In nowadays is international standard for the meteorological data publication and interchange in air traffic management (ATM) across the world METAR format. This format is defined and standardized by World Meteorological Organization (WMO) and International Civil Aviation (ICAO). Reader can find list and explanation of all codes in messages regarding to standard in [6] where are also some examples of reports and its structures. Detailed information about implementation of OPMET (Operational meteorological data) can be find in [4].

In a simple way, METAR can be defined as text format message which contain summary information about current meteorological conditions on any airbase or measuring location.

Nice example of METAR message is published in [2]:

```
METAR LBBG 041600Z 12012MPS 090V150 1400 R04/P1500N
R22/P1500U +SN BKN022 OVC050 M04/M07 Q1020 NOSIG
8849//91=
```

As you can see, message is represented by several information in one continuous string. First is indication of message type. It can be METAR or SPECI. Difference between these type of message is just about the time and situation when has been the message published. METAR is published regularly every hour in 365/24/7 mode. SPECI on the other hand is special type of METAR with completely same format (except keyword at the start) but it is published outside of the standard publishing window. This can happen because of technical issues, unexpected significant change of meteorological situation, wrong information in regular METAR message etc. After the message type keywords follows these data fields – **ICAO airport code, time and date, wind information, prevailing visibility, runway visual range, snow situation, cloud information, temperature and dew point, altimeter setting, trend forecast, runway condition, CAVOK information** (cloud and visibility ok).

2.1 Current Architecture of Data Distribution

From international data distribution point of view looks current situation in Czech Republic very similar like in other countries. There is on central collecting point which is usually operated by one central institution which guarantee data collection and distribution for the whole country or region. This central point then distribute data into international interchange network or to its parent collecting point.

As you may notice, it is basically classical pyramid topology with all its cons and pros as you can see on Fig. 1.

In our case is central collection and distribution point VGHMU Dobruska (military geographical and hydro meteorological office). This point is used as meteorological

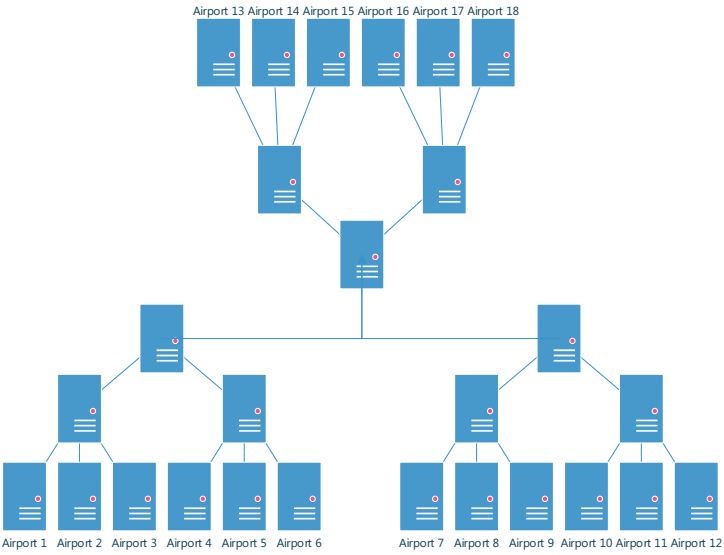

Fig. 1. Current architecture of collection and distribution

data (METAR/SPECI) source for all military ATMS and locations. All process and data exchange of meteorological information in Czech Republic is defined in [5].

2.2 Disadvantages of the Current State

Inflexibility and dependence

One of the biggest disadvantages of the pyramid topology is dependence on the central collecting points because each of it represents potential problems in case of errors but not only for the parent's points, but also for the points in a same region. It is because of that many real-life topologies or systems uses central points as exchange place also for the servers on a same hierarchy level so in case of unavailability of the central point, even neighbors' servers cannot exchange its' data.

It goes without saying that these points should use the high availability architecture and they should be redundant but in our opinion, this is not enough for example in a military environment where we can expect attack on the central datacenters during conflict.

Amount of data

Because in pyramid topology data are collected in a way up, the amount of data to keep is bigger and bigger as collection point is closer to top. That leads to situations when top points have all information from child points, but they cannot handle and store nothing detailed than hours information (METAR/SPECI).

For readers' imagination about data size, we can do a little calculation. During analysis and first tests of our project, we have found that one airbase of ACR generates about 64 GB of RAW data. If we consider that ACR have four active airbases we get

256 GB of RAW data per year. Then we, of course, needs data from civil airports in Czech Republic (let's count just the bigger ones – Prague, Brno, Karlovy Vary, Ostrava, Vodochody) we get 0.5 TB of RAW data and that's just from the Czech Republic (CZ).

On the other hand, in [1] is written that in United States of America was in 2013 totally 15 513 airports. That means that in case we would like to store all RAW data we would have to have solution for storing and processing 992 TB of data per year.

So as reader can see this was also the reason for using just the METARs which represents just the fraction of RAW data (about 100 B per message). Of course, the main question is if this is sufficient and accurate.

Data message transmissions

There are no general rules for the data collection and transmission between end localities and collection points so national organizations usually choose their own way how to handle it. Czech institutions for example usually uses FTP protocol to the central storage which basically represents batch processing than online data distribution so there can be smaller or bigger delay and in a same time different system can have different information.

Data quality

Another disadvantage of current solutions is absence of validation and data quality control. Data generation for the ATM is usually solved by two modes – automatic and manual.

Automatic mode

If the measuring system is in automatic mode, it automatically reads current values from the sensors then generates message and sends it for publishing. In this mode systems also usually enables modification of messages before its publishing.

Problem of this mode could be situation when something happens with sensors so it indicates wrong data. This mode is also usually unable to detect short term external influences. Point is, that in many cases is measure "garden" close to the runway or taxiway which is necessary for having accurate data on the edge of the runway for example. So hypothetically can occur situations when airplanes with started engine can directly influence the sensors like wind measure, temperature etc. That can lead to publication of wrong data and to unexpected situations.

Manual mode

In manual mode is message generated by worker of the meteorological service on airbase. System for data measuring just indicates current value and its evaluation is up to worker who fill it to the final message.

Disadvantage of this mode is high dependency on human which can lead to mistakes. There also potentially exists same problems with sensor error or short term external influence as in automatic mode.

As can be seen from the above, the current situation and working procedures are functional and proven, but certainly not ideal, and in our opinion, there is space for improvement.

3 Aim of Project

The main aim of our project is development of solution which will deals with most of the disadvantages of current systems for distribution of meteorological data with focus on distribution to the ATMS and its quality.

When we were looking for similar research projects, we found out that many of them are focusing more on data collection and simulation like in [3], others for data analysis and their use for decision making [7], but we haven't found any that would be focused on data distribution. Lot of research projects also focuses on centralized architecture which we believe has more disadvantages than advantages so we decided to try to solve this problem kind different than others.

The proceeding text will be describing our pilot project with the ACR were we would like to apply all our ideas.

4 Planned System Architecture

As it was written in chapter A, in Czech Republic is used architecture with central collection and distribution point operated by VGHMU. All the ACR airbases and its meteorological systems send data directly on this sever via FTP. That means there exists only one connection and in case of its failure none of the airbases has data from the others which is not quite ideal.

If consider that it is a military environment, it should be our main aim to develop decentralized system architecture with similar principles like telecommunications networks with great emphasis on security, resistant and flexibility of whole system.

On the other hand, we must also consider the backward compatibility of system because lot of applications and systems are proprietary and it its reconfiguration or modification will be possible only its future upgrade.

That leads us to design system which will works on full mesh topology and which will also have central analytical cluster. By full mesh topology is meant such a connection when every server of our system has connection to any part of our system across the decentralized military communication network. The reader should not understand topology in terms of directly connected physical data carriers. The topology is in fact deployed across the Czech Republic.

On Fig. 2 is shown current architecture of our pilot project. The reader can see that every airbase has its owns server pro data processing and distribution of meteorological information. At the same time, we have also central analytic cluster, which has three main roles.

The first role is replacement of the VGHMU collection and distribution server (from inside of our system). This provide us backward compatibility solution for old systems or system waiting for its upgrade. Another effect is that we can act as common system to the "outside" world without need of reconfiguration at national data collecting point.

Second role is planned advance real-time analytics over data from all airbases where would like to evaluate current situation, calculating short and long-term trends, historical analytics etc.

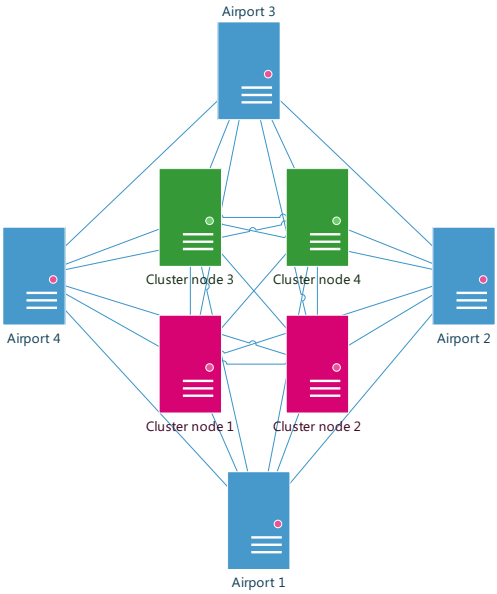

Fig. 2. Proposed architecture

Third role is backup of active servers on every airbase. This is basically only protection for every airbase before hardware problems but it saves us part of the budget because we don't necessarily need two active servers on every airbase.

The color difference of cluster nodes on the Fig. 2 indicates its locations. As you can see, we spread them into two independent datacenters and unlike other projects (for example [3]) we are focusing on decentralized architecture with central support instead of building large central computational cluster.

5 Data Processing and Distribution

5.1 Data Processing on Airbase

On every airbase is deployed on independent server which can provide all functions of system even in case when the whole airbase is disconnected from network (in that case provides just local data). The procedure workflow of services on servers look like this:

5.2 Data Mining from Measuring System

System is directly connected into meteorological measuring system which sends current sensor values in predefined intervals via TCP/IP – defined by manufacturer of measuring device so it is basically in real-time mode.

5.3 Data Storing

Once system receive any data, it validates its source and saves it into the SQL server. Before final commit into the database system is passing standard data procedure like writing RAW data, cleaning, sorting, basic checking on invalid characters etc.

5.4 Validation and Evaluation

Once are RAW data stored system starts with its validation. This step is crucial in the whole project, because it is this feature that differentiates our system from others.

In common we can say that data validation is examine these areas:

- Comparing with previous values
- Validation against common values
- Validation based on calculated long-term and short-term trend
- Validation against historical and statistics data

This process is passed for every data value of received data and based on its result, every value gets indication of its state – ok, error, waring, unexpected change etc. These indications are then passed with data during it publications so end user now if value is save or not.

The main idea is of this process is not deleting of data which looks suspicious or which fails on validation but passing that information to the end user of that value no matter if he accesses it via web interface of our system or if get it in ATMS.

It can happen that for example unexpected change of wind speed or direction is not error of sensor or error because of external influences but it can be simply just gust of wind. In case of ATMS is then up to worker how he will deal with that information.

This part of system is one of the biggest challenge right now because we trying to find such a method, which eliminates false alarms on minimum and this needs lot of testing, data observing, analytics etc.

5.5 Data Publishing

Once data have been validated and tagged, they will be published. Unlike standard systems where data is distributed over a central collection point, we have decided to provide a complete public API for system and data access. In addition, the data will not be published in any periodic cycles (except for the reports like METAR), but it will be send via PUSH notifications to each of currently registered and listening client.

This solution has a huge advantage and gives the entire system a huge potential for the integration with ATM systems of all current vendors and practically with any system because we will provide full description of API and we will keep it open as much as possible.

This API also helps in decentralize topology because server can talk directly to each other over standardized interface and they don't need to keep any information (except its address) from other locations. It is also important to keep in mind that every data is published with validation indications.

5.6 Archive

At this point of research, we have no valid data about archive but our planned approach is to keep all data in a SQL at least for two years (depends on HW). Once the data reach the deadline, we are going to flush detailed data into files and saved them on place, where we can index it and access it very fast. But we will keep the summary data in the SQL for the maximum performance and common statistical task. We are going to use data in the files only in case when someone call API request on it with maximal granularity.

The archive also must be accessible via API so the archive storage cannot be offline storage.

6 Technical Background

The system is currently based on Microsoft technologies – Windows Server, SQL Server, C#, ASP.NET MVC/CORE. It is mainly because we are counting on fact, that big environments need big analytics power so we build system from the start for compatibility with Microsoft Azure because it offers great ratio between cloud features, power and integration with local environment so we can deploy completely hybrid solutions.

In a future, we count we will be Linux compatible once Microsoft release its SQL on Linux.

7 Future Potential

If everything will be fine, we think that our system has huge potential for the future use. Our philosophy is to build solution in the box which will be compatible with as many meteorological measure systems as possible and which will be able to communicate with whole world right after the initial configuration. If you imagine situation when many locations would be equipped with our system and all of them would be connected into the internet. That could totally change the way how we use meteorological information in air traffic now.

For example, in nowadays is common thing that airplanes have direct data communication to the ground or into the internet. If they would be able to communicate with big network of our systems, the crew on board can know about change of weather conditions miles before they reach the destinations and system can offer them the closest airport with good conditions for landing or the airplane can inform closest system about current condition in its flight altitude to accurate the data of ground systems.

8 Conclusion

This article introduced to the reader our project which is still in prototyping and research phase. We introduced our motivation, basic functions of system and our plans into the future development.

We would like to thanks to all of readers and you have any questions do not hesitate to contact us.

References

1. Central Intelligence Agency: Total Number of Airports by Country (2011). https://www.cia.gov/library/publications/the-world-factbook/fields/2053.html. Accessed 20 June 2017
2. Wikimedia Foundation, Inc.: Wikipedia - METAR, 22 April 2017. https://en.wikipedia.org/wiki/METAR. Accessed 21 June 2017
3. Tascón, C.S., Gonzalo, J.: Advances in digital meteorological services (DMET) for ATM: Aviation meteorology in support of air traffic optimization and automation. In: SIDs 2011 - Proceedings of the SESAR Innovation Days (2011)
4. International Civil Aviation Organization: Guidelines for the Implementation of OPMET Data Exchange using IWXXM in the EUR Region (EUR Doc 033), 23 September 2016. https://www.icao.int/EURNAT/EUR%20and%20NAT%20Documents/EUR%20Documents/033%20%E2%80%93%20CONOPS%20for%20the%20Transition%20of%20OPMET%20Data%20Exchange%20using%20IWXXM/EUR%20Doc%2033%20%20(EN)%20-%20Edition%202,%20Amd%200.pdf. Accessed 20 June 2017
5. Civil aviation authority Czech Republic: Letecký predpis L3: Meteorologie, 10 November 2016. https://lis.rlp.cz/predpisy/predpisy/dokumenty/L/L-3/data/print/L-3_cely.pdf. Accessed 20 June 2016
6. World Meteorological Organization: WMO Publication No. 306: Manual on Codes, International Codes, Volume I.1, Annex II to the WMO Technical Regulations, Part A – Alphanumeric Codes (2016). http://www.wmo.int/pages/prog/www/WMOCodes/WMO306_vI1/Publications/2016update/WMO306_vI1_en_2011UP2016.pdf. Accessed 20 June 2017
7. Klüver, C., Klüver, J.: A self-enforcing neural network as decision support system for air traffic control based on probabilistic weather forecasts. In: 2017 International Joint Conference on Neural Networks (IJCNN), Anchorage (2017)

Neural Interface: The Potential of Using Cheap EEG Devices for Scientific Purposes

Radim Bednář(✉) and Josef Brozek

Faculty of Electrotechnical Engineering and Informatics,
Laboratory of the Application of Software Technologies,
University of Pardubice, Studentska 95, 532 10 Pardubice, Czech Republic
asote.pce@gmail.com

Abstract. Alternative input devices for computing have come to the forefront of interest of scientific teams. The idea of controlling the computer with mind has great potential. The popularization of this topic has led to a greater public interest and the creation of a market for cheap EEG devices. The article focuses on the evaluation of affordable EEG devices usage by scientific teams. Two different devices were used. The validation programs were created in the C# programming language. On a test sample composed of students, University staff and other suitably selected test subjects, the potential of affordable science devices was evaluated. In the conclusion of the article there is a discussion, as the device cannot be used for high-quality scientific work. The article also deals with the scientific teams that use the equipment for "serious" research and marks the specific errors and deficiencies that teams have committed and therefore may have the impression that the device is usable.

Keywords: EEG · Alternative user interface · User interface · Neural interface Neurosky · Brain · Validation · Effectivity

1 Introduction

The current input devices used in information technologies were developed more than 50 years ago. Use of mouse and keyboard is very often effective - but this efficiency is usually built on the user's training. At present time, however, alternative input devices must be taken into account as well. In addition to resistive, optical and familiar touch devices, the use of EEG signals can be considered. The consequence of the EEG option would be to remove the intermediate level and control the computer through actual decisions of the user.

For a deeper understanding of the issue, it is necessary to understand the EEG principle, or the creation of human thoughts - so literature [1, 2] are recommended. Consequently, it is desirable to understand the principle of capturing EEG signals [3], their processing in software, especially with emphasis on the application of the Fourier transform [4]. The article does not deal with the direct implementation and the source code samples are not part of the article. Knowledge of programming techniques is an advantage for the reader. For a better understanding of the case study, it is desirable to have a basic overview of the topics of representative sample production, case study and

K. Ntalianis and A. Croitoru (Eds.): APSAC 2017, LNEE 489, pp. 127–132, 2019.
https://doi.org/10.1007/978-3-319-75605-9_18

its evaluation. The used statistical apparatus is available, for example, in [5], using statistics of reliability, validity, obliquity, and punctuality. Verification of values was based on a good match test.

2 State of the Art

Current experiments with the creation of bridge between mind and information technology can be tracked at several different levels. The key is the information technology loop - a person, where actual results are already very sophisticated and demonstrable. The fields of EEG signal research include primarily medicine - which focuses on the EEG as such and serves primarily for patient diagnosis. Information technology is being processed on a different level and uses different resources.

2.1 Influencing the Mind Through Information Technology

The basic link between the user and the computer, so that it can be influenced by the user's EEG can be achieved by means of frequent displacement methods. In fact, it is a simple method, used by, for example, the so called "psychowalkmans". Through the headphones, a 50 Hz frequency is transmitted to one of the user's ears, and 55 Hz to the second ear. The brain is gradually "tuned" to the inter-frequency - the two frequencies are actually deducted. Because the frequency of 5 Hz corresponds to Delta waves EEG, a man exposed to this effect falls asleep relatively quickly, as he tunes his brain to the Delta sleep waves. Indirectly, this influence of the mind can be observed, for example, in means of transport, such as a train, where gentle jiggles often manifest strongly. The ability to tune the brain to selected EEG frequencies is evidenced by studies [1].

2.2 Processing Signals for Medical Purposes

Knowledge of EEG signals and their composition in various activities is a key way of diagnosing many diseases and brain disorders - epilepsy, Alzheimer's disease, post-stroke conditions and others. In the field of medicine, it is not crucial what particular waves mean specifically (e.g. "seeing the red colour"), but the key is the correct ratio of each class of brain waves. Especially when monitoring individual waves in the context of resting, normal activities or sleep, which makes human bodies very similar, it is relatively easy to find deviations from normal and diagnose diseases. See literature [3].

2.3 Advanced Processing of EEG Signal

From EEG signals, it is possible to track a number of other information besides the standard frequency representation of individual waves. In the last decade of the last century, the first experiment was developed to use EEG as a lie detector. The use of this principle was that the representation of the frequencies in the brain is different in the case of a man trying to remember and in case of making something up. The problem

with this method was the fact that the tested person only had to prepare the lie in advance, and then remember it - the notorious liar then succeeded in the test.

The research itself, however, laid the foundations of a very sophisticated discipline, which seeks to find similar patterns in behaviour, but at a much more detailed level. The disadvantage of these methods, however, is, at present, that the results are always strictly individual. So, if any two people start thinking about the publisher Springer, the manifestation of this will in the EEG in each of them will be completely different. However, if these two people begin to think again about Springer, their own result (though among people unique) will match their own EEG formulas.

The above mentioned technique is very often abused in order to demonstrate the efficiency of the operation of EEG devices. The actual sophisticated formula for a particular publisher is sifted from about 50 different partial frequency bindings and is not easy to distinguish for a particular individual. It requires very precise equipment and very high computing power. However, this applies only when we distinguish one particular idea from another. The situation will change dramatically if we create a very limited set of ideas, such as “Springer”, “Cow”, “Sun”, “Wet”. If we have enough time and diagnostic data for individuals, it is not difficult to distinguish these ideas. In practice, such use is almost inapplicable because the experiment is built so that it cannot fail. This is the case for simplifying the baseline set of questions so that only two or three data sets can be tracked from the need to monitor 50 frequency occurrences. In addition, data no longer need to be tracked in the context of the entire brain (i.e., to search for a particular location). In a properly designed test, it is possible to demonstrate the functioning of any EEG device.

2.4 Sensor Location and Typology

To correctly understand the problematics, it is necessary to accentuate the different typology and placement of EEG device sensors. The most complicated is scanning a general field through an electromagnetic detector – magnetic resonance with deactivated actuating field. This solution is very expensive, and unusable in practice.

In practice (medical and general), electromagnetically-sensitive electrodes are commonly used. The accuracy of these electrodes is acceptable in the field of medicine (and others sciences as well), as any precision greater than 7 bits/value is considered acceptable.

A practical problem is the segmentation and complexity of the brain. Waves are defined not only be their shape, but also by the location where they emanate from, how they distribute etc. (that is how we can tell sleep riddled with nightmares from sleep with pleasant dreams). For this reason, electrode count and localization is crucial. The minimal number of needed electrodes is two. The problem with using two electrodes is that the location from where a wave propagates cannot be precisely determined. Most affordable EEG devices, including the one used in the case study, use only two electrodes. The result of using only two electrodes is evident; during the lie-detecting test, all the tested subjects had to do to simulate intensive thinking is think of breasts (although it may sound sexist, it has been scientifically proven that for males, breasts are a stimulus that alters the results the most).

High quality medical facilities, including the medical ones, have by European standards 10–20, where the numbers do not represent electrode count, but distances in percent from other electrodes in vertical and horizontal planes. Such a facility usually uses a minimum of 20 electrodes, distributed all over the scalp.

3 Case Study

For the case study, several devices NeuroSky MindWave devices were used. No differences were found among these devices, and that is why they are discussed generally. The devices boast two electrodes, one of which is placed on an ear (grounding electrode) and the other in the middle of the forehead. The device looks like a headband. The NeuroSky company provides a program library thinkgear64.dll with and open interface, which allows further work in C#. The company admits that the device is capable of measuring two primary values, generally called "focus" and "relaxation". The manufacturer was however not capable of identifying precisely what is measured, even after further questioning.

The actual case study is a collection of questions – a variant of a didactic test. However, before the actual case study is introduced, it must be noted that more application were made. During solution testing, a game called SnakeEEG was crated. This game aims to use the measured values to move a snake – a game very similar to the famous game of old Nokia phones. The second application that was created is called Space Adventure EEG – a simple space game controlled only by the values of focus and relaxation. It was discovered that it is possible to learn how to control applications through EEG signals. It is not possible to reach any other states (except for focus, meditation and nervousness). For basic game controls it is enough.

3.1 Case Study

The actual case study took place at the University of Pardubice in spring of 2017. A total of 42 persons took part, with a variety of students, faculty staff and public. Pictures used along with questions can be seen in Fig. 1.

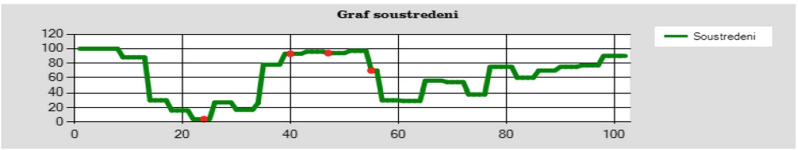

Fig. 1. Test result graph

The following questions were asked:

a. How many windows does the house have?
b. Solve the equation.
c. What colour is the model's underwear?

d. How many triangles are in the picture?
e. Find 6 differences between the two pictures.

During the process, the user was wearing an EEG headband, and the EEG activity of the user was tracked. Illustration of activity can be seen in Fig. 2.

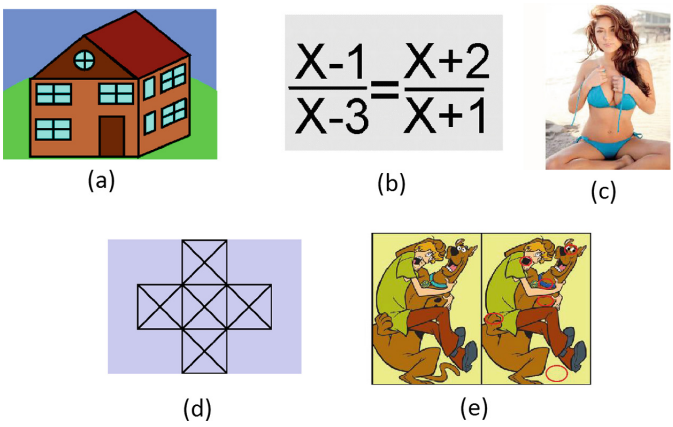

Fig. 2. Questions of the validation test

The graph's X axis represents time, Y axis represents focus. The moment the question is asked is marked by a point on the focus line. In the depicted example, we can see that the focus levels correspond to the difficulty of the questions. The focus levels are quite high when solving the most difficult question. On the other hand, the underwear question lowers the focus level to minimal values, and has a lasting effect. Following values are typical of a person solving logical problems.

The Figure shows fluctuations of focus levels for various questions. However, common patterns can be found. Especially with the question about the colour of the model's underwear, male subjects showed a significant drop in focus level, and took almost 10x the time to answer than female subjects. Generally, it can be said that the test was a success, and it was proven that the device can be used for focus level tracking. However, it is important to note that other factors and external influences, e.g. distracting the subject, has a significant influence on the whole measurement.

3.2 Discussion

On the basis of executed experiments and three application, some results may be drawn. The first conclusion is thought distinction – although changes of focus level are generally dependent on mental activity and the presumptions of this process may be generalized, it is simple to bias the measurements. Bias errors can be introduced through external influences (acoustic interference, or even strong eye contact with the testing subject), or through internal influences (instead of solving the question at hand,

it is possible to think intensively about any other topic). Measurements done with only one electrode (and grounding) are ineffective.

Hypotheses stated in for example [6] or [7] which point out the risks of spying passwords through EEG interfaces are, as of today, exaggerated and pointless. Without the complex knowledge of the user's behaviour patterns and his complete EEG image, such spying ruled out.

The theory stated in [6] and similar expert articles can be qualified as very precise experiments, the environment of which is controlled so strictly that results other than positive were not possible.

4 Conclusion

The contemporary marked is highly saturated with simple devices with two, four or eight electrodes. These devices were tested during the research part, and the results will be follow. The price of these devices is in the range of tens to hundreds of dollars. They can often be connected to mobile devices or computers, and are supposed to help with concentration.

Price of high-quality medical-gra de devices moves in the thousands of euros, high-quality devices with professional software can cost up to hundreds of thousands of euros.

In our research, it was discovered that the prices are not pointlessly exaggerated. Affordable devices with few electrodes and sub-par quality level of the software (which, considering the input quality, cannot be very good in the first place) cannot replace the professional solutions.

Affordable devices have a substantial approximation of the actual values – and although the EEG principles apply even on this approximation, the data loss is so severe that the solutions cannot be recommended for any practical uses apart from the entertainment industry.

References

1. What are Brain Waves (Theta, Delta, Alpha, Beta Brain Waves?). In: Hub Pages, Berkeley (2013)
2. Neurofeedback. In: Therapy Centre, Prague (2015)
3. Polak, R.: Mereni EEG signalu. In: Baechelor Work. CVUT Prague (2009)
4. Husek, M., Pyrih, P., et al.: Fourrier transform. Charles University in Prague (2017)
5. Svoboda, V., Marek, J., Brozek, J.: Reliability of the test. Elektro 2016. University of Zilina (2016)
6. Simonite, T.: Using Brainwaves to Guess Passwords. MIT Technology Review (2017)
7. Sulleiman, A.: Hackers can steal passwords using brainwave signals. Independent Mag. (2017)

Optimal Information Paths in Social Media: Personalized Consumption of Tweets

Klimis Ntalianis[1(✉)] and Nikolaos Mastorakis[2]

[1] Department of Business Administration, University of West Attica, Agiou Spyridonos Street, 12210 Egaleo, Athens, Greece
kntal@teiath.gr
[2] Industrial Engineering Department, Technical University of Sofia, Sofia, Bulgaria
mastor@tu-sofia.bg

Abstract. During the last decade Twitter has undergone a massive growth and several algorithms have been proposed for analysing its content. A common challenge is identifying user interests. In this work, we focus on personalizing the consumption of tweets by taking into consideration the tweets profile of each user (average tweet). In particular for each user an average vector is estimated that maps her/his interests. Then the distance between tweets that are posted on a user's wall is estimated. In this process the average tweet is also considered. Finally a graph of tweets is constructed and the minimum distance path is estimated. Experimental results on real life data exhibit the advantages and limitations of the proposed scheme.

Keywords: Twitter · Information path · Personalization · Integer programming

1 Introduction

Content personalization based on social networks' activities is gaining much interest lately. The personalized content for each user is determined by using various information queues such as clicks, likes, shares, cookies etc. A common focus of several existing approaches is to use current behaviors for providing personalization.

In this work, we also address this problem but now from the view of putting all information into a minimum distance optimal order. Towards this direction initially the tweets of each user are textually analyzed and an average vector is created representing the *average tweet* of the user. Since these tweets are pieces of information that the user has deliberately posted, we assume that they reveal her/his interests. In the next step we analyze the tweets posted on the user's wall (tweets from persons that the user follows). Then the distance among all tweets is estimated, including the *average tweet*. Next all tweets are connected to form a graph and the problem to find the appropriate order of tweets is transformed to a problem of finding the optimal minimum distance path in the graph. Finally formulation is further demoted to an integer programming problem. Experimental results on real world data exhibit the merits of the proposed scheme.

K. Ntalianis and A. Croitoru (Eds.): APSAC 2017, LNEE 489, pp. 133–139, 2019.
https://doi.org/10.1007/978-3-319-75605-9_19

The rest of this paper is organized as follows: Sect. 2 compactly presents some previous works. In Sect. 3 the proposed scheme is fully described while Sect. 4 provides experimental results. Finally Sect. 5 concludes this paper.

2 Previous Works

Much research has been done on tweet recommendations. In [1] a tweet recommendations methodology is proposed based on collaborative filtering. A graph co-ranking technique is presented in [2] while Uysal et al. [3] leverage retweet signals and a user's likelihood of retweeting tweets for generating personalized tweet rankings. In [4] collaborative filtering is also incorporated for generating keyword tags for profiles. In [5] the bag-of-phrases model is used to capture the underlying topics of posted microblogs. In [6] except of microblog posting history, reposting history, relations with other users and contextual knowledge, the authors also utilize sentimental information for microblog recommendations.

There are also other interesting recent works such as [7–9]. However all these works just recommend new content, without putting into a both semantically meaningful and minimum distance order all posted information.

3 Estimation of Optimal Information Paths

Let us consider a specific twitter user UR_i. In UR_i's wall, new content appears as soon as new tweets are posted from the followed accounts. Let us assume that each tweet i is an information piece which is gathered and analyzed to produce a vector $\mathbf{v}_i$:

$$\mathbf{v}_i = [wr_1, wr_2, \ldots, wr_k] \tag{1}$$

where $wr_1 = 1$ if the tweet i contains the word #1 or 0 if it does not contain it. In this case a vocabulary of k words is considered. Let $\mathbf{AU}v_i$ be the average vector for UR_i, which accumulates the information of all tweets posted by UR_i. Let us also assume that a correlation value among all tweets is estimated including $\mathbf{AU}v_i$. Now let us define a graph G with $n + 1$ vertices, where each vertex V represents a tweet (except of the "base" where $\mathbf{AU}v_i$ is located) and each edge E represents the connection between tweets. In our case two vertices are connected only if the respective vectors are correlated. Additionally the more correlated two vertices are the less their distance.

Twitter presents tweets using the first-come first-served (FCFS) rule. However when several tweets are posted, the FCFS may not be the best approach. This is due to the fact that UR_i has specific interests, which can be discovered by UR_i's previous tweets. In this case we estimate an optimal information path so that UR_i consumes the posted tweets in a personalized manner and according to her/his interests.

Towards this direction, UR_i is supposed to read each of the n tweets, indexed by 1, 2, …, n. She/he starts from the "base tweet" indexed by 0, reads each of the n other tweets once, and ends up to her/his base. During her/his reading, she/he can return to 0 exactly t times, including her/his final return (here t may vary), and she/he is supposed

to read no more than p tweets in one session. By a session we mean a succession of readings without returning to tweet number 0. In this case it is required to find such an information path which minimizes the total distance between tweets. In other words UR_i is supposed to read all tweets by following a minimum distance path. In reality this is a semantic distance among the different tweets.

If t is fixed, then for the problem to have a solution we must have $t \cdot p \geq n$. For $t = 1$, p $\geq$ n. In this case UR_i reads all tweets just once without checking her/his interests that are mapped onto $\mathbf{AU}v_i$. Let $d_{i,j}$ ($i \neq j$, $i, j = 0, 1, \ldots, n$) be the distance between tweet i and tweet j. Then our problem can be transformed into an integer programming problem. In particular minimize the linear form:

$$\sum_{0 \neq i \neq j \leq n} \sum d_{i,j} \cdot x_{i,j} \tag{2}$$

over the set determined by the following relations

$$\sum_{\substack{i=0 \\ i \neq j}}^{n} x_{i,j} = 1, \quad j = 1, \ldots, n \qquad \sum_{\substack{j=0 \\ j \neq i}}^{n} x_{i,j} = 1, \quad i = 1, \ldots, n \tag{3}$$

$$u_i - u_j + p x_{i,j} \leq p - 1, \qquad 1 \leq i \neq j \leq n \tag{4}$$

where $x_{i,j}$ are non-negative integers and u_i (i = 1, …, n) are arbitrary real numbers.

If t is fixed it is necessary to add the additional relation:

$$\sum_{i=1}^{n} x_{i,0} = t \tag{5}$$

Note that the constraints require that $x_{i,j}$ = 0 or 1, so that a natural correspondence between these two problems exists if $x_{i,j}$ are interpreted as follows: UR_i proceeds from tweet i to tweet j if and only if $x_{i,j}$ = 1. Under this correspondence the form to be minimized in Eq. (2) is the total distance among different tweets.

Let us consider a feasible solution to Eq. (2). The number of returns to the base tweet $\mathbf{AU}v_i$. is given by:

$$\sum_{i=1}^{n} x_{i,0} \tag{6}$$

The constraints of the form:

$$\sum x_{i,j} = 1, \qquad all\, x_{i,j}\, non - negative\ integers \tag{7}$$

represent the conditions that each tweet is presented to UR_i exactly once. The parameters u_i play a role similar to node potentials in a network and the inequalities involving them serve to eliminate paths that do not begin and end at tweet 0 ($\mathbf{AU}v_i$) and

paths that present more than p tweets. Consider any $x_{r_0,r_1} = 1$ ($r_1 \neq 1$). There exists a unique r_2 such that $x_{r_1,r_2} = 1$. Unless $r_2 = 0$, there is a unique r_3 with $x_{r_2,r_3} = 1$. We proceed in this way until some $r_j = 0$. This must happen since the alternative is that at some point we reach an $r_k = r_j$, $j + 1 < k$. Since none of the r's are zero we have:

$$u_{r_i} - u_{r_{i+1}} + p x_{r_i,r_{i+1}} \leq p - 1 \quad \text{or} \quad u_{r_i} - u_{r_{i+1}} \leq -1 \tag{8}$$

Summing from $i = j$ to $k-1$, we have

$$u_{r_j} - u_{r_k} = 0 \leq j + 1 - k \tag{9}$$

which is a contradiction. Thus all paths include tweet 0. It remains to observe that no path is of length greater than p. Let us suppose that such a tour exists, $x_{0,r_1}, x_{r_1,r_2}, \ldots, x_{r_p,r_{p+1}} = 1$, with all $r_i \neq 0$. Then:

$$u_{r_i} - u_{r_{p+1}} \leq -p \quad \text{or} \quad u_{r_{p+1}} - u_{r_i} \geq p \tag{10}$$

But we have:

$$u_{r_{p+1}} - u_{r_i} + p x_{r_{p+1},r_1} \leq p - 1 \quad \text{or} \quad u_{r_{p+1}} - u_{r_i} \leq p(1 - x_{r_{p+1},r_1}) - 1 \leq p - 1 \tag{11}$$

which is a contradiction.

Conversely, if the $x_{i,j}$, correspond to a legitimate path, it is clear that the u_i, can be adjusted so that $u_i = j$ if tweet i is the jth tweet presented in the path which includes tweet i, for we then have:

$$u_i - u_j = -1 \quad \textit{if} \quad x_{i,j} = 1 \quad \text{and always} \quad u_i - u_j \leq p - 1 \tag{12}$$

The above program involves $n^2 + n$ constraints in $n^2 + 2n$ variables. Since the inequality form of constraint is fundamental for integer programming calculations, one may eliminate $2n$ variables, say the $x_{i,0}$ and $x_{0,j}$, by means of the equation constraints and produce an equivalent problem with $n^2 + n$ inequalities and n^2 variables. The solution procedure used was the Tabu search method [10, 11].

4 Experimental Results

In order to evaluate the proposed scheme, experiments were contacted on 120 Twitter users, the majority of which are undergraduate students at the Department of Marketing of the Athens University of Applied Sciences (TEI of Athens). We used the Twitter API to collect the tweets, posted on the 31st of May 2017. In total 57,000 tweets were gathered or on average 475 tweets per wall. Of course in the wall of each user the numbers of tweets were varying, due to the different numbers of followed profiles, the different rates of postings among followed profiles etc. The "tweets to user walls" distribution is shown in Fig. 1.

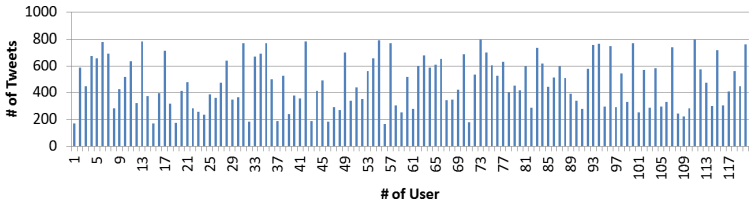

Fig. 1. Number of tweets posted on each user's wall

As it can be observed, the largest number of tweets is 799 (on the wall of user #111) while the smallest number of tweets is 167 (on the wall of user #56). Next and due to space limitations, results are presented for user #27 for two reasons: (a) the wall of user #27 contained 471 tweets (very near the average of 475 tweets/wall) and (b) user #27 tweets in English and the tweets on the wall are also in English. In particular initially the average vector $\mathbf{AU}v_{27}$ for the user has been estimated. The top five words of the vector are "University", "Education", "Students", "Exams" and "Innovation". Then correlation among the 471 tweets has been calculated (after discarding stop-words), by correlating their respective vectors. Zero correlation between two tweets means that they are not connected in the tweets graph. The greatest the correlation between two tweets the less their distance in the graph. Each isolated (not connected to any other tweets) tweet was discarded. By this way 443 tweets have remained to create the graph. After creating the graph, the optimal information path was estimated by the proposed algorithm. Due to space limitations, in Table 1 only the top 5 nodes (tweets) are presented. In the wall of user #27 they were presented in the following order (according to the time instance they were posted): 98, 64, 336, 299 and 156.

Table 1. Top 5 tweets for user #27

Ranking	Tweet
1st	*Important information for #students about to undertake #exams.*
2nd	*Corbyn: We will return the educational maintenance allowance, & end the University fees system.*
3rd	*Controversy strikes on Aligarh Muslim University campus, no food provided to students during Roza hours*
4th	*Meet twins Paula and Peter Imafidon. They passed the University of Cambridge Advanced Maths A level at age 8*
5th	*Some fun stuff going on at the Innovation Fair*

Furthermore the evolution of the normalized total distance was also calculated for a computing time between 100 and 1,000 s. Results are presented in Fig. 2. As it can be observed the solution at 1,000 s is better than the one at 100 s by 16%. However the reduction rate falls significantly after the 450 s.

Last but not least, an experiment to measure satisfaction has also been carried out. Towards this direction we have presented to each user the top 30 tweets as they were

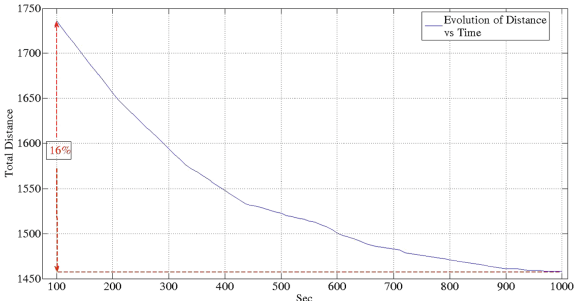

Fig. 2. Evolution of total distance through computational time

provided by Twitter (chronological order) and the top 30 tweets as provided by the minimum path within the graph. Then the 120 users that participated in these experiments were asked to express their preference. Three choices where provided: "Proposed", "Twitter" and "None". In total 120 subjective evaluation sessions have been carried out. Results are provided in Fig. 3, where the proposed scheme received 44.17%, Twitter's approach received 32.5%, while none received 23.33%. As it can be observed the answer "None" received a high percentage (28 users). This may be due to the fact that users are not satisfied by the quality of tweets themselves. Finally the proposed scheme outperforms Twitter's chronological order, since it is also able to personalize the consumption of information for each user.

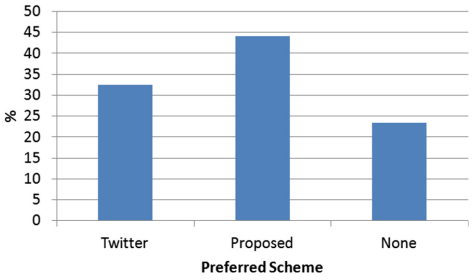

Fig. 3. Users' preference

5 Conclusion

In this paper we have presented a scheme to organize tweets in a non-chronological content-based order. Towards this direction a graph was created and the minimum distance path in the graph was estimated. Experimental results on real data illustrated the promising performance of the proposed scheme.

References

1. Chen, K., Chen, T., Zheng, G., Jin, O., Yao, E., Yu, Y.: Collaborative personalized tweet recommendation. In: Proceedings SIGIR (2012)
2. Yan, R., Lapata, M., Li, X.: Tweet recommendation with graph co-ranking. In: ACL (2012)
3. Uysal, I., Croft, W.B.: User oriented tweet ranking: a filtering approach to microblogs. In: Proceedings CIKM (2011)
4. Zhou, X., Wu, S., Chen, C., Chen, G., Ying, S.: Real-time recommendation for microblogs. Inf. Sci. **279**, 301–325 (2014)
5. Gong, Y., Zhang, Q., Han, X., Huang, X.: Phrase-based hashtag recommendation for microblog posts. Science China - Information Sciences, January 2017
6. Cui, W., Du, Y., Shen, Z., Zhou, Y., Li, J.: Personalized microblog recommendation using sentimental features. In: IEEE International Conference on Big Data and Smart Computing (2017)
7. Yuan, Z.–M., Huang, C., Sun, X.-Y., Li, X.X., Xu, D.-R.: A microblog recommendation algorithm based on social tagging and a temporal interest evolution model. Front. Inf. Technol. Electron. Eng. (2015)
8. Liu, S., Liu, Y., Xie, Q.: Personalized resource recommendation based on regular tag and user operation. In: Li, F., Shim, K., Zheng, K., Liu, G. (eds.) Web Technologies and Applications. Lecture Notes in Computer Science, vol. 9932. Springer (2016)
9. Karidi, D.P., Stavrakas, Y., Vassiliou, Y.: Tweet and followee personalized recommendations based on knowledge graphs. J. Ambient Intell. Hum. Comput. (2017)
10. Glover, F.: Tabu Search - Part 1. ORSA J. Comput. **1**(2) (1989)
11. Glover, F.: Tabu Search - Part 2. ORSA J. Comput. **2**(1) (1990)

Solving Sparse Matrices: A Comparative Analysis Between FPGA and GPU

Khaled Salah(✉) and Mohamed AbdelSalam

Mentor, A Siemens Business, Cairo, Egypt
{khaled_mohamed, mohamed_abdelsalam}@mentor.com

Abstract. In this paper, the performance improvement from using FPGAs and GPUs to solve sparse matrices is evaluated. GPU and FPGA are formally compatible but the results are very sensitive to the particular calculation task, the architecture of DSP blocks in particular FPGA, and the architecture of the designed core for particular calculation in FPGA. The results show that GPUs have superior performance over FPGAs for this particular type of problems.

Keywords: GPU · FPGA · Matrix · FEM · Linear equations

1 Introduction

Electromagnetic (EM) simulation is currently a highly-needed planning tool in high frequency systems. It enables the enhancement and the optimization of the performance of systems while they are still in the design phase.

The precise modeling of the relevant physical interactions in the simulation environment helps significantly in the optimization process and ensures that the system is optimally adapted to blend into its environment.

The main objective of EM simulation is to find an approximate solution for Maxwell's equations that satisfies the given boundary conditions and a set of initial conditions. Many numerical techniques are used for solving Maxwell's equations, e.g., the finite difference method (FDM) [1], finite element method (FEM) [2], finite volume method (FVM) [3], and the boundary element method (BEM) [4]. Computations involved in FEM consume too much time, which affects the final time-to-market value. Profiling shows that the most time-consuming part in the simulation process is the solver part, which is responsible for solving the resultant system of linear equations generated from the FEM.

The total number of equations may reach thousands or millions of linear equations. Thus, software-based EM solvers are often too slow. Several alternatives are introduced to accelerate the solver part including Application-specific Integrated Circuits (ASICs) for their high speed, Graphics Processing Units (GPUs) for their parallelization power, Field Programmable Gate Arrays (FPGAs) for their high speeds and relatively low cost and finally multi-FPGA systems for their abundance of logic resources. Although all these several solutions [5, 6], there is still a room to improve the speed and scalability of these solvers.

K. Ntalianis and A. Croitoru (Eds.): APSAC 2017, LNEE 489, pp. 140–147, 2019.
https://doi.org/10.1007/978-3-319-75605-9_20

In this work, we propose hardware architecture for the conjugate gradient method to be used in solving linear equation. This algorithm is implemented on both FPGA and GPU to evaluate the performance improvement between them. For the best of our knowledge, this is the first work to address such a comparison for linear equation solvers.

This paper is organized as follows: In Sect. 2, the background for FEM and conjugate gradient (CG) is presented. In Sect. 3, the proposed methodology is introduced. In Sect. 4, Results are discussed.

2 Background

In this section, we provide a brief overview of the FEM. Then, we describe the details of the conjugate gradient method used to solve the matrices resulting from using the FEM. Moreover, we give a quick introduction about GPU and CUDA.

2.1 Finite Element Method

The Finite Element Method (FEM) is a numerical technique, which is widely used in engineering to solve boundary-value problems, characterized by a partial differential equation (PDE) and a set of boundary conditions. The basic procedures of using FEM are: (1) discretizing the computational domain into finite elements, (2) rewriting the PDE in a weak formulation, (3) choosing proper finite element spaces and forming the finite element scheme from the weak formulation, (4) calculating those element matrices on each element and assembling the element matrices to form a global linear system, (5) applying the boundary conditions, solving the SLS, and finally, (6) post-processing the numerical solution.

2.2 Conjugate Gradient Method

Conjugate gradient method can reach the required tolerance after a relatively small number of iterations compared to Jacobi AND Gauss Method [7–10]. The conjugate gradient algorithm used in this work is shown in Listing 1.

The conjugate gradient algorithm used in this work can be formalized as follows:

```
Conjugate gradient algorithm: The algorithm is detailed
below for solving Ax = b.
Input: Number of linear equations.

Variables: A is a real, symmetric, positive-definite
matrix.

The input vector x0 can be an approximate initial
solution or 0.

Output: Solution.

     r_0=b-Ax_0
     p_0=r_0
     k=0
     Repeat
     α_n=(r_n^T r_n)/(p_n^T Ap_n )
     x_(n+1)=x_n+α_n p_n
     r_(n+1)=r_n-α_n [Ap]_n
     If r_(n+1) is very small then exit the loop else
     p_(n+1)=r_(n+1)+β_n p_n
     n=n+1
     End repeat
     The solution is x_(n+1)
```

2.3 GPU and CUDA

GPUs had been mostly used for computation of computer graphics. They have only lately been explored for their parallel computation power that can be used to accelerate algorithms that can be parallelized. Speed-ups resulting from using GPU-parallelized algorithms can reach 100x compared to algorithms running on Central Processing Units (CPUs) [11, 12].

CUDA is a parallel computing platform and programming model invented by NVIDIA. The CUDA platform is designed to work with programming languages such as C, C++ and FORTRAN. It allows software developers to use GPUs for general purpose processing – an approach known as GPGPU.

3 Proposed Architecture

In order to gain a high performance on the hardware for solving system of linear equations, we need to solve them in parallel. We could not solve linear equation in parallel as long as there are high dependencies between them, so we need a way to reduce those dependencies between equations.

There is a property in the output matrix of the finite element method that can be used to reduce those dependencies named clustering. This property appears in the output matrix as the finite element method divides the test element into square meshes and calculations takes place on the edges of the mesh. Vertical edges in one row and horizontal edges in one column each contribute in the main output matrix with equations with high dependencies between them and low dependencies with other equations in the matrix. We named each group of those equations a cluster (Fig. 1).

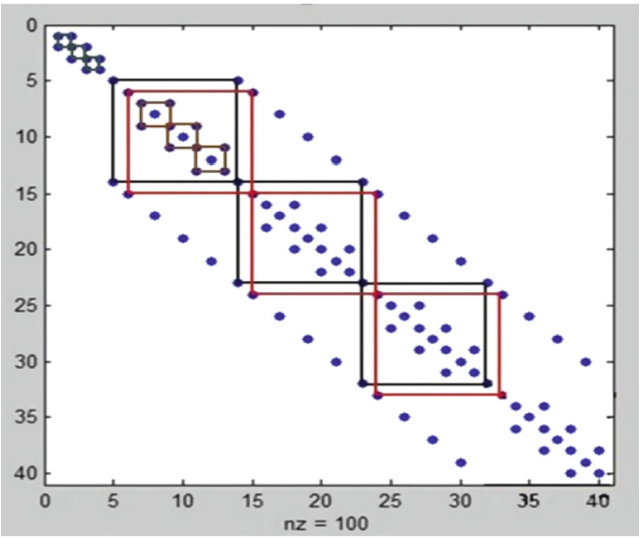

Fig. 1. Clustering: the finite element method divides the test element into square meshes and calculations takes place on the edges of the mesh.

The proposed architecture for this method is shown in Fig. 2, where the architecture consists of the following modules:

Top Module. This module encapsulates all of the design modules and connects them together.

Control Unit. The control unit is responsible for handling the interaction between the ALU and the memories in the design.

Memories. The algorithm makes use of various kinds of matrices and vectors, which we need to store in our design implementation in memories. Those memories are: *memA*, this memory is used to store the square coefficient matrix A. *memR*, this memory is used to store the dense vector (r) used in the algorithm. Initially vector (r) is loaded with the right hand vector (b), then it is updated each iteration as the algorithm requires. *memP*, this memory is used to store the dense vector (p). Just like vector (r), it is initially loaded with the right hand vector (b), then it is updated each iteration as the algorithm requires. *memX*, this is the solution vector.

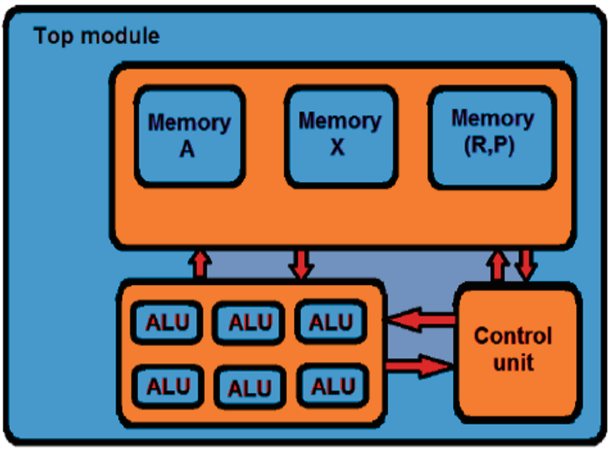

Fig. 2. The proposed architecture for Conjugate Gradient method, where A, X, R, and P represent the coefficient matrix, solution, residue and conjugate vectors respectively.

ALU. The ALU is responsible for all arithmetic operations performed on data. It has the following modules: *Dot product module*, the algorithm requires a number of dot product operations. *Matrix by vector module*, the algorithm requires to perform one matrix by vector operation A * P. *Mult_add module*, this module is responsible for performing operations of the kind (X = Y ± c * Z).

The most important operation in conjugate gradient method is the dot product as depicted in Fig. 3 and the most critical part in the dot product is the summation at the end stage. So, we proposed to implement it as a tree adder (Fig. 4).

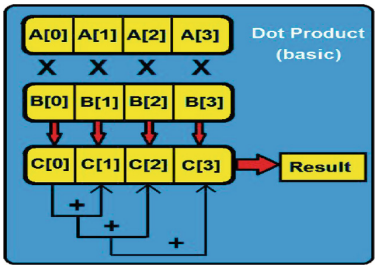

Fig. 3. Basic dot product operation.

Moreover, the summation in the Inner Product is implemented using parallel reduction as the process is done as if a binary tree is being constructed. This reduced the complexity of the summation from O(N) to O(logN) as illustrated by Fig. 5.

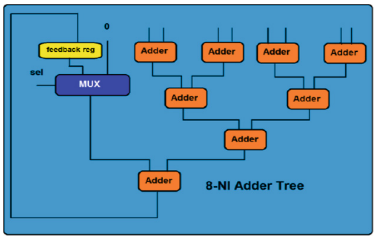

Fig. 4. Adder tree implementation.

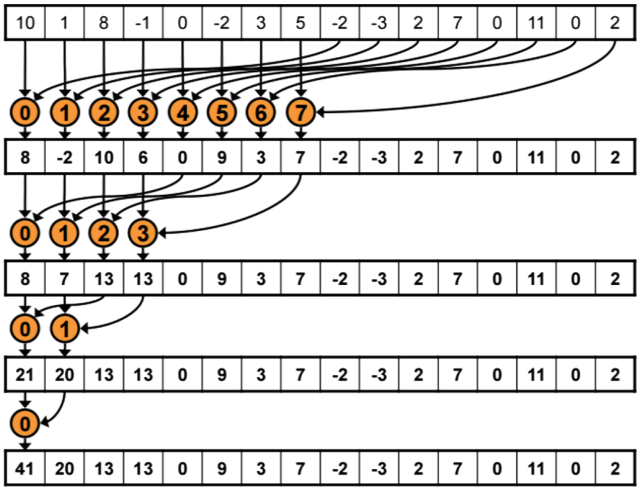

Fig. 5. Parallel reduction algorithm.

4 Results and Discussions

GPU and FPGA are formally compatible but the results are very sensitive to the particular calculation task, the architecture of DSP blocks in particular FPGA, and the architecture of the designed core for particular calculation in FPGA.

The proposed architecture is implemented on hardware FPGA using Verilog and on GPUs using CUDA. For GPU, our results were verified using Intel core i5-4510U and GeForce 920 m graphics card. GeForce 920 m is based on NVIDIA's Maxwell architecture; it has a global memory of size 2048 MBs and clock rate 900 MHz, 384 CUDA cores, a shared memory per block of size 49152 Bytes and number of threads that can reach 1024 threads per block. For FPGA, our results were verified using VERTEX-7 from Xilinx. GPU-based implementation of Jacobi versus conjugate gradient results is shown in Fig. 6. Comparison between GPUs and Emulators/FPGAs in terms of run time is shown in Table 1, where GPUs showed superior performance.

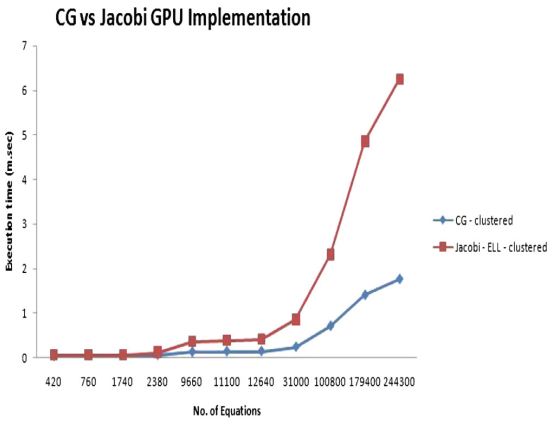

Fig. 6. Jacobi clustered Vs. CG clustered.

Table 1. Comparison between run-time (*msec*) on both GPU & FPGA platforms.

#Equations	FPGA platform	GPU platform
420	2.6	0.02
760	3.5	0.042
1740	5.2	0.043
2380	6.1	0.05
9660	12.1	0.12
11100	13	0.13
12640	13.8	0.14
31000	21.6	0.2
100800	38.8	0.7
179400	51.7	1.7
244300	60.3	1.8

For FPGA implementation, the resources used by the algorithm including the total number of lookup tables (LUTs), slice registers, and digital signal processing blocks (DSPs), as well as the throughput obtained, are shown in Table 2.

Table 2. FPGA utilization.

Platform	Virtex 7
LUTs	27,000
Registers	29,000
Total DSPs	64
Freq (MHz)	300
Slices	16000

References

1. Smith, G.D.: Numerical Solution of Partial Differential Equations: Finite Difference Methods. Oxford University Press, Oxford (1978)
2. Fix, G., Strang, G.: An Analysis of the Finite Element Method. Prentice-Hall, Englewood Cliffs (1973)
3. LeVeque, R.: Finite Volume Methods for Hyperbolic Problems. Cambridge University Press, Cambridge (2002)
4. Banerjep, K.: Boundary Element Methods in Engineering. McGraw-Hill, New York (1994)
5. Carvalho, R.F., Martins, C.A.P.S., Batalha, R.M.S., Camargos, A.F.P.: 3D parallel conjugate gradient solver optimized for GPUs. In: Digests of the 2010 14th Biennial IEEE Conference on Electromagnetic Field Computation, p. 1 (2010)
6. Wu, G., Xie, X., Dou, Y., Wang, M.: High-performance architecture for the conjugate gradient solver on FPGAs. IEEE Trans. Circuits Syst. II Express Briefs **60**(11), 791–795 (2013)
7. Atkinson, K.A.: An Introduction to Numerical Analysis, 2nd edn. Wiley, New York (1989)
8. Avriel, M.: Nonlinear Programming: Analysis and Methods. Dover Publishing (2003)
9. Golub, G.H., Van Loan, C.F.: Matrix Computations, 3rd edn. Johns Hopkins University Press (2011). Chapter 10
10. Saad, Y.: Iterative methods for sparse linear systems, 2nd edn. SIA (2005). Chapter 6 http://www.nvidia.com/object/cuda_home_new.html
11. Kirk, D.B., Hwu, W.-M.W.: Programming Massively Parallel Processors - A Hands-On Approach. Morgan Kaufmann, New York (2012)
12. Salah, K.: IP cores design from specifications to production: modeling, verification, optimization, and protection. In: IP Cores Design from Specifications to Production. Springer International Publishing (2016)

Making a Shift from Believing to Knowing by the Help of RDF CFL Formal Representation

Martin Žáček(✉) and Alena Lukasová

Department of Computers and Informatics, University of Ostrava, Ostrava, Czech Republic
{martin.zacek,alena.lukasova}@osu.cz

Abstract. In the frame of seeking an optimal formal language means for semantic web inferences a model and language RDF CFL has been developed. Using an intensional approach to the language semantics in its graph-based style of representation a demand of open world has been fulfilled. On the other side the RDF CFL system contains a package of inference methods working especially in closed-worlds, that have been developed in the clausal form of first order predicate logics, useful for solving a lot of tasks over corresponding knowledge bases. The article shows one of the capabilities of our RDF CFL graph language using as an example a well-known Castaněda's puzzle that has been before used by some authors of new formal approaches, like for example Shapiro's SNaPS for testing their possibilities. The believing versus knowing problem accompanying the puzzle brings into a discussion a further dimension.

Keywords: RDF · CFL · NLC · Castaněda · Puzzle · Logic · Language

1 Introduction

In the frame of seeking an optimal formal language means for semantic web inferences a model and language RDF CFL has been developed. Using an intensional approach to the language semantics in its graph based style of representation a demand of open world has been fulfilled. On the other side the RDF CFL [4] system contains a package of inference methods working especially in closed-worlds, that have been developed in the clausal form of first order predicate logics, useful for solving a lot of tasks over corresponding knowledge bases. The article shows one of the capabilities of our RDF CFL graph language using as an example a well-known Castaněda's puzzle that has been before used by some authors of new formal approaches, like for example Shapiro's SNaPS for testing their possibilities. The believing versus knowing problem accompanying the puzzle brings into a discussion a further dimension.

K. Ntalianis and A. Croitoru (Eds.): APSAC 2017, LNEE 489, pp. 148–155, 2019.
https://doi.org/10.1007/978-3-319-75605-9_21

2 Knowing and/or Believing a Think

From the web discussion on a difference between knowing and believing [2] we have chosen the following statements fulfilling enough our seeing the topic, corresponding to our knowledge level of cognitive science.

1. 'Believing' means that you have chosen a truth, but 'knowing' means that you are certain about that truth.
2. 'Believing' always leaves room for doubt, but 'knowing' leads to confidence.
3. 'Believing' is blind trust, while 'knowing' is trusting with awareness (Fig. 1).

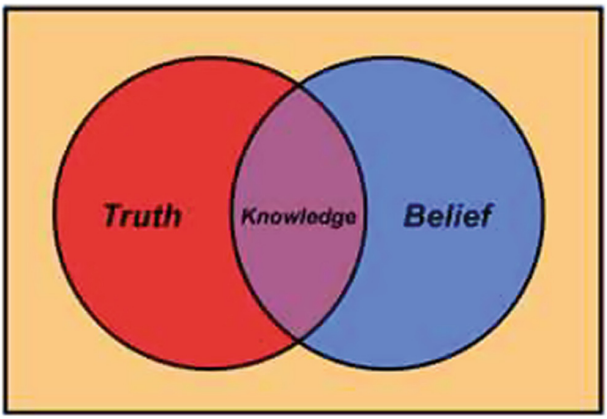

Fig. 1. Knowledge. (http://www.differencebetween.net/miscellaneous/difference-between-knowing-and-believing/#ixzz4PsivjUyL)

When you say 'I believe', you indicate that you don't know about this thing, because, in your personal experience, it has not yet occurred. Beliefs are based on your words, or a particular train of thought. You apply these beliefs to your life because they are appealing. As a result, you feel and begin to believe that they are true.

To have got any assurance that what we just believe in, is true or not we should delve deeper into the meaning instead of follow blindly our belief, without letting know whether it is a truth or not, and try to have known what it is speaking about.

An element of doubt should be put in between 'believing' and 'knowing', but doubt with shrewdness or intelligence. Even if we know useful information, it should be tested with respect to the believed think, so that it turns into knowledge, and is then converted from a belief into knowledge. It is extremely important that we feed our mind with the right information. We create the world with our knowledge and beliefs. So better be careful in what we believe.

We take into account the real knowledge about a think as an end member of a step by step more precise chain of coming out from a rather vague stage of knowledge like beliefs to an expected goal – the real facts about the think.

Moreover our approach leads also to seeing all the process of the children education in a similar manner. It means at the beginning we cannot speak about a real knowledge of an educated subject. The process of step by step education we can take as a cleaning a rather uncertain concept believed in child's mind towards a conceptual term with a clear meaning.

3 Castaněda's Puzzle with Both Believing and Knowing Input Information

Following the test of capabilities of SNePS system (Shapiro and Rapaport [1]) we decided to use in the following paragraphs the known Castaněda's puzzle of Hector Neri Castaněda [3] with the data background coming out from the Sophocles' tragedy as an example how to reconcile belief and knowledge about a concrete think.

A short explanation of the Sophocles' tragedy:

Oedipus has become the king of Thebes while unwittingly fulfilling a prophecy that he would kill his father, Laius (the previous king), and marry his mother, Jocasta (whom Oedipus took as his queen after solving the riddle of the Sphinx). The action of Sophocles' play concerns Oedipus' search for the murderer of Laius in order to end a plague ravaging Thebes, unaware that the killer he is looking for is none other than himself. At the end of the play, after the truth finally comes to light, Jocasta hangs herself while Oedipus, horrified at his patricide and incest, proceeds to gouge out his own eyes in despair.

Input data for a solving of the Castaněda's puzzle consists of three sentences, two of them (1), (3) we use as beliefs and one (2) as a description of a real fact:

1. At the time of the pestilence, Oidipus believed that: Oedipus's father was the same as his own father but the previous King of Thebes was not the same as his own father.
2. Oedipus's father was the same as the previous King of Thebes.
3. It was not the case that at the time of pestilence Oidipus believed that: the previous King of Thebes was the same as his own father but the previous King of Thebes was not the same as his own father.

Input sentences (1) and (3) express two beliefs of Oidipus, the first at the positive approach, the second from the negative point of view.

Authors of the paper [1] completed input information by four theorems:

(T1) For any individuals x and y: if x is (genuinely or strictly) identical with y, than whatever is true of x is true of y and vice versa.

(T2) The sentential matrix occurring in (1) and (3), namely: "at the time of pestilence, Oidipus believed that:__ was the same as his own father but the previous King of Thebes was not the same as his own father", expresses something true of (a property of) the individual denoted by the singular term that by filling the blank in the matrix produces a sentence expressing a truth.

(T3) The expression "was the same as" in (2) expresses genuine or strict identity.

(T4) The singular terms "the previous King of Thebes" and "Oidipus's father" have exactly the same meaning and denotation in both direct and indirect speech.
Our method needs for an analyzing the puzzle the theorem (T5) more. It is one of the known deMorgan rules:
(T5) Negation of a conjunction of statements implies a disjunction of the negated statements.

3.1 Representing Sentences (1)–(3) in RDF CFL Language

Representing the Belief (1)

1. *At the time of the pestilence, Oidipus believed that: Oedipus's father was the same as his own father but the previous King of Thebes was not the same as his own father.* Figure 2 shows an antecedent of the clause without a consequent.

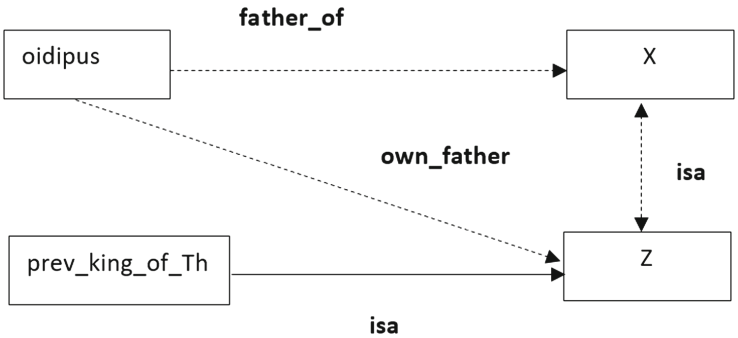

Fig. 2. An antecedent of the clause without a consequent.

After an application of the substitution rule (laius/X, @anybody/Y) the network (1) becomes (1′). "Substitution rule" is one of the two inference rules within the system RDF CFL. The substitution rule is usable in both of the clauses (1) and (3) because both of them are here representing networks of inference prerequisites of processes with variables of universal quantified elements in representative clauses (Fig. 3).

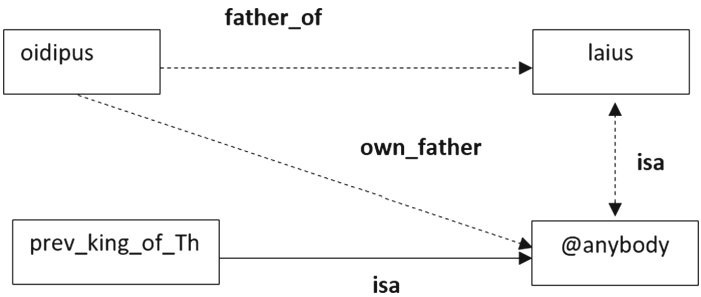

Fig. 3. Next step of deduction.

Representing the Belief (3)
It was not the case that at the time of pestilence Oidipus believed that: the previous King of Thebes was the same as his own father but the previous King of Thebes was not the same as his own father.

The Fig. 4 represents the Oidipus's belief in its positive variant, having the conjunction of vectors **isa**(prev_king_of_Th, Y) & **father_of**(Oidipus, Y) in the antecedent of a clause without a consequent.

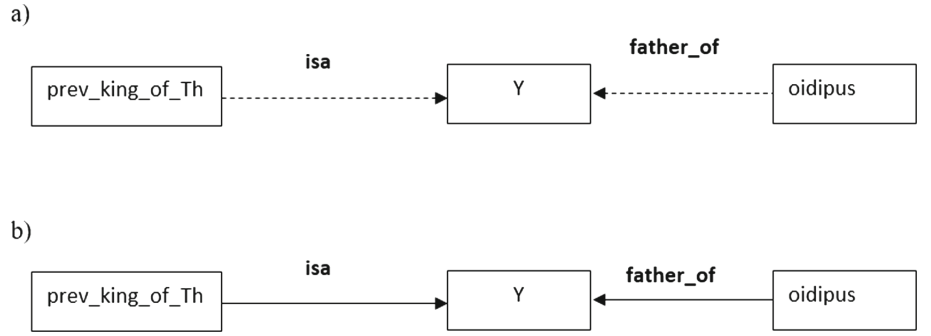

Fig. 4. The Oidipus's belief in its positive variant.

After the using of (T5) the Fig. 4a represents the original negative Oidipus's belief as the consequent (disjunction) of a clause without an antecedent.

Representing the Knowledge (2) of the Sophocles's Mythological Tragedy

2. *Oidipus's father was the same as the previous King of Thebes.*

3.2 Adding Relevant Rules or Facts to Make a Knowledge from the Belief as It Has Been Given

Authors of [1] as well as [3] use four relevant theorems (T1)–(T4) to investigate believes (1) and (3) to become a knowledge.

The same four theorems (T1)–(T3) we use now for solving the question from the point of view of our RDF CFL graph language.

(T1) expresses a law holding in predicate logics and of course must hold in RDF CFL as its modified system (see at the Fig. 5 in the form of clause of RDF CFL) (Fig. 6).

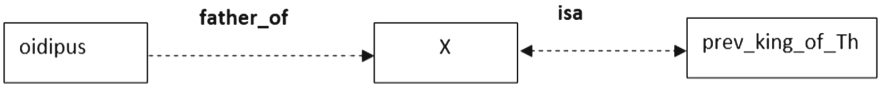

Fig. 5. The form of clause of RDF CFL.

Theorem (T2) represents the corresponding RDF CFL "substitution rule" [1].

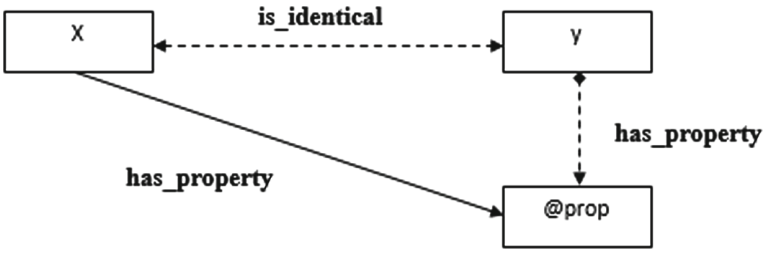

Fig. 6. The clause form of RDF CFL.

(T2) rule applying in the (1′) graph returns the statements **father_of**(oudipus, laius).

After an using resolution rule on clauses of the Fig. 7:

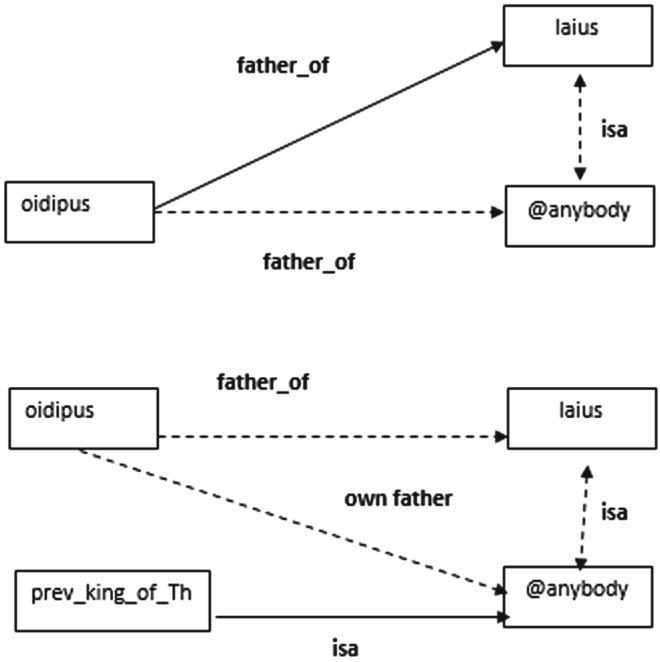

Fig. 7. Applying resolution rule.

After a further using of (T1) rule: father_of(oidipus, prev_king_of_Th) (Figs. 8 and 9).

(1′) after previous instance of (T2) rule and after a using resolution rule the network says at the consequent of the corresponding clause the same as the statement (2): *Oidipus's father was the same as the previous King of Thebes* (Fig. 10).

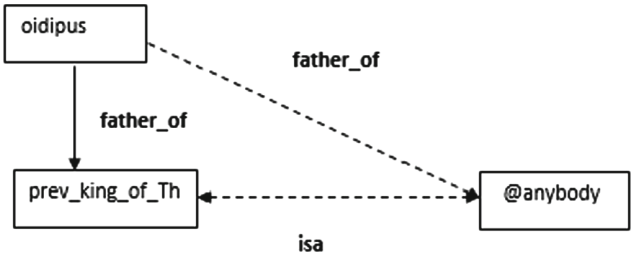

Fig. 8. Further using of (T1) rule.

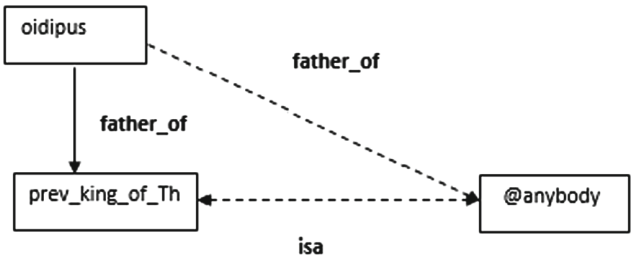

Fig. 9. father_of (oidipus, prev_king_of_Th)

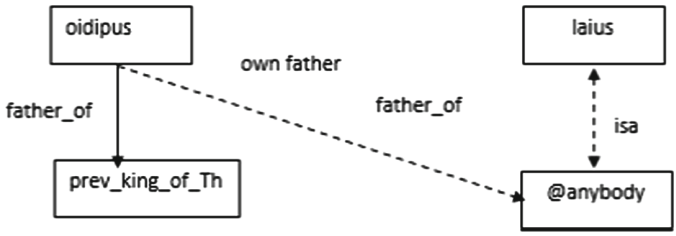

Fig. 10. The result.

4 Conclusion

Our system RDF CFL [4–7] can represent and reason about entities whose meaning can have an extensional character but also it can use means to express as well as systems like SNePS the meaning pure intensionally. So, our language of representation is able to be in an environment of semantic web a useful natural communication language not only for people but also for human-robot interaction.

By means of the RDF CFL graph representation apparat is there a possibility to construct relevant intensional bindings between concepts of the real domain in the form of networks shearing all their original properties.

We can take into account a real knowledge about a think as an end member of a step by step more precise chains that are coming out from a rather vague stage of knowledge like beliefs to an expected goal – knowledge as real facts about the think.

Moreover our approach leads also to seeing all the process of the children education in a similar manner. It means at the beginning we cannot speak about a real knowledge of an educated subject. The process of step by step education we can take as a cleaning a rather uncertain concept believed in child's mind towards a conceptual term with a clear meaning.

Acknowledgments. The research described here has been financially supported by University of Ostrava grant SGS10/PřF/2017. Any opinions, findings and conclusions or recommendations expressed in this material are those of the authors and do not reflect the views of the sponsors.

References

1. Shapiro, S.C., Rapaport, W.J.: The SNePS family. Comput. Math Appl. **23**, 243–275 (1992)
2. Shapiro, S.C., Rapaport, W.J.: Models and minds. In: Knowledge Representation for Natural-Language Competence. (1991)
3. Castaněda, H.N.: Philosophy as a science and as a worldview. In: Cohen, A., Dascal, M. (eds.) The Institution of Philosophy, Peru, IL. Open Court (1989)
4. Lukasová, A., Vajgl, M., Žáček, M.: Knowledge represented using RDF semantic network in the concept of semantic web. In: Proceedings of the International Conference of Numerical Analysis and Applied Mathematics 2015 (ICNAAM 2015), USA. AMER INST PHYSICS (2016)
5. Lukasová, A., Žáček, M., Vajgl, M.: Reasoning in graph-based clausal form logic. IJCSI Int. J. Comput. Sci. Issues **9**(1–3), 37–43 (2012). ISSN (Online) 1694-0814
6. Žáček, M., Lukasová, A., Miarka, R.: Modeling knowledge base and derivation without pre-defined structure by graph-based clausal form logic. In: Proceedings of the 2013 International Conference on Advanced ICT and Education, France, pp. 546–549. Atlantis Press: AISR (2013). ISBN 978-90786-77-79-6
7. Žáček, M., Lukasová, A.: English grammatical rules representation by a meta-language based on RDF model and predicate clausal form. Inf. Int. Interdisc. J., 4009–4015 (2016). ISSN 1343-4500

Utilization of NFV in Cloud Data Center

Tomas Svoboda[1(✉)] and Josef Horalek[2]

[1] Faculty of Electrical Engineering and Informatics, University of Pardubice, Pardubice, Czech Republic
tomas.svoboda5@student.upce.cz

[2] Faculty of Informatics and Management, University of Hradec Kralove, Hradec Kralove, Czech Republic
josef.horalek@uhk.cz

Abstract. Problematics of reliable and secure set up of virtual network service for orchestrators in cloud environment is a part with high degree of risk within its implementation from the functionality and security point of view. This degree of risk is greatly influenced by the implementer who can make, intentionally or unintentionally, a number of mistakes that may have both security and economic implications. The aim of this article is to introduce the SaltStack orchestration procedure by which the virtual network service can be deployed automatically. The introduced procedure that allows to install cluster of the Avivantage software load-balancer controller is automated. Procedure also includes all necessary dependencies in a specific OpenStack environment by calling a single command. The created procedure shows the general procedures for creating a VNF rule for orchestrators. The introduced rule has been successfully tested on a real-world environment running on the OpenStack cloud platform with OpenContrail's network solution.

Keywords: NFV · Datacenter · OpenStack · OpenContrail · Framework SaltStack

1 Introduction

Nowadays, the cloud providers utilized datacenters, for providing cloud services, where all computing performance is installed and distributed to individual customers or services [1]. NFV (network function virtualization) is a framework that unifies individual parts of cloud network infrastructure and also allows its creation, management and supervision [2]. NFV is a computer network architecture concept where traditional physical network devices are replaced by virtual devices, in the form of virtual machines that perform the same functionality and operates on standard, high-performance servers [3, 6]. Using virtualized solutions, compatibility issues can be avoided when devices from different manufacturers are utilized [4]. Software solutions can be developed as open-source and virtualization is not dependent on the manufacturer as in the case of physical devices. The NFV was introduced in 2013 by the European Telecommunications Standards Institute (ETSI). The NFV framework architecture consists of three

K. Ntalianis and A. Croitoru (Eds.): APSAC 2017, LNEE 489, pp. 156–162, 2019.
https://doi.org/10.1007/978-3-319-75605-9_22

main components [5]: **Virtual Network Function (VNF)** - is a software implementation of a network device's feature that runs in one or more virtual machines or containers. NFV infrastructure typically contains several VNF. **Network Function Virtualization Infrastructure (NFVI)** – is a subsystem that consists of all utilized physical devices, such as servers, switches, mass storage, and software technologies that enables virtualization, typically hypervisors. **Management and Orchestration (MANO)** - is a subsystem that provides access to the entire framework administration. VNF management is provided by Virtual Networks Functions Manager (VNFM), Virtualization Infrastructure Manager provides virtualization infrastructure and Network Function Virtualization Orchestrator (NFVO) provides orchestration and automation of NFV infrastructure as a whole [7].

2 Architecture and Utilized Technologies

Figure 1 depicts the individual parts of NFV framework and the specific implementation of software components, which were chosen for the implementation of the individual layers. The OpenStack [8] platform with OpenContrail SDN extension has been selected as the Network Functions Virtualization Infrastructure (NFVI) a Virtualized Infrastructure Manager (VIM). The SaltStack [10] tool has been selected to provide Network Functions Virtualization Orchestrator (NFVO) and Virtual Network Functions Manager (VNFM) functions.

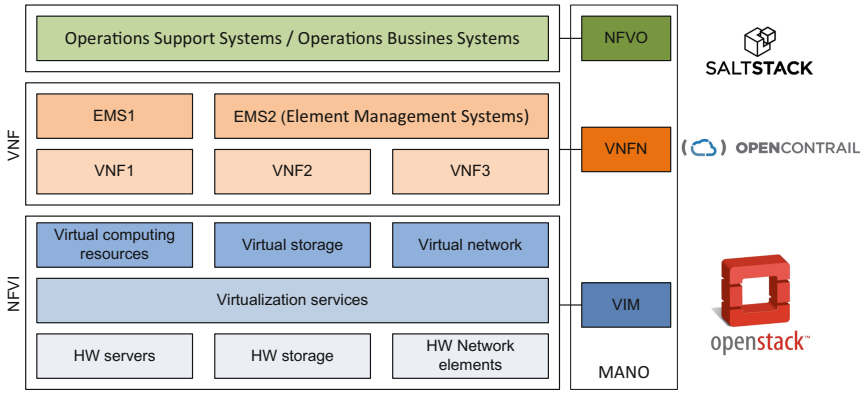

Fig. 1. NFV framework architecture (source: authors)

OpenStack was selected for its stability, great variability and a large number of implementations in production environments. It is a very stable and tuned platform for cloud implementation with NFV. OpenContrail is directly available for use with NFV since it has been developed for this type of usability from the very beginning [9].

Compared to OpenStack's standard network solution (Neutron), OpenContrail is more scalable and more stable, especially for large number of virtual machines. The main advantage of OpenContrail over Neutron is distributed vRouter, which means in practice that communication between computing servers, which hosting a virtual machines can take place directly. This communication goes through Neutron via network nodes, which are servers, that provides all communication over virtual networks. It means, that all network traffic is oriented in one place, and thus to a large number of instances, to its eventual collapse. This problem can be eliminated by using distributed access, because the load is evenly spread across all computing nodes for achieving better scalability, stability, and, of course, higher network throughput. In addition, OpenContrail offers some other capabilities over Neutron, including, for example service chaining, load-balancing, analytics, or a more advanced firewall. Figure 2 depicts the flow of packets by using Neuron and OpenContrail.

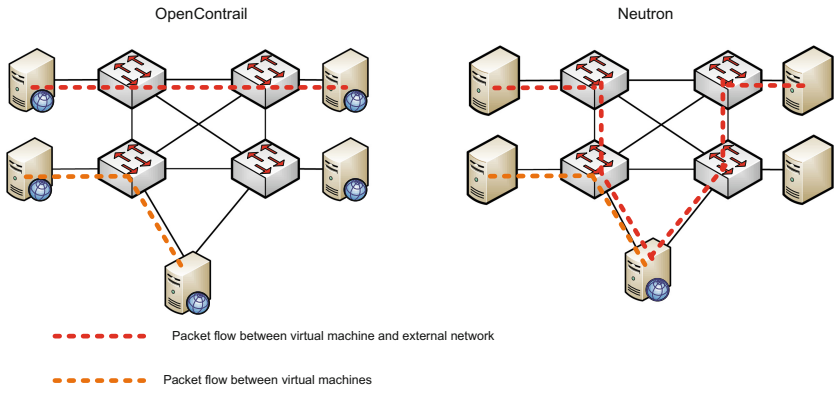

Fig. 2. The difference in the packet stream between Neutron and OpenContrail (source: authors)

SaltStack was selected because it provides the widest range of orchestration options. In addition to managing NFV, it's easy to control the entire cloud environment. In addition, it provides very good native support for OpenStack features.

3 VNF Deployment Technology

The premise is that OpenStack and OpenContrail are installed and are fully functional. The Avi Vantage software load-balancer from Avi Networks was selected as the VNF. However, AviVantage deployment and its functionality and safety is dependent on implementer. The core of presented solution is to automatize this process using the Salt orchestrator. Load-balancer takes care of the even distribution of load, typically from service users, among all servers that provide it. It is only relevant if two or more servers provide identical service on the network. AviVantage installation has three operating modes.

The AvimanagedLBaaS mode was selected for the presented solution, in which a special tenant for Avi Controller with a user with administrative rights is created. Administrator is able to create Avi Service Engine (Avi SE) in the cloud users. Users can then manage Avi SE in their tenant. Within the installation, administrator must first create a tenant for controllers, create at least one rule for controller instances, upload a controller disk image to Glance, create network management for controllers, SE and security-group with specified firewall rules, and finally create a controller instance.

3.1 Salt Pillar and Formula Creation

The formula is created based on the requirements set forth above and reflects the procedure at the end of the previous chapter. Salt state formulas have a .sls ending, so the file called avinetworks.sls is created in the directory where the Salt formula is stored. The first level contains the individual roles of the Salt, the second level lists their subrole. The solution presented here is the role of *avinetworks*, which contains one subrole *controller*. The subrole contains a list of variables.

```
avinetworks:
    controller:
          enabled: true
          identity: cloud1
          image_location: http://...
          disk_format: qcow2
          public_network: INET1
```

In the next step, we need to define the underlying condition, whether the role is enabled.

```
{%- if server.enabled %}
{%- endif %}
```

Here is a section of the formula that contains steps for creating network resources using the Neutron Application Interface. This is a network, subnet, and router that provides communication with an external network.

```
avinetworks_network:
    neutronng.network_present:
    - profile: {{ server.identity }}
     - name: avinetworks
     - tenant: avinetworks
     - require:
          - keystone: avinetworks_user
avinetworks_subnet:
    neutronng.subnet_present:
     - profile: {{ server.identity }}
     - name: avinetworks
     - tenant: avinetworks
     - network: avinetworks
     - cidr: 10.1.0.0/24
     - require:
          - keystone: avinetworks_user
          - neutronng: avinetworks_network
avinetworks_router:
    neutronng.router_present:
    - profile: {{ server.identity }}
    - name: avinetworks
    - tenant: avinetworks
    - interfaces:
        - avinetworks
    - gateway_network: {{ server.public_network }}
    - require:
        - keystone: avinetworks_user
    - neutronng: avinetworks_network
    - neutronng: avinetworks_subnet
```

Creating instances of a virtual machine controller is briefly presented below.

```
avinetworks_instance_01:
    novang.instance_present:
    - profile: {{ server.identity }}
    - tenant_name: avinetworks
    - name: avi_ctl01
    - flavor: avinetworks
    - image: avinetworks
    - security_groups:
        - avinetworks
    - networks:
        - name: avinetworks
        v4_fixed_ip: 10.1.0.10
```

Consequently, a command for syncing all modules and roles on the Saltmaster, pillar sync command, and an avinetworks application for the particular minion can be executed.

```
$ Salt -C 'I @ avinetworks: controller' saltutil.sync_all
$ Salt - 'I @ avinetworks: controller' saltutil.refresh_
pillar
$ Salt -C 'I @ avinetworks: controller' state.sls
avinetworks
```

Now, the web interface of one of the controllers can be executed to make sure it runs correctly. Figure 3 depicts a web interface Access Setup Form. The services between which load-balancing is to take place can be added and set up the services.

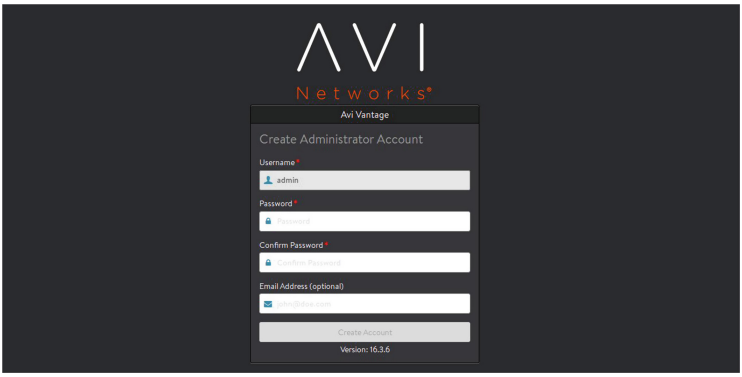

Fig. 3. Avi vantage load balancer loan form (source: authors)

4 Copyright Forms

This work and contribution is supported by the project of the student competition of the University of Pardubice, Faculty of Electrical engineering and Informatics "Usage of ambient intelligence in the area of information systems and their communication".

5 Conclusion

The presented solution describes the deployment of a functional prescription and pillar for the Salt orchestrator that allows automated cluster installation of three instances of the AviVantage software load-balancer controller, by calling a single command, including all the necessary dependencies in the OpenStack environment. The more general procedure for creating a VNF rule for orchestrators was presented. Regardless of the chosen platform, VNF or orchestration, it is always necessary to familiarize user with the manual installation of the selected VNF and then try to transform these manual actions into the chosen rule, whether it is template for Tacker, Cloudify blueprints, salt formula, or any other formulas for orchestrators. The introduced and tested solution is

fully usable for automated controller installation. Introduced VNF rule for orchestration significantly reduces the risk of deploying the required tool in OpenStack, thanks to the ability to independently test automated installation against intentionally or unintentionally errors and thereby reducing security and economic impacts.

References

1. Reddy, K.H.K., Mudali, G., Sinha Roy, D.: A novel coordinated resource provisioning approach for cooperative cloud market. J. Cloud Comput. **6**(1), 1–8 (2017). https://doi.org/10.1186/s13677-017-0078-z
2. Trajkovska, I., Kourtis, M.-A., Sakkas, C., Baudinot, D., Silva, J., Harsh, P., Xylouris, G., Bohnert, T.M., Koumaras, H.: SDN-based service function chaining mechanism and service prototype implementation in NFV scenario. Comput. Stand. Interfaces **54**, 247–265 (2017). https://doi.org/10.1016/j.csi.2017.01.002
3. Hausheer, D., Hohlfeld, O., Lopez, D.R., Maggs, B.M., Raiciu, C.: Network function virtualization in software defined infrastructures. In: Dagstuhl Seminar 17032. Dagstuhl Reports, vol. 7(1). Schloss Dagstuhl-Leibniz-Zentrum fuer Informatik (2017)
4. Maresova, P., Sobeslav, V., Krejcar, O.: Cost–benefit analysis–evaluation model of cloud computing deployment for use in companies. Appl. Econ. **49**(6), 521–533 (2017). https://doi.org/10.1080/00036846.2016.1200188
5. Sobeslav, V., Komarek, A.: Opensource automation in cloud computing. Lecture Notes in Electrical Engineering, vol. 355, pp. 805–812 (2015). https://doi.org/10.1007/978-3-319-11104-9_93
6. Ramalho, F., Neto, A.: Virtualization at the network edge: a performance comparison. In: IEEE 17th International Symposium on a World of Wireless, Mobile and Multimedia Networks (WoWMoM), pp. 1–6. IEEE, June 2016
7. Bellavista, P., Foschini, L., Venanzi, R., Carella, G.: Extensible orchestration of elastic IP multimedia subsystem as a service using Open Baton. In: Proceedings of the 5th IEEE International Conference on Mobile Cloud Computing, Services, and Engineering, MobileCloud 2017, Art. no. 7944877, pp. 88–95 (2017). https://doi.org/10.1109/MobileCloud.2017.31
8. Scott-Hayward, S., Natarajan, S., Sezer, S.: A survey of security in software defined networks. IEEE Commun. Surv. Tutor. **18**(1), 623–654 (2016). https://doi.org/10.1109/COMST.2015.2453114. Art. no. 7150550
9. Wang, L., Zhang, D.: Research on OpenStack of open source cloud computing in colleges and universities' computer room. IOP Conf. Ser. Earth Environ. Sci. **69**(1), 012140 (2016). https://doi.org/10.1088/1755-1315/69/1/012140
10. Benson, J.O., Prevost, J.J., Rad, P.: Survey of automated software deployment for computational and engineering research. In: 10th Annual International Systems Conference, SysCon 2016 (2016). https://doi.org/10.1109/SYSCON.2016.7490666

Autonomic Machine Learning for Intelligent Databases

Keon Myung Lee[1(✉)], Jaesoo Yoo[2], and Jiman Hong[3]

[1] Department of Computer Science, Chungbuk National University, Cheongju, Korea
kmlee@cbnu.ac.kr
[2] School of Information and Communication Engineering, Chungbuk National University, Cheongju, Korea
yjs@cbnu.ac.kr
[3] School of Computer Science and Engineering, Soongsil University, Seoul, Korea
jiman@ssu.ac.kr

Abstract. Various machine learning algorithms are available off the shelf, even for free. It takes an expert to choose a proper algorithm for given task and to set hyperparameters of the algorithm. This paper addresses an architecture of autonomic machine learning platform with which developers get some assistance in choosing a machine learning algorithm appropriate to a task and in selecting the values of hyperparameters of the algorithm. Due to massive computation demands on executing machine learning algorithms, the platform is designed to utilize the external computing resources such as cloud computing systems and distributed computing systems. This paper presents the design choices and architecture of the proposed platform, and a possible application to intelligent databases.

Keywords: Machine learning · Distributed computing · Autonomic computing Machine learning platform

1 Introduction

Many machine learning algorithms have been developed and in use for various tasks [1–16]. Machine learning algorithms are very effective in extracting knowledge in the form of patterns or models from a collection of data. The adoption of machine learning could increase productivity, quality, or profit by saving much cost and labor in various domains. Excellent machine learning tools have been developed and available in public even in open software or open source software [1–4]. Machine learning takes experts to be successfully applied to a specific problem due to the following reasons: First, appropriate machine learning task should be identified to the problem. The tasks include classification, regression, clustering, recommendation, density estimation, dimensionality reduction, feature representation, and so on. Second, it is of paramount importance to use proper features by selecting or extracting features from data sets with various attributes. Third, there are many candidate machine learning algorithms for a

K. Ntalianis and A. Croitoru (Eds.): APSAC 2017, LNEE 489, pp. 163–169, 2019.
https://doi.org/10.1007/978-3-319-75605-9_23

specific task, each of which has some advantages or disadvantages over others. Fourth, most machine learning algorithms have some hyperparameters which are a kind of parameters that influence on the algorithm's behavior. The existence of hyperparameters requires the engineering work for selecting their proper values. With some insight of experts and mainly generate-and-test manner, many hyperparameter combinations should be examined by executing the employed machine learning algorithms with the hyperparameter values.

Recent progresses in machine learning, especially in deep learning and probabilistic graphical models, take considerable amount of computations due to their model complexity, i.e., the number of parameters in a model. Machine learning algorithms with hyperparameters take considerable computing resources for training and inference [6–11]. External computing resources such as cloud services or distributed computing systems allow us to harness the computing power for machine learning service systems [12–14]. As mentioned above, however, the well-trained human experts on machine learning is a rare resource to take. Even though there are many open machine learning tools are available, most sectors in industry, business, and government have difficulty in adopting machine learning techniques to their work because they do not have such machine learning experts.

There have been some works to automate machine learning tasks with less human involvement [7–10]. This paper addresses a new platform for machine learning which automates machine learning for a given data set and uses the external computing resources. The platform works in an autonomic manner of which architecture is organized so that some components take care of machine learning planning, some components manage executing of specific machine learning task, some components evaluate the learned models, and others take care of distributed computing resource management.

2 Related Work

There have been some efforts to automatically determine hyperparameters in machine algorithm algorithms. Grid method [12] generates candidate hyperparameter combinations each of which hyperparameters is equally spaced in its domain, and chooses a combination which gives the best performance by executing the corresponding ML algorithm for each candidate. Random method [9] generates candidate hyperparameter combinations randomly which gives empirically better chances to find better hyperparameters within the given computation budget. Sequential model-based algorithm configuration method [7] selects a hyperparameter combination based on a model rather than uniformly at random. Tree-structured Parzen estimator method [10] sequentially constructs models to approximate the performance of hyperparameters based on historical measurements, and then subsequently chooses new hyperparameters to test based on this model. Gaussian process-based method [6] is also used, which uses a Gaussian process as a surrogate for hyperparameter distributions and updates the Gaussian process by combining sampling results and prior distribution.

Due to considerable computation demands, there have been various works on distributed processing and parallel processing in machine learning. OptiML, GraphLab,

SystemML, SimSQL, and MLBase are such machine learning platform that provide programming and runtime support [4]. OptiML is developed to allow the machine learning practitioner to write code in a MATLAB-like declarative manner of which code runs on various hardware platforms such as a multi-core CPU, a GPU, a clusters of computing nodes, and other specialized accelerators. GraphLab is a graph-based, distributed computation framework which uses the graph-parallel abstraction for sparse iterative graph algorithms and works in pull-based and asynchronous manner. SystemML is an ML framework in which a declarative ML language is used to describe ML algorithms and the codes expressed in the ML language are compiled and optimized into hybrid runtime plans of multi-threaded, in-memory operations in a single node or distributed map-reduce or Spark operations on a cluster of nodes. SimSQL is an SQL-based platform which runs on top of Hadoop, and is designed for supporting scalable Bayesian machine learning. MLBase is an ML framework which is based on Spark for lower-level data processing and works on Hadoop platform.

Giraph, Spark, and DryadLinq are some of frameworks with which ML tasks are programmed and executed even though they have been not designed only for ML tasks [17]. Giraph is a graph-based, distributing computing framework, in which models are push-based and synchronous. Spark is a cluster computing framework for large scale data analytics, which utilizes Resilient Distributed Datasets (RDDs) that allows in-memory computation and provides fault-tolerance by managing data lineage. DryadLinq is a distributed computing framework which uses the distributed execution engine Dryad and the .Net language integrated query LINQ, and allows to easily develop ML algorithms as well as other distributed computing applications.

3 Autonomic Machine Learning Platform

Despite many available ML tools, it takes an expert to effectively use them in a real problem because there are various factors to be selected in the applications of ML algorithms. Even an expert is devoted to develop an ML application, it also takes considerable computing resources for multiple trials in finding a model with satisfactory performance. Hence, it will be great to have a platform to help ML applications without an ML expert and to take care of computing resources required to search for a best model and its hyperparameters. Such a system is called as an autonomic ML platform because it works with least human involvement.

3.1 Requirements of Autonomic Machine Learning

An autonomic ML platform aims to provide an environment in which a non-expert on ML develops an ML-based application in his/her problem. There are some requirements that such a ML platform meets: First, the platform needs to provide the mechanism which can use the existing public ML frameworks and tools.

Second, the platform allows non-experts to build their ML application even though they do not have enough understanding of ML algorithms and capability to implement them. Here the ML platform needs to provide five autonomicity levels as follows: The autonomicity levels are specified in terms of the existences of specified data set, of

specified input attributes, of specified ML task, of specified ML algorithms, and of hyperparameters. At the autonomicity level 0, all pieces of the above-mentioned information are supposed to be provided by the developer. At the autonomicity level 1, the developers are free from choosing the proper input attributes in the development of ML applications. At the autonomicity level 2, the platform has the functionality of automatically determining the hyperparameters for the given algorithm, which has the capability of level 1. At the autonomicity level 3, only the training data set and its ML task are given, and all other ML works are done by the platform. The highest autonomicity level is level 4 in which only the training data is provided.

Third, the platform needs to have the capability of using the external computing resources and executing the learning and inference tasks with them. Fourth, the platform needs to provide a script language with which the autonomic ML tasks are expressed in a distributed and parallel manner.

3.2 Architecture of the Proposed Autonomic Machine Learning Platform

To realize an autonomic ML platform, we designed an architecture that meets the above-mentioned requirements as shown in Fig. 1. The architecture supports both the black box and white box modes. In the black box mode, the ML platform does not ask the developers to write some codes of ML tasks, but just asks them to specify the components corresponding to the autonomicity level employed at the moment. The remaining details on ML tasks are taken care of by the platform which uses the existing ML platforms and tools integrated. In the white box mode, the developers write some codes for ML tasks according to their own logic and design choices, using the provided script language.

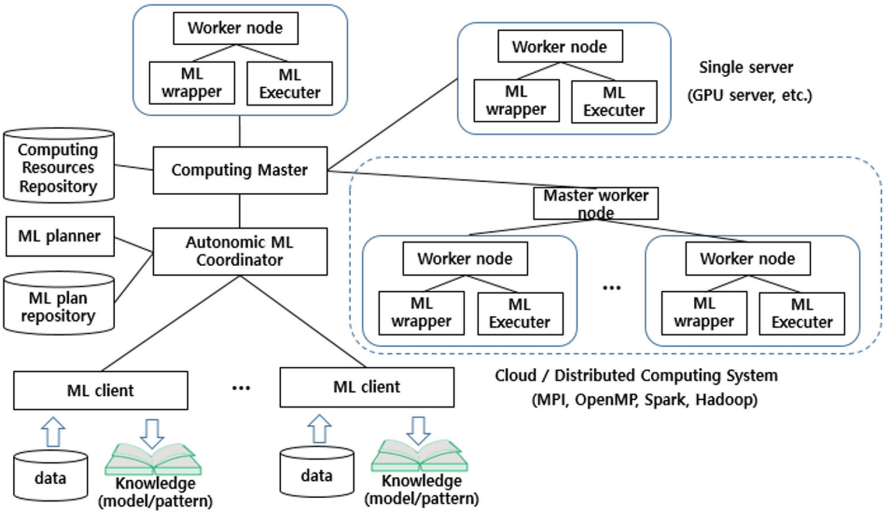

Fig. 1. The architecture of the proposed autonomic ML platform

In the architecture, a developer interacts with the platform through the ML client. The ML client delivers the developer' request to the Autonomic ML Coordinator, monitors the progress of the deployed tasks, and receives the results of learning and inference. It maintains the connection between the database system and the platform so that the data sets in the database can be used in ML tasks and the results of learning and inference are stored and maintained in the database. The Autonomic ML coordinator takes charge of coordinating the autonomic ML tasks by generating ML task plans for plausible configurations, executing them with the available computing platforms, and selects the best models and patterns from the results of the ML tasks. Due to enormous number of candidate ML configurations, the demands on computing resources are soaring up as the autonomicity level grows high. Expert knowledge can be helpful to set up the initial configurations and to bound the ranges of candidate hyperparameters under consideration. Such knowledge is maintained in the ML plan repository to which the execution profiles including configurations and their performance are maintained to incrementally enhance the knowledge. The ML plan repository also includes the cost model for configurations and data characteristics. The cost model is updated to reflect the execution profiles collected during the ML tasks conducted on the platform. The ML planner is in charge of determining the model configuration, the hyperparameters, and/or feature selection and extraction, as well as ML tasks deployment.

The Computing Master receives the ML tasks from the Autonomic ML coordinator, deploys them over the computing resources, monitors their progresses, reconfigures the deployments of ML tasks, if needed, and reports the status and the results to the Autonomic ML coordinator. The computing resources include the single servers like a GPU server and a multi-core server, the cloud services and distributed computing systems. Each computing resource has a master worker node which communicates with the Computing Master and manages its own computing resources to conduct the ML tasks. The proposed platform supports to use the existing ML platform and tools. Hence, the ML wrappers are implemented to invoke the ML tools to execute the corresponding ML tasks, to report their progresses and results, and to terminate the deployed tasks, if needed. When the ML tasks are expressed in the script language, the codes are executed by the ML Executer which launches the corresponding ML platform and conducts the execution of the codes on the platform according to the corresponding configuration. When a cloud service or a distributed computing system is used as a computing resource, the master worker node is installed on it. The master worker node communicates with the deployed ML platform or framework which takes care of the ML tasks. If the ML codes in the script language are delivered, the master worker node distributes the ML codes to the Worker nodes which next invokes the ML Executers. The master worker nodes of the computing resources that support the proposed ML platform to register themselves into the Computing Resource Registry with their access method, functionality, capability, workload, and billing policy. The Registry checks the registered computing resources on a regular basis, and maintains the current states. The Computing Master refers to the Computing Resource Registry when distributing the ML tasks and monitoring their progress.

4 Implementation of the Proposed ML Platform

The proposed autonomic ML platform is a huge system to integrate the existing ML platforms and frameworks and to use many external computing resources. In addition, it is an ambitious approach to try to realize the full range of the autonomicity levels from the primitive level to the completely autonomic level. To evaluate the feasibility of the proposed architecture, we have developed an initial stage prototype which realizes a preliminary platform of the proposed architecture. The Single server node has been implemented to provide the GPU-based ML framework to execute the Tensorflow programs. The prototypes of the ML client, the Autonomic ML coordinator, the ML planner, the ML plan repository, the Computing Resource Registry, and the Computing Master have been implemented. The autonomicity levels 0 and 1 have been supported by the ML planner. The prototype system has been tested to execute the deep learning algorithms like CNN and RNN algorithms.

5 Conclusions

The autonomic ML platform can be an enabler for non-experts of ML to employ ML techniques in solving their real domain problems. We defined the autonomicity levels from the primitive level to the ultimate level. To handle the vast demands on computing resources in autonomic ML, we proposed an architecture to realize the ML platform which uses the external computing resources and the existing ML platforms and frameworks. To evaluate the feasibility of the proposed platform, we have developed a primitive prototype of the proposed architecture for the autonomic ML platform.

The proposed ML architecture can be an important enabling technique to convert a database into an intelligent database. With the advances and widespread deployment of sensor technology like IoT, large volumes of data have been accumulated with the expectation of finding business opportunities from them. It is, however, not easy to transform such data into valuable knowledge. The autonomic ML platform can help extract valuable and confident knowledge from data. There yet remains much work in realizing the functionalities of the autonomic computing platform. Once it is implemented, the ML technology can be easily adopted in many domains without ML experts. Especially, the databases can be evolved into intelligent databases with the help of the autonomic ML platform. Such intelligent databases allow the dream that once data are stored, the knowledge are developed automatically.

Acknowledgments. This research was supported by the MSIP (Ministry of Science, ICT and Future Planning), Korea, under the ITRC (Information Technology Research Center) support program (IITP-2017-2013-0-00881) supervised by the IITP (Institute for Information & communication Technology Promotion).

References

1. Kraska, T., Talwalkar, A., Duchi, J., Griffith, R., Franklin, M.J., Jordan, M.: MLbase: a distributed machine-learning system. In: CIDR, vol. 1 (2013)

2. Bello-Orgaz, G., Jung, J.J., Camacho, D.: Social big data: recent achievements and new challenges. Inf. Fusion **28**, 45–59 (2016)
3. Jha, S., Qiu, J., Luckow, A., Mantha, P., Fox, G.C.: A tale of two data-intensive paradigms: applications, abstractions, and architectures. In: 2014 IEEE International Congress on Big Data (BigData Congress), pp. 645–652. IEEE, June 2014
4. Cai, Z., Gao, Z.J., Luo, S., Perez, L.L., Vagena, Z., Jermaine, C.: A comparison of platforms for implementing and running very large scale machine learning algorithms. In: Proceedings of the 2014 ACM SIGMOD International Conference on Management of Data, pp. 1371–1382. ACM, June 2014
5. Lee, K.M., Lee, S.Y., Lee, K.M., Lee, S.H.: Document density and frequency-aware cluster identification for spatio-temporal sequence data. Wirel. Pers. Commun. **93**(1), 1–5 (2017)
6. Brochu, E., Cora, V.M., De Freitas, N.: A tutorial on Bayesian optimization of expensive cost functions, with application to active user modeling and hierarchical reinforcement learning (2010). arXiv preprint: arXiv:1012.2599
7. Bergstra, J.S., Bardenet, R., Bengio, Y., Kégl, B.: Algorithms for hyper-parameter optimization. In: Advances in Neural Information Processing Systems, pp. 2546–2554 (2011)
8. Johnson, V.E., Wong, W.H., Hu, X., Chen, C.T.: Image restoration using Gibbs priors: Boundary modeling, treatment of blurring, and selection of hyperparameter. IEEE Trans. Pattern Anal. Mach. Intell. **13**(5), 413–425 (1991)
9. Bergstra, J., Bengio, Y.: Random search for hyper-parameter optimization. J. Mach. Learn. Res. **13**, 281–305 (2012)
10. Bergstra, J., Yamins, D., Cox, D.: Making a science of model search: hyperparameter optimization in hundreds of dimensions for vision architectures. In: International Conference on Machine Learning, pp. 115–123, February 2013
11. Thornton, C., Hutter, F., Hoos, H.H., Leyton-Brown, K.: Auto-WEKA: combined selection and hyperparameter optimization of classification algorithms. In: Proceedings of the 19th ACM SIGKDD International Conference on Knowledge Discovery and Data Mining, pp. 847–855. ACM, August 2013
12. Larochelle, H., Erhan, D., Courville, A., Bergstra, J., Bengio, Y.: An empirical evaluation of deep architectures on problems with many factors of variation. In: Proceedings of the 24th International Conference on Machine Learning, pp. 473–480. ACM (2007)
13. Kang, S.J., Lee, S.Y., Lee, K.M.: Performance comparison of OpenMP, MPI, and mapreduce in practical problems. Adv. Multimed. **2015**, 7 (2015)
14. Lee, K., Lam, M., Pedarsani, R., Papailiopoulos, D., Ramchandran, K.: Speeding up distributed machine learning using codes. In: 2016 IEEE International Symposium on Information Theory (ISIT), pp. 1143–1147. IEEE, July 2016
15. Lee, K.M., Jeong, Y.-S., Lee, S.H., Lee, K.M.: Document bucket-size balancing locality sensitive hashing using the map reduce paradigm (2017)
16. Li, M., Andersen, D.G., Park, J.W., Smola, A.J., Ahmed, A., Josifovski, V., Su, B.Y.: Scaling distributed machine learning with the parameter server. In: OSDI, vol. 1(10.4), p. 3, October 2014
17. Sparks, E.R., Talwalkar, A., Smith, V., Kottalam, J., Pan, X., Gonzalez, J., Kraska, T.: MLI: an API for distributed machine learning. In: 2013 IEEE 13th International Conference on Data Mining (ICDM), pp. 1187–1192. IEEE, December 2013
18. Singh, D., Reddy, C.K.: A survey on platforms for big data analytics. J. Big Data **2**(1), 8 (2015)

Recommender System for Post-editing of Machine Translation

Jozef Kapusta[1,2(✉)] and Ľubomír Benko[3]

[1] Department of Informatics, Faculty of Natural Sciences, Constantine the Philosopher University in Nitra, Nitra, Slovakia
jkapusta@ukf.sk
[2] Faculty of Mathematics, Physics and Technical Science, Institute of Computer Science, Pedagogical University of Cracow, Cracow, Poland
jkapusta@up.krakow.pl
[3] Institute of System Engineering and Informatics, University of Pardubice, Pardubice, Czech Republic
lubomir.benko@gmail.com

Abstract. This paper is focused on improving the output of post-edited Machine Translation. A novel recommender system is introduced in this paper that was created to help post-editors to correct translation created by the Machine Translation. The aim of the paper is to describe the design and functionality of the proposed system. With the usage of automated parser were analysed pairs of segments from Machine Translation and corresponding post-edition. The calculation of the likelihood of the recommendation was used to get the word with the highest probability that was selected based on the similarity in words, tags and lemmas. The introduced approach can help to create a versatile recommender system that helps post-editors to improve their translation.

Keywords: Recommender system · Machine Translation · Natural language processing · Tokenization · POS tagging

1 Introduction

In comparison to human translation offers Machine Translation (MT) low cost and faster translation of texts. Statistical Machine Translation is an approach to MT characterized by the use of machine learning methods where it takes translation as machine learning problem [1]. The main aim of Statistical Machine Translation is the creation of the system to automatically discover translation rules of the large bilingual corpus, merging input data with output data and "learn" from the results of statistical analysis of relevant data [2].

This research is focused on improving the output of MT, especially the output of post-edited MT. This article contains the proposed recommender system created for post-editors of MT. The attempt is not focused on improving the MT system itself. The newly created system analyses segments that were translated using MT. The aim of the paper is to describe the design and functionality of the system that supports post-edition of translated text. The system is based on previous research in the field of MT and

K. Ntalianis and A. Croitoru (Eds.): APSAC 2017, LNEE 489, pp. 170–175, 2019.
https://doi.org/10.1007/978-3-319-75605-9_24

evaluation of MT. The following sections will describe the steps needed to create the recommender system for post-edition.

The paper is structured as follows: in Sect. 2 is summarized the related work of the field of recommender systems. Section 3 deals with creating the Translation Memory. The following sections deal with the presented approach of a recommender system for post-editors. Subsequently the discussion and conclusion are offered in the last section.

2 Related Work

Some authors already work on the idea of creating a recommender system in the field of machine translation. The aim of this paper is to describe a recommender system for post-editing the machine translation output. Such system would offer a translation recommendation for the post-editor. Dara et al. [3] provide a commercially viable platform of a recommender system. The system allows an integration of Machine Translation with legacy Translation Memory systems to provide the most effective translation options to human translators. He et al. [4] proposed a translation recommender system which integrates Statistical Machine Translation (SMT) output with Translation Memory systems. The authors used Support Vector Machines (SVM) for Translation Quality Estimation. The paper by Espla-Gomis et al. [5] proposed an approach to help users of computer-aided translation systems to identify the target word in the translation proposals that need to be changed or kept unedited.

Lops et al. [6] present a sematic content-based recommender system for providing cross-language recommendations. The results of the experiment showed that the accuracy of cross-language recommendations is comparable to classical one language content-based recommendations. Recommender systems for solving data processing and analysis tasks are considered by Vodyaho and Zhukova [7]. The proposed recommender systems are designed as agile knowledge based systems that allow the integration of new methods and algorithms. Manzato et al. [8] developed a post-processing module based on ensemble learning which combines rankings of content-based recommenders using various description types. The proposed module offers options to the developers to use various text mining algorithms and attribute-aware recommenders and the module could be extended to the recommendation of non-textual items.

The proposed work differs from the aforementioned since it is based on lexical analysis of parallel texts and for the recommendations are used not only words but also information about lemma and tag. From the point of view of parallel text, the texts of MT and post-edition were analyzed.

3 Creation of Translation Memory

Translation Memory (TM) is a database in that are stored all sentences that the users translate within the Translation Memory System. The TM system is a type of translation support tool that is used to avoid the need to re-translate segments of text that

already have been translated [9]. If the system encounters segments that match the segment in TM, its translation is retrieved and proposed to the translator.

The newly created recommender system is oriented to improve the work of post-edition of MT. The key parts of the system are parallel text of MT and post-edition.

For the need of post-edition of MT was created a system for recording MT errors [10]. The system offers an interface for effective post-edition, i.e. logged-in user will be allowed to correct the translation as well as to determine the basic typology of machine translation system errors. This way will be the user allowed to flag the error typology of corrected segments. Using the created system was performed post-edition of MT by professional translators.

As a new element, experts for the target language were called in to this process. It was assumed that the work will be done quite mechanically. For this reason, their work has been reviewed by the specialist in the target language.

The results of this process were parallel texts source language – machine translation to target language and post-edited translation of target language. Currently our system contains 47 634 segments that consist of 406 280 words (454 528 tokens).

4 Lexical Analysis of Parallel Texts

The translated target language segments and their post-edited versions were analysed after the post-edition. After the post-edition were the translated segments to target language and their post-edited versions analysed. Morphology analysis for each segment was done using the analysing tool TreeTagger [11], where segments were divided to tokens. Tag and lemma were assigned to each token. To each token was assigned a tag and also a lemma.

This way were achieved two sets for each segment (Fig. 1); first set consisted of tokens from MT segments together with corresponding tags and lemmas; second set consisted of tokens from post-edited MT segments together with corresponding tags and lemmas.

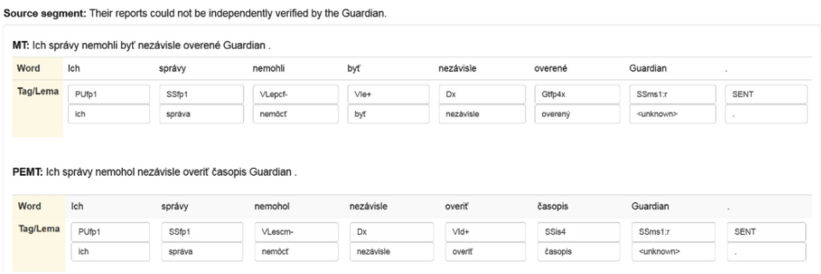

Fig. 1. Sample of input data for pair of segments from machine translation and post-editing

An automatic parser was created for further analysis that analysed pairs of segments (sentences) from MT and corresponding post-edition. According to the following steps were from the pairs of segments extracted pairs of words.

1. In the first step were chosen words that were for MT segment and also for post-edited segment the same and as well as had the same tag and lemma;
2. From the remaining text were chosen pairs that had the same word and tag;
3. Followed by a pair where only words were the same;
4. And finally were chosen pairs with the same lemma.

Words that were not chosen remained after the analysis in both segments. These words were flagged as unassigned. For the mean time they are kept in the database. In the future work, the most common n-tuple sets will be created using association analysis and this data will be implemented into the improved recommender system.

The resulting set is the basic layer of data of the recommender system as shown on Fig. 2.

parser_info	parser_info	word	tag	lema	source
…					
word	W	Ich	PUfp1	ich	machine_translate
word	W	Ich	PUfp4	ich	postedit
word	W	správy	SSfp1	správa	machine_translate
word	W	správy	SSfp4	správa	postedit
lema	L	nemohli	VLepcf-	nemôcť	machine_translate
lema	L	nemohol	VLescm-	nemôcť	postedit
word_tag_lema	WTL	nezávisle	Dx	nezávisle	postedit
unclassified_MT	OTH_MT	byť	VIe+	byť	machine_translate
word_tag_lema	WTL	nezávisle	Dx	nezávisle	machine_translate
word_tag_lema	WTL	.	Z	.	postedit
word_tag_lema	WTL	.	Z	.	machine_translate
…					

Fig. 2. Sample of source data of the recommender system

5 Design of the Recommender System

The created recommender system is based on selection of all words that may be recommended for the token for post-editing. The system looks for the number of words from the modified segments that match the words, tags, lemmas and their combinations. Weights are then assigned to the specific combinations (Fig. 3) and number of these combinations in the source file was determined. It is obvious that the highest weight was assigned in the case of the word-tag-lemma match and the lowest in the case of the same lemma.

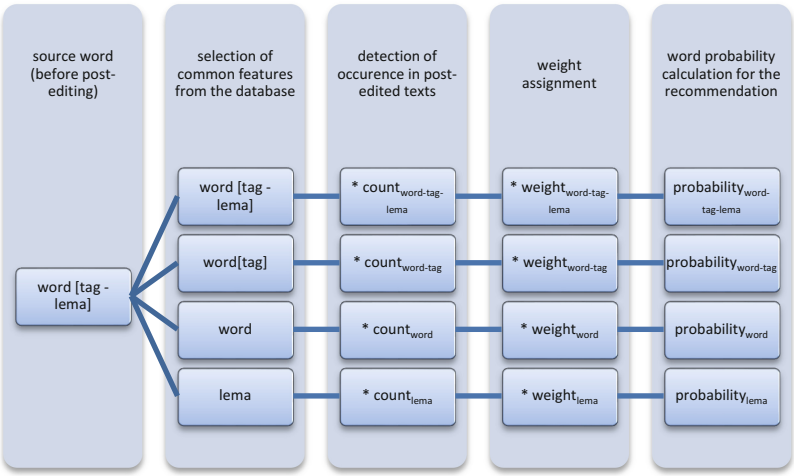

Fig. 3. Determining the appropriateness of the word for the recommendation

After calculation of the likelihood of the recommendation was the word with the highest probability displayed in the system and offered for the user as a proposal for correction. The aim of the creators of the recommender system is always to offer the user a proposal of post-edition correction. Obviously, when calculating the probability, many situations arise when the word with the highest probability for recommendation is the same word as the post-edited. In that case the system does not recommend changing the source word from the MT. For this reason was the word offered for recommendation compared to the post-edited word. In this case were the words the same and the system has chosen the word with the second highest probability.

6 Discussion and Conclusion

This work offers a novel approach focused onto the translated target text and its post-edition. The paper is not oriented on improving the machine translation itself. Using parallel texts of MT and their corresponding post-edited versions can this approach help post-editors to improve their work and also to improve the final text in the target language. Using the presented design it is possible to create a versatile recommender system that is source language and MT system independent.

Similar issues dealt in the field of recommender systems are solved using basic classification approach as also the issues that are dealt with by our designed recommender system. Because the system uses Translation Memory, it cannot be personalized. Obviously every post-editor has his/her own post-editing style and uses his/her favourite language “schemas”. For this reason will be learning implemented into the system in the future, i.e. the co-occurrence matrix generated from the parallel texts is constantly expanding. At the same time, the information about the post-editor is associated to the parallel texts. This will be used to increase the weight from which will

be calculated the probability of the recommendation of the word with the aim to personalize the recommendation.

The second issue of the system seems to be the creation of the source file of the pairs of words. Here are also the unassigned words. In the future work it is planned to find appropriate parallel n-tuples using association or sequence analysis. The system will then recommend not only "word by word" but will also provide a recommendation for n-grams.

The success of the recommender systems is the robustness of the source file. The source file used by the proposed recommender system contains currently 406 280 words. Its expansion is the most important task that will lead to increasing the accuracy and relevance of the recommendations.

Acknowledgements. This paper is published with the financial support of the project of the Slovak Research and Development Agency under the contract No. APVV-14-0336.

References

1. Lopez, A.: Statistical machine translation. ACM Comput. Surv. **40**, 1–49 (2008)
2. Koehn, P.: Statistical Machine Translation. Cambridge University Press, Cambridge (2010)
3. Dara, A., Dandapat, S., Groves, D., van Genabith, J.: TMTprime: a recommender system for MT and TM integration. In: Proceedings of the NAACL HLT 2013 Demonstration Session, Atlanta, Georgia, pp. 10–13. Association for Computational Linguistics (2013)
4. He, Y., Ma, Y., van Genabith, J., Way, A.: Bridging SMT and TM with translation recommendation. In: Proceedings of the 48th Annual Meeting of the Association for Computational Linguistics, Uppsala, Sweden. pp. 622–630. Association for Computational Linguistics (2010)
5. Espla-Gomis, M., Sánchez-Martínez, F., Forcada, M.L.: Using machine translation in computer-aided translation to suggest the target-side words to change. In: Machine Translation Summit, pp. 172–179 (2011)
6. Lops, P., Musto, C., Narducci, F., de Gemmis, M., Basile, P., Semeraro, G.: Cross-language personalization through a semantic content-based recommender system (2010)
7. Vodyaho, A., Zhukova, N.: Implementation of agile concepts in recommender systems for data processing and analyses, 9 April 2015
8. Manzato, M.G., Domingues, M.A., Fortes, A.C., Sundermann, C.V., D'Addio, R.M., Conrado, M.S., Rezende, S.O., Pimentel, M.G.C.: Mining unstructured content for recommender systems: an ensemble approach. Inf. Retr. J. **19**, 378–415 (2016)
9. Simard, M.: Translation spotting for translation memories. In: Proceedings of the HLT-NAACL 2003 Workshop on Building and Using Parallel Texts Data Driven Machine Translation and Beyond, Morristown, NJ, USA, pp. 65–72. Association for Computational Linguistics (2003)
10. Munková, D., Kapusta, J., Drlík, M.: System for post-editing and automatic error classification of machine translation. In: DIVAI 2016: 11th International Scientific Conference on Distance Learning in Applied Informatics, Sturovo, 2–4 May 2016, pp. 571–579. Wolters Kluwer, Sturovo (2016). ISSN 2464-7489
11. Schmid, H., Baroni, M., Zanchetta, E., Stein, A.: The enriched TreeTagger system. In: Proceedings of the EVALITA 2007 Workshop (2007)

Neural Network Methods for Image Segmentation

Manami Barthakur[1(✉)], Kandarpa Kumar Sarma[1], and Nikos Mastorakis[2]

[1] Department of Electronics and Communication Engineering, Gauhati University, Guwahati, Assam, India
manamibarthakur@gmail.com, kandapaks@gmail.com
[2] Department of Electrical Engineering and Computer Science, Hellenic Naval Academy, Piraeus, Greece
mastor@hna.gr

Abstract. Segmentation is the fundamental step in many image processing algorithms. In this paper, a simplified neuro-computing structure in feed forward form for use in segmentation of images in complex background is proposed. The work considers the formation and training a neuro-computing structure in which the pixel values of various region of the image are used as target. The method does not require any feature extraction, labeling of objects, region growing or splitting methods to configure and train a neuro-computing structure, which for the work is a Multi Layer Perceptron (MLP) trained with (error) Back Propagation learning. The neuro-computing structure is trained with different training functions. The network is also trained with single, double and triple hidden layers. The training is also done with Generalized Regression Neural Network for different values of spread function. Then the mean square error between the output image and desired image and the time required for training has been calculated.

Keywords: GRNN · MLP · Segmentation

1 Introduction

The goal of image segmentation is to obtain a representation of an image with distinct partitions of common content with something meaningful. The representation should enable subsequent analysis. It is typically used to locate objects and boundaries in images. There are many approaches to segment an image. Most of these methods rely on the image characteristics they are measuring. Therefore, they work well in certain cases and not in others. For example, edge detection based image segmentation methods do not work well for images with ill defined edges. Similarly, thresholding based methods do not work well with images without any obvious peaks or with broad layout and at valleys. Therefore, when dealing with complex image, some prior knowledge may be necessary to disambiguate the segmentation process. For that purpose learning and neuro-computing structures have been used extensively in the literature [1–6].

K. Ntalianis and A. Croitoru (Eds.): APSAC 2017, LNEE 489, pp. 176–182, 2019.
https://doi.org/10.1007/978-3-319-75605-9_25

Several learning based methods for segmentation have been developed until now. An Artificial Neural Network (ANN) architecture had been developed for region of interest (ROI) segmentation of fingerprint images in [1] where the authors trained ANNs with 10000 samples extracted from 20 fingerprint images. Arumugadevi et al. in [2] proposed a method in which supervised feed forward neural network are trained where the labels obtained from the clustering method FCM are used as a target. ANNs had also been used in medical image segmentation. In [3], ANN based segmentation method for lesion in brain MRI where training was done using gray levels and extracted statistical features from the training data with the labeled ground truth. Moghaddam et al. [4] had developed a method of segmentation where deep brain structures were segmented using Geometric Moment Invariants (GMIs) and MLP ANNs.

In most of the above cited methods feature extraction techniques, labeling of objects etc. are required for segmentation of the images. In this paper, a simplified ANN based approach for segmentation of images in complex background is proposed. The work considers the formation and training an ANN in which the pixel values of various region of the image used as target. The method does not require any feature extraction, labeling of objects, region growing or splitting methods to configure and train an ANN, which for the work is a MLP trained with (error) Back Propagation learning. The training is also done Generalized Regression Neural Network (GRNN) for different values of spread function.

The paper is organized as follows. In Sect. 2 the review ANN and GRNN is presented. In Sect. 3 the proposed algorithm is discussed. Then in Sect. 4 the experimental results are shown. At last the conclusion is given in Sect. 5.

2 A Brief Overview of ANN and GRNN

2.1 ANN

An ANN is a mathematical or computational model inspired by biological neural networks. It consists of an interconnected group of artificial neurons and processes information using a connectionist approach to computation. The ANN in a feed forward form called MLP is configured to learn applied patterns. The process of learning patterns by an ANN is called training. MLPs are trained using (error) Back Propagation (BP) depending upon which the connecting weights between the layers are updated. This adaptive updating of the MLP is continued till the performance goal is met [5]. The steps are as below,

- **Initialization:** Initialize weight matrix W with random values between [0, 1].
- **The training samples:** The input is $\mathrm{I}_p = \left[i_{p1}, i_{p2}, \ldots\ldots\ldots i_{pn}\right]$. The desired output is, $\mathrm{T}_p = \left[t_{p1}, t_{p2}, \ldots\ldots\ldots t_{pn}\right]$. The hidden nodes are computed as follows,

$$N_{py}^{q} = \sum_{x=1}^{n} w_{yx}^{q} I^{px} + \phi_{y}^{q} \tag{1}$$

The output from the hidden layer are calculated as-

$$O_{py}^{q} = f_{y}^{q}(N_{py}^{q}) \tag{2}$$

Where, f(X) depends upon the choice of activation function.
The values of the output nodes are calculated as-

$$O_{pl}^{r} = f_{l}^{r}(N_{py}^{r}) \tag{3}$$

- **Computation of errors:** The errors are computed as-

$$E_{ye} = T_{ye} - O_{ye} \tag{4}$$

The mean square error (MSE) is calculated as-

$$MSE = \frac{\sum_{y=1}^{N}\sum_{e=1}^{n} E_{ye}^{2}}{2N} \tag{5}$$

The errors for the output layer is calculated as follows-

$$\partial_{pm}^{r} = O_{pm}^{r}(1 - O_{pm}^{r})E_{pe} \tag{6}$$

The errors for the hidden layer is calculated as-

$$\partial_{pm}^{q} = O_{pm}^{q}(1 - O_{pm}^{q})\sum_{y} \partial_{py}^{r}\omega_{ym} \tag{7}$$

One cycle through the complete training set forms one epoch. The above is repeated till MSE meets the performance criteria.

2.2 GRNN

A GRNN is a variation of the Radial Basis Function (RBF) ANN. As back propagation networks, a GRNN does not require an iterative training procedure. It consists of four layers: input layer, pattern layer, summation layer and output layer. Input layer feeds the input to the next layer i.e. the pattern layer. The pattern layer is connected to the summation layer. The summation layer has two different types of summation, which are a single division unit and summation units. In training of network, radial basis and linear activation functions are used in pattern and output layers. Each pattern layer unit is connected to the two neurons in the summation layer. One summation neuron computes the sum of weighted responses of the pattern layer and the other summation neuron is used to calculate un-weighted outputs of pattern neurons. The output layer merely divides the output of each summation neuron, yielding the predicted value Y(x) to an unknown input vector x as [6]-

$$Y(x) = \frac{\sum Y_i e^{-\left(\frac{d_i^2}{2\sigma^2}\right)}}{\sum e^{-\left(\frac{d_i^2}{2\sigma^2}\right)}} \tag{8}$$

Where, $d_i^2 = (x - x_i)^T (x - x_i)$.

Here x is the input sample and x_i is the training sample. Output of the input sample x_i is Y_i, d_i^2 is the Euclidean distance from x and x_i and $e^{-\left(\frac{d_i^2}{2\sigma^2}\right)}$ is the activation function. Only one parameter is unknown here, which is spread constant σ. That can be tuned by training process to an optimum value where the error will be very small.

3 The Proposed Method

The block diagram for the proposed method is shown on Fig. 1. The block diagram is explained below.

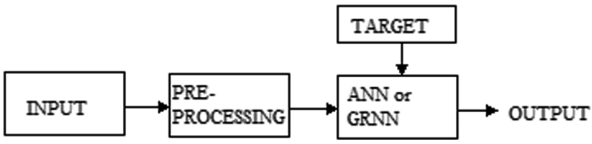

Fig. 1. Block diagram of the proposed method

i. **Input and Preprocessing:** The input in this work is a RGB image with complex background. The image contains seven regions namely sky, house, leaves, trunk, river, mountain and background which are to be segmented. As preprocessing step the image is resize to 101_177 size. Then the pixel values are normalized to [0, 1] values.
ii. **Target:** The target to system is pixel values of the different regions. If sky region of the image is to be segmented, then in the image the sky region is selected using 'impixel' command of MATLAB. Then keeping pixel values of the region as it is, other values are set to 255. Similarly for the other region also target will be the pixel values of the particular region.
iii. **ANN and GRNN:** FF ANNs are trained with back-propagation algorithm as explained in Sect. 2. Batch training method is adopted as it accelerates the speed of training and the rate of convergence of the MSE to the desired value. At first the MLP is trained with one hidden layer and then it is trained with two and three hidden layers. The input and output layers use log-sigmoid activation while the hidden layers use tan-sigmoid activation functions. The training is also performed with GRNN with different values of spread function as explained in Sect. 2 B.
iv. **Output:** The output will be pixel values of the region which is to be segmented.

4 Experimental Results and Discussion

The image used for the experiment shown in Fig. 2(a). The network is trained with single, double and triple hidden layers with different numbers of hidden neurons. Here the training function used is Levenberg-Marquardt (LM) back-propagation. Then, again MSE between the output image and desired image and the time required for training is calculated for all the region of the image. The results are shown in Table 1 below. The training is also done with GRNN with different values of spread function. Then MSE and the time required for training is calculated for all region of the image. The results are shown in Table 2.

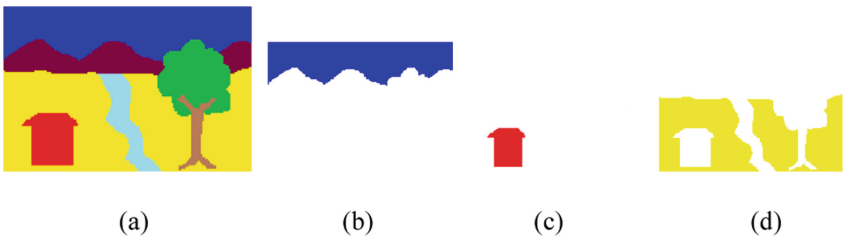

Fig. 2. (a) Input Image, Output Image for (b) 'Sky' region (c) 'House' region (d) 'Background' region.

From Table 1, at first ANN is trained with LM Back-propagation with hidden layer neuron number 10, 20, 50, 100 in all the regions, (Sky, house and background). Then ANN is trained with double and triple hidden layer with LM Back-propagation as

Table 1. Experimental results when trained with single, double and triple hidden layer of MLP.

Methods	ANN with single hidden layer			ANN with double hidden layer			ANN with triple hidden layer		
	No. of hidden required	Time required in second	MSE	No. of hidden required	Time required in second	MSE	No. of hidden required	Time required in second	MSE
Sky	10	22.79	0.0438	[20 10]	46.94	0.0019	[20 20 10]	140.63	0.0513
	20	23.79	0.0058						
	50	35.69	0.0059	[20 50]	119.83	0.0027	[50 20 10]	161.19	0.0041
	100	52.67	0.0582						
House	10	29.76	0.0511	[20 10]	42.95	0.0019	[20 20 10]	123.71	0.0233
	20	34.11	0.0308						
	50	51.80	0.0683	[20 50]	149.32	0.0128	[50 20 10]	253.12	0.0103
	100	57.51	0.0052						
Background	10	31.34	0.0065	[20 10]	41.92	0.0599	[20 20 10]	78.20	0.0239
	20	31.67	0.0093						
	50	44.66	0.0086	[20 50]	143.45	0.0453	[50 20 10]	86.71	0.0493
	100	48.05	0.0462						

Table 2. Experimental results when trained with GRNN

Methods	$\sigma = 0.1$		$\sigma = 0.5$		$\sigma = 1$		$\sigma = 5$		$\sigma = 10$	
	Time required in second	MSE	Time required in second	MSE	Time required in second	MSE	Time required in second	MSE	Time required in second	MSE
Sky	11.70	0	11.71	0	13.120	0	10.68	1.6329×10^{-275}	9.85	1.2846×10^{-66}
House	11.07	0	11.87	0	12.45	0	17.28	0	24.19	2.14×10^{-8}
Background	14.11	0	17.16	0	16.17	0	15.82	2.3825×10^{-275}	17.68	6.2380×10^{-10}

training algorithm. It was seen that the double hidden layer gives better result than triple layer and single layer. The MSE value for double layer was calculated as around 0.0019 to 0.0599 and that for triple layer was around 0.0103 to 0.0703. It was also seen that for most of the region when ANN is trained with double hidden layer, it gives better MSE than single hidden layer ANN. When training is performed with GRNN, it gives better result than ANN both in terms of MSE and required time. The GRNN is trained with spread function values from 0.1 to 10. In most of the cases MSE values calculated as 0. When the values of spread function increase from 0.1 to 10, the MSE also slightly increases (around 10^{-8}). The time required for training is also less than ANN (10–25 s).

5 Conclusion

An ANN based approach for segmentation of images in complex background is proposed in this paper. The method does not require any feature extraction, labeling of objects, region growing or splitting methods to configure and train an ANN. The ANN is trained with single, double and triple hidden layer. The training is also done with GRNN for different values of spread function. Then the mean square error between the output image and desired image and the time required for training had been calculated. From the experimental results it is seen that GRNN gives better result.

References

1. Stojanovic, B., Nekovic, A., Popovic, Z., Lukic, V.: ANN based fingerprint image ROI segmentation. In: Proceedings of 22nd Telecommunications Forum Telfor (TELFOR), pp. 1–6, Belgrade, Serbia (2014)
2. Arumugadevi, S., Seenivasagam, V.: Color image segmentation using feed forward neural networks with FCM. Int. J. Autom. Comput. **13**(5), 491–500 (2016). https://doi.org/10.1007/s11633-016-0975-5. Springer, Heidelberg
3. Si, T., De, A., Bhattacharjee, A.K.: Artificial neural network based lesion segmentation of brain MRI. Commun. Appl. Electr. **4**(5), 1–5 (2016). Foundation of Computer Science (FCS), New York

4. Moghaddam, M.J., Zadeh, H.S.: Medical image segmentation using artificial neural networks. In: Artificial Neural Networks - Methodological Advances and Biomedical Applications, Chap. 6, pp. 121–138 (2011)
5. Haykin, S.: Neural Networks A Comprehensive Foundation, 2nd edn. Pearson Education, New Delhi (2003)
6. Hannan, S.A., Manza, R.R., Ramteke, R.J.: Generalized regression neural network and radial basis function for heart disease diagnosis. Int. J. Comput. Appl. **7**(13), 7–13 (2010)

An HPC-Data Center Case Study on the Power Consumption of Workload

Marta Chinnici[1(✉)], Davide De Chiara[2], and Andrea Quintiliani[1]

[1] ENEA- ICT Division, C.R Casaccia via Anguillarese 301, 00123 Rome, Italy
{marta.chinnici,andrea.quintiliani}@enea.it
[2] ENEA-ICT Division, C.R. Portici Piazzale Enrico Fermi, 1,
80055 Portici, NA, Italy
davide.dechiara@enea.it

Abstract. With the increasing popularity of Data Center (DCs), the energy efficiency issue is becoming more important than before. Due to their complex nature, the analysis and in particular the measurement of DCs' energy efficiency is articulated and open issue. Therefore, the analysis of energy efficiency in DCs, through a set of globally accepted metrics, is an ongoing challenge. In particular, the area of productivity metrics is not complete explored and existing proposed metrics none provides a direct measure of the useful work in a DC. To this end, this paper study and analyses the relationship between the power consumption by server' workload and the relative number of cores used. In details, through the ENEA-HPC'DC facility, we analyse the real data collected during one year to understand the link between workload' power consumption and cores. In this way, we present to advance beyond the state of the art of the productivity metrics, and in the meantime, a step forward regarding server performance and power management since through the statistical data analysis provides the behaviour of server energy consumption.

Keywords: Data Center · HPC · Energy efficiency · Computer applications
Energy metrics

1 Introduction

Nowadays, reducing energy consumption and provide metrics to monitoring the energy efficiency of computing infrastructure is an important goal of "big" data centres. Indeed, data centre energy consumption has risen dramatically over the past decade and will continue to grow in-step with the High-Performance Computing (HPC)- Data Centers (DCs) intensive workloads, which are crucial for our modern life [2–4]. Currently, advances in the technology have driven the DCs into a new phase of an expansion featuring solutions with higher density. For this reason, much has been done to increase server efficiency and IT space utilisation [12]. In particular, regarding the servers, the usage rate of resources is not so efficiency. Furthermore, some server and internal processors are completely idle [13]. Therefore, the enormous amount of energy consumed per year by DCs could be reduced through high-performance computing of resources scheduling and optimisation. The servers represent a significant component of

K. Ntalianis and A. Croitoru (Eds.): APSAC 2017, LNEE 489, pp. 183–192, 2019.
https://doi.org/10.1007/978-3-319-75605-9_26

DCs and the nature of the software that is run on them, called workload can have a considerable impact on the energy use. Indeed, the workloads can have a significant impact on the productivity and energy use of a server. Although, benchmarks - the deliberate process of data collection to provide an early indication of how your DC will perform - are presented in HPC' world (e.g. High Performance Linpack (HPL) Benchmark and the Green500 Challenge), but there are still few efforts to investigate on HPC' DC performance and productivity metrics. Indeed, only limited attention has been given to concern the definition and estimation the effectiveness of a DC thought the productivity metrics with the aim to understand the "useful work" in DCs [2, 6, 10]. Since the quantification of "useful work" is relevant to the assessment of the DC energy efficiency, the recent works are addressed to advance beyond the different techniques respect to the advanced to the state of the art of productivity metrics. Since the quantification of "useful work" is relevant to the assessment of the DC energy efficiency, the recent works are addressed to advance beyond the different techniques respect to the advanced to the state of the art of productivity metrics. In detail, the various methods include running on the actual SW stack, running a proxy workload, using the results of existing industry benchmarks, measured server power, and server power specs. Using industry benchmarks can be a research effort to gather data and make an approximate prediction of how a given solution stack should perform, but the most industry benchmarks cover either productivity or energy but none both. To investigate at productivity metrics, a good start is represented by the server power consumption.

This paper is organized as follows. Section 2 presents an introduction to the related work on measuring power consumption in HPC' DCs. Section 3 addresses the criteria and methodologies that can be considered to measure power consumption in CRESCO4 (HPC'DC) through a statistical data analysis is provided by ENEA-C.R. Portici facility. The Sect. 4 discusses the real power consumption provided by workloads running in ENEA'DC collected during the experimental campaign that covers one year. Section 5 is devoted to the conclusion on workload power management and the future challenges, considering the productivity metrics and recommendation for further development are given.

2 Related Works

There are many works on the characterization of servers' energy use [8]. In the present work, we will focus on the analysis of the job management systems to understand in details the workload power consumption associated with the different phase of the computing resources (idle time, sleep time, work time). The current techniques regarding the processor resources scheduling and optimisation are not taking into account in this manuscript. Regarding the server' power consumption techniques, an interesting survey associated with appropriate metrics - to achieve energy proportionality at DCs level, it is presented in [12]. The concept of energy proportionality emphasises the increase in power consumption of a system in proportion to the work done by the system. In [12], yet, an expanded treatment of the energy consumption related to the energy proportionality it was presented at the server level. In [11] the authors provide a technique to make progress to provide a practical solution and

metrics for computing and comparing the different workload energy consumptions with the aim of advancing current understanding on the calculation of the useful work of a DC. In the present work, we will provide an energy consumption evaluation method of workloads as regards energy-efficiency in High-Performance Computing (HPC) facilities. Moreover, describing the open challenges related to the work done metrics for DCs. The work presents a procedure to understand and predict the energy consumption of a DC. The developed solution is based on Platform Load Sharing Facility (LFS) that accounting job scheduler and the consumption data are stored on Zabbix. The solution employs experiments that were carried out at ENEA premises. The continued demand for new DCs capacity and computing power requires particularly careful consideration of computational infrastructure's energy consumption. The research community is about face many challenges on its way to create faster and more energy-efficient computing systems. Therefore, significant step forward regarding the energy efficiency of DCs are made, also in the niche of High-Performance Computing (HPC). Indeed, the recent years, the demands for High-Performance Computing (HPC) services have become widespread. The latest advancements in the HPC system size and processing power at computing nodes led to a significant increase in power consumption. For this reason, recently there have several studies on server power management. These works have proposed solutions, which reduce and characterise the server's energy consumption by adjusting power levels to track the resource demands of the workloads. Currently, the technique of power-aware task scheduling (PATS), based on dynamic voltage scaling (DVS), has been most widely used in the energy saving research topic of processors. This technique may reduce the power consumed by processors through flexible task scheduling. Chinnici et al. [11] address the DVFS approach to evaluate the servers' power consumption and to compare the DVFS (more parameters that come into play in a server configuration) with other servers' configurations.

Even if in literature several studies consider the power management of resources scheduling, servers resources scheduling and optimisation, workloads methods, however, not works supported by the practical approach to understanding and testing in depth from an energy efficiency side. In particular, investigate the workloads management methods will carry to advantages both regarding energy efficiency, low-cost and productivity metrics for DCs. Indeed, for a comprehensive framework on energy efficiency metrics for DCs is mandatory to understand in depth the work related to the computing and then the useful work done by workloads [2, 11].

3 ENEA HPC-Data Center

The work focuses on the evaluation and statistical data analysis of the power consumption at DC' cluster level. The procedure correlates accounting data from the Platform LSF (Load Sharing Facility) Job scheduler and the corresponding energy consumption obtained by data stored by Zabbix. LSF is a workload management platform and job scheduler, for distributed HPC systems. This platform is concerned with deciding which process is to be run and is designed to keep CPUs as busy as possible. It stores a log file that contains all information on executed jobs and the usage of computing nodes (cores). Our experiment uses the LSF log file to understand the

usage of the cores by the users and the Zabbix database that contains the consumptions detected by the PDUs of our DC during job execution. The experiments were performed on CRESCO4 HPC' facility (hosted by ENEA-R.C. Portici). In detail, the experimental campaign evaluates the global energy consumption of the cluster CRESCO4 that consists of 38 Supermicro F617R3–FT chassis, each hosting 8 dual CPU nodes. Each CPU, specifically an Intel E5–2670, hosts in its turn 8 cores, for a total number of 4864 cores. These operate at a clock frequency of 2.6 GHz. The system is provided with a RAM memory of 4 GB per core. Computing nodes access a DDN storage system, for a total storage amount of 1 Pbyte. Computing nodes are interconnected via an Infiniband 4xQDR QLogic/Intel12800-180 switch (432 ports, 40 Gbps). The data that came from the installed PDUs and LSF job scheduler accounting data was observed for one year (from February 2016 to February 2017).

4 Characterization of Workload Consumption

In this study, the data of workloads that have been analysed carry out of CRESCO4 cluster. The purpose is to find the correspondence between the workload power consumption and the cores used. This kind of measure could be necessary to drive the step forward in the way to measure the useful work within the DC, and the corresponding energy consumption. In detail, the power load needed to perform a task for a single core was evaluated. As aforementioned, we use the real data from a production HPC-ENEA-DC and the data is collected during one year time period from Feb. 2016 to Feb. 2017. It contains 47150 jobs ran out on more than 304 nodes. Moreover, this analysis does not take into account the cooling aspect of the external environment [18]. Management systems in HPC-DC store the information about past usage of the system; the information is found in a log format, namely workload. These records provide information about job execution in the system and our case as mentioned before, the LSF' platform stores the job scheduler' information. To understand in depth the energy performance of system we associate to each Zabbix interval (timestamp = 1 h) the number of jobs that are running within this range which know the number of cores. However, the timestamp of Zabbix' DB and LSF' data is different: the first one presents a timestamp equal to 1 h while the second one allows the rule of job allocations (in which arrival rate job comes from the user, what different size of jobs what length of job all the jobs related questions divert the system' administrator). Hence, we characterise the real DC' consumption from the workload point of view in this paper, and the first step to understanding the workload' consumption, it is required to have a robust and DB. For this reason, we have revised all data (coming from Zabbix and LSF) with a MATLAB procedure that allowed us to allocate better the cores used in time intervals. Unfortunately, the data from Zabbix are much less frequent and have a much larger sampling rate than LSF data. We have obtained many values for each row of Zabbix, so for each time interval of one hour we managed to get six values, that is, the minimum, average and maximum values of the number of core used and the minimum, average and maximum values for energy consumption (Fig. 1).

To provide the idea of the procedure testing, we show the analysis of the data collected during one month (Feb. 2016). This analysis in shown in Fig. 2; where the

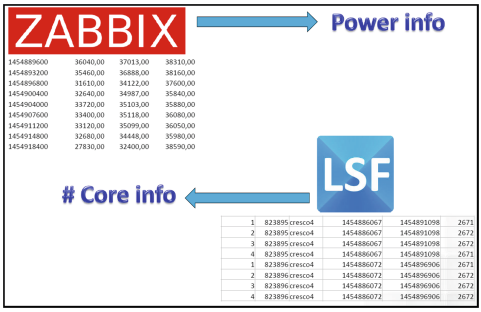

Fig. 1. Example of matching of data tuples from Zabbix to LSF

curve in 2-a represents the hourly trend of the electrical load (Watt) of CRESCO4 related for one month while 2-b curve shows the number of cores used in the same period. For each time step the ratio between the total electrical load (Fig. 2-a) and the number of working cores (Fig. 2-b) represents the power load related to each core in Fig. 2-c is reported. In this way, it was possible to evaluate the average value in the period analysed of electrical load of a single core. In the Fig. 2-c, a sketch of the deviation for each hour of the core power consumption respect to the average value (W8.02) for one month is presented. The analysis of this difference (or deviation) makes it possible to detect when the electrical load of a single core assumed value very distant from the mean. To evaluate the relationship between the power consumption and core the Pearson coefficient has been calculated.

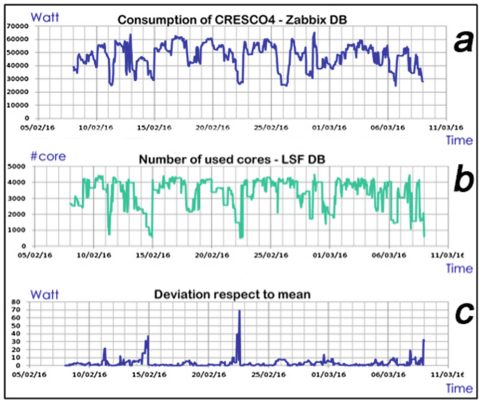

Fig. 2. The graphs represent the power profile, respectively of (a) power consumption (b) number of cores used (c) deviation of the core power consumption respect to the average value, during 1 month on CRESCO4

The calculated Pearson correlation coefficient for the period of one month resulted in being equal to 0.6. Figure 3 show the deviation of the ratio power consumption and the number of the core from its average value.

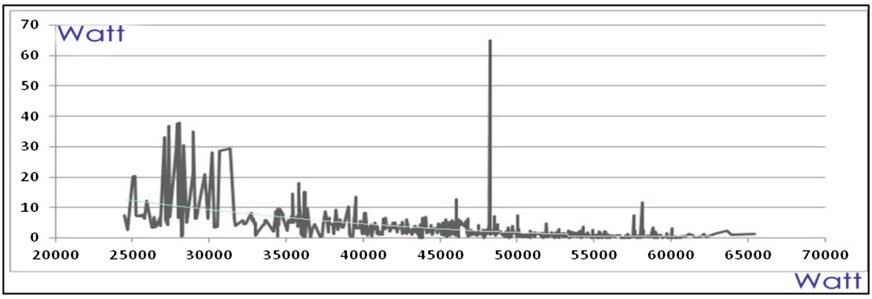

Fig. 3. Deviation of the ratio power consumption and number of core from its average value (data set = 1 month)

The curve in Fig. 3 shows the data coming from the Fig. 2c) according to increasing power size the axes represent the total power consumption of cluster CRESCO4 - x-axis and the power usage by the deviation of the ratio power/#core, y-axis respectively). To note that as the power grew the value of single core' power, it approaches to the mean value (e.g., take into account the value 25000 W, around this value the deviation of the ratio power/number of core respect to the average value is 20 W). Notice that when the power increases, the number of cores approaches more to the mean value. Moreover, probably due to the systematic error of Zabbix and LSF, a peak is presented between 45000 W and 50000 W. So obviously there is a problem in the first 30000 watts. Between the analysed data it is immediately noticed that the deviation is much higher and unstable in the first 30000 W. This small case study is a preliminary analysis that has been extended to the larger version that covers a data set of one year of data. Indeed, in the following, we present a new case study related to this larger set of data where we have to apply the same method of the previous small case.

The graphs in Fig. 4 represent the profile respectively of (a) power consumption (b) number of cores used (c) deviation of the core power consumption respect to the average value, during one year on CRESCO4. In the Fig. 4-c, we found the curve that represents the deviation for each hour of the core power consumption respect to the average value (W7.28) for one-year data. In Fig. 5 is reported the deviation of the ratio power consumption and the number of the core from the mean value. It possible to apply at this deviation' curve the same considerations as before in Fig. 3 and in particular the peaks load presented within the range 35000–40000, around the point 46000, and the position 58000 are caused by the systematic error of Zabbix and LSF.

Starting to the considerations about the last chart, an additional analysis regarding the idle issue is necessary. Hence, the procedure consists of isolating the amount of energy consumed when the DC is idle (Idle CRESCO4: 28635 W), with a regression method that would also allow understanding the inclination (slope of the regression line) of the cloud of points using the regression line of the active core on x-axis vs. power consumption on the y-axis (see Fig. 6). A linear equation $y = mx + b$ was obtained respectively with coefficient $m = 7{,}01$ and $b = 28635$, where m is the slope of the line and b is the y intercept, which is the y coordinate of the location where the line crosses the y axis. In our case slope m represents the consumption of a single core and b provides indications about idle consumption of the datacentre CRESCO4.

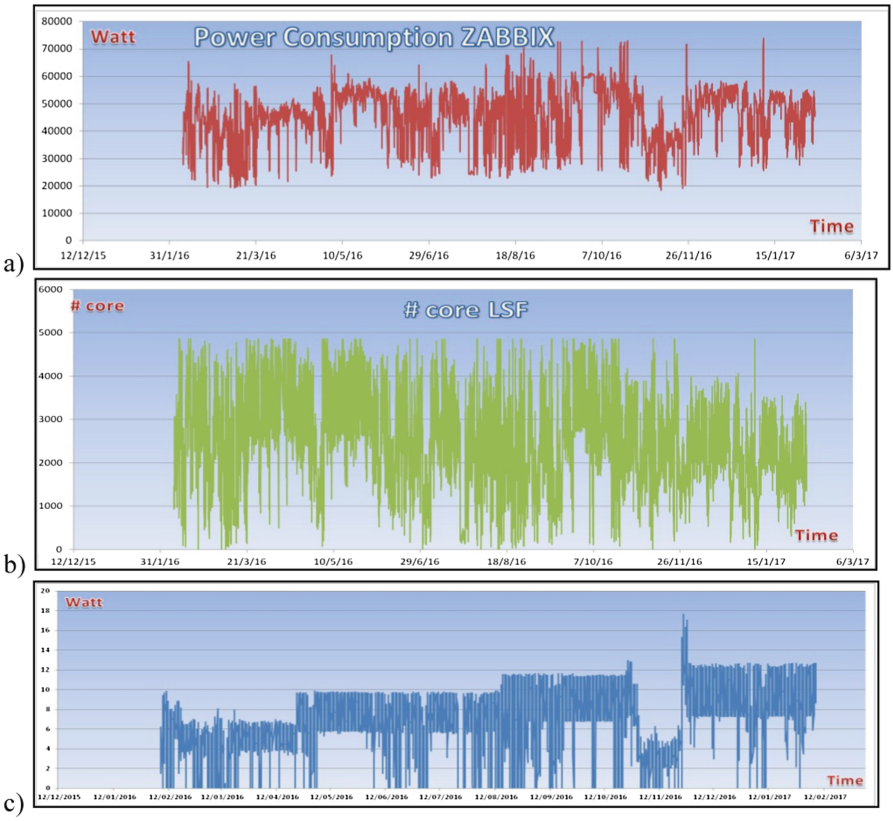

Fig. 4. The graphs represent the profile respectively of (a) power consumption (b) number of cores used (c) deviation of the core power consumption respect to the average value, during 1 year on CRESCO4

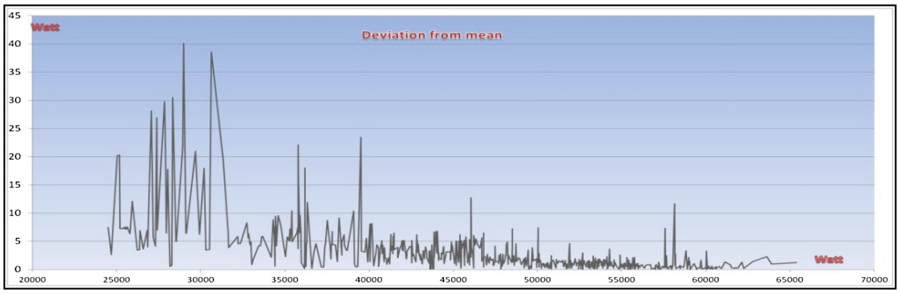

Fig. 5. Deviation of the ratio power consumption and number of core from its average value (data set = 1 year)

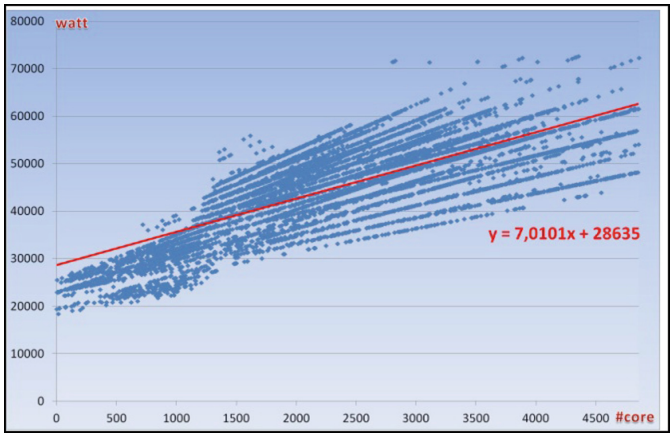

Fig. 6. Linear equation for regression line

The statistical parameters such as Pearson coefficient, harmonic mean, standard deviation and variance have been calculated and shown below:

- Pearson (Power, Core) = 0.768319246
- Avg (Power/Core) = 7.288367014
- Standard deviation (Power/Core) = 2.672695437
- Variance (Power/Core) = 7.1433009

It is notable as the variance has risen and therefore we have obtained through the procedure more significant data and with less probability of error. With these new data we have again built the scatter plot, and through the well-known mathematical formulas, we obtained the equations of the regression lines. We have worked with both linear and polynomial regression of different order. With linear regression, we have obtained the equation y = 7.01x + 28635, trivially indicated us a cluster idle consumption of about 28635 (W) and a single core consumption of 7.01 (W). The idle is calculated by the smooth intersection of the regression line with the y-axis (when the number of cores is zero) and the consumption of the single core given by the angular coefficient of the regression line. In order to test for nonlinear relationship, polynomial regression (Fig. 7) has been adjusted. However, the linearity of the curve is still present when both the power and the number of cores used increase.

Currently, with the aim of improving the measures and methods used and providing a more reliable calculation model, we are completing procedures that best identify the core utilised in the job scheduler sampling timeframe. The ultimate goal is to provide a customizable forecast model that can be employed on different architectures using measuring instruments other than Zabbix and LSF.

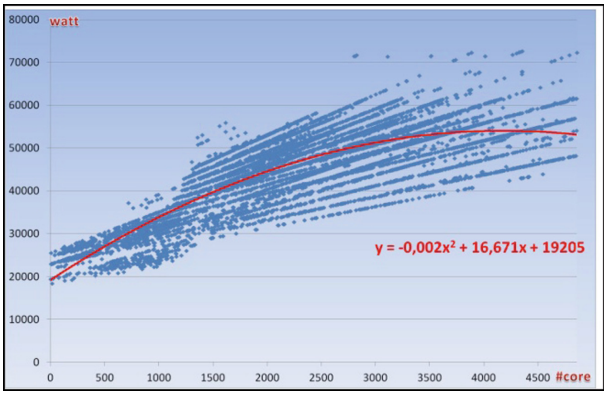

Fig. 7. Polynomial equation for regression line

5 Conclusion

Currently, results on productivity metrics for predicting energy consumption are still in an embryonic state but this is a hard and important problem above all when we want to approach the power consumption when the applications were running. We believe that some of the aspects we have proposed here regarding the correlation between the power consumption and core used by workload will be helpful for future works in the interpretation and calculation of the useful work. Indeed, thanks to the collection of a big set of real consumption data trying to gain knowledge on the useful work of computing process that contribute the most to the DC' energy consumption. Through the interpretation of the trend of the power curve about the amount of the busy number of cores relatively to an extended period, could provide substantial information for the estimate of power output and therefore of energy required for certain tasks. Obviously, the study is also useful to calculate the energy consumptions of a given computing infrastructure. Basically what we do is primarily a study of data, which starts from the acquisition, filtering and then comes wing classification. Then we correlate the power data with those of the resources used (in our case the number of the core) to perform a regression analysis, to analyse a set of data that consists of a dependent variable and one independent variable. The experiment we run relates the number of the core with the power delivered, but in general, it could be replicated to estimate any functional relationship between the dependent variable and the independent variables. Nowadays in statistics, the regression analysis is associated with the linear model resolution, but once valid and useful data is obtained, we can opt for non-linear regression methods, and therefore we can estimate the trends of a "power output/resource usage" pattern through an interpolating curve that best approximates such a trend.

Acknowledgements. This work is an extended version of the poster "Data Center, a cyber-physical system: improving energy efficiency through the power management" presented in the conference proceedings of Cyberscitech'17 will be held on Nov. 2017. Moreover, the authors would like to thank the research HPC group at the ENEA-R.C. Portici for the helpful discussions and useful advice on modelling and control of ENEA-DC.

References

1. Sehgal, P., Tarasov, V., Zadok, E.: Evaluating performance and energy in file system server workloads. In: Proceeding FAST 2010 of the 8th USENIX Conference (2010)
2. Chinnici, M., Capozzoli, A., Serale, G.: Measuring energy efficiency in data centers. In: Pervasive Computing Next Generation Platforms for Intelligent Data Collection, pp. 299–351 (2016). ISBN: 978-0-12-803663-1
3. Capozzoli, A., Chinnici, M., Perino, M., Serale, G.: Review on performance metrics for energy efficiency in data center: the role of thermal management. In: Klingert, S., Chinnici, M., Rey, M. (eds.) Third International Workshop on Porto Energy Efficient Data Centers, E2DC 2014, Cambridge, UK, 10 June 2014, Revised Selected Papers, Cambridge, UK (2015)
4. Capozzoli, A., Serale, G., Liuzzo, L., Chinnici, M.: Thermal metrics for data centers: a critical review. In: Energy Procedia, vol. 62, pp. 391–400. Elsevier (2014). ISSN: 1876-6102
5. Capozzoli, A., Primiceri, G.: Cooling systems in data centers: state of art and emerging technologies. In: Energy Procedia, pp. 484–493. Elsevier (2015). ISSN: 1876-6102
6. Chinnici, M., Quintiliani, A.: An example of methodology to assess energy efficiency in data centers. In: IEEE Third International Conference on Cloud Green Computing, Karlsruhe, pp. 459–463 (2013). https://doi.org/10.1109/cgc.2013.78
7. Basmadjian, R., de Meer, H.: Evaluating and modeling power consumption of multi-core processors. In: Third International Conference on Future Energy Systems: Where Energy, Computing and Communication Meet (e-Energy), pp. 1–10. IEEE (2012)
8. Shen, S., van Beek, V., Iosup, A.: Workload characterization of cloud datacenter of bit brains. pp. 1387–2109 (2014)
9. Parolini, L., Sinopoli, B., Krogh, B.H., Wang, Z.: A cyber–physical systems approach to data center modeling and control for energy efficiency. In: Proceedings of the IEEE, vol. 100 (1), January 2012. ISSN: 0018-9219
10. http://www.dc4cities.eu/en/wp-content/uploads/2016/05/D7.3-Final-DC4Cities-standardization-framework-and-results-description-of-the-European-Cluster.pdf
11. Quintiliani, A., Chinnici, M., De Chiara, D.: Understanding 'workload-related' metrics for energy efficiency in Data Center. In: 20th International Conference on System Theory, Control and Computing, ICSTCC 2016, pp. 830–837. ISBN: 978-150902720-0 7790771
12. Khan, S., Zomaya, A.Y.: Handbook on data centers. Springer (2015). ISBN: 978-1-4939-2091-4
13. Barroso, L.A., Holzle, U.: The datacentre as a computer: an introduction to the design of warehouse-scale machines. Synth Lect. Comput Archit. **4**, 1–108 (2009)
14. Pillai, P., Shin, K.: Real time dynamic voltage scaling for low power embedded operating systems. ACM SIGOPS Oper. Syst. Rev. **35**, 89–102 (2001)
15. Martin, S., Flautner, K., Mudge, T., et al.: Combined dynamic voltage scaling and adaptive body biasing for low power microprocessors under dynamic workloads. In: ACM International Conference Computer-aided Design, pp. 721–725 (2002)
16. Jrjurikar, R., Pereira, C., Gupta, G.: Leakage aware dynamic voltage scaling for real time embedded systems. In: Proceedings of the 41st Annual Design Automation Conference, pp. 275–280 (2004)
17. Yan, L., Luo, J., Jha, N.: Joint dynamic voltage scaling and adaptive body biasing for heterogeneous distributed real time embedded systems. IEEE Trans. Comput. Aided Des. Integr. Circ. Syst. **24**, 1030–1041 (2005)
18. Capozzoli, A., Primiceri, G.: Cooling systems in data centers: state of art and emerging technologies. In: Proceedings of SEB 2015, vol. 83, pp. 484–493 (2015)

Identifying Problematic E-courses Content Based on Students Behaviour

Dominik Halvoník[1(✉)] and Jozef Kapusta[1,2]

[1] Department of Informatics, Faculty of Natural Sciences, Constantine the Philosopher University in Nitra, Nitra, Slovakia
{dominik.halvonik, jkapusta}@ukf.sk
[2] Institute of Computer Science, Faculty of Mathematics, Physics and Technical Science, Pedagogical University of Cracow, Cracow, Poland
jkapusta@up.krakow.pl

Abstract. When analyzing students' behavior, it is possible to use a variety of web mining techniques and techniques in addition to basic descriptive statistics. These techniques are applied in order to identify the most frequent way how student is exploring courses, frequent problems in passing the e-learning course, identifying problems in individual tests or identification problematic parts of educational materials. The aim of this paper is to introduce our own methodology for identifying problematic parts of educational content. We use two areas of mining web: web content and web usage mining. By applying basic web content mining techniques, we created a site size metrics for the training course. We experimented with time spent on educational pages. The content size of the individual training course parts will predict the time spent by students in their study. We analyzed the dependence between number of words of the web page with the educational content and the time spent by students on this site. We deal with the problematic parts of the analysis differences in content length of educational materials and time spent on them in discussion and also in the conclusion of this paper. We also assume other metrics for comparison of these variables.

Keywords: Web usage mining · Web content mining · Educational content Time spent

1 Introduction

Educational data mining includes methods and techniques for analyzing the behavior of users - students during the learning process, most often in virtual learning environments (VLE). When analyzing students' behavior, it is possible to use a variety of web mining techniques and techniques in addition to basic descriptive statistics. These techniques are applied in order to identify the most frequent way how student is exploring courses, frequent problems in passing the e-learning course, identifying problems in individual tests or identification problematic parts of educational materials. This information is an important part of the teacher's work. It serves as support for decision-making within teachers course creation.

The aim of this paper is to introduce our own methodology for identifying problematic parts of educational content. We use two areas of mining web: web content and

K. Ntalianis and A. Croitoru (Eds.): APSAC 2017, LNEE 489, pp. 193–198, 2019.
https://doi.org/10.1007/978-3-319-75605-9_27

web usage mining. By applying basic web content mining techniques, we will create a site size metrics page for the training course. In this article, we will experiment with time spent on educational pages. The content size of the individual training course parts will predict the time spent by students in their study.

We use our web mining methods to process the data from the VLE of our university. Base on this these logs, we estimate the student's average time spent on each course page. Our aim is to analyze students' behavior and identify parts of educational materials that may be problematic from the point of presented subject. We focus on pages where their content studying time is relatively high compared to their content size. It is likely that the identified parts of educational content represent a problematic content that the teacher can improve or redesigned for its better clarity and readability.

2 Related Work

In this paper we analyze one of the discovered variables and which is student's time spend on a single page of educational content. We assume that it is possible for sake of this analysis apply results of Rayner's experiment that discovered base on the observations of college-level readers reveal that most read is at a rate of between 200–400 words per minute [1]. We also took into account that average speed of ordinary reading is higher than average speed of reading for education purpose.

Comprehending expository reading material is a challenge for many students. Research has shown that students' expository reading comprehension can improve with the help of text structure instructions [2]. Currently there are several structural and content frameworks that increase student's ability to understand and reuse learned knowledge from educational materials. The theoretical bases for this frameworks are reading comprehension models, such as Cromley and Azevedo's [3] direct and inferential mediation (DIME) model which in turn is based on Kintsch's [4] construction-integration model. The DIME model hypothesizes the relationships between background knowledge, vocabulary, word reading, reading strategies, and inference that together result in reading comprehension. Reading vocabulary and background knowledge directly contribute to the reading comprehension and also have effects that are mediated by inference. The model further suggests that the effect of strategies on comprehension is mediated by inference. Reading comprehension is correlated with a number of cognitive and metacognitive strategies, such as [5]: activating background knowledge, summarizing text, generating questions to capture the main idea of the passage.

Most of previous research was done on educational materials in paper form. However base on the D'Haenens [6] findings we can use the results of these research because there is no significant difference between learning new information from text that is in online and paper form.

Intelligent tutoring systems commonly record their interactions in the form of log files. Log files are easy to record, flexible in what information they can capture, (sometimes) human-understandable to read, and useful in debugging. However, they are unwieldy to aggregate across multiple sessions and computers, and difficult to parse and analyze in ways not anticipated when they were designed. Consequently, we have found

that logging interactions stored directly in a database make such analysis easier, more flexible, less bug-prone, and more powerful than analyzing conventional log files [7].

Base on these findings we decided to avoid using Common Log File as a resource of user behavior information. Instead we used Moodles logging table.

3 Data Pre-processing

We mentioned previously, that we tried to connect information represented time spent on site with educational content extracted from the VLE's log file and information about the educational content size and structure. We describe the details of the proposed approach in this section.

For the experiment, the Computer Network course was selected from the bachelor study program Applied Informatics. Individual educational materials, which were in the form of web pages, were translated into non-formatted text. Subsequently, we calculated the number of text characters, the number of words and the number of images. The input data consisted of 294 educational pages that were identified by: URL, number of characters, number of words, which was added to each page.

We used the log files of the university VLE. With the complete log file, we only selected logs related to the selected e-learning course. The final log file contained 50346 records over a period of 2 years 3 months and 5 days.

We prepared data with session identification using standard time threshold technique (STT) [8]. The session identification method using standard time threshold (time-window) represents the most common technique. Using this method, each time we had found subsequent records about the web page requests where the time of the web page displaying had been higher than explicitly selected time, we divided the user visits into several sessions. We used STT = 90 min.

We worked with VLE Moodle log, where users must use their name and password to access the system. For this reason, it was not necessary to use the standard web log mining steps - cleaning a file from robots.

The reconstruction of the web site visitor's activities represents another issue for WUM. This technique does not belong to the session identification approaches. VLE Moodle is an environment with a rich offer of links and a thorough linking of learning pages. It was proved in research [8] that in the log file from the Moodle VLE there is no need to use this technique.

In the next step, we analysed the log file and we added the information about time spent by individual user on the web page into each record. This time was calculated as the difference between two consecutive records from one user.

4 Finding Potentially Problematic Parts of Educational Content

We analysed the dependence between number of words of the web page with the educational content and the time spent by students on this site. We considered the comparable values for the comparison of web page with educational content size (variable *word_count*) and time spent on this page (variable *time_spend*).

The variables *word_count* and *time_spend* were normalised using min-max normalisation function. The min-max normalizer linearly rescales every feature to the < 0, 1 > interval. The normalization of the variables *word_count* and *time_spend* creates an important part of the proposed method. It ensures the comparability of both variables. However, it is possible to use also other normalization methods like normalization with decimal scale, normalization with zero being the central point, etc.

We assume that the number of words in the study material predicts the time spent by students studying this material. To compare variables *word_count* and *time_spent.*

We calculated the value of difference from the normalized values. The Table 1 shows the difference calculation. In total, the table shows 294 values for all the educational pages studied from the course and is arranged according to the value of difference.

Table 1. Table of the difference

Id	Url	Norm. word_count	Norm. time_spent	Difference
p133	view.php? id=42910&chapterid=14984	0,459919391	1	0,540081
p45	view.php? id=42914&chapterid=15024	0,335423197	0,747350108	0,411927
p80	view.php? id=47234&chapterid=17995	0,019704433	0,417189955	0,397486
p11	view.php? id=42911&chapterid=14993	0,081504702	0,421551322	0,340047
p194	view.php? id=49532&chapterid=19232	0,11150918	0,440574775	0,329066
	…			
p289	view.php? id=56426&chapterid=22645	0,008508733	0,008779272	0,000271
p68	view.php? id=47231&chapterid=17984	0,13658755	0,136474662	–0,00011
p122	view.php? id=49523&chapterid=19148	0,176444245	0,175954698	–0,00049
	….			
p221	view.php?id=49541	0,485893417	0,012290981	–0,4736
p109	view.php? id =49523&chapterid=19135	0,808329601	0,164734963	–0,64359
p107	view.php?id=49523	0,657411554	0,005267563	–0,65214
p75	view.php? id=47231&chapterid=17991	1	0,282446214	–0,71755

We present the values of difference visualization also in the graph (Fig. 1), where the axis X represents the individual pages with the educational content and the Y axis represents the value of difference for the individual pages.

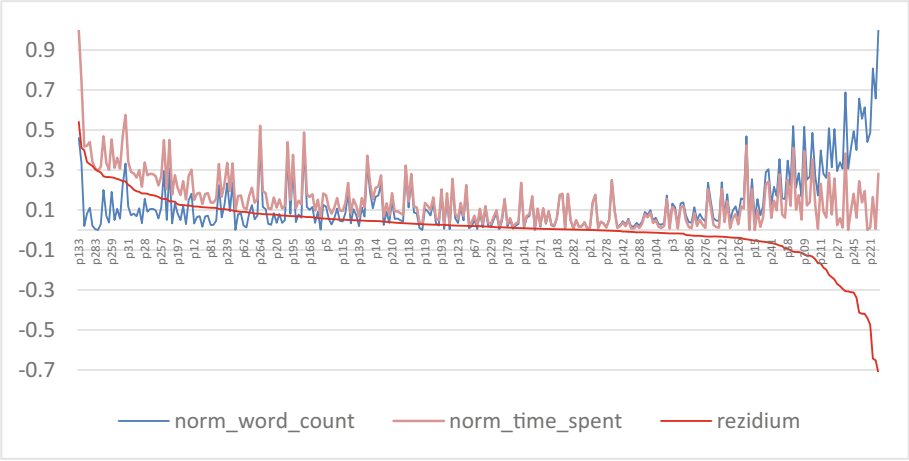

Fig. 1. Difference visualization in the graph

5 Discussion

Base on the analysis presented in Sect. 4, we found web pages that can be considered as inadequately structured educational content. As we defined in the beginning of this paper the criteria for this classification is the difference between student`s time spend on specific web page and its content length, respectively number of words on the educational page. In described course they were, for example pages dedicated to problematic of OSI model, WPA2 etc. This method quickly and relatively easily points to the e-course pages that need to be edited, respectively modified.

An important step in the method is the normalization that normalizes both values - the number of words on page and the average time spent on the page - into comparable values.

The determination of outlier values is an another important part of the method. Their determination will accurately identify pages with educational content that are problematic and need to be redesigned. We could identify the outliers using the standard rule $\pm\ 2\sigma$. It means that we considered the cases that were out of the interval

$$\textit{Average of differences} \ \pm\ 2\ \textit{standard deviation of differences}.$$

The second option for determining outlier values is to use the rule for quartile interval

$$(Q_I - 1,5Q; Q_{III} + 1,5Q),$$

where Q is quartile interval, Q_I and Q_{III} are lower and upper quartile.

Due to the scope of the article, we did not write the progress and results for determining the outlying values in the course we analysed.

6 Conclusion and Future Work

In the article, we focused on analyzing the content of educational materials and the time spent on them. We introduced a simple method to find potential problematic pages with educational content. The problem of this method appears to be a comparison of relatively different data: the number of words on the educational page and the average time spent on the page. For this reason, in the future, we want to focus on estimating the time spent on the site, based on reading text learning theories. Based on the number of words, respectively characters, we get an estimate of time spent on a page that we can compare with the actual, average time spent on the page. Then, we will be able to use a residual analysis. As a prediction, we take into account the estimated time spent on the page (calculated by the number of words or characters). Observed data will be the average time spent by students on the site. The residues are defined as difference between observed values and expected values.

Another way of looking at the data is to use a linear regression. We assume that the average time spent on the educational content page depends on the number of words on this page. Therefore, the average time will be the dependent variable and the size of the educational content by the independent variable in the regression model. Once it's created, we'll be able to find problematic educational pages by specifying the deviation from the model.

Acknowledgement. This article was supported by the project UGA VII/6/2017.

References

1. Rayner, K.: Eye movements in reading and information processing: 20 years of research. Psychol. Bull. **124**(3), 372–422 (1998)
2. Roehling, J.V., Hebert, M., Nelson, J.R., Bohaty, J.J.: Text structure strategies for improving expository reading comprehension. Read. Teach. **71**(1), 71–82 (2017)
3. Cromley, J.G., Azevedo, R.: Testing and refining the direct and inferential mediation model of reading comprehension. J. Educ. Psychol. **99**(2), 311–325 (2007)
4. Kintsch, W.: Comprehension: A Paradigm For Cognition. Cambridge University Press, Cambridge (1998)
5. Spörer, N., Brunstein, J.C., Kieschke, U.: Improving students' reading comprehension skills: effects of strategy instruction and reciprocal teaching. Learn. Instr. **19**(3), 272–286 (2009)
6. d'Haenens, L., Jankowski, N., Heuvelman, A.: News in online and print newspapers: differences in reader consumption and recall. New Media Soc. **6**(3), 363–382 (2004)
7. Tell, W., Mostow, J., Beck, J., Cen, H., Cuneo, A., Gouvea, E., Heiner, C.: An Educational Data Mining Tool to Browse Tutor-Student Interactions: Time (2005)
8. Munk, M., Drlik, M.: Influence of different session timeouts thresholds on results of sequence rule analysis in educational data mining. CCIS, vol. 166, pp. 60–74 (2011)

Dyscalculia: A Behavioural Vision

Filipa Ferraz[1], José Neves[1(✉)], Victor Alves[1], and Henrique Vicente[2]

[1] Department of Informatics, University of Minho, Braga, Portugal
filipatferraz@gmail.com, {jneves,valves}@di.uminho.pt
[2] Department of Chemistry, University of Évora, Évora, Portugal
hvicente@uevora.pt

Abstract. *Learning Disabilities* (*LD*) constitute a diverse group of disorders in which children who generally possess at least average intelligence have problems processing information or generating output, i.e., *LD* may be interpreted as a neurologically-based processing problem. The causes and treatment of *LD*, namely reading disorders has been the subject of considerable thought and study. Being one among others, this is the reason why this work will focus on dyscalculia and in its different manifestations and how they may interfere with the children natural development. It will be assessed it in terms of a measurement of the child's entropy, a thermodynamic quantity representing the unavailability of a child brain energy for conversion into mental work, and seen as the degree of disorder or randomness in the brain, i.e., lack of order or predictability; gradual decline into disorder; an arena where entropy reigns supreme. In one's work it reigns in a specific interval, i.e., one may have two scenarios, namely the worst and the best one. The formal background will be grounded in the use of *Logic Programming* to set the architecture of a *Function Machine* to assess *LD* and built on base of a *Deep Learning* approach to *Knowledge Representation and Reasoning*.

Keywords: Learning Disabilities · Entropy · Logic Programming
Knowledge Representation and Reasoning · Deep Learning · Function Machine

1 Introduction

Learning Disabilities (*LD*) are one of the main concerns when it comes to scholar ratings of success. Specific mathematical *LD* are, yet, not so deeply approached when there is an attempt to mitigate the learning ones affecting the rates. Even so, there is more research work on this issue that will make a sustainable difference to the quality and consistency with which safe and therapeutic services for people with *LD*, not only regarding the children evolution. Indeed, *developmental dyscalculia* is a specific mathematical *LD* that has been studied and it is understood as *a difficulty in leading with arithmetical issues*. There is not, yet, a standard screening test, but there are several tools to help assess the type of *LD* that affect children.

Following Kosc [1], one may be faced to six distinct types of dyscalculia that comprehend the *lexical one*, which concerns troubles reading and understanding mathematical symbols and numbers, as well as mathematical expressions or equations. The children who has *lexical dyscalculia* can understand spoken views, but have

K. Ntalianis and A. Croitoru (Eds.): APSAC 2017, LNEE 489, pp. 199–206, 2019.
https://doi.org/10.1007/978-3-319-75605-9_28

trouble in writing or understanding them, presenting difficulty in reading symbols, such as numerals, and cannot understand them when they occur in number sentences or equations; *verbal dyscalculia*, in which children have problems in naming and comprehending the mathematical concepts exposed verbally. The children are able to read or write a number, but cannot recognize them when they are revealed verbally – they present some strain when talking about mathematical concepts or relationships; *graphical dyscalculia*, manifested as not easy task when writing mathematical symbols. The children that have this type of dyscalculia are able to understand the mathematical concepts but do not have the ability to read, write, or use the mathematical symbols – a difficulty with writing such icons including but not limited to numbers; *operational dyscalculia*, which presents itself with a difficulty to complete arithmetical operations or mathematical computations, both written and verbal. Someone with *operational dyscalculia* will be able to understand the numbers and the relationships between them, but will have trouble manipulating numbers and mathematical symbols in computational process; *practognostic dyscalculia*, which denotes difficulty in the process of translating their abstract-mathematical concepts to real and ideal aspects of human life. These children are able to understand mathematical concepts but have trouble in listing, comparing or manipulating mathematical equations, demonstrating difficulty in translating their abstract mathematical knowledge into real-world actions or procedures; and *ideagnostic dyscalculia*, a snag when carrying out mental operations without using numbers to arrive at a solution or to understand concepts or ideas related to mathematics or arithmetic. These children have a challenging time in remembering mathematical concepts once having learned them and difficulties with tasks that require understanding of mathematical notions and relationships, such as identifying which sequence of numbers is larger or smaller.

As stated above, the distinction between each type of dyscalculia can be done through tasks directed towards a certain objective and its assessment. So, the board games, puzzles and other type of educative tools are the best instruments to use in order to evaluate the stage and type of *LD*.

Additionally, questionnaires filled by teachers, educators or relatives (preferentially someone that deals daily with children) are an asset to complete a primary diagnosis of the several types of dyscalculia.

On the other hand, *Artificial Intelligence* (*AI*), in touch with reality, is in the evolving and testing of theories and aspects of intelligent behaviour, including *Knowledge Representation and Reasoning*, *Learning*, *Decision-making*, *Communication*, *Coordination*, *Action*, *Interaction*, where *Machine Learning* (*ML*) is concerned with the scientific study, design, analysis, and applications of algorithms that learn concepts, predictive models and behaviours. Indeed, *AI* is transforming the world of different disciplines. *AI* can help teachers, doctors and other practitioners to make faster, more accurate diagnoses. It will be used here to improve children care, supporting a *Deep Learning* approach to *Knowledge Representation and Reasoning* (*KRR*).

Therefore, a brief description of an innovative *KRR* it is set in the next section, followed by the presentation of a case study focused on screening the types of dyscalculia in children. Finally, conclusions are gathered and directions for future work are outlined.

2 Knowledge Representation and Reasoning

On the one hand, many approaches to integrate *Deep Learning* with *Knowledge Representation and Reasoning* (*KRR*) are based on the fact that one must give up on having a fixed symbolic *structure*, i.e., it must be set a process of *relaxation* when going from symbolic to sub-symbolic, where the *KRR's* process is induced by learning algorithms, with an outcome mostly opaque to the users. This view stands for the key distinction between such approaches where it is asserted that when it is used symbolic logic in vector spaces, the essential features of a universe of discourse remain discrete, and as a result nothing is gained. On the other hand, in one's approach, although presenting a symbolic logic in vector spaces, the functions' elements or attributes go from discrete to continuous, allowing for *unknown*, *incomplete*, *forbidden* and even *self-contradictory information* or *knowledge*, with no opaqueness at all for the users. Thus, the universe of discourse in this work will be engendered according to predicate's extensions of the type:

$$predicate_i - \bigcup_{1 \le j \le m} clause_j(([A_{x_1}, B_{x_1}](QoI_{x_1}, DoC_{x_1})), \cdots, ([A_{x_n}, B_{x_n}](QoI_{x_m}, DoC_{x_m}))) :: QoI_j :: DoC_j$$

where $[A_{x_j}, B_{x_j}]$, QoI_{x_j} and DoC_{x_j} denote, respectively, the scope where the unknown $attribute_j$ for $predicate_i$ is expected to appear, the attribute's *Quality-of-Information* and, finally, the *Degree-of-Confidence* that one may have on such a value. Therefore, we will look at approaches to *KRR* that have been proposed using the *Logic Programming* (*LP*) epitome, namely in the area of *Model Theory* [2, 3] and *Proof Theory* [4, 5]. In the present work, the *Proof Theoretical* approach in terms of an extension to the *LP* language is followed. An *Extended Logic Program* is, therefore, given by a finite set of clauses, in the form:

$$\begin{{l}}
\neg p \leftarrow not\ p, not\ exception_p \\
p \leftarrow p_1, \cdots, p_n, not\ q_1, \cdots, not\ q_m \\
?(p_1, \cdots, p_n, not\ q_1, \cdots, not\ q_m)(n, m \ge 0) \\
exception_{p_1}, \cdots, exception_{p_j}(0 \le j \le k), \quad being\ k\ an\ integer\ number \\
\} :: scoring_{value}
\end{{l}}$$

where the first clause stand for predicate's closure, "," denotes "*logical and*", while "*?*" is a domain atom denoting falsity, the p_i, q_j, and p are classical ground literals, i.e., either positive atoms or atoms preceded by the classical negation sign $\neg$ [5]. Indeed, $\neg$ stands for a strong declaration that speaks for itself, and *not* denotes *negation-by-failure*, or in other words, a flop in proving a given statement, once it was not declared explicitly. Under this formalism, every program is associated with a set of *abducibles*

[2, 3], given here in the form of exceptions to the extensions of the predicates that make the program, i.e., clauses of the form:

$$exception_{p_1}, \cdots, exception_{p_j}(0 \leq j \leq k), being\ k\ an\ integer\ number$$

that stand for data, information or knowledge that cannot be ruled out. On the other hand, clauses of the type:

$$?(p_1, \cdots, p_n, not\ q_1, \cdots, not\ q_m)\ (n, m \geq 0)$$

also named *invariants*, allows one to set the context under which the universe of discourse has to be understood. The term $scoring_{value}$ stands for the relative weight of the extension of a specific predicate with respect to the extensions of peers' ones that make the inclusive or global program.

3 Case Study

3.1 Data Collection

On the one hand, one's approach to the problem referred to above will focus on the study of sensory problems in children diagnosed with specific *LD*, where cognition of visual stimuli is of the utmost importance, i.e., a special attention would be given not only to the sensing of the children physical characteristics but also to their sentiments and emotions or even our own soul. On the other hand, it is also imperative to focus on the social perspective and its assessment, which will be done in terms of a *Function Machine* (i.e., a writing board for presentations), set as a computational environment comprising children, teachers and other practitioners and technology, interacting and producing actions and information that would not be possible to extract without having all parties present. Therefore, regarding the factors that influence *LD*, focus should be given to national policies, such as economic strategies and the conditions in which children live and learn.

Regarding data collection, the technique used was observation. Teachers from *N* schools evaluated *N*N* students following a criteria list. The target group, the *N*N* students, is characterized by a set of children between 5 to 8 years-old, attending the first, second and third grades. These annotations focused not only on students that were already diagnosed with, or suspected of having dyscalculia but also on non-affected ones. The process consisted in fill a data registry regarding each student where the teachers and other practitioners assess the student`s difficulty in performing the tasks described in the criteria list, based on the previous knowledge and daily contact with the child. The criteria list contained mixed tasks concerning the six types of dyscalculia, delivered to the lecturers and other experts and built by the research team. Such records are stored in a *Case Base*, according to productions of the type:

$$Case\ Records = \{Raw_{data}, Normalized_{data}, Description_{data}\}$$

where the attributes Raw_{data} and $Normalized_{data}$ stand for themselves, and the last one, $Description_{data}$ denotes a set of procedures that may be used in order to set a diagnosis or even free text that explains the *Case Records* in more detail, namely presenting a diagnosis and validating it.

3.2 Feature Extraction

The feature extraction's process focused on the more relevant tasks associated with each type of dyscalculia. Given the criteria list that guided the teachers, it were selected five to eight tasks related to a type of dyscalculia and stored in the respective table, as shown in Fig. 1. The remaining data from the criteria list was discarded.

The data used in this study will be given in terms of the extensions of the relations/tables *Lexical Dyscalculia*, *Verbal Dyscalculia*, *Graphical Dyscalculia*, *Operational Dyscalculia*, *Practognostic Dyscalculia* and *Ideagnostic Dyscalculia* (Fig. 1), where the attributes 'values speak for themselves. For example, *Understanding Relationships Between Numbers* stands for an attribute that belongs to the

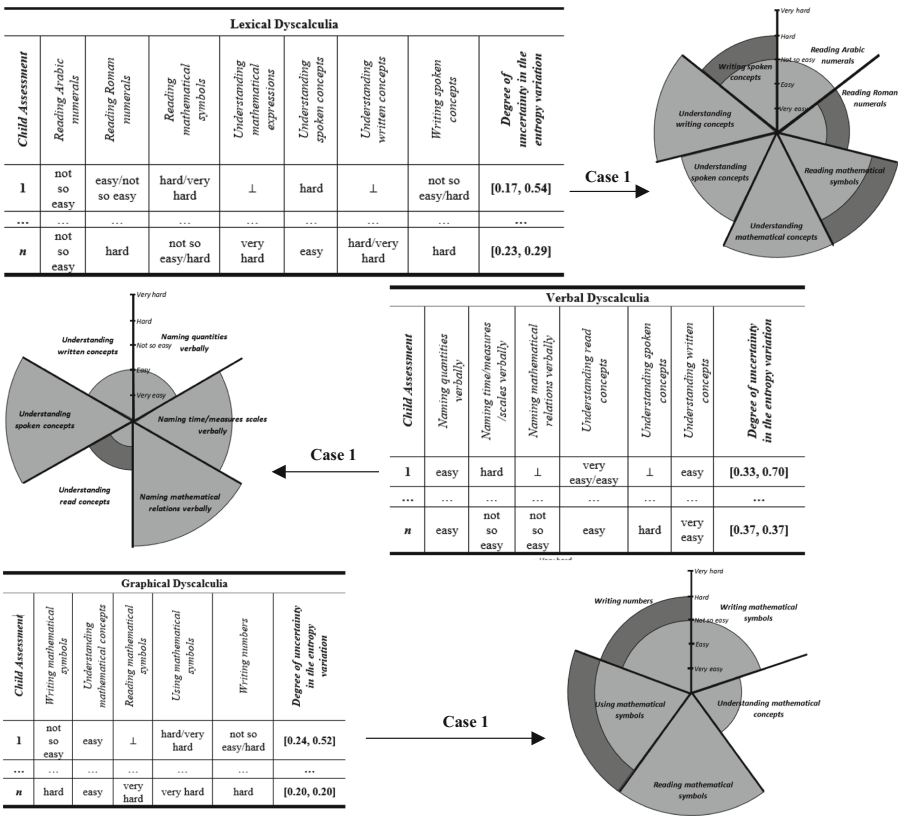

Fig. 1. A knowledge based fragment of an extension of the relational database for the different types of dyscalculia's screening.

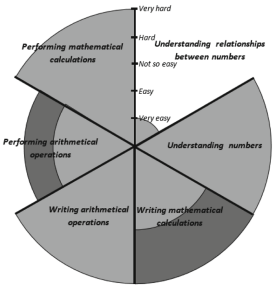

Case 1

Operational Dyscalculia

Child Assessment	*Understanding relationships between numbers*	*Understanding numbers*	*Writing mathematical calculations*	*Writing arithmetical operations*	*Performing mathematical calculations*	*Performing arithmetical operations*	*Degree of uncertainty in the entropy variation*
1	very easy	⊥	not so easy/very hard	⊥	not so easy/hard	very hard	**[0.17, 0.60]**
…	…	…	…	…	…	…	**…**
n	easy	very easy	hard	very hard	not so easy	hard	**[0.37, 0.37]**

Practognostic Dyscalculia

Child Assessment	*Understanding mathematical equations*	*Comparing mathematical equations*	*Performing mathematical equations*	*Using mathematical equations in real situations*	*Calculating measures*	*Measuring objects*	*Calculating amounts*	*Counting money exchange*	*Degree of uncertainty in the entropy variation*
1	easy/ /not so easy	very hard	hard	⊥	very easy/ /easy	hard/ /very hard	⊥	hard	**[0.18, 0.50]**
…	…	…	…	…	…	…	…	…	**…**
n	easy	hard	hard	very hard	easy	very hard	not so easy	very hard	**[0.25, 0.25]**

Case 1

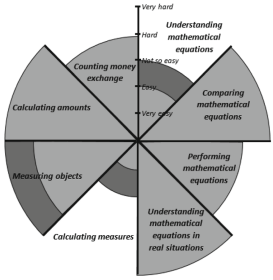

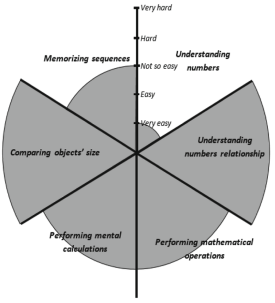

Case 1

Ideagnostic Dyscalculia

Child Assessment	*Understanding numbers*	*Understanding numbers relationship*	*Performing mathematical operations*	*Performing mental calculations*	*Comparing objects ' size*	*Memorizing sequences*	*Degree of uncertainty in the entropy variation*
1	very easy	⊥	hard	hard	very hard	not so easy	**[0.27, 0.43]**
…	…	…	…	…	…	…	
n	easy	not so easy	not so easy	very hard	hard	very hard	**[0.27, 0.27]**

Fig. 1. (*continued*)

Operational Dyscalculia table, a situation that occurs when the educator presents the numbers 5 and 10 to a child, and asks him/her about the relationship between them, expecting an answer that should sustain of the greatness of one be above the other, or even the use of term *double of*.

The qualitative values also used to classify the children difficulties are given in terms of the scale *very easy, easy, not so easy, hard* and *very hard*. These values are posteriorly converted in quantitative ones, according to the method described in the work of Ramalhosa *et al.* [6]. It is now possible to set the *degree of uncertainty in the entropy variation* associated to the diverse types of dyscalculia that may affect each child (Fig. 1). It must also be denoted that the scenario that was workout assume that the distinct types of dyscalculia understudy affect every child.

Therefore, one may have:
Best Scenario's Entropy:

$$entropyBestScenario = 1 - (0.54 \times 0.70 \times 0.52 \times 0.60 \times 0.50 \times 0.43) = 0.975$$

Worst Scenario's Entropy:

$$entropyWorstScenario = 1 - (0.17 \times 0.33 \times 0.24 \times 0.17 \times 0.18 \times 0.27) = 0.99989$$

i.e., the ***entropy*** with respect to the 1st child listed in Table 1 and in terms of the different types of dyscalculia that he/she may present is set in the interval 0.975. . .0.99989. Therefore, the entropy for the children' set will be given in the form:

$$entropyBestScenario = \frac{\sum_{i=1}^{N}\left(1 - \prod_{j=1}^{K} Minimum_{area_j}\right)_i}{N}$$

$$entropyWorstScenario = \frac{\sum_{i=1}^{N}\left(1 - \prod_{j=1}^{K} Maximum_{area_j}\right)_i}{N}$$

where K and N stand, respectively, for the cardinality of the set of the different types of dyscalculia and the cardinality of the children's set.

Table 1. Overall entropy dyscalculia assessment.

Overall Dyscalculia Assessment								
Child assessment	*Lexical dyscalculia*	*Verbal dyscalculia*	*Graphical dyscalculia*	*Operational dyscalculia*	*Practognostic dyscalculia*	*Ideagnostic dyscalculia*	*Entropy Best scenario*	*Entropy Worst scenario*
1	[0.17, 0.54]	[0.33, 0.70]	[0.24, 0.52]	[0.17, 0.60]	[0.18, 0.50]	[0.27, 0.43]	0.975	0.99989
…	…	…	…	…	…	…	…	…
n	[0.23, 0.29]	[0.37, 0.37]	[0.20, 0.20]	[0.37, 0.37]	[0.25, 0.25]	[0.27, 0.27]	0.99946	0.99957

4 Conclusions

LD can affect neurocognitive processes and may manifest as an imperfect ability to listen, speak, read, spell, write, reason, concentrate, solve mathematical problems, or organize information. It may interfere with children reaching their full potential. In particular, the inability to read and comprehend is a major obstacle to learning that may have long-term educational, social, and economic implications. Teaching children with reading difficulties is a challenge for the student, parents, and educators.

Indeed, *LD* has become a major cause of concern. This in itself shows the increased attention paid to improving safety of the most vulnerable people on the society, our children. Thus, considering our previous studies on this subject [7], it becomes essential to accommodate the system with the ability to reason on data that may be unknown, incomplete or even self-contradictory. One's approach not only proved

successful in such a task, but also explain workings on qualitative data. Considering how social factors may put children at risk, we have gone further and yield result on data from a set of immaterial variables that glimpse social perception and how to expose children. Focusing on such attributes, which may be indicative of dissimilarities in the cognition arena, we were able to quantify the degree of disorder, i.e., its level of entropy. Undeniably, it was set the fundamentals of a *Function Machine* based on a *Deep Learning* approach to *Knowledge Representation and Reasoning*. This is extremely valuable as it strengths the systems' confidence, reliability, reduces unpredictability and ensures stability among all the actors. It is now possible to start employing different *AI* based techniques, such as *Artificial Neural Networks* or *Case-Based Reasoning* for the construction of predictive models to handle such situations. Such models will be essential to reveal possible dangerous situations and behaviours, allowing the enhancement of the *children's natural development*.

Acknowledgements. This work has been supported by *COMPETE: POCI-01-0145-FEDER-007043* and *FCT – Fundação para a Ciência e Tecnologia* within the *Project Scope: UID/CEC/00319/2013*.

References

1. Kosc, L.: Developmental dyscalculia. J. Learn. Disabil. **7**(3), 164–177 (1974)
2. Kakas, A.C., Kowalski, R.A., Toni, F.: The role of abduction in logic programming. In: Handbook of Logic in Artificial Intelligence and Logic Programming, pp. 235–324. Oxford University Press Inc., (1998)
3. Pereira, L.M., Anh, H.T.: Evolution prospection. In: Nakamatsu, K., Phillips-Wren, G., Jain, L.C., Howlett, R.J. (eds.) New Advances in Intelligent Decision Technologies: Results of the First KES International Symposium IDT 2009, pp. 51–63. Springer, Heidelberg (2009)
4. Neves, J., Machado, J., Analide, C., Abelha, A., Brito, L.: The halt condition in genetic programming. In: Neves, J., Santos, M.F., Machado, J.M. (eds.) Progress in Artificial Intelligence, pp. 160–169. Springer, Heidelberg (2007)
5. Ferreira Maia Neves, J.C.: A logic interpreter to handle time and negation in logic data bases. In: Proceedings of the 1984 Annual Conference of the ACM on the Fifth Generation Challenge - ACM 1984, pp. 50–54 (1984)
6. Ramalhosa, I., et al.: Diagnosis of Alzheimer disease through an artificial neural network based system. In: Advances in Intelligent Systems and Computing, pp. 162–174. Springer, Cham (2018)
7. Ferraz, F., Costa, A., Alves, V., Vicente, H., Neves, J., Neves, J.: Gaming in dyscalculia: a review on disMAT. In: Advances in Intelligent Systems and Computing, vol. 570, pp. 232–241 (2017)

Enhancing the Development of Interaction Between Authorities in Maritime Surveillance

Ilkka Tikanmäki(✉) and Paresh Rathod

Research, Development and Innovation, Laurea University of Applied Sciences, Vanha maantie 9, 02650 Espoo, Finland
ilkka.tikanmaki@gmail.com, paresh.rathod@laurea.fi

Abstract. Research study clearly indicates, there is a need for cooperation and information sharing between authorities and other Maritime related actors in security and safety issues on the European level. This study deals with European Common Information Sharing Environment (CISE) for the maritime domain. The purpose of this study was to enhance the development of authorities' interaction in maritime surveillance. The European testbed for the maritime Common Information Sharing Environment in the 2020 perspective (EUCISE 2020) and Finnish National Common Information Sharing Environment for Maritime Surveillance (FiNCISE) are also surveyed within this study. The research was conducted as a qualitative study and the research method is principally descriptive. The material of this paper consists mainly of the documents of the FiNCISE and EUCISE2020 projects, unclassified material of the Border Guard, and attending to and observing project meetings. In this research, it was found out, that during the FIMAC cooperation, maritime activities have been developed. As a result, organizations have become streamlined by combining overlapping systems and, thus, each operator is able to focus on its own core competence. Significant economic benefits have been achieved in technical surveillance and communication systems' constructing and maintenance of maritime traffic.

Keywords: Information sharing · Authorities' interaction · Cooperation
Maritime surveillance · Maritime safety
Common Information Sharing Environment

1 Introduction

The cooperation between public authorities consists of common preparation, cooperation, sharing of information and coordination of activities. National cooperation between authorities is one way of maintaining a sufficient level of resources. Another way is cooperation between countries, which provides opportunities for the development of maritime cooperation. Joint Chiefs of Staff- Interorganizational Cooperation report presents and argues that "Commitment to interorganizational cooperation can facilitate cooperation in areas of common interest, promote a common operational picture, and enable sharing of critical information and resources" [1]. The aim of the integrated maritime surveillance is to generate better situational awareness (SA) of activities on the maritime domain, and "Cross-sectorial interoperability for better

K. Ntalianis and A. Croitoru (Eds.): APSAC 2017, LNEE 489, pp. 207–214, 2019.
https://doi.org/10.1007/978-3-319-75605-9_29

Maritime Governance" [2]. According to [3] "The primary objective of the Union's Integrated Maritime Policy ('IMP') is to develop and implement integrated, coordinated coherent, transparent and sustainable decision-making in relation to the oceans, seas, coastal, insular and outermost regions and in the maritime sectors".

The European Border Surveillance System (EUROSUR) will establish an information sharing and cooperation mechanism that will enable Member State authorities to carry out border surveillance activities and the European Agency for the Management of Operational Cooperation at the External Borders of the Member States of the European Union (FRONTEX) to collaborate [4]. The EUROSUR development plan is to create a Roadmap for the Common Information Sharing Environment (CISE) for the EU maritime domain [5].

A Common Information Sharing Environment (CISE) will be developed together with the European Commission and thus, the Member States aim to integrate existing national maritime surveillance systems and networks [6]. Once completed, CISE will provide participating authorities needed access to information, and offering national and EU decision-makers' real-time situational information to process security events affecting their borders and security. There are seven user communities at the European Union level; (1) border control, (2) fisheries, (3) defence, (4) maritime safety and security, (5) marine environment, (6) customs, and (7) general law enforcement.

The research question of this study is: What processes will be needed for the efficient use of common information sharing environments on the European maritime domain?

1.1 Methodology

This study was conducted as a qualitative study and the research method is principally descriptive. This research focuses on the processes needed to efficiently use the Common Information Sharing Environment (CISE), which is being developed within the EU. Sect. 2 of this paper presents some known best practices examples of cooperation between authorities on the maritime domain, Sect. 3 is discussion on user processes and finally Sect. 4 presents the conclusions of this study.

The collected source material for this study is based on participatory observations, conversations, scientific reports, collected articles, and literary reviews. The main strength of case study is this context is the ability to use many different sources of evidence to gain more information on issues than by using a single method [7]. The research problem has been evaluated through a constructive research approach [8]. This study uses an ethnographic method to collect data within phenomena. The most important ethnographic data collection method is the observation of participants, where the researcher is both an observer and a participant, and aims to gather information on human values and practices [9]. The main material of this paper consists of the documents of the EUCISE2020 and FiNCISE projects, unclassified material of the Border Guard, and attending to and observing project meetings. The study included co-operation between experts from different authorities and a researcher with the aim of utilizing practical experience.

2 Cooperation Between Authorities on the Maritime Domain

Interorganizational cooperation enables unity of effort, common objectives and common understanding [1]. [10] describes cooperation between authorities in his formal concept analysis as follows: "Cooperation between authorities is coordinated by the competent authority of cooperation between authorities and other obligated or authorized entities functioning together to achieve the goals of cooperation". The objectives of the co-operation are; (1) to increase situational awareness, (2) to share best practices, (3) to improve interoperability, (4) to avoid overlapping activities, and (5) to achieve focus and synergy by promoting cooperation.

Maritime Surveillance in the Northern Sea Basins (MARSUNO) was a pilot project to make existing monitoring and tracking systems more interoperable between the coastal Member States of Northern Europe. MARSUNO had six work groups that focused on: (1) Integrated Border Management and Law Enforcement IBM-LE), (2) Vessel Traffic Monitoring and Information Systems (VTMIS), (3) Maritime Pollution Response (MPR), (4) Search and Rescue (SAR), (5) Fisheries Control (FC), and (6) Maritime Situational Awareness MSA). The project's objective was to support Common Information Sharing Environment (CISE) by identifying practical solutions to cross-sector and cross-border information sharing between maritime authorities. [11].

2.1 Finnish Maritime Authorities Co-operation

The Finnish Maritime Authorities Co-operation (FIMAC) has been operating cross-sector nationwide cooperation between authorities since 1994. FIMAC parties are the Finnish Transport Agency (FTA), the Finnish Transport Safety Agency (TRAFI), the Finnish Border Guard (FBG) and the Finnish Defence Forces (NAVY) [12]. Maritime surveillance sensor information is shared by TRAFI, FBG, NAVY, FTA and other relevant authorities as well as international actors. FIMAC cooperation goals are to increase maritime safety, to the development of information management and information exchange, international influence, and joint use of capabilities. Formatting of the national maritime situational picture (NMSP) and distributing it to cooperation partners is a significant mission of FIMAC [13].

Over 20 years of continued cooperation and efficiency in maritime activities have achieved savings merely in technical surveillance data communication systems investments, and maintenance expenditure [14]. In addition, each of FIMAC authority's specialists and equipment could be used for the common benefit. FIMAC actors have, in several aspects, implemented joint maritime surveillance, search and rescue (SAR), and maritime traffic control system with sensors, data transfer arrangement and applications.

2.2 Common Information Sharing Environment

A Common Information Sharing Environment (CISE), which the European Commission is currently working to develop, together with the EU and EEA countries, will unite the different control systems and networks. With CISE the different authorities are going to get access to all the information necessary for maritime surveillance missions.

The European Council adopted union-wide maritime security strategy on June 2014 [3]. One of the most important strategic goals is to create the integrated maritime policy for the EU to improve the exchange of information between the supervisory authorities of the sea. Further CISE development should direct to user demand and support operational user requirements [15].

The European Cooperation Project (Cooperation Project Maritime Surveillance, CoopP) aim was paving the way for smooth data transmission and easy access between public authorities. CoopP aimed to define the future Common Information Sharing Environment (CISE) for European maritime surveillance [15].

2.3 EUCISE 2020

A European testbed for the maritime Common Information Sharing Environment in the 2020 perspective (EUCISE 2020) addresses to steps forward along the accomplishment of the European roadmap for Common Information Sharing and Distributed Systems and Services Environment [16]. The project attains the widest possible experimental environment of innovative and collaborative services and processes between European maritime institutions. It also takes as reference a broad spectrum of factors in the field of European Integrated Maritime Surveillance, arising from the European legal framework, as well as from studies, pilot and related R&D projects [17].

The integrated maritime surveillance's aim is to generate situational awareness (SA) activities at sea areas. CISE is a set of specifications for interoperability and it is based on the work of pilot projects Blue Maritime Surveillance System Mediterranean (BluemassMed), Maritime Surveillance in the Northern Sea Basin (MARSUNO) and of the Cooperation Project (CoopP). [15, 18].

EUCISE will reuse building blocks of Electronic Simple European Networked Services (eSens) and other previous projects that have developed European Digital Market through innovative ICT solutions [19]. One objective for EUCISE is to make a test-bed network of multiple nodes connected to participating authorities for cross-sector information services and exchange of data [2].

2.4 FiNCISE

FIMAC -authorities and the Finnish Environment Institute (SYKE) launched a project, Study to promote Finnish National Common Information Sharing Environment for Maritime Surveillance (FiNCISE). The project aims to develop surveillance information systems in the Finnish sea areas. The project goals are to obtain developed systems to be compatible for the future maritime common information sharing environment (CISE) and to allow the exchange of information of national surveillance systems with other authorities through interfaces. FiNCISE supports directly the implementation of the European Maritime Security Strategy and its action plan [20]. The general objective of the FiNCISE project is to improve the interoperability of Finnish maritime surveillance systems nationally across sectors and cross-borders within EU. The focus is on system-to-system information exchange. One of the aims of the project is to develop a national enterprise architecture description related to the production and sharing of maritime surveillance information.

In addition, studies are carried out by developing data catalogue of existing national information service interfaces and data models. Comparing them to the CISE data model and defining the necessary changes will be studied as well. The exchange of national maritime information will be tested from a technical point of view with information service interfaces and data models at the national level and towards the CISE. FiNCISE focuses on designing of the information exchange and requirement development, as well as, takes into account current and future requirement [21].

The objectives of the FiNCISE project are (1) coordination of the Finnish maritime surveillance information exchange systems with the future CISE information exchange environment, and (2) to permit the exchange of information nationally through surveillance systems interfaces (FiNCISE, 2015). The project consists of four work packages (WP) which are: WP1 Project Management, WP2 Architecture descriptions, WP3 Interoperability and compatibility considerations, and WP4 Testing and demonstration.

Finland has a long history of sharing operatively maritime information among multiple governmental actors. As a result of this development, many systems are already implemented and used operationally nowadays. Full-scale system-to-system integration has not been implemented. However, FiNCISE project will lead actors to an enhanced level of interoperability. The project will develop primarily existing systems and information-sharing channels. The achievements of the project will be taken into action and the stakeholders will be benefitting the results in a sustainable way after the project has been successfully implemented [21].

The main Finnish national authorities with tasks or responsibilities for maritime safety functions are Border Guard, Defence Forces, Transport Safety Agency, Transport Agency, Finnish Environment Institute, Police, and Customs. At the legislative level, maritime security functions are provided for one authority's monitoring and implementing responsibility. However, particular functions have given to several authorities' responsibility while some functions are set to certain authority's control and entrusted to the other authority as participate in concept [22].

3 Discussion

First it is worth noting that cooperation between maritime authorities is a model that could be applied to the other areas of government. Yet, in many countries, national legislation does not allow the authorities to cooperate. There is a concern that the distributed information could end up to an operator, which is not desired to receive such information. The problem was seen particularly in the collection, analysis and lack of information sharing, which can be used in creating an effective maritime picture for the support of operational decision-making [9].

The relevant information related to the decision-making is collected from different sources. This requires the exchange of information between different parties. The results of [23] research show that 'trust' can be said to be the main issue in multi-government cooperation. As [23] state: "The exchange of information is always a matter of trust". According to [24], development of the cooperation activity requires a particular trust, continuity and shared vision of the rationality of action.

Cooperation must be part of the everyday activities and not only be based on cooperation exercises or treatment of exceptional situations. Authorities' activities will be intensified in the future. One of the most sensible ways is to find more effective interfaces to work and to combine the resources of those concerned [25].

4 Conclusions

The purpose of this study was to enhance the development of authorities' interaction in maritime surveillance, safety and security. The other aim of this study was to find out the good practices observed during the projects and to share them with other parties. In this research, it was found out, that during the FIMAC cooperation, maritime activities have been developed. As a result, organizations have become streamlined by combining overlapping systems and, thus, each operator is able to focus on its own core competence. Significant economic benefits have been achieved in technical surveillance and communication systems' constructing and maintenance of maritime traffic.

It is difficult to concretize all the savings brought by this operating model. The value of the common situational awareness (CSA) and trust cannot be measured by money; its high value appears at the level of activity almost every day. Close cooperation has facilitated negotiations on difficult issues even other than the FIMAC-operating matters. FIMAC cooperation model began as technical cooperation and is today a low-threshold approach that ensures the functioning of operational cooperation. Cooperation has become routine and a part of everyday life.

Therefore, the decision-makers should consider approving agreements that are needed to ensure a coordinated implementation of the information sharing. Authorities need to continue interconnecting systems, focusing on cross-border and cross-sector information services. Distributed architecture enables this kind of stakeholders' operating model.

International cooperation requires the creation of unified operating models. By harmonizing the practices and unifying operating models, national and international co-operation comes more efficiency; shipping will be safer and systems become more efficient usage. Establishing trust among different CISE participants, CISE system can be improved by building a security policy by defining the minimal safety requirements that all CISE users and communities must comply with. The authorities stressed the main obstacle to the information exchange is differences in mind-sets. Fundamental aspects of cross-sector and cross-border information exchange are to amend the way of thinking and to build trust between authorities.

CISE is important for the European Union and its security. EUCISE2020 project must take into account not only the project, but as a stepping stone for a common European data exchange environment, which will give added value to security and safety. The work needs to be transparent and it also has to be clearly led into because lack of information sharing between actors causes confusion. Maritime Security Strategy and the European Common Maritime Policy will provide a solid basis for this kind of work.

Acknowledgments. This project has received funding from the European Union's EMFF programme under grant agreement No EASME/EMFF/2014/1.2.1.2/5/SI2.715264. Study to promote Finnish National Common Information Sharing Environment for Maritime Surveillance (FiN-CISE).

References

1. Joint Chiefs of Staff: Interorganizational Cooperation. Joint Publication, 3 August 2016. http://www.dtic.mil/doctrine/new_pubs/jp3_08.pdf
2. EUCISE: EUCISE 2020 project meeting: EUCISE2020, European testbed for the maritime Common Information Sharing Environment in the 2020 perspective (2015)
3. European Commission: COM(2010) 584 Final. Communication from the Commission to the Council and the European Parliament: on a Draft Roadmap towards establishing the Common Information Sharing Environment for the surveillance of the EU maritime domain (2010)
4. Laitinen, I.: Key Note as Executive Director of FRONTEX. "Role of Border Control in the new EU security architecture and an update on Frontex activities", Situation Scope Seminar presentation, Äkäslompolo Finland, 11 March 2011
5. European Commission: Directorate-General, Maritime Affairs and Fisheries, The development of the CISE for the surveillance of the EU maritime domain and the related Impact Assessment. Part 2: Combined Analysis (2017). http://www.cowi.com
6. European Commission: Security in 2020: Meeting the challenge. Publications Office of the European Union, Luxembourg (2014). ISBN 978-92-79-43762-5
7. Yin, R.: Case Study Research: Design and Methods. SAGE Publications, London (2009)
8. Lukka, K.: Constructive research: nature, process and evaluation. Transl. Konstruktiivinen tutkimusote: luonne, prosessi ja arviointi. In: Rolin, K., Kakkuri-Knuuttila, M-L., Henttonen, E. (eds.). Applied Social Science and Philosophy, pp. 111–133. Hakapaino Oy, Helsinki (2006)
9. Vuorisalo, V.: Developing Future Crisis Management - An Ethnographic Journey into the Community and Practice of Multinational Experimentation. University of Tampere, Tampereen Yliopistopaino Oy – Juvenes Print: Tampere (2012)
10. Valtonen, V.: Collaboration of Security Actors – an Operational-Tactical Perspective, Transl. Turvallisuustoimijoiden yhteistyö – operatiivis- taktisesta näkökulmasta. Dissertation. The National Defence University, Edita Prima Oy, Helsinki (2010)
11. European Commission: COM (2012) 491 final. Report from the Commission to the European Parliament, the Council, the European Economic and social committee and the Committee of the regions; Progress of the EU's Integrated Maritime Policy. Brussels, 11 September 2012
12. Finnish Maritime Authorities (FIMAC): Strategy 2013 (2013)
13. FiNCISE Monitoring visit. Helsinki, 12 September 2016
14. Finnish Defence Forces: Maritime activities are developed through co-operation, Transl. "Merellisiä toimintoja kehitetään yhteistyöllä" (2014). http://www.mil.fi

15. Finnish Border Guard: Test Project on cooperation in executing various maritime functionalities at sub-regional or sea-basin level in the field of integrated maritime surveillance (CoopP). Final Report, March 2014. Elan Graphic, Paris (2014). ISBN 978-952-491-901-2
16. Council of the European Union: Council conclusions on integration of Maritime Surveillance: Towards the integration of maritime surveillance: A common information sharing environment for the EU maritime domain. 3092nd General Affairs Council meeting (2011)
17. European Commission: Communication from the Commission to the European Parliament and the Council, COM (2014) 451 final. Better situational awareness by enhanced cooperation across maritime surveillance authorities: next steps within the Common Information Sharing Environment for the EU maritime domain (2014)
18. BlueMassMed: Final Report: Cross-border and Cross-Sectoral Maritime Information Sharing for a control of activities at sea (2012). http://www.statewatch.org/news/2014/jul/eu-2012-bluemassmed-final-report.pdf
19. e-SENS: e-SENS white paper; Short, Medium and Long-term Governance Models Scenario. Electronic Simple European Services (2016). http://www.esens.eu
20. European Union: Maritime Security Strategy, 11205/14 (2014)
21. Finnish Border Guard: FiNCISE application form to European Commission, European Agency for Small and Medium Enterprises (EASME) (2015)
22. Osola, K.: An Integrated Maritime Policy for the European Union - Horizontal maritime security missions, Transl. Euroopan Unionin yhdennetty meripolitiikka – monialaiset merelliset turvallisuustehtävät. Pro Gradu, The National Defence University (2012)
23. Rajamäki, J., Knuuttila, J.: Cyber security and trust: tools for multi-agency cooperation between public authorities. In: 7th International Joint Conference on Knowledge Discovery, Knowledge Engineering and Knowledge Management (KMIS 2015), pp. 397–404 (2015)
24. Räsänen, T.: Complexity theoretical viewpoint of cooperation between the authorities, Transl. Kompleksisuusteoreettinen näkökulma viranomaisten yhteistoimintaan. Pro Gradu. National Defence University (2011)
25. Anttonen, J.: Building a common security. The possible synergies of developing the police and officer professions in tandem, Transl. Yhteistä turvallisuutta rakentaen - Poliisi- ja upseeriprofessioiden yhteiskehittelyn mahdollisuuksista. The National Defence University. Series 1: Research Publications No. 6. Doctoral Dissertation. Juvenes Print: Tampere (2016)

System Science

Characterisation of the Vibration of an Ultrasonic Transducer for Guided Waves Applications

Marco Zennaro[1(✉)], Alex Haig[2], Dan J. O'Boy[3], and Stephen J. Walsh[3]

[1] NSRIC, Cambridge CB21 6AL, UK
M.Zennaro@lboro.ac.uk
[2] TWI, Cambridge CB21 6AL, UK
[3] AACME, Loughborough University, Loughborough LE11 3TU, UK

Abstract. Dry coupled thickness-shear piezoelectric transducers are typically used to excite guided waves in plate-like or tubular structures in the frequency range of 20–150 kHz. The dispersive behavior of guided waves and the excitation of unwanted modes require a precise tuning of the excitation frequency to facilitate effective inspection. A natural frequency analysis of a typical piezoelectric transducer has been performed to identify the shape of vibration in the frequency range indicated. Moreover, an experimental analysis of the vibration of the piezoelectric element through a scanning laser Doppler Vibrometer has been conducted. The numerical and experimental results agree in indicating no longitudinal mode is present up to 94 kHz. Experiment also have shown that the higher the frequency the higher the longitudinal component of displacement.

Keywords: Piezoelectric transducers · Guided waves · Laser vibrometer
Natural frequency analysis

1 Introduction

1.1 Industrial Motivation of the Project

In the last twenty years a method known as ultrasonic guided wave testing has found its area of application within the field of non-destructive testing [1], i.e. the transmission of ultrasonic guided waves over relatively long distances (often tens of meters) in objects whose geometry form a waveguide. The ultrasonic guided waves travel along a fixed boundary. Therefore the wavelength of the guided wave must be comparable to the thickness of the structure. It is typical to make use of frequencies in the range of 20 to 150 kHz, where the generation of guided waves is most commonly obtained through piezoelectric coupling. In this study the focus will be on the piezoelectric transducer and its characterization in terms of vibration, a first step toward a long term goal, which is the miniaturization of the transducers. Section 1.2 has a brief background, the numerical results of a finite element prediction are provided in Sect. 2, with corresponding experiment measurements from a laser vibrometer in Sect. 3.

K. Ntalianis and A. Croitoru (Eds.): APSAC 2017, LNEE 489, pp. 217–222, 2019.
https://doi.org/10.1007/978-3-319-75605-9_30

1.2 Guided Waves and Piezoelectric Transducers

Alleyne and Cawley were the first to use dry-coupled thickness-shear transducers to generate guided waves [1]. The mechanical resonance of these devices for guided wave applications was later studied by Engineer [2], who proved experimentally how changing the clampling force on the dry-coupled transducers shifts the resonance of the transducers. Subsequently Marques used thickness-shear transducers in plate-like structures. He showed that optimal ultrasonic output indicated by his simulations could not be obtained due to the relatively large size of the transducers limiting the array layout [3], pointing out the necessity of a miniaturization of the transducers.

In regards to the miniaturization Comyn and Tavernor showed that there are minimum aspect rations of length-thickness (20:1) and length-width (6:1) to be kept to avoid mode coupling in these types of transducers. [4]. Also Pardo et al. proved experimentally and numerically the presence of mode coupling in thickness shear piezoelectric transducers [5]. Thus a careful characterization of the transducer is required. The numerical and experimental results presented in this publication regard just the piezoelectric material, shown in Fig. 1(b).

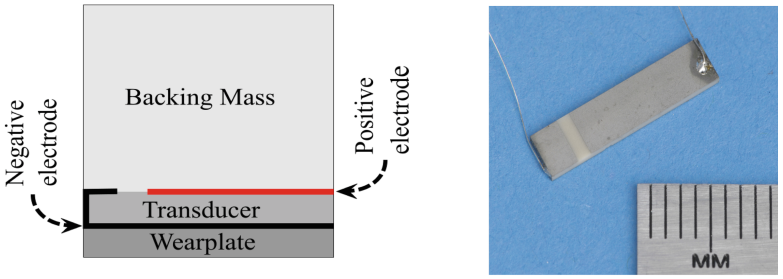

(a) Cross-section of the assembly (b) Piezoelectric transducer

Fig. 1. Cross-section of the assembly (left) and picture of the piezoelectric transducer (right)

2 Numerical Modelling

2.1 Methodology

The use of finite element analysis (FEA) to solve thickness shear transducers problems is well documented in the literature [5]. In this study the natural frequencies and mode shapes of a piezoelectric transducer are predicted to understand in which frequency region the transducer should be tuned; since it is desired that the thickness-shear transducer should only create in-plane motion, the frequency must be tuned where the out of plane component is low.

The FEA software COMSOL was employed to model both the natural frequencies of the piezoelectric element and the piezoelectric attached to a wearplate, consisting of 15167 elements and 30514 of free tetrahedral type respectively, with free-free boundary conditions. The analysis in COMSOL produces eigenvalues and eigenvectors showing the natural frequencies and corresponding mode shapes in the frequency range

20–150 kHz. Note that the material is polarized along the longitudinal axis [6]. The material properties of the thickness-shear transducer and the wearplate are provided by the manufacturer, PI Ceramic.

2.2 Numerical Results

It is well known that various eigenmodes can arise in the calculation of the eigenfrequencies of a structure. Although not all of them will be significantly excited in a forced excitation, the natural frequency analysis is a first step to identify the potential natural motion of the structure. For example, for an element polarized along the horizontal axis, the application of an alternating voltage would lead to a symmetric stress pattern along that axis hence the torsional mode would be unlikely to be excited at high amplitude.

Figure 2 shows the mode shapes corresponding to the first two natural frequencies. The analytical indication [7] and the numerical calculation show that no thickness-shear resonance is to be found in the range of operation. However, as suggested by [2] and by the comparison of natural frequencies of Table 1 a shift of natural frequencies is likely to happen when the whole assembly is considered.

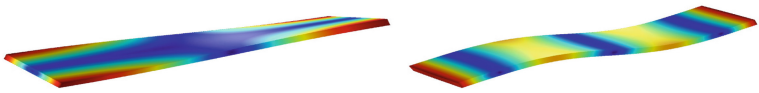

(a) First torsional mode n=1 (b) First flexural mode, n=2

Fig. 2. First two eigenshapes of the piezoelectric element calculated with Comsol

3 Experimental Analysis

In order to have confidence in the finite element predictions, and the subsequent response shapes, an experimental validation test was performed, to obtain the response frequencies and the amplitudes of a PZT strip when an alternating voltage is applied.

3.1 Methodology

Measuring the velocity of the active surface of a transducer often requires the use of a non-contact technique to avoid any interaction between the measuring equipment and the transducer, especially for small, lightweight structures such as this PZT element. One of the most successfully applied techniques is Laser Doppler Vibrometer (LDV), which is capable of detecting the Doppler frequency shift of an infrared light back scattered from the surface of a specimen in motion.

The Laser Vibrometer PSV-400-3D-M used in this experiment is composed of three scanning heads each capable of measuring one component of surface velocity, as seen in Fig. 3. The velocity is measured over a grid of points defined on the upper surface of the piezoelectric element. The measurement over the grid is covered by

Table 1. Table of first four natural frequencies

Frequency order	Frequency of piezo element [Hz]	Wearplate added [Hz]
n = 1	20375, first torsional	25224, first flexural
n = 2	20619, first flexural	62964, first torsional
n = 3	38987, first shear horizontal	67897, second flexural
n = 4	40242, second flexural	84111, first shear horizontal

repeated measurements where the excitation was performed for the measurement of each point separately. A Teletest Focus system was used as a waveform generator to drive the transducer into vibration and to trigger the vibrometry measurement [8].

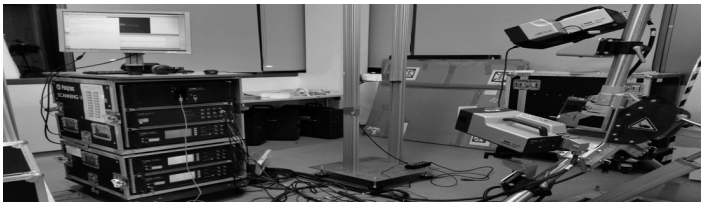

Fig. 3. Picture of the experimental setup

To cover a relatively wide excitation bandwidth, a chirp signal was used as the input signal for the transducer, i.e. a sinusoidal signal with a linear increase in frequency over time (between 20–150 kHz). The amplitude of the voltage was 200 Vpp, spanning for 500 microseconds, as shown in Fig. 4. It is well known that in the real application there is no transducer in free air, that is every transducer must be attached to the surface of the object being inspected. However, since it is well known that any mechanical coupling changes the response of the ultrasonic transducer [2], the transducer was attached to polystyrene foam.

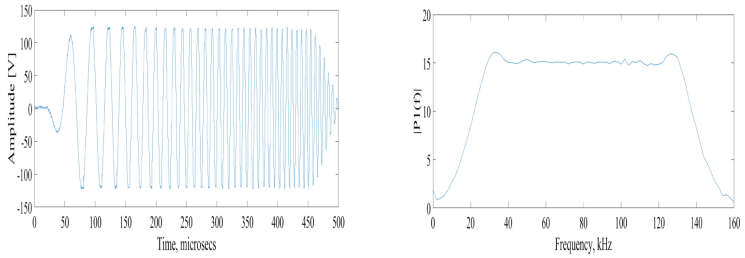

(a) Amplitude of the signal (b) Fast Fourier Transform

Fig. 4. Plot of the chirp signal and its Fast Fourier Transform

3.2 Experimental Results

The surface displacement plotted against excitation frequency is shown in Fig. 5. Interestingly it is shown that in regards to frequencies up to 60 kHz the higher component of motion is the z-component, which is the undesired out-of-plane component. For the higher frequencies the longitudinal component (the x-component) becomes higher. However this component is still undesirable because the excitation of the surface results is not uniform.

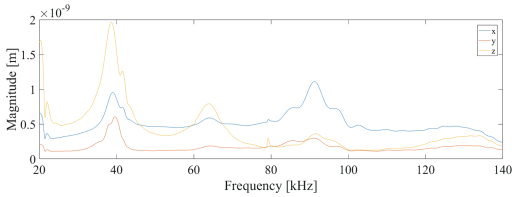

Fig. 5. Plot of the three components of displacement as a function of frequency

This trend of frequencies is confirmed by the natural frequency analysis: as a matter of fact the first longitudinal resonance does not appear until 91 kHz.

Thus, the modes actually excited in the range of applications represent modes which need to be avoided. As far as the mode shape is concerned, in Fig. 6 it is shown as an example the shapes at the resonance frequency for 22 kHz and 39 kHz. The first excited resonance is the first flexural resonance and the second one corresponds to the second flexural resonance. These results confirm the validity of the numerical simulations.

(a) First mode, 22 kHz (b) Second mode, 39 kHz

Fig. 6. Plot of the experimental shape of the upper surface

4 Conclusion

The numerical prediction has been confirmed experimentally by the analysis with the PSV-400-3D-M vibrometer. Moreover, the presence of the wearplate shifts the position of the natural frequencies. Not all the modes calculated numerically appear in the experiments. Therefore there is a matter of mode excitability which needs to be carefully investigated. Since the electrical load is uniform across the width, it is expected that no torsional and shear horizontal modes are excited. However, as suggested in [4, 5], this is not always the case: since it has been clearly shown how the geometry plays an important role in the mode excitation, the influence of geometry on the mode excitability needs to be investigated through a parametric study. Furthermore,

the experimental analysis will be compared with a numerically computed forced excitation model, for all the elements of the assembly. After that, since the coupling with a waveguide is likely to shift to the resonance of the transducers [2], the influence of the waveguide on the performance of the piezoelectric transducer will be analyzed.

Acknowledgments. The support of Lloyd's Registered Foundation and Loughborough University for this publication is fully acknowledged.

References

1. Lowe, M.J.S., Alleyne, D.N., Cawley, P.: The excitation of Lamb waves in pipes using dry-coupled piezoelectric transducers. J. Nondestruct. Eval. **5**(1), 11 (1996)
2. Engineer, B.A.: The mechanical and resonant behaviour of a dry coupled thickness-shear PZT transducer used for guided wave testing in pipe line. Diss. Brunel University (2013)
3. Marques, H.R.: Omnidirectional and Unidirectional SH0 Mode Transducer Arrays for Guided Wave Evaluation of Plate-Like Structures. Brunel University, Diss (2016)
4. Comyn, T., Tavernor, A.W.: Aspect ratio dependence of d15 measurements in Motorola 3203 material. J. Eur. Ceram. Soc. **21**, 9–12 (2001)
5. Pardo L., Garcia, A., de Espinosa, F.M., Breøl, K.: Shear resonance mode decoupling to determine the characteristic matrix of piezoceramics for 3-D modeling. IEEE Trans. Ultrason. Ferr. **58**(3), 646–657 (2011)
6. Benjeddou, A., Trindade, M. A., Ohayon, R., A: A unified beam finite element model for extension and shear piezoelectric actuation mechanisms. J. Intel. Mat. Syst. Str. **8**(12), 1012–1025 (1997)
7. Aurelle, N., Roche, D., Richards, C., Gonnard, P.: Sample aspect ratio influence on the shear coefficients measurements of a piezoelectric bar. In: Proceedings of the Ninth IEEE International Symposium on Applications of Ferroelectrics, 1995, ISAF 1994, pp. 162–165 (1991)
8. Mudge, P.J.: Field application of the Teletest long-range ultrasonic testing technique. Insight (2001)

Asymptotic Stability of Partial Difference Equations Systems with Singular Matrix

Guido Izuta(✉)

Department of Social and Information Science, Yonezawa Women's Junior College, 6-15-1 Toori Machi, Yonezawa, Yamagata 992-0025, Japan
izuta@yone.ac.jp

Abstract. This paper is concerned with the asymptotic stability of partial difference equations representing 2-d (two dimensional) discrete systems that appear in practical fields as electrical engineering, automation and control, and computer and communication, among others. The partial difference equations are expressed in the state space description format and its composing matrix is singular. The aim is to establish the conditions under which the system is asymptotically stable. In order to accomplish it, the system is first augmented by means of the orthonormal matrix, then the Lagrange method for solving partial difference equations is considered to examine the stability of the overall system. Finally, a numerical example is presented to show how to apply the procedure suggested here.

Keywords: 2-d discrete systems · Asymptotic stability · Row full rank system Lagrange method · Diagonalization

1 Introduction

Modeling engineering systems with partial difference equations dates back to the 1960's [1], and since then a great deal of research has been carried out so far on the grounds of basically two types of state space descriptions - FM model [2] and Roesser model [3] - which are equivalent to each other.

As far as the investigations on the stability of this kind of systems are concerned, many approaches have been adopted with the main frameworks being as briefly described hereafter. Indeed, details related to works on z-transform can be found in [4] and references therein in, whereas on linear matrix inequalities in [5], on operator calculus in [6] and on transformation based methods in [7]. Yet, in recent years the Lagrange method [7] has been used to explore the stability and control design issues of 2-d systems [8–10], and it has been a useful framework to make it explicit the relationships between stability and eigenvalues of the matrix defining the system of partial difference equations.

Motivated by these developments, this work aims to extend previous results on the stability analysis of 2-d systems on the basis of the Lagrange method [8–10], in the sense that the system is here expressed by a with row full rank matrix expressing the set of partial difference equations. To accomplish it, the system is augmented by means of

K. Ntalianis and A. Croitoru (Eds.): APSAC 2017, LNEE 489, pp. 223–229, 2019.
https://doi.org/10.1007/978-3-319-75605-9_31

the orthonormal matrix, then the Lagrange method is used to establish the conditions under which the system is asymptotically stable.

Finally, this paper is organized as follows. The concepts and definitions used in the sequel as well as the problem formulation are provided in Sect. 2. The mathematical tools need to prove the findings of this paper are gathered in Sect. 3, whereas the results are given in Sect. 4. Section 5 presents a numerical example to show how to carry out the stability analysis and establish an explicit solution when it exists; and Sect. 6 yields some final comments.

2 Problem Formulation

The kind of systems of partial difference equations considered here is given next.

Definition 1. Let the systems be given by the following set of partial difference equations with coefficients over $\Re$, and indices over $\mathbb{Z}$.

$$\begin{bmatrix} x_1(i+1,j) \\ \vdots \\ x_k(i+1,j) \\ x_{k+1}(i,j+1) \\ \vdots \\ x_n(i,j+1) \end{bmatrix} = \overbrace{\begin{bmatrix} a_{11} & \cdots & a_{1n} \\ \vdots & & \vdots \\ a_{n1} & \cdots & a_{nn} \end{bmatrix}}^{\mathrm{M}_{n\times n}} \begin{bmatrix} x_1(i,j) \\ \vdots \\ x_k(i,j) \\ x_{k+1}(i,j) \\ \vdots \\ x_n(i,j) \end{bmatrix} \tag{1}$$

$$\text{and } \operatorname{rank}(\mathrm{M}_{n\times n}) = l, \quad 1 \le l < n,$$

in which the over-braced $\mathrm{M}_{n\times n}$ is a short notation for the matrix it encloses with n meaning the dimensions of matrix.

Next, let the concept of stability adopted hereafter be given as next.

Definition 2. System (1) is asymptotically stable if the following conditions are fulfilled for every set of solutions provided by x(i, j)'s.

$$\lim_{(i+j)\to\infty} |x_*(i,j)| \to 0, \quad \forall * = 1, \cdots, n. \tag{2}$$

Moreover, the frame of reference for the solutions are the so-called Lagrange solutions, which in this work are assumed to be as follows:

Definition 3. Let the non-null Lagrange solutions to (1) be

$$x(i,j) = \textstyle\sum_{k=1}^{l} \mathrm{I}_k \alpha_k^i \beta_k^j, \tag{3}$$

in which I's are the initial values and α's and β's and are non-null real numbers.

Taking these definitions into account, the problem to be solved in this paper reads:

Problem 1. To establish conditions for the existence of asymptotically stable Lagrange solutions to (1).

3 Some Mathematical Facts

This section gives the mathematical framework and gathers the facts needed to prove the results of this paper. Indeed, to begin with, note that basic linear algebra of matrices allows us to rearrange the rows and columns so that the system (1) can be rewritten as follows:

$$\begin{bmatrix} x_1(i+1,j+1) \\ x_2(i+1,j+1) \end{bmatrix} = \overbrace{\begin{bmatrix} \mathbb{A}_{l\times l} & \mathbb{B}_{l\times(n-l)} \\ \mathbb{C}_{(n-l)\times l} & \mathbb{C}\mathbb{A}^{-1}\mathbb{B} \end{bmatrix}}^{\bar{\mathbb{A}}} \begin{bmatrix} x_1(i,j) \\ x_2(i,j) \end{bmatrix} \tag{4}$$

in which

$$x_1(i+1,j+1) \stackrel{\text{def}}{=} \begin{bmatrix} x_1(i+1,j) \\ \vdots \\ x_p(i+1,j) \\ x_{(p+1)}(i,j+1) \\ \vdots \\ x_l(i,j+1) \end{bmatrix}, \quad x_1(i,j) \stackrel{\text{def}}{=} \begin{bmatrix} x_1(i,j) \\ \vdots \\ x_p(i,j) \\ x_{(p+1)}(i,j) \\ \vdots \\ x_l(i,j) \end{bmatrix},$$

$$x_2(i+1,j+1) \stackrel{\text{def}}{=} \begin{bmatrix} x_{(l+1)}(i+1,j) \\ \vdots \\ x_{\diamondsuit}(i+1,j) \\ x_{(\diamondsuit+1)}(i,j+1) \\ \vdots \\ x_n(i,j+1) \end{bmatrix}, \quad x_2(i,j) \stackrel{\text{def}}{=} \begin{bmatrix} x_{(l+1)}(i,j) \\ \vdots \\ x_{\diamondsuit}(i,j) \\ x_{(\diamondsuit+1)}(i,j) \\ \vdots \\ x_n(i,j) \end{bmatrix},$$

$$\diamondsuit \stackrel{\text{def}}{=} l+n-k-p$$

and $\mathbb{A}_{l\times l}$ is a non-singular matrix block.

Remark 1. For the sake of clarity and without loss of generality, the vectors $x_i(i,j)$'s and $x_i(i+1,j+1)$'s were here written orderly as in (4) from x_1 to x_l then $x_{(l+1)}$ to x_n. However, the computations do not always yield a vector consisting of two separate blocks as the one defined by x_1 to x_p and $x_{(p+1)}$ to x_l.

Now, the theory of generalized inverse of matrices [11] states that the matrix

$$\mathbb{G} = \begin{bmatrix} \mathbb{A}_{l\times l}^{-1} & 0_{l\times(n-l)} \\ 0_{(n-l)\times l} & 0_{(n-l)\times(n-l)} \end{bmatrix} \tag{5}$$

is an inverse matrix of $\bar{\mathbb{A}}$, and that the set of partial difference equations in (5) can be solved if and only if

$$\bar{\mathbb{A}}\mathbb{G}\begin{bmatrix} x_1(i+1,j+1) \\ x_2(i+1,j+1) \end{bmatrix} = \begin{bmatrix} x_1(i+1,j+1) \\ x_2(i+1,j+1) \end{bmatrix} \tag{6}$$

is satisfied. In addition, (6) leads to

$$x_2(i+1,j+1) = \mathbb{C}\mathbb{A}^{-1}x_1(i+1,j+1). \tag{7}$$

And since a particular solution is provided by

$$\mathbb{G}\begin{bmatrix} x_1(i+1,j+1) \\ x_2(i+1,j+1) \end{bmatrix} = \begin{bmatrix} x_1(i,j) \\ x_2(i,j) \end{bmatrix}, \tag{8}$$

thus (7) can be established by means of

$$x_1(i+1,j+1) = \mathbb{A}x_1(i,j). \tag{9}$$

Remark 2. Note that matrix theory [12] also allows to say that the general solution has the form of

$$\begin{bmatrix} x_1(i,j) \\ x_2(i,j) \end{bmatrix} = \mathbb{G}\begin{bmatrix} x_1(i+1,j+1) \\ x_2(i+1,j+1) \end{bmatrix} + \left(\mathbb{I} - \mathbb{G}\bar{\mathbb{A}}\right)\begin{bmatrix} v_1(i,j) \\ v_2(i,j) \end{bmatrix} \tag{10}$$

for some $v_1(i,j)$ and $v_2(i,j)$.

4 Results

The main results of this investigation are gathered in the following theorem.

Theorem 1. Let the system be given by (4) and assume that each different eigenvalue of matrix $\mathbb{A}$ is such that their algebraic and geometric multiplicities are equal. Then system is asymptotically stable in the sense of Lagrange method of solving partial difference equations as provided by (4), if the eigenvalues of $\mathbb{A}$ are all non-null numbers with absolute values less than unit for given $\alpha_*\,(* = 1,\cdots,p)$ and $\beta_{\#}\,(\# = p+1,\cdots,l)$ such that $0 \neq |\alpha_*| < 1$ and $0 \neq |\beta_{\#}| < 1$.

Proof 1. Note that it suffices to consider only the particular solution given by (9). Now, take the matrix $\mathbb{T}$ composed by the eigenvectors of $\mathbb{A}$ to carry out the vector transformation defined by

$$\mathbf{z}(i,j) = \mathbb{T}^{-1}\mathbf{x}(i,j) \tag{11}$$

Thus, substitution of (11) into (9) leads to

$$\mathbf{z}(i+1,j+1) = \overbrace{\mathbb{T}^{-1}\mathbb{A}\mathbb{T}}^{\mathbb{D}}\mathbf{z}(i,j). \tag{12}$$

Since, by hypothesis, the algebraic and geometric multiplicities of the eigenvalues are equal, $\mathbb{D}$ is a diagonal matrix composed by the eigenvalues of $\mathbb{A}$, namely $\mathbb{D} = diag\{\lambda_1, \cdots, \lambda_l\}$

Thus, the general expression for the entries of (12) is either

$$\mathbf{z}(i+1,j) = \lambda\mathbf{z}(i,j), \quad or \quad \bar{\mathbf{z}}(i,j+1) = \bar{\lambda}\bar{\mathbf{z}}(i,j)\,, \tag{13}$$

in which λ and $\bar{\lambda}$ are the eigenvalues of $\mathbb{A}$.

Now, let the Lagrange solution candidates to equations in (13) be

$$\mathbf{z}(i,j) = K\alpha^i\beta^j, \quad or \quad \bar{\mathbf{z}}(i,j) = \bar{K}\bar{\alpha}^i\bar{\beta}^j\,, \tag{14}$$

in which K and $\bar{K}$ stand for the initial values, whereas α, $\bar{\alpha}$, β and $\bar{\beta}$ are the composing terms of Lagrange solutions. It turns out that the left and right equations in (14) become respectively:

$$K\alpha^{i+1}\beta^j = \lambda K\alpha^i\beta^j, \quad \text{and} \quad \bar{K}\bar{\alpha}^i\bar{\beta}^{j+1} = \bar{\lambda}\bar{K}\bar{\alpha}^i\bar{\beta}^j, \tag{15}$$

from which

$$\alpha = \lambda, \quad \text{and} \quad \bar{\beta} = \bar{\lambda} \tag{16}$$

hold.

Hence, recalling that $\mathbf{x}(i,j) = \mathbb{T}\mathbf{z}(i,j)$ along with the definition of stability (2), the particular solutions (9) reduce to definiton 3, namely

$$x(i,j) = \textstyle\sum_{k=1}^{l} \mathrm{I}_k\lambda_k^i\beta_k^j. \tag{17}$$

5 Numerical Example

In this section, a simple numerical example is given to show how the results aforementioned are used to decide whether the system is asymptotically stable. Consider the simple system already given in the form (4)

$$\begin{bmatrix} x_1(i+1,j) \\ x_3(i,j+1) \\ x_4(i,j+1) \\ x_2(i+1,j) \end{bmatrix} = \begin{bmatrix} 0.45 & 0.13 & 0.08 & 0.10 \\ 0.14 & -0.28 & -0.15 & 0.17 \\ 0.70 & -0.25 & 0.31 & 0.35 \\ 0.34 & 0.23 & -0.30 & 0.02 \end{bmatrix} \begin{bmatrix} x_1(i,j) \\ x_3(i,j) \\ x_4(i,j) \\ x_2(i,j) \end{bmatrix}. \tag{18}$$

Then (18) can be solved if and only if

$$x_2(i+1,j) = \begin{bmatrix} 0.34 & 0.23 & -0.30 \end{bmatrix} \begin{bmatrix} 0.45 & 0.13 & 0.08 \\ 0.14 & -0.28 & -0.15 \\ 0.70 & -0.25 & 0.31 \end{bmatrix}^{-1} \begin{bmatrix} x_1(i+1,j) \\ x_3(i,j+1) \\ x_4(i,j+1) \end{bmatrix}, \tag{19}$$

in which a particular solution is given by

$$\begin{bmatrix} x_1(i+1,j) \\ x_3(i,j+1) \\ x_4(i,j+1) \end{bmatrix} = \begin{bmatrix} 0.45 & 0.13 & 0.08 \\ 0.14 & -0.28 & -0.15 \\ 0.70 & -0.25 & 0.31 \end{bmatrix} \begin{bmatrix} x_1(i,j) \\ x_3(i,j) \\ x_4(i,j) \end{bmatrix}. \tag{20}$$

Thus applying the transformation

$$\begin{bmatrix} z_1(i,j) \\ z_3(i,j) \\ z_4(i,j) \end{bmatrix} = \begin{bmatrix} -0.369389 & -0.180235 & 0.177970 \\ 0.097002 & -0.307769 & -0.857873 \\ -0.924198 & 0.934235 & -0.482059 \end{bmatrix}^{-1} \begin{bmatrix} x_1(i,j) \\ x_3(i,j) \\ x_4(i,j) \end{bmatrix}, \tag{21}$$

and since substitution of (21) into (20) gives the diagonal matrix composed by the eigenvalues, the following Lagrange solutions are obtained

$$\begin{aligned} z_1(i,j) &= K_1(0.616019)^i \beta_1^j, \\ z_3(i,j) &= K_3 \alpha_3^i (0.257313)^j, \\ z_4(i,j) &= K_4 \alpha_4^i (-0.393332)^j. \end{aligned} \tag{22}$$

Thus, back substitution of (22) into (21) yields

$$\begin{bmatrix} x_1(i,j) \\ x_3(i,j) \\ x_4(i,j) \end{bmatrix} = \begin{bmatrix} -0.369389 & -0.180235 & 0.177970 \\ 0.097002 & -0.307769 & -0.857873 \\ -0.924198 & 0.934235 & -0.482059 \end{bmatrix} \begin{bmatrix} K_1(0.616019)^i \beta_1^j \\ K_3 \alpha_3^i (0.257313)^j \\ K_4 \alpha_4^i (-0.393332)^j \end{bmatrix}. \tag{23}$$

Thus, for any β_1, $0 \neq |\beta_1| < 1$; $0 \neq |\alpha_3| < 1$ and α_4, $0 \neq |\alpha_4| < 1$, the solutions vanish as the indices increase. Yet, this is also true for the general solution if one chooses appropriate v's in (10). Finally, x_2 is obtained by solving (23) for each x and then inserting them into (19) with the indices correctly adjusted.

6 Final Remarks

This paper was concerned with the stability analysis of 2-d discrete systems expressed by a set of partial difference equations in the state space description with a singular matrix composing it. As a result, we established an analysis procedure on the grounds of the Lagrange method for solving partial difference equations. A relevant key point here is that when the system is asymptotically stable we can determine an explicit

solution to the system. Another point is that it shows the relationship between the eigenvalues of the matrix and asymptotic stability of the system. Finally, a numerical example was presented to illustrate these points.

Acknowledgments. The author would like to thank the school for providing fruitful research environment and financial support to carry out this research.

References

1. Ozaki, H., Kasami, T.: Positive real functions of several variables and their applications to variable network. IRE Trans. Circ. Theor. **CT-7**, 251–260 (1960)
2. Fornasini, E., Marchesini, G.: Doubly indexed dynamical systems: state space models and structural properties. Math. Syst. Theor. **12**, 59–72 (1978). https://doi.org/10.1007/BF01776566
3. Givone, D.D., Roesser, R.P.: Multidimensional linear iterative circuits - general properties. IEEE Trans. Comput. **C-21**, 1067–1073 (1972)
4. Tzafestas, S.G.: Multidimensional Systems: Techniques and Applications. Marcel Dekker, New York (1986)
5. Izuta, G.: Stability and disturbance attenuation of 2-d discrete delayed systems via memory state feedback controller. Int. J. Gen Syst **36**(3), 263–280 (2007)
6. Cheng, S.S.: Partial Difference Equations. Taylor Francis, London (2003)
7. Jerri, A.J.: Linear Difference Equations with Discrete Transform Methods. Kluwer Academic Publishers, Netherlands (1996)
8. Izuta, G.: Stability analysis of 2-d discrete systems on the basis of lagrange solutions and doubly similarity transformed systems. In: 35th IEEE Industrial Electronics Soc. IEEE Press, New York (2010)
9. Izuta, G.: Networked 2-d linear discrete feedback control systems design on the basis of observer controller. In: 16th International Conference on System Theory, Control and Computing, IEEE CS (2012)
10. Izuta, G.: An observer controller design method for 2-d linear discrete control systems. In: Proceedinigs of 2015 IEEE International Conference on Information and Automation. IEEE AC (2015)
11. Ben-Israel, A., Greville, T.N.E.: Generalized Inverses: Theory and Applications (Sect. 1.1), Wiley, New York (1974)
12. Rao, C.R., Mitra, S.K.: Generalized Inverse of Matrices and its Applications (Sect. 2.4). Wiley, New York (1971)

Chaos and Stability of the Financial System

Adam Altăr-Samuel(✉)

Department of Computer Science, Statistics and Mathematics,
Romanian-American University, Bucharest, Romania
adam.altar@profesor.rau.ro

Abstract. Financial stability is one of the most widely discussed issues in today's economic literature. The relevance of analyses on financial stability was first recognized during the international financial crises at the end of the 90s, also strengthened by the financial and economic crisis emerging in 2007. Even if an economical system possesses deterministic characteristics, a chaotic behavior can occur in the financial system. Because of slight errors, chaotic dynamical systems can lead to completely different trajectories. Hence, the chaos control in the financial systems is required. In this paper, we analyze the stability of equilibria of a financial system described by three dynamic equations and apply stabilization techniques for the unstable equilibrium state of the system. Our results are essentially based on the Theorem of allotting the characteristic polynomial (see, e.g. [1], Theorem 2.2.3). We also suggest the use of optimal stabilization, by means of a quadratic loss-function.

Keywords: Financial system · Stability of the financial system
Chaotic finance system · Stabilization by linear feed-back
Optimal stabilization

1 Introduction

Financial stability is one of the most widely discussed issues in today's economic literature. The relevance of analyses on financial stability was first recognized during the international financial crises at the end of the 90s, also strengthened by the financial and economic crisis emerging in 2007. A stable financial system is one in which financial intermediaries, markets and market infrastructure facilitate the smooth flow of funds between savers and investors and, by doing so, help promote growth in economic activity. Conversely, financial instability is a material disruption to this intermediation process with potentially damaging implications for the real economy.

Lately, many central banks, through their financial stability reports (FSRs), attempt to assess the risks to financial stability by focusing on a small number of key indicators.

A financial system is governed by extremely complex laws. Its dynamics depend in a nonlinear way of a series of factors as interest rate, price of goods and shares, investment demand, etc. Even if an economic system possesses deterministic characteristics, a chaotic behavior can occur in the financial system. One of the main characteristics of chaotic system is the high sensitivity to initial conditions. Since 1989, chaos control has attracted a great quantity of attention, after Hübler published the first paper on chaos control [2]. Particularly, some useful methods have been developed in

K. Ntalianis and A. Croitoru (Eds.): APSAC 2017, LNEE 489, pp. 230–236, 2019.
https://doi.org/10.1007/978-3-319-75605-9_32

case of chaos suppression, including sliding mode control, time-delayed feedback control, double delayed feedback control, robust control, optimal control, intelligent control. In this respect, we can mention the papers [3–15].

The present paper achieves chaos control of a three-dimensional model of a financial system based essentially on the Theorem of allotting the characteristic polynomial (see, e.g. [1], Theorem 2.2.3). We also suggest the use of optimal stabilization, by means of a quadratic loss-function. The paper is structured as follows: after this Introduction, we present, in Sect. 2, the Mathematical prerequisites necessary for the analysis and stabilization of the financial model, which are performed in Sect. 3. The paper ends with Conclusions and References.

2 Mathematical Prerequisites

2.1 Stability

Theorem 1 (Theorem for Non-linear Systems of Differential Equations - Stability Theorem after the First Approximation). Assume

$$\dot{x} = f(x), x \in \mathbb{R}^n, n \in \mathbb{N} \text{ and } \hat{x} \; - \; \text{the equilibrium } (f(\hat{x}) = 0). \tag{1}$$

If all the eigenvalues of the matrix $A = \frac{\partial f}{\partial x}(\hat{x})$ have strictly negative real parts, then the equilibrium $\hat{x}$ is exponentially stable, i.e.:

$$\begin{gathered}(\exists)\delta > 0, \alpha > 0, \beta \geq 1 \text{ such that } \|x_0 - \hat{x}\| < \delta \Rightarrow \\ \Rightarrow \|x(t) - \hat{x}\| \leq \beta e^{-\alpha t}\|x_0 - \hat{x}\|, (\forall)t \geq 0.\end{gathered} \tag{2}$$

Proposition 1 (Necessary and Sufficient Conditions for Exponential Stability in the Case of a third order matrix). The eigenvalues of a 3×3 matrix A have strictly negative real parts if and only if $\beta > 0, \delta > 0, \beta\gamma - \delta > 0$, where β, γ, δ are the coefficients of the characteristic polynomial

$$P(r) = r^3 + \beta r^2 + \gamma r + \delta = \det(rI - A). \tag{3}$$

Remark. Let $A = \left(a_{ij}\right), i, j = 1, 2, 3$. We denote

$$trA = a_{11} + a_{22} + a_{33}, \quad \delta_{ij} = \begin{vmatrix} a_{ii} & a_{ij} \\ a_{ji} & a_{jj} \end{vmatrix}, i, j = 1, 2, 3. \tag{4}$$

We have

$$P(r) = r^3 - (trA)r^2 + (\delta_{12} + \delta_{13} + \delta_{23})r - \det A. \tag{5}$$

Therefore, the exponential stability conditions become

$$\begin{array}{l} trA < 0, \det A < 0, \beta\gamma - \delta > 0, \text{ where} \\ \beta = -trA; \delta = -\det A; \gamma = \delta_{12} + \delta_{13} + \delta_{23}. \end{array} \tag{6}$$

2.2 Stabilization

Controllability. Let A be an $n \times n$ matrix and $B \in \mathbb{R}^{n\times m}$. The pair (A, B) is called controllable, if the rank of the matrix $C = \begin{pmatrix} B & AB & A^2B & \dots & A^{n-2}B & A^{n-1}B \end{pmatrix}$ is equal to n.

Remark. If b is a column vector, $b \in \mathbb{R}^3$ and A is a square matrix of order 3, then

$$A \text{ is controllable } \Leftrightarrow \det\begin{pmatrix} b & Ab & A^2b \end{pmatrix} \neq 0. \tag{7}$$

Theorem 2 (Theorem of Allotting the Characteristic Polynomial). Let A be a $n \times n$ matrix, $b \in \mathbb{R}^n$. If the pair (A, b) is controllable, then for any monic polynomial $P(r)$ of degree n, there exists a matrix F such that $P(r)$ is the characteristic polynomial of the matrix $M = A + BF$.

3 The Model

The model of the financial system consists of three dynamic equations [3, 4]:

$$\begin{cases} \dot{x} = z + (y - a)x \\ \dot{y} = 1 - by - x^2 \\ \dot{z} = -x - cz. \end{cases} \tag{8}$$

where x is the interest rate, y represents the demand for investment, z is the price exponent (determines the variance of the price distribution) and a, b, c are positive parameters, representing the saving amount, the per-investment cost, and the elasticity of demand for commercials, respectively.

An equilibrium $(\hat{x}, \hat{y}, \hat{z})$ of the system (8) is a solution to the system:

$$\begin{cases} z + (y - a)x = 0 \\ 1 - by - x^2 = 0 \\ x + cz = 0. \end{cases} \tag{9}$$

If $\theta = 1 - ab - \frac{b}{c} \leq 0$, the system (9) has only one solution:

$$E_1 = \left(0, \frac{1}{b}, 0\right). \tag{10}$$

If $\theta > 0$, then there exist two more equilibria:

$$E_2 = \left(\sqrt{\theta}, a + \frac{1}{c}, -\frac{\sqrt{\theta}}{c}\right) \text{ and } E_3 = \left(-\sqrt{\theta}, a + \frac{1}{c}, \frac{\sqrt{\theta}}{c}\right). \tag{11}$$

We remark that in state E_3, the interest rate $\hat{x}$ would be negative, which is unacceptable from the financial viewpoint, so we will not discuss E_3.

On the other hand, applying Proposition 1 for the characteristic polynomial:

$$\begin{aligned} P(r) =& r^3 + (a + b + c - y)r^2 + (ab + ac + bc \\ & - \hat{y}(b + c) + 2\hat{x}^2 + 1)r + 2\hat{x}^2 c + b - bc\hat{y} + abc, \end{aligned} \tag{12}$$

we find that the equilibrium E_2 is exponentially stable. Therefore, the only equilibrium worth discussing is E_1.

The corresponding characteristic polynomial is:

$$P(r) = r^3 + \left(a + b + c - \frac{1}{b}\right)r^2 + \left(ab + ac + bc - \frac{c}{b}\right)r + b - c + abc. \tag{13}$$

This equilibrium can be unstable, e.g. if $\beta = a + b + c - \frac{1}{b} < 0$.

Stabilization. In this case, we can try to stabilize this equilibrium by using a feedback control of the form:

$$u(x, y, z) = F_1 x + F_2\left(y - \frac{1}{b}\right) + F_3 z = (F_1, F_2, F_3)\begin{pmatrix} x \\ y - \frac{1}{b} \\ z \end{pmatrix}. \tag{14}$$

We consider the control system:

$$\begin{cases} \dot{x} = z + (y - a)x + u(x, y, z) \\ \dot{y} = 1 - by - x^2 + u(x, y, z) \\ \dot{z} = -x - cz. \end{cases} \tag{15}$$

In matrix form, we have:

$$\dot{w} = f(w, u) = f(x, y, z, u),\ \mathrm{w} = \begin{pmatrix} x \\ y \\ z \end{pmatrix},\ \mathrm{f} = \begin{pmatrix} \mathrm{f}_1 \\ \mathrm{f}_2 \\ \mathrm{f}_3 \end{pmatrix}. \tag{16}$$

Applying Theorem 1 to system (16), we obtain the requirement that the matrix $M = A + bF$ has eigenvalues with negative real parts, where

$$A = \frac{\partial f}{\partial w} = \begin{pmatrix} \frac{1}{b} - a & 0 & 1 \\ 0 & -b & 0 \\ -1 & 0 & -c \end{pmatrix}, b = \begin{pmatrix} 1 \\ 1 \\ 0 \end{pmatrix}. \tag{17}$$

In order to find the stabilizing feedback control, we apply Theorem 2 to the matrices A, b above. First, we check the controllability of the pair (A, b). We have:

$$C = \begin{pmatrix} b & Ab & A^2b \end{pmatrix} = \begin{pmatrix} 1 & \frac{1}{b} - a & \left(\frac{1}{b} - a\right)^2 - 1 \\ 1 & -b & b^2 \\ 0 & -1 & -\frac{1}{b} + a + c \end{pmatrix}. \tag{18}$$

We have controllability if $\det C = b^2 + 2 - ab + ac - bc - \frac{c}{b} \neq 0$.

Remark. If we took $b = \begin{pmatrix} 1 \\ 0 \\ 0 \end{pmatrix}$, then we would get $\det C = 0$. Further, we have

$$M = A + bF = \begin{pmatrix} \frac{1}{b} - a + F_1 & F_2 & 1 + F_3 \\ F_1 & -b + F_2 & F_3 \\ 0 & -1 & -\frac{1}{b} + a + c \end{pmatrix}. \tag{19}$$

According to the remark from Sect. 2.1, the characteristic polynomial of M is:

$$P(r) = r^3 - (trM)r^2 + (\Delta_{12} + \Delta_{13} + \Delta_{23})r - \det M. \tag{20}$$

On the other hand, according to Theorem 2, we can arbitrarily choose negative eigenvalues r_1, r_2, r_3, which would be the roots of polynomial:

$$\pi(r) = r^3 - (\mathrm{r}_1 + \mathrm{r}_2 + \mathrm{r}_3)r^2 + (\mathrm{r}_1\mathrm{r}_2 + \mathrm{r}_1\mathrm{r}_3 + \mathrm{r}_2\mathrm{r}_3)r - \mathrm{r}_1\mathrm{r}_2\mathrm{r}_3. \tag{21}$$

By identifying (20) and (21), we obtain:

$$trM = \mathrm{r}_1 + \mathrm{r}_2 + \mathrm{r}_3, \Delta_{12} + \Delta_{13} + \Delta_{23} = \mathrm{r}_1\mathrm{r}_2 + \mathrm{r}_1\mathrm{r}_3 + \mathrm{r}_2\mathrm{r}_3, \det M = \mathrm{r}_1\mathrm{r}_2\mathrm{r}_3. \tag{22}$$

This leads to the linear algebraic system with unknowns F_1, F_2, F_3:

$$\begin{cases} \mathrm{F}_1 + \mathrm{F}_2 = (a + b + c) - \frac{1}{b} + \mathrm{r}_1 + \mathrm{r}_2 + \mathrm{r}_3 \\ -(b + c)\mathrm{F}_1 + \left(\frac{1}{b} - a - c\right)\mathrm{F}_2 + \mathrm{F}_3 = \frac{c}{b} - (ab + ac + bc) + \mathrm{r}_1\mathrm{r}_2 + \mathrm{r}_1\mathrm{r}_3 + \mathrm{r}_2\mathrm{r}_3 \\ -bc\mathrm{F}_1 + \left(\frac{c}{b} - ac - 1\right)\mathrm{F}_2 + b\mathrm{F}_3 = -b + c - abc - \mathrm{r}_1\mathrm{r}_2\mathrm{r}_3. \end{cases} \tag{23}$$

We remark that the determinant of system (23) coincides with $\det C$, which means that the controllability of the pair (A, b) is equivalent to system (23) having exactly one solution $F = (F_1, F_2, F_3)$, corresponding to the chosen eigenvalues r_1, r_2, r_3.

Remark. Since the choice of r_1, r_2, r_3 is mostly arbitrary, it would be advisable to select an "optimal" feedback control, by means of an optimality criterion, for instance a quadratic loss function, which should be minimized:

$$\min J(x, y, z, u) = \int_0^{\infty} \left(q_1 x^2 + q_2 \left(y - \frac{1}{b} \right)^2 + q_3 z^2 + u^2 \right) dt. \tag{24}$$

4 Conclusions

The present paper achieves chaos control of a three-dimensional model of a financial system, based essentially on the Theorem of allotting the characteristic polynomial (see, e.g. [1], Theorem 2.2.3). We also suggest the use of optimal stabilization, by means of a quadratic loss-function. In an extension of this paper, we will apply the theoretical results obtained for some real systems.

Acknowledgement. This work was supported by a grant of the Romanian National Authority for Scientific Research, CNCS – UEFISCDI, project number PN-II-RU-TE-2014-2499 entitled "Coordinating Monetary and Macroprudential Policies".

References

1. Halanay, A., Dragan, V.: Stabilization of Linear Systems. Birkhäuser, Switzerland (1999)
2. Hübler, A.: Adaptive control of chaotic systems. Helvetica Physica Acta **62**, 343–346 (1989)
3. Ma, J., Chen, Y.: Study for the bifurcation topological structure and the global complicated character of a kind of non-linear finance system (I). Appl. Math. Mech. **22**(11), 1240–1251 (2001)
4. Ma, J., Chen, Y.: Study for the bifurcation topological structure and the global complicated character of a kind of non-linear finance system (II). Appl. Math. Mech. **22**(11), 1375–1382 (2001)
5. Cai, G., Huang, J.: A new finance chaotic attractor. Int. J. Nonlinear Sci. **3**(3), 213–220 (2007)
6. Cai, G., Yu, H., Li, Y.: Stabilization of a modified chaotic finance system. In: 4th International Conference on Information and Computing, pp. 188–191. IEEE Press, New York (2011)
7. Chen, W.: Dynamics and control of a financial system with time-delayed feedbacks. Chaos Solitons Fractals **37**(4), 1198–1207 (2008)
8. Ding, J., Yang, W., Yao, H.: A new modified hyperchaotic finance system and its control. Int. J. Nonlinear Sci. **8**(1), 59–66 (2009)

9. Emiroğlu, S., Uyaroğlu, Y., Köklükaya, E.: Control of a chaotic finance system with passive control. In: 3rd International Symposium on Sustainable Development, Sarajevo, pp. 125–130. International Burch University, Sarajevo (2012)
10. Gelberi, H., Emiroğlu, S., Uyaroğlu, Y, Yalçin, M.A.: Time delay feedback control of chaos in a hyperchaotic finance system. In: 3rd International Symposium on Sustainable Development, Sarajevo, pp. 139–144. International Burch University, Sarajevo (2012)
11. Hou, Y.Y., Liau, B.Y., Chen, H.C.: Synchronization of unified chaotic systems using sliding mode controller. Math. Prob. Eng. **2012** (2012). Article 632712
12. Lukyanov, A.G., Utkin, V.I.: Methods of reducing equations for dynamic systems to a regular form. Autom. Remote Control **42**(4), 413–420 (1981)
13. Rigatos, G.G.: State-Space Approaches for Modelling and Control in Financial Engineering. Springer, Cham (2017)
14. Sundarapandian, V., Sivaperumal, S.: Global chaos synchronization of hyperchaotic Chen system by sliding mode control. Int. J. Eng. Sci. Technol. **3**(5), 4265–4271 (2011)
15. Uyaroğlu, Y., Temel, R., Kırlıoğlu, H.: Feedback control of chaos in a hyperchaotic finance system. In: 3rd International Symposium on Sustainable Development, Sarajevo, pp. 135–139. International Burch University, Sarajevo (2012)
16. Altăr-Samuel, A., Alupoaiei, A.: Dynamics in a New-Keynesian model with financial accelerator and uncertainty. In: Economic Computation and Economic Cybernetic Studies and Research, vol. 51. Editura Academia de Studii Economice, Bucharest (2017)
17. Azar, A.T., Sundarapandian, V.: Advances in Chaos Theory and Intelligent Control. Springer, Cham (2016)
18. Azar, A.T., Zhu, Q.: Advances and Applications in Sliding Mode Control. Springer, Cham (2015)

A Simple Econophysics Model of the Stock Market as a Nonequilibrium Open System

Andrey Dmitriev(✉), Vitaly Silchev, and Victor Dmitriev

School of Business Informatics, National Research University Higher School of Economics, 33 Kirpichnaya Street, 105187 Moscow, Russia
a.dmitriev@hse.ru

Abstract. Mathematical modeling of a stock market functioning is one of the actual and at the same time complex task of the modern theoretical economics. From our point of view, building such mathematical models "ab initio", by using analogy between the stock market and a certain physical system (in our work, laser), is the most promising approach. This paper proposes a simple econophysical model of stock market as an open nonequilibrium system in form of Lorenz–Haken equation. In this system, variation of ask price, variation of bid price, and instantaneous difference between numbers of agents in active and passive state are intensity of external information flow is a control parameter. This model explains the impossibility of existence of an equilibrium state of the market and shows the presence of deterministic chaos in a stock market.

Keywords: Deterministic chaos · Lorenz–Haken equation · Stock market
Ask price · Bid price

1 Introduction

From the second half of the XX century the general trend of science development is the penetration of the ideas and methods of physics into other natural and humanitarian disciplines. Methods of physical modeling are often used in sciences such as demography, sociology and linguistics.

An interdisciplinary research field, known as econophysics, was formed in the middle 1990s as an approach to solve various problems in economics, such as uncertainty or stochastic processes and nonlinear dynamics, by applying theories and methods originally developed by physicists. H. Eugene Stanley coined the term "econophysics" in order to describe the large number of papers written by physicists in the problems of stock markets (for econophysics reviews see refs. [1–4]).

Current state of theoretical economics allows one to effectively use advanced methods of physico-mathematical modeling for economical system. A remarkable example is applying nonlinear dynamics to analysis of financial time series [5, 6]. Moreover, in 1963 Mandelbrot [7] during his research of cotton prices found out that the prices follows a scaled distribution in time. That discovery originated a new approach in market research called fractal market analysis [8]. A systematic research of deterministic chaos in financial markets started from works of Savit [9].

K. Ntalianis and A. Croitoru (Eds.): APSAC 2017, LNEE 489, pp. 237–243, 2019.
https://doi.org/10.1007/978-3-319-75605-9_33

By the end of 20th century there were formed two lines of research of deterministic chaos in financial markets. The first one is related to discovery and analysis of deterministic chaos in the structure of financial markets. Studies of that kind are usually based on qualitative characteristic and quantitative measures of chaos [10], and their results show conclusively that deterministic chaos exists in financial markets [11–19]. The second line connected to retrieval of explicit form of such dynamical systems. Definitely, construction of such models is far more complex problem. That is why the number of relevant publications on this topic is relatively small. The most comprehensive survey of mathematical models of financial markets can be found in the book of Elliott and Kopp [20]. Although the book and other relevant publications contain numerous conceptual models, we have not found any "ab initio" econophysical model of a stock market that can explain its fundamental functioning mechanisms. Thus, the purpose of this work is building of econophysical model of a stock market using parallels between market functioning and physical principles of laser operation.

2 Construction of the Model

2.1 Model Assumptions

1. Stock market is a macroscopic system. Assume that the stock market is a dynamical system that consists of numerous market agents (investors) ($N \gg 1$). Modeling of such systems does not require detailed analysis of interactions between the agents on the micro-level. For macrosystem description we use macroscopic parameters and dynamic variables of the system. For macroscopic dynamic variables we have chosen aggregated flows of ask and bid price changes and dynamical difference of market agents in specific states.
2. Stock market is a point autonomous dynamical system.

$$\dot{\mathbf{X}} = \mathbf{F}(\mathbf{X}, \boldsymbol{\beta}). \tag{1}$$

This statement goes without saying, as it depends only on chosen modeling approach and objectives. However, the choice of (1) as the base model is made for reason. It is based on tests that the constructed mathematical model agrees with empirical (observed) data, for which we used available financial time series of ask/bid stock prices.

3. Every market agent can be in one of two possible states: active ($|\boldsymbol{a}\rangle$-state) or passive ($|\boldsymbol{p}\rangle$-state). A particular market agent being in $|a\rangle$-state has maximum amount of valuable information about financial asset ($I_{|a\rangle}$) and has minimum information ($I_{|p\rangle}$) otherwise. In $|a\rangle$-state the agent can generate local demand on deal with the asset and send an "ask-quantum" to other agents. If the agent is in $|p\rangle$-state, then the agent's rational decision is do not generate demand on deal ("bid-quantum"). Moreover, for the agent in $|p\rangle$-state generating of a deal offer depends on the agent's reaction on received "ask-quantum" (Fig. 1a) or can be his or her own

decision (Fig. 1b). General pattern in stock markets is that local "ask" waves ("quanta") induce local "bid" waves ("quanta").

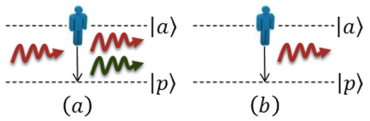

Fig. 1. Agents generate «ask-quanta» (red) and «bid-quanta» (green). (a) Forced generation of an «bid-quantum». (b) Spontaneous generation of an «ask-quantum».

4. Stock market is a nonequilibrium open system. Indeed, stock market is an open system that continuously interacts with the external world. Sources of external information include corporate financial reports, financial news feeds, stock-ticker data and others. This information flow, in some sense, "pump up" the stock market, making inverse population of market agents: $N_{|a\rangle} \gg N_{|p\rangle}$, where $N_{|a\rangle}$ is the number of agents being in $|a\rangle$-state, $N_{|p\rangle}$ is the number of agents being in $|p\rangle$-state.

With acceptable accuracy, the distribution of number of agents by their states can be represented as follows:

$$N_{|a\rangle} = N_{|p\rangle} \exp\left(-\left(I_{|a\rangle} - I_{|p\rangle}\right)/\theta\right), \tag{2}$$

where θ is average intensity of stochastic interactions between market agents Simple analysis of Eq. (2) allows to identify two macroscopic states of the market: stable equilibrium state and nonequilibrium state. If $I_{|a\rangle} - I_{|p\rangle} \gg \theta$, then $N_{|p\rangle} \gg N_{|a\rangle}$. In this case, the system is in stable equilibrium state. Otherwise, if $I_{|p\rangle} - I_{|a\rangle} \gg \theta$, then $N_{|a\rangle} \gg N_{|p\rangle}$. This case corresponds to nonequilibrium state of the system.

Taking into account continuous information pumping, stock market is always functioning in nonequilibrium state, making "avalanches" of ask and bid "quanta". Due to information pumping, the equilibrium state is almost unreachable. It is crucially important, that existence of chaotic states is a fundamental property of nonequilibrium open systems [24, 25].

2.2 Dynamic Variables of the Model and the Relationship Between Them

Let us define dynamic variables in Eq. (1) for constructing nonlinear dynamical model of stock market: $x_1(t) \equiv X_{ask}(t) - X_{ask}^{eq}$ is the variation of "ask" price ($X_{ask}(t)$) relative to equilibrium value (X_{ask}^{eq}) is the "ask" price in equilibrium state); $x_2(t) \equiv X_{bid}(t) - X_{bid}^{eq}$ is the variation of "bid" price ($X_{bid}(t)$) relative to equilibrium value (X_{bid}^{eq}) is the "bid" price in equilibrium state); $x_3(t) \equiv N_{|a\rangle}(t) - N_{|p\rangle}(t)$ instantaneous difference between numbers of agents in $|a\rangle$-state and $|p\rangle$-state.

The choice of these dynamic variables responds to possibility to test whether the constructed dynamical system agrees with empirical data, for which we have chosen available time series of ask and bid prices from real stock markets. However, it is

impossible to compare the third dynamic variable with actual data, due to available datasets does not contain these values. Thus, the fit test can be performed only with two dynamic variables.

Let us establish connections between dynamic variables and their change rates. Variation rate of the ask price is defined by concurrency of two factors: rate decrease due to market relaxation ($-\alpha x_1(t)$) and rate increase due to growing bid price variation ($+\beta x_2(t)$):

$$\dot{x}_1(t) = -\alpha x_1(t) + \beta x_2(t) \tag{3}$$

Term $-\alpha x_1(t)$ in (3) is necessary due to relaxation of nonequilibrium system. According to Le Chatelier's principle [26], when the system at equilibrium is subjected to change by external force, then the system readjusts itself to counteract (partially) the effect of the applied change. Indeed, without term $+\beta x_2(t)$ the Eq. (3) has the following form:

$$\dot{x}_1(t) = -\alpha x_1(t). \tag{4}$$

A solution of differential Eq. (4) is a function of form $x_1(t) = A\exp(-\alpha t)$. Therefore, $X_{ask}(t) \to X_{bid}^{eq}$ when $t \to \infty$ (stock market tend to stable equilibrium). In Eq. (4) α – relaxation parameter, related to relaxation time (τ_1) according to: $\alpha = 1/\tau_1$. Term $+\beta x_2(t)$ in (3) refers to the fact, that increase of bid price variation leads to increase of variation rate of ask prices.

Variation rate of the bid price is defined by concurrency of two factors: rate decrease due to market relaxation ($-\gamma x_2(t)$) and rate increase due to $+cx_1(t)x_3(t)$.

$$\dot{x}_2(t) = -\gamma x_2(t) + cx_1(t)x_3(t) \tag{5}$$

Presence of the first term in (5) is explained by Le Chatelier' s principle. Term $+cx_1(t)x_3(t)$ is explained as follows: "bid quantum", on which every market agent reacts considering "ask quanta" flow, is proportional to ask price variation and depends on the agent's current state ($|a\rangle$-state or $|p\rangle$-state).

Dynamics of difference between numbers of market agents in $|\boldsymbol{a}\rangle$-state and $|\boldsymbol{p}\rangle$-state is defined as follows.

$$\dot{x}_3(t) = \varepsilon(I_0 - x_3(t)) + kx_1(t)x_2(t) \tag{6}$$

Again, term $-\varepsilon x_3(t)$ is in Eq. (6) due to Le Chatelier's principle. Parameter I_0 refers to intensity of external information pumping, so instantaneous difference between numbers of agents in $|a\rangle$-state and $|p\rangle$-state grows with increase of I_0.Term $+kx_1(t)x_2(t)$ represents the power that the aggregated ask price variation spends on creation of the aggregated bid price variation.

2.3 Modeling Results and Their Interpretation

The system of differential Eqs. (3), (5) and (6) represents the well-known Lorenz–Haken equation [27]:

$$\dot{x}_1 = -\alpha x_1 + \beta x_2, \dot{x}_2 = -\gamma x_2 + c x_1 x_3, \dot{x}_3 = \varepsilon(I_0 - x_3) + k x_1 x_2 \tag{7}$$

System (7) is one of the most studied 3-dimensional dynamical systems. General properties of (7) are presented in works [28, 29]. Let us consider (7) as a system with one control parameter I_0. From changing control parameter's value, we can make two important conclusions about system (7).

If $\beta c/\alpha\gamma \cong 1$ and $0 < I_0 < 1$, then $X_{ask}(t) \to X_{ask}^{eq}$, $X_{bid}(t) \to X_{bid}^{eq}$ and $N_{|a\rangle}(t) \to N_{|p\rangle}(t)$ as $t \to \infty$. In case of relatively small intensity of external information pumping, the stock market tends to stable equilibrium. However, practically this stable equilibrium state cannot be reached, since the market is an open system with permanent eternal information pumping. If $\beta c/\alpha\gamma \cong 1$ and $I_0 \cong 28$, then the stock market functions as an open nonequilibrium system with deterministic chaos. It is worth to mention that such behavior is typical for a financial market with considerably intense external information.

3 Conclusion

The constructed simple econophysical model of a stock market as an open nonequilibrium system allows explaining the unrealizability of equilibrium state of the market as well as appearance of deterministic chaos in the market. These phenomena are explained only by quantitative characteristics of external information pumping as a control parameter of the system.

However, this simple model cannot explain several other important phenomena, such as heavy-tailed distribution of financial time series, financial bubbles and economic downfalls. Actually, time series of ask and bid price variations has trimodal centered distribution with "cropped tails". Local maxima of the PDF represent three stable equilibrium points of the dynamical system (7). Formally, by increasing the number of stable equilibrium points one can fit theoretical PDF to empirical PDF. That will lead to significant growth of dynamical system dimension. Although such modification is possible, it also removes low-dimensional (deterministic) chaos, which is a characteristic feature of stock markets. We suppose, that explanation of heavy-tailed distribution of financial time series requires modification of dynamical system by introducing the noise of specific kind. Particularly, the form of time series with heavy-tailed distribution can be achieved by including a power-law multiplicative noise [30], what is the subject of our further research.

References

1. Chakraborti, A., Toke, I., Patriarca, V., Abergel, F.: Econophysics review: I. Empir. Facts Quant. Finan. Quant. Fin. **11**, 991–1012 (2011)
2. Chakraborti, A., Toke, I., Patriarca, V., Abergel, F.: Econophysics review: II. Agent-based Models. Quant. Fin. **11**, 1013–1041 (2011)
3. Richmond, P., Mimkes, J., Hutzler, S.: Econophysics and Physical Economics. Oxford University Press, United Kingdom (2013)
4. Savoiu, G.: Econophysics: Background and Applications in Economics, Finance, and Sociophysics. Elsevier, Amsterdam (2013)
5. Hsieh, D.A.: Chaos and Nonlinear Dynamics: Application to Financial Markets. J. Fin. **46**, 1839–1877 (1991)
6. Small, M., Tse, C.K.: Determinism in Financial Time Series. Stud. Nonlin. Dyn. Econom. **7**, 1–29 (2003)
7. Mandelbrot, B.B.: The Variation of Certain Speculative Prices. J. Bus. **36**, 394–419 (1963). University of Chicago
8. Hudson, R.L., Mandelbrot, B.B.: The (Mis)Behavior of Markets: A Fractal View of Risk, Ruin, and Reward. Basic Books, New York (2004)
9. Savit, R.: When random is not random: an introduction to chaos in market prices. J. Fut. Mark. **8**, 271–290 (1988)
10. Lai, Y.C., Ye, N.: Recent developments in chaotic time series analysis. Int. J. Bif. Chaos **13**, 1383–1422 (2003)
11. Murray, F., Stengos, T.: Measuring the strangeness of gold and silver rates of return. Rev. Econom. Stud. **56**, 553–567 (1989)
12. Blank, S.: Chaos in futures markets? a nonlinear dynamical analysis. J. Fut. Mark. **11**, 711–728 (1991)
13. Decoster, G.P., Labys, W.C., Mitchell, D.W.: Evidence of chaos in commodity futures prices. J. Fut. Mark. **12**, 291–305 (1992)
14. Abhyankar, A., Copeland, L.S., Wong, W.: Nonlinear dynamics in real-time equity market indices: evidence from the United Kingdom. Econom. J. **105**, 864–880 (1995)
15. Andreou, A.S., Pavlides, G., Karytinos, A.: Nonlinear time-series analysis of the Greek exchange-rate market. Int. J. Bif. Chaos **10**, 1729–1758 (2000)
16. Panas, E., Ninni, V.: Are oil markets chaotic? a non-linear dynamic analysis. Energ. Econ. **22**, 549–568 (2000)
17. Antoniou, A., Vorlow, C.E.: Price clustering and discreteness: is there chaos behind the noise? Phys. A **348**, 389–403 (2005)
18. Hafner, C.M., Reznikova, O.: On the estimation of dynamic conditional correlation models. Comp. Stat. Data Anal. **56**, 3533–3545 (2012)
19. Urrutia, J.L., Gronewoller, P., Hoque, M.: Nonlinearity and low deterministic chaotic behavior in insurance portfolio stock returns. J. Risk Insur. **69**, 537–554 (2002)
20. Elliott, R.J., Kopp, P.E.: Mathematics of the Financial Markets. Springer, Berlin Heidelberg (2005)
21. Cai, G., Huang, J.: A new finance chaotic attractor. Int. J. Nonlin. Sci. **3**, 213–220 (2007)
22. Chen, W.C.: Dynamics and control of a financial system with time-delayed feedbacks. Chaos, Solitons Fractals **37**, 1188–1207 (2008)
23. Holyst, J.A., Zebrowska, M., Urbanowicz, K.: Observations of the deterministic chaos in financial time series by recurrence plots, can one control chaotic economy? Europ. Phys. J. B **20**, 531–535 (2001)

24. Loskutov, A.Y.: Dynamical chaos: systems of classical mechanics. Phys. Uspekhi **177**, 989–1015 (2007)
25. Loskutov, A.Y.: Fascination of Chaos. Phys. Uspekhi **180**, 1305–1329 (2010)
26. Atkins, P.W.: The Elements of Physical Chemistry. Oxford University Press, United Kingdom (1993)
27. Haken, H.: Analogy between higher instabilities in fluids and lasers. Phys. Lett. A **53**, 77–85 (1975)
28. Sparrow, C.: The Lorenz Equations: Bifurcations Chaos and Strange Attractors. Springer, Germany (1982)
29. Hilborn, R.C.: Chaos and nonlinear dynamics: an introduction for scientists and engineers. Oxford University Press, United Kingdom (2000)
30. Kaulakys, B., Alaburda, M.: Modeling scaled processes and $1/f^{\beta}$ noise using nonlinear stochastic differential equations. J. Stat. Mech. **P02051**, 1–16 (2009)

Mathematical Modeling and Simulation of Selected Multi-pulse Rectifiers, Used in "Conventional" Airplanes and Aircrafts Consistent with the Trend of "MEA/AEA"

Lucjan Setlak(✉) and Rafał Kowalik

Aviation Division, Department of Avionics and Control Systems,
Polish Air Force Academy, ul. Dywizjonu 303 nr 35, 08-521 Deblin, Poland
{l.setlak, r.kowalik}@wsosp.pl

Abstract. The subject of this paper is the advanced architecture of the power of modern aircrafts in the field of key components, power electronics power supply system PES, which are multi-pulse rectifiers (6-, 12- and 18-, 24-) pulse, and even (48-, 60-) pulse applied to the "classical" aircrafts and the aircrafts consistent with the concept of aircraft partially/fully electric "MEA/AEA". The main objective of the paper is to make a comparative analysis and presentation of the mathematical model and simulation of selected multi-pulse rectifiers. Also, in the final part of the work comparative characteristics of selected rectifiers was carried out and their analysis presented in terms of simulation and on this basis practical conclusions were drawn.

Keywords: Modeling · Multi-pulse rectifiers · More/All electric aircraft

1 Introduction

In modern aircraft, in the context of civil aviation (Airbus, Boeing), taking into account both "conventional" planes (A-320, B-777), as well as so-called civilian more electric aircrafts (A-380 and A-350XWB, B-787) and military aircrafts (Lockheed Martin) in the field of "classic" aircrafts (F-18, F-16) and those in line with the modern trend of More/All Electric Aircraft ("MEA/AEA") Joint Strike Fighter (JSF) F-35 and F-22 Raptor, you can see many significant changes, in particular in the field of on-board Electric Power Systems (EPS). Among other things, you can see the dynamic development of on-board power architectures in terms of Power Electronics Systems (PES), which are key components of the multi-pulse rectifiers (6-, 12-, and 18-, 24-) pulse [1–3]. Modern aircrafts are equipped with advanced modern power supply systems (EPS), together with the systems of HVDC (High Voltage Direct Current) and power systems of HVAC (High Voltage Alternating Current), power electronics systems (PES) and the innovative avionics systems [4–7].

K. Ntalianis and A. Croitoru (Eds.): APSAC 2017, LNEE 489, pp. 244–250, 2019.
https://doi.org/10.1007/978-3-319-75605-9_34

2 Comparative Analysis and Mathematical Model of Multi-pulse Rectifiers of "Conventional" Aircraft and Aircraft Consistent with the Concept of "MEA/AEA"

2.1 Comparative Analysis of Multi-pulse Rectifiers (6-, 12- and 18-, 24-) and (48-, 60-) Pulse as Regards the System PES

Please no Example of a comparative analysis of multi-pulse rectifiers and their mathematical models are presented basing on the rectifiers (12- and 24-) pulse selected from the group of (6-, 12- and 18-, 24-) pulse rectifiers. These rectifiers and their mathematical models were compared with the 48-pulse rectifier selected from the group of (48- and 60-) pulse rectifiers (Fig. 1).

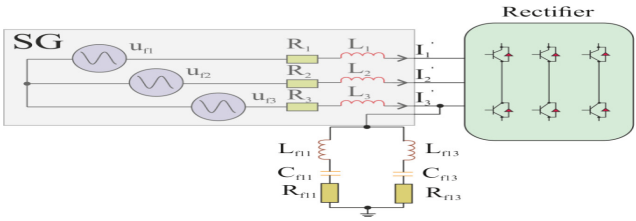

Fig. 1. Exemplary block diagram of PES system consistent with the concept of MEA/AEA

The figure above illustrates the modern architecture of the power system, used on the most advanced aircrafts (Airbus, Boeing) as regards the PES, which is also the main component of the ASE. A main power supply of 3-phase AC of this architecture is an electric machine (motor/generator) that uses permanent magnets instead of rotor windings. It is referred to in the literature as a PMSM (Permanent Magnets Synchronous Machine). For practical applications it is used for electronic control of the excitation with integrated power inverter and rectifier, sensor and electronics inverter. Therefore, in the structure of the rectifier, using multi-pulse rectifiers (12- and 24-) pulse, set of filters was applied, developed on the basis of two parallel-connected RLC elements. This kind of solution in the final stage will eliminate some unwanted signals, affecting the final shape of the waveform of the output voltage of the multi-pulse rectifier. As a result, basing on a block diagram of the power system architecture in terms of PES system, mathematical notation of physical phenomena of the power of MEA for the voltage at the input of the energy-electronic transducer unit AC/DC will take the following form [8, 9]

$$\begin{aligned} u_1 &= U_m \sin\left(\omega t + \frac{\pi}{2}\right) \\ u_2 &= U_m \sin\left(\omega t - \frac{\pi}{6}\right) \\ u_3 &= U_m \sin\left(\omega t - \frac{5\pi}{6}\right) \end{aligned} \tag{1}$$

Basing on the above expression (1), we see that the waveform shape (waveform), which shows the input voltage of the same amplitude U_m, is different only by phase shift value. In the case of the voltage flowing through the filter unit, mathematical notation (model) takes the following form [10]

$$\begin{aligned} u_{f1} &= u_1 + R_1 i_1 + L_1 \frac{di_1}{dt} \\ u_{f2} &= u_2 + R_2 i_2 + L_2 \frac{di_2}{dt} \\ u_{f3} &= u_3 + R_3 i_3 + L_3 \frac{di_3}{dt} \end{aligned} \tag{2}$$

After adoption of the initial assumptions and determinations, where u_1, u_2 and u_3 are voltages of 3-phase AC generated by an open circuit at the terminals of the electric machine PMSM with a maximum value of the amplitude U_m; u_{f1}, u_{f2} and u_{f3} determine the value of voltage in the electrical filter circuit RLC and ω indicates the angular speed of the electric machine PMSM. Therefore, the resistance in the filter circuit is analyzed is expressed as the sum of the resistance elements, included in the electric machine PMSM and the resistance of the wires connecting the various components of the power PES in accordance with a trend of MEA/AEA. Also, the mathematical notation of occurring phenomena is as follows

$$R_{z1} = R_{f11} - R_{f13} \tag{3}$$

Analyzing the architecture of the system PES for the case of inductance in the filter circuit, as illustrated in the Fig. 1, a mathematical notation takes a similar form

$$L_{z1} = L_{f11} - L_{f13} \tag{4}$$

After adoption of the following indications and assumptions for analysis in the field of power architecture PES, where i_1, i_2 and i_3 are the values of the currents in a 3-phase set for the branch base from 1 to 3; $I_p^{'}$ is the electric current that occurs at the rectifiers input, which is responsible for the performance of key functions, which is to transform the voltage and AC on the DC power (AC/DC), implemented by the TRU (Transformer Rectifier Unit). Based on the above, and taking into account the above Eq. (1)–(4) you can determine the equations describing all physical electrical phenomena in the considered filtering circuit. Therefore [11, 12]

$$\begin{gathered} L_{f11} \frac{d^2 i_{f11}}{dt^2} + R_{f11} \frac{di_{f11}}{dt} + \frac{1}{C_{f11}} i_{f11} = \frac{du_f}{dt} \\ = L_{f13} \frac{d^2 i_{f13}}{dt^2} + R_{f13} \frac{di_{f13}}{dt} + \frac{1}{C_{f13}} i_{f13} \\ i_{f11} + i_{f13} = I_f = I_p^{'} - I_p \end{gathered} \tag{5}$$

where L_{f11}, C_{f11} and L_{f13}, C_{f13} are respectively the inductance and capacitance on the respective elements L, C in the filter circuit in each branch of the circuit concerned.

This filter is designed to filter individual harmonics (in our case harmonics of 11 and 13 are filtered). Additionally, as in the case of EPS supply system for an electric machine PMSM, also in the case of a PES system there is the resistance of the filter present in the circuit architecture, which is denoted by R_{f11} and R_{f13}. The individual harmonic voltages of the current are produced by the 12-pulse rectifier selected from the group of multi-pulse rectifiers (6-, 12- and 18-, 24-) pulse [13].

2.2 48-Pulse Rectifiers

For the currently used power electronics supply systems PES elements responsible for the conversion of the AC to DC power, are multi-pulse sensors, and in most cases 12-pulse or 24-pulse rectifiers are used. However, in the scientific literature [8, 14] developed models of 48-pulse rectifiers can be found. The results presented in the literature [9, 14] contained the simulation from which it can be seen that instability of 48-pulse rectifier is possible resulting from overloading the system and the possibility of changes in the voltage harmonics. Emerging inconsistencies can be eliminated indirectly by using the appropriately phased voltage in three-phase system of 7.5°, this value will provide valuable full effect of a 48-pulse rectifier. The remainder of the paper are examples of simulations of multi- pulse rectifiers of 12- and 24-pulse and their comparison with the 48-pulse rectifiers was made [15].

3 Simulation of Selected Multi-pulse Rectifier of "Conventional" Aircraft and Aircraft Consistent with the Concept of "MEA/AEA"

3.1 Simulation of 12- and 24-Pulse Rectifiers

However, due to limitations in the volume of this paper (6 pages), the authors were unable to provide in-depth comparative analysis and simulations of (12- and 24-) pulse power electronics rectifiers. Considerations in this area have been made in other articles [2, 15]. Authors have confined themselves only to the analysis and simulation of 48-pulse rectifiers in the context of (12- and 24-) pulse rectifiers.

3.2 Simulation of 48-Pulse Rectifiers

The results obtained at this stage of the study are presented below (Figs. 2, 3, 4 and 5).

In the shown graphs there is a noticeable jump of waveforms of AC currents for the time of 0.025 s which is caused by the switching of the rectifier circuit. At the same time load receivers were connected.

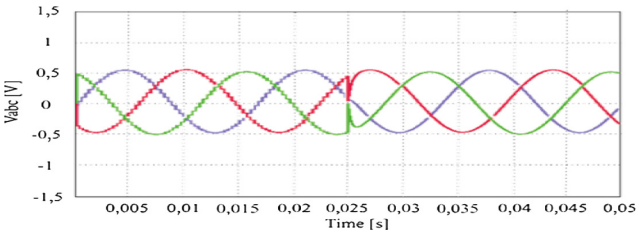

Fig. 2. Voltage waveform in the TRU in accordance with the concept of MEA/AEA for the angle of the voltage harmonic 7.5°

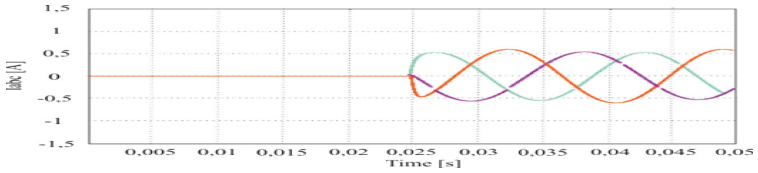

Fig. 3. The waveform of the current in the TRU in accordance with the concept of MEA/AEA for the angle of the voltage harmonic 7.5°

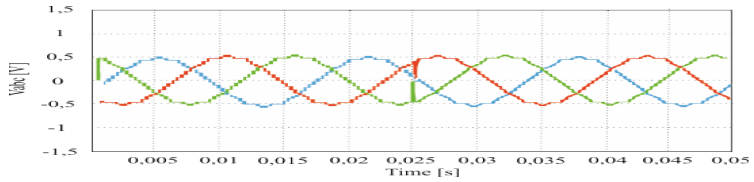

Fig. 4. Voltage waveform in the TRU in accordance with the concept of MEA/AEA for the angle of the voltage harmonic 30°

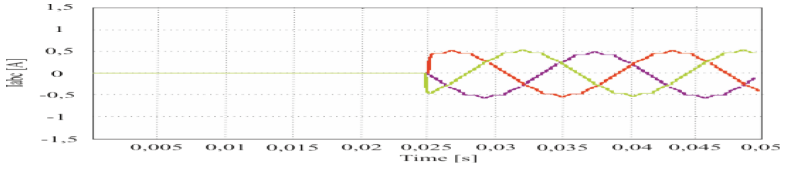

Fig. 5. The waveform of the current in the TRU in accordance with the concept of MEA/AEA for the angle of the voltage harmonic 30°

4 Conclusion

Based on results of calculations and measurements of the simulation model of modern power systems ASE in terms of the system PES it can be concluded that the systems comply with the concept of a MEA, based on the presented graphs showing voltage and

current waveforms (Figs. 2 and 3) they have a higher efficiency of operation than in the case of systems used on "classical" aircraft. In addition, the two 24-pulse circuits convert the voltage harmonics in phase by 7.5° from each other, which in turn ensures the correct operation of the 48-pulse transmitter (Figs. 4 and 5). In addition, in this system when we are dealing in various loads, system power will level a problem of voltage instability. In turn, changing the phase angle of voltage at a value of 30° makes the final effect of the voltage waveform and currents be significantly distorted than in the previously discussed case, which could affect unstable operation of all electrical devices, which specific plane is supplied with (Figs. 2, 3, 4 and 5). This effect is connected with mutual harmonic voltages generated by the primary power source in the form of a generator.

References

1. Wu, B.: High-Power Converters and AC Drives. IEEE Press, John Wiley & Sons Inc., Hoboken (2006)
2. Setlak, L., Ruda, E.: Review, analysis and simulation of advanced technology solutions in power electronics systems (PES) of more electric aircraft. World Acad. Sci. Eng. Technol. **9** (10), 1–13 (2015)
3. Abu-Rub, H., Malinowski, M., Al-Haddad, K.: Power Electronics for Renewable Energy Systems, Transportation, and Industrial Applications, 1st edn. John Wiley-IEEE Press, Hoboken (2014)
4. Emandi, K., Ehsani, M.: Aircraft power systems: technology state of the, and future art trends, Aerospace and Electronic Systems Magazine, IEEE (2000)
5. Setlak, L., Ruda, E.: Analysis and Simulation of Advanced Technological Solutions in the Field of Power High-Voltage Direct Current (HVDC) of Modern Aircraft in line with the Trend of More Eelectric Aircraft (MEA), Technical Transactions Electrical Engineering, 3-E/2016. Cracow University and Technology, Cracow (2016)
6. Bozhko, S., Tao, Wu,Y., Asher, G.M.: More-electric aircraft electrical power system accelerated functional modeling. In: International Power Electronics and Motion Control Conference, Ohrid, Republic of Macedonia, Ohrid (2010)
7. Setlak, L., Kowalik, R.: Mathematical modeling and simulation of selected components on-board autonomous power supply system (ASE), in accordance with the concept of a more electric aircraft (MEA). In: 18th International Scientific Conference on Electric Power Engineering, Kouty nad Desnou, Czech Republic, pp. 1–6. IEEE (2017)
8. Singh, B., Gairola, S., Singh, B.N., Chandra, A., Haddad, K.A.: Multi-pulse AC-DC converter for improving power quality: a review. IEEE Trans. Power Deliv. **23**(1), 260–281 (2008)
9. Raghuvanshi, S., Singh, N.: Comparative analysis of 36, 48, 60 pulse AC-DC controlled multipulse converter for harmonic mitigation. Int. J. Adv. Res. Comput. Eng. Technol. (IJARCET) **3**(4), 1159–1163 (2014)
10. Hernadi, A., Taufik, T., Makbul, A.: Modeling and Simulation of 6-Pulse and 12-Pulse Rectifiers under Balanced and Unbalanced Conditions with Impacts to Input Current Harmonic, IEEE (2008)
11. Gong, G., Drofenik, U., Kolar, J.W.: 12-pulse rectifier for more electric aircraft applications. ETH Zurich, Power Electronic Systems Laboratory, ICIT (2003)

12. Monroy, A.O., Le-Huy, H., Lavoie, C.: Modeling and Simulation of a 24-pulse Transformer Rectifier Unit for More Electric Aircraft Power System, Electrical Systems for Aircraft, Railway and Ship Propulsion (ESARS) (2012)
13. Singh, B., Singh, B.N., Chandra, A., Al-Haddad, K., Pandey, A., Kothari, D.P.: A review of three-phase improved power quality AC-DC converters. IEEE Trans. Power Deliv. **51**(3), 641–660 (2004)
14. El-Moursi, M.S., Sharaf, A.M.: Novel controllers for the 48-pulse VSC STATCOM and SSSC for voltage regulation and reactive power compensation. IEEE Trans. Power Syst. **20** (4), 1985–1997 (2005)
15. Setlak, L., Kowalik, R.: Review, comparative analysis and simulation of selected components of modern power systems (EPS, PES) of 'classical' aircraft and 'More/All Electric Aircraft' (MEA/AEA). WSEAS Trans. Power Syst. **11**, 338–346 (2016)

A Sufficient Asymptotic Stability Condition in Generalised Model Predictive Control to Avoid Input Saturation

Paolo Mercorelli(✉)

Institute of Product and Process Innovation, Leuphana University of Lueneburg, Volgershall 1, 21339 Lueneburg, Germany
mercorelli@uni.leuphana.de

Abstract. The goal of this contribution is presenting a Theorem which states the asymptotic stability of a feedback controlled system with a Linear Generalized Model Predictive Control (LGMPC). Concerning the asymptotic stability, a sufficient and constructive condition on the weight matrices of the cost function used in the optimization problem in LGMPC for one step prediction horizon is demonstrated. The condition consists of a lower bound for one of these matrices. The obtained condition is explained and discussed by means of some physical considerations. The second part of this contribution is devoted to the saturation case and proves a sufficient condition for obtaining asymptotic stability and saturation avoidance.

Keywords: Model predictive control · Optimization · Matrix algebra
Discrete systems · Linear systems

1 Introduction

Improvements of the tracking of a desired trajectory are very often achieved by means of a Model predictive control approach. The linear prediction algorithm is used for improvement of the tracking performances of an adaptive controller. Because of that, MPC is commonly used in drives control applications [1, 2]. Constraints and multivariable industrial processes can be successfully managed by MPC, that is why this control approach has been applied in a wide range of automotive and process control communities [3]. In the meantime, the MPC applications are usually limited by slow dynamic systems because of the computation burden in solving optimization problems on-line [3]. Studying of application of MPC in mechatronic systems for servo design has attracted interest of a great number of researchers. The reason for that is development of a microprocessor technology. There are some advantageous examples in many mechatronic systems such as electrical motor control [4], two stage actuation system control and machine tool chattering control [5]. There is also a fast development of different advanced techniques integrated within MPC for the performance improvement [6]. One of the most interesting problems in the contest of optimization consists of finding conditions on the asymptotic stability. In this contribution, lower bounds of matrix which characterizes the cost function are found to guarantee the

K. Ntalianis and A. Croitoru (Eds.): APSAC 2017, LNEE 489, pp. 251–257, 2019.
https://doi.org/10.1007/978-3-319-75605-9_35

asymptotic stability of the optimal solution for one step prediction horizon. The condition is a constructive one and straightforward to be interpreted. This contribution is divided into the following parts. Section 2 proves a property of the LGMPC in case without and with saturation for one step prediction horizon. Conclusions close the paper.

2 Asymptotic Stability Sufficient Constructive Condition in GMPC

Let us take the discrete SISO linear system into consideration:

$$\mathbf{z}(\mathrm{k}+1) = \mathbf{A}_\mathrm{k}\mathbf{z}(\mathrm{k}) + \mathbf{B}_k u_{mpc}(k), \tag{1}$$

$$\mathrm{y}(\mathrm{k}) = \mathbf{H}_\mathrm{k}\mathbf{z}(\mathrm{k}), \tag{2}$$

which is obtained by a discretization of a linear continuous system using a sampling time which equals T_s .$u_{mpc}(k)$. represents the first element of the vector of the optimal solution as calculated in [7] for the following cost function:

$$\begin{aligned} J = &\tfrac{1}{2}\sum_{j=1}^{N}(y_d(k+j)-\hat{y}(k+j))^T \boldsymbol{Q}_p(y_d(k+j)-\hat{y}(k+j)) \\ &+ \sum_{j=1}^{N}\left(\Delta u_{mpc}(k+j-1)\right)^T \boldsymbol{R}_p \Delta u_{mpc}(k+j-1), \end{aligned} \tag{3}$$

where $\Delta u_{mpc}(k) = \Delta u_{mpc}(k) - \Delta u_{mpc}(k-1), y_d(k+j), j = 1, 2\ldots\mathrm{N}$ is the output reference trajectory and N is the prediction horizon, and $\mathbf{Q}_\mathrm{p}$ and $\mathbf{R}_\mathrm{p}$ are non-negative definite matrices. Furthermore, the solution minimizing performance index (3) may be obtained by solving:

$$\frac{\partial \mathbf{J}}{\partial \Delta \mathbf{U}_\mathrm{mpc}} = 0. \tag{4}$$

It is known for instance from [7] that the optimal solution is:

$$\Delta u_{mpc}(k) = (\mathbf{F}_{1p}^T\mathbf{Q}_p\mathbf{F}_{1p} + \mathbf{R}_p)^{-1}\mathbf{F}_{1p}^T\mathbf{Q}_p\left(\mathbf{Y}_{\mathrm{d}_p}(k) - \mathbf{G}_p\mathbf{z}(\mathrm{k})\right). \tag{5}$$

In case of one step prediction horizon $\mathbf{F}_{1_p} = \mathbf{H}_k\mathbf{B}_k$ and $\mathbf{G}_p = \mathbf{H}_k\mathbf{A}_k$ and where $\mathbf{Y}_{\mathrm{d}_p}(k)$ is the desired output column vector. Matrices $\mathbf{Q}_p$ and $\mathbf{R}_p$ are diagonal and positive defined. It is to notice that matrix $\mathbf{R}_p$ collapses in a scalar in case of one step prediction horizon, $\mathbf{R}_p = \mathrm{r}$.

Theorem 1. Under the hypothesis that system (1) is asymptotically stable, i.e. $\left(\|\mathbf{A}_k\|_2 < 1\right)$, where

$$\|\mathbf{A}_k\|_{2=}\sqrt{max\lambda_{\mathrm{i}}\left(\mathbf{A}_k^T\mathbf{A}_k\right)}\ \text{for i = 1,2,. . ., n} \in \mathrm{N}$$

represents the root of the maximal eigenvalue of matrix $\mathbf{A}_k^T\mathbf{A}_k$, then $\forall\mathbf{R}_p$ diagonal and positive defined matrix such that:

$$\left\|\mathbf{R}_p\right\|_2 > \frac{\left\|\mathbf{B}_k\mathbf{F}_{1p}^T\mathbf{Q}_p\mathbf{G}_p\right\|_2}{1-\|A_k\|_2} \tag{6}$$

and

$$\begin{aligned}&\left\|\mathbf{A}_k-\mathbf{B}_k(\mathbf{F}_{1p}^T\mathbf{Q}_p\mathbf{F}_{1p}+\mathbf{R}_p)^{-1}\mathbf{F}_{1p}^T\mathbf{Q}_p\mathbf{G}_p\right\|_2 <\\&\left\|\mathbf{A}_k+\mathbf{B}_k(\mathbf{F}_{1p}^T\mathbf{Q}_p\mathbf{F}_{1p}+\mathbf{R}_p)^{-1}\mathbf{F}_{1p}^T\mathbf{Q}_p\mathbf{G}_p\right\|_2,\end{aligned} \tag{7}$$

the system (1) controlled with (5) results to be asymptotically stable for one step prediction horizon.

Proof 1. For one prediction step is considered, then according to [7], it follows that:

$$\mathbf{F}_{1_p} = [\mathbf{H}_k\mathbf{B}_k], \tag{8}$$

$$\mathbf{G}_p = [\mathbf{H}_k\mathbf{A}_k]. \tag{9}$$

Combining Eq. (1) with (5), this expression is obtained:

$$z(\mathrm{k}+1) = \mathbf{A}_{\mathrm{k}}\mathbf{z}(\mathrm{k}) + \mathbf{B}_k(\mathbf{F}_{1p}^T\mathbf{Q}_p\mathbf{F}_{1p}+\mathbf{R}_p)^{-1}\mathbf{F}_{1p}^T\mathbf{Q}_p\left(\mathbf{Y}_{\mathrm{d}_p}(k)-\mathbf{G}_p\mathbf{z}(k)\right), \tag{10}$$

which is equivalent to write:

$$\mathbf{z}(\mathrm{k}+1) = \left(\mathbf{A}_k-\mathbf{B}_k(\mathbf{F}_{1p}^T\mathbf{Q}_p\mathbf{F}_{1p}+\mathbf{R}_p)^{-1}\mathbf{F}_{1p}^T\mathbf{Q}_p\mathbf{G}_p\right)\mathbf{z}(k) + \mathbf{B}_k(\mathbf{F}_{1p}^T\mathbf{Q}_p\mathbf{F}_{1p}+\mathbf{R}_p)^{-1}\mathbf{F}_{1p}^T\mathbf{Q}_p\mathbf{Y}_{d_p}(\mathrm{k}). \tag{11}$$

$$\text{If}\quad \left\|\mathbf{R}_p\right\|_{2>}\frac{\left\|\mathbf{B}_k\mathbf{F}_{1p}^T\mathbf{Q}_p\mathbf{G}_p\right\|_2}{1-\|A_k\|_2}, \tag{12}$$

considering that $\left\|\mathbf{R}_p\right\| > 0$,

$$\|\mathbf{A}_k\|_2 + \left\|\mathbf{R}_p\right\|_2^{-1}\left\|\mathbf{B}_k\mathbf{F}_{1p}^T\mathbf{Q}_p\mathbf{G}_p\right\|_2 < 1. \tag{13}$$

Considering that $\left\|\mathbf{R}_p\right\|_2 = \mathrm{r}$ is a scalar one, the following condition can be derived:

$$\|\mathbf{A}_k\|_2 + \left\|\mathbf{B}_k r^{-1}\mathbf{F}_{1p}^T\mathbf{Q}_p\mathbf{G}_p\right\|_2 < 1. \tag{14}$$

Being expression $\mathbf{F}_{1p}^T\mathbf{Q}_p\mathbf{F}_{1p}$ a scalar for one step prediction horizon and

$$\mathbf{F}_{1p}^T\mathbf{Q}_p\mathbf{F}_{1p} > 0,$$

as a consequence, it follows that:

$$\|\mathbf{A}_k\|_2 + \left\|\mathbf{B}_k(\mathbf{F}_{1p}^T\mathbf{Q}_p\mathbf{F}_{1p} + \mathrm{r})^{-1}\mathbf{F}_{1p}^T\mathbf{Q}_p\mathbf{G}_p\right\|_2 < 1. \tag{15}$$

Considering the norm properties and condition (7), then:

$$\begin{aligned}\left\|\mathbf{A}_k - \mathbf{B}_k(\mathbf{F}_{1p}^T\mathbf{Q}_p\mathbf{F}_{1p} + \mathrm{r})^{-1}\mathbf{F}_{1p}^T\mathbf{Q}_p\mathbf{G}_p\right\|_2 &< \left\|\mathbf{A}_k + \mathbf{B}_k(\mathbf{F}_{1p}^T\mathbf{Q}_p\mathbf{F}_{1p} + \mathrm{r})^{-1}\mathbf{F}_{1p}^T\mathbf{Q}_p\mathbf{G}_p\right\|_2 \\ &< \|\mathbf{A}_k\|_2 + \left\|\mathbf{B}_k(\mathbf{F}_{1p}^T\mathbf{Q}_p\mathbf{F}_{1p} + \mathrm{r})^{-1}\mathbf{F}_{1p}^T\mathbf{Q}_p\mathbf{G}_p\right\|_2 < 1.\end{aligned} \tag{16}$$

To conclude:

$$\left\|\mathbf{A}_k - \mathbf{B}_k(\mathbf{F}_{1p}^T\mathbf{Q}_p\mathbf{F}_{1p} + \mathrm{r})^{-1}\mathbf{F}_{1p}^T\mathbf{Q}_p\mathbf{G}_p\right\|_2 < 1. \tag{17}$$

Condition (17) states that the eigenvalues of the controlled system described by (11) are all inside the complex unit circle and thus system (11) results to be asymptotically stable.

The asymptotic stability represents the necessary condition of the optimality of a controlled system. In order to interpret the result, let us observe a linear mechanical system including a mass-spring system in which it is known that the eigenvalues can variate in the whole real and complex domain as functions of the mass which state the system dynamics. The following considerations can be done:

- Case of high inertial system:
  This is the case in which mass $\mathrm{m} \to +\infty$, then, because of the discretisation, it follows:
  $\left(\|\mathbf{A}_k\|_2 - 1\|\right) \to 0$, with, according to the Landau notation, $\mathcal{O}\left(\|\mathbf{A}_k\|_2 - 1\right) = \mathcal{O}\left(\frac{1}{m}\right)$, but in the meantime, $\mathcal{O}\left(\mathbf{B}_k\mathbf{F}_{1p}^T\right) = \mathcal{O}\left(\mathbf{B}_k\mathbf{B}_k^T\right) = \mathcal{O}\left(\frac{1}{m^2}\right)$. For a very slow system $\left\|\mathbf{R}_p\right\|_2 \to 0$, and parameter $\left\|\mathbf{R}_p\right\|_2$, according to (6), is present in the denominator function of the optimal solution of (5) and in this case, small values are devoted to speed up the system.
- Case of low inertial system:
  This is the case in which mass $\mathrm{m} \to 0$, then, because of the discretisation, it follows:

$\|\mathbf{A}_k\|_2 \rightarrow 0.$,with $\mathcal{O}(\|\mathbf{A}_k\|_2) = \mathcal{O}(\frac{1}{m})$, but in the meantime, $\mathcal{O}\left(\mathbf{B}_k\mathbf{F}_{1p}^T\right) = \mathcal{O}(\mathbf{B}_k\mathbf{B}_{\mathrm{k}}^T) \rightarrow +\infty$ in which $\mathcal{O}(\mathbf{B}_k\mathbf{B}_{\mathrm{k}}^T) = \mathcal{O}(\frac{1}{m^2})$. For a very fast system $\|\mathbf{R}_k\|_2 \rightarrow +\infty$ and $\mathbf{R}_p$, according to (6), is present in the denominator function of the optimal solution (5) and in this case, large values are devoted to slow down the system.

So, it is possible to conclude that a high inertial system needs relatively small values of $\|\mathbf{R}_p\|_2$ to be stabilised. On the contrary, a low inertial system needs large values of $\|\mathbf{R}_p\|_2$ to be stabilised.

3 The Saturation Case

Proposition 1. Let us take the following discrete SISO linear system as before into consideration:

$$\mathbf{z}(\mathrm{k}+1) = \mathbf{A}_{\mathrm{k}}\mathbf{z}(\mathrm{k}) + \mathbf{B}_k u_{mpc}(\mathrm{k}), \tag{18}$$

$$\mathrm{y}(\mathrm{k}) = \mathbf{H}_{\mathrm{k}}\mathbf{z}(\mathrm{k}), \tag{19}$$

and let U_{max} be a real value with

$$\left|u_{mpc}(\mathrm{k})\right| < \mathrm{U}_{\max} \forall k, \tag{20}$$

then (18) with the input saturation defined in (20) and controlled with the control law in (5) is asymptotically stable and its input avoids the saturation constraint if the following conditions hold:

$$\mathrm{r} = \|\mathbf{R}_p\|_2 > max\left\{\frac{\left\|\mathbf{B}_k\mathbf{F}_{1p}^T\mathbf{Q}_p\mathbf{Y}_{\mathrm{d}_p}(k)\right\|_2}{\mathrm{U}_{max}} - \left\|\mathbf{F}_{1p}^T\mathbf{Q}_p\mathbf{F}_{1p}\right\|_2, \frac{\left\|\mathbf{B}_k\mathbf{F}_{1p}^T\mathbf{Q}_p\mathbf{G}_p\right\|_2}{1 - \|\mathbf{A}_k\|_2}\right\}, \tag{21}$$

and

$$\left\|\mathbf{A}_k - \mathbf{B}_k(\mathbf{F}_{1p}^T\mathbf{Q}_p\mathbf{F}_{1p} + \mathbf{R}_p)^{-1}\mathbf{F}_{1p}^T\mathbf{Q}_p\mathbf{G}_p\right\|_2 < \left\|\mathbf{A}_k + \mathbf{B}_k(\mathbf{F}_{1p}^T\mathbf{Q}_p\mathbf{F}_{1p} + \mathbf{R}_p)^{-1}\mathbf{F}_{1p}^T\mathbf{Q}_p\mathbf{G}_p\right\|_2 \tag{22}$$

Proof 2. The demonstration is straightforward. In fact, just considering that:

$$\left|u_{mpc}(\mathrm{k})\right| < \mathrm{U}_{\max} \forall k,$$

and thus, considering the input of the optimal predicted expression (11), it is enough that the following condition holds:

$$\left\|\mathbf{B}_k(\mathbf{F}_{1p}^T\mathbf{Q}_p\mathbf{F}_{1p}+\mathbf{R}_p)^{-1}\mathbf{F}_{1p}^T\mathbf{Q}_p\mathbf{Y}_{\mathrm{d}_p}(k)\right\|_2 <\mathrm{U}_{\max}. \tag{23}$$

This can be written as:

$$\left\|\mathbf{B}_k(\mathbf{F}_{1p}^T\mathbf{Q}_p\mathbf{F}_{1p}+\mathbf{R}_p)^{-1}\mathbf{F}_{1p}^T\mathbf{Q}_p\mathbf{Y}_{\mathrm{d}_p}(k)\right\|_2 <\left\|(\mathbf{F}_{1p}^T\mathbf{Q}_p\mathbf{F}_{1p}+\mathbf{R}_p)^{-1}\right\|_2\left\|\mathbf{B}_k\mathbf{F}_{1p}^T\mathbf{Q}_p\mathbf{Y}_{\mathrm{d}_p}(k)\right\|_2 <\mathrm{U}_{\max}. \tag{24}$$

Considering that $\mathbf{R}_p$ and $\mathbf{F}_{1p}^T\mathbf{Q}_p\mathbf{F}_{1p}$ are both positive scalars in case of one step prediction horizon, then:

$$\left\|\mathbf{F}_{1p}^T\mathbf{Q}_p\mathbf{F}_{1p}\mathbf{R}_p\right\|_2 <\frac{\left\|\mathbf{B}_k\mathbf{F}_{1p}^T\mathbf{Q}_p\mathbf{Y}_{\mathrm{d}_p}(k)\right\|_2}{\mathrm{U}_{max}}. \tag{25}$$

And thus, to guarantee the asymptotic stability and anti-saturation input of system (18), it follows:

$$\mathrm{r}=\left\|\mathbf{R}_p\right\|_2 > max\left\{\frac{\left\|\mathbf{B}_k\mathbf{F}_{1p}^T\mathbf{Q}_p\mathbf{Y}_{\mathrm{d}_p}(k)\right\|_2}{\mathrm{U}_{max}}-\left\|\mathbf{F}_{1p}^T\mathbf{Q}_p\mathbf{F}_{1p}\right\|_2,\frac{\left\|\mathbf{B}_k\mathbf{F}_{1p}^T\mathbf{Q}_p\mathbf{G}_p\right\|_2}{1-\left\|\mathbf{A}_k\right\|_2}\right\}. \tag{26}$$

4 Conclusion

One of the most important problems in the context of optimization using LMPC is represented by conservative conditions on the asymptotic stability. This paper presents a sufficient and constructive condition for the asymptotic stability of an LMPC for one step prediction horizon calculating lower bound of the unique element of matrix $\mathbf{R}$ which represents the weight of the input in a typical given cost function. A physical interpretation of the result is given in the light of some physical considerations. In the second part of the paper the saturation case is considered and a sufficient condition to obtain the asymptotic stability and saturation avoidance is proven.

References

1. Mercorelli, P.: A switching Kalman Filter for sensorless control of a hybrid hydraulic piezo actuator using MPC for camless internal combustion engines. In: Proceedings of the IEEE International Conference on Control Applications, pp. 980–985 (2012)
2. Mercorelli, P.: A switching model predictive control for overcoming a hysteresis effect in a hybrid actuator for camless internal combustion engines. In: Proceedings of the IEEE PRECEDE 2011 – International Workshop on Predictive Control of Electrical drives and Power Electronics, pp. 10–16 (2011)

3. Qin, S.J., Badgwell, T.A.: A survey of industrial model predictive control technology. Control Eng. Pract. **11**(7), 733–764 (2003)
4. Bolognani, S., Peretti, L., Zigliotto, M.: Design and implementation of model predictive control for electrical motor drives. IEEE Trans. Ind. Electron. **56**(6), 1925–1936 (2009)
5. Neelakantan, V.A., Washington, G.N., Bucknor, N.K.: Model predictive control of a two-stage actuation system using piezoelectric actuators for controllable industrial and automotive brakes and clutches. J. Intell. Mater. Syst. Struct. **19**(7), 845–857 (2008)
6. Hu, Z., Farson, D.F.: Design of a waveform tracking system for a piezoelectric actuator. In: Proceedings of the Institution of Mechanical Engineers, vol. 222, pp. 11–21 (2008)
7. Sunan, H., Kiong, T.K., Heng, L.T.: Applied Predictive Control. Springer, London (2002). https://doi.org/10.1007/978-1-4471-3725-2

Harmonic Analysis in a Node Where Exist a Deformed Regime

Eleonora Darie[1(✉)] and Emanuel Darie[2]

[1] Technical University of Civil Engineering, Bucharest, Romania
eleonora.darie@gmail.com
[2] Police Academy, Bucharest, Romania
edarie@gmail.com

Abstract. In this paper, we analyze the deforming regime, present in a 0.4 kV electrical network node, node in which, at present, no compensatory measures are applied. Depending on the results of the analysis, the compensation measures for the deforming regime present in the analyzed node will be adopted. The existence of harmonic currents increases the actual values of currents in power line conductors and neutral conductors, which can cause fire in buildings and can cause phenomena that induce inadvertent disconnections of power lines and thus interruption of consumer operation.

Keywords: Harmonic analysis · Deforming regime · Nonlinear receiver
Power quality · Active filters · Passive filters · Harmonic current
Harmonic voltage

1 Introduction

The deforming phenomenon is widespread in all areas of human activity and is continually accentuated as a consequence of the modernization of all activities through the use of non-linear receivers and electrical installations [6]. Therefore, for the most part, the permanent functioning regime of the energy system has become non sinusoidal. As a result, new phenomena, which accompany the deforming regime, will appear both now and in the next stages. It is possible to highlight faults of the capacitor batteries as well as the malfunctions of the protection and signaling installations, which can have important technical and economic consequences. Also, the quality of the power supply is affected, thus creating great problems in ensuring it to the appropriate parameters according to the regulations in force. As the deforming regime is discovered in different network nodes, especially industrial consumers, measures are taken to mitigate it. In general, measures consist of installing active or passive filters [6].

The filters retain, partially or totally, the harmonic currents injected into the respective nodes by the nonlinear receivers existing to the consumers. Regardless of the type of filter used, its efficiency is a maximum for upstream electrical installations at the node where the filter is installed and is zero in all downstream installations at the node where it is installed and the consequences are severe.

K. Ntalianis and A. Croitoru (Eds.): APSAC 2017, LNEE 489, pp. 258–263, 2019.
https://doi.org/10.1007/978-3-319-75605-9_36

The effectiveness of the filters is reduced if they are installed further away from the deforming receivers.

2 Sources of Deformation

Sources that cause deformation are the electricity receivers installed at low-voltage end consumers. When connected to the mains, these receivers receive from the mains the sinusoidal current, but at the same time they produce and inject into the power supply a spectrum of sinusoidal electrical currents with frequencies different from the fundamental frequency (50 Hz). The theoretical and experimental analyzes show that important values in the produced spectra have odd harmonic currents. The range of these harmonics can reach 50, which corresponds to the frequency of 2500 Hz, generally higher values, have the currents up to the 15 ÷ 20 ranges, after which their magnitude and influence is gradually reduced.

In the power plants there are two categories of harmonic sources: voltage and current, but most of them are the sources of harmonic currents [2, 6]. In stationary non-sinusoidal regime (deforming regime), the state quantities of the electric circuits (voltage and current) are periodic functions, which correspond to the relation:

$$f(t) = f(t + m \cdot T), m \in Z \tag{1}$$

in which: Z – is the set of integers; T – the period of function.

According to the theory of signals, a periodic signal of finite energy and satisfying the Dirichlet conditions can be represented by a Fourier series [1, 3]. In the theory of electric circuits, the harmonic Fourier series is frequently used:

$$f(t) = \sum_{k=0}^{\infty} A_k \cdot \sin(k\omega t + \varphi_k), \tag{2}$$

in which the harmonic sinusoidal components, infinite number, having the rank k ($k \in N$), the amplitude of A_k and the angular phase φ_k are emphasized. The term $k = 1$, is the fundamental harmony and, in the European electricity system, has the frequency $f_1 = 50$ Hz.

Fourier analysis of a periodic function consists in determining the parameters in relation (2) – amplitudes and angular phases - which define the Fourier series associated with this function. Fourier analysis of periodic functions is also called harmonic analysis.

2.1 Characteristic Sizes of Deforming Regime

Among the characteristic sizes of deformed electric currents circulating through various installations, some are more representative [1]:

2.1.1 Effective Value of the Deformed Curve of the Current

Determine the relative values of the harmonic currents resulting from the harmonic analysis that are related to the effective value of the fundamental sinusoidal curve:

$$I_{def} = \sqrt{I_1^2 + \sum_{k=2}^{n} I_k^2} = I_{RMS}, \tag{3}$$

in which: I_{def} - The effective RMS (Root Mean Square) value of the deformed curve of the electrical current; I_1 - The effective reference value of the fundamental sinusoidal curve (50 Hz); $\sum_{k=2}^{n} I_k^2$ – The square of the deforming residue; k – An index that designates the harmonic rank [4].

2.1.2 Current Deformation Residue

It is defined by the expression:

$$I_{rezid} = \sqrt{\sum_{k=2}^{n} I_k^2}, \tag{4}$$

is an important size, as it indicates the additional charge [1] of the conductors to the fundamental current.

2.1.3 Distortion Factors (Reported to Fundamental)

They are associated with the curves of electric current in the measuring nodes and must not exceed certain values provided by the regulations in force.

The calculated and displayed values of the measuring instruments are expressed for the electrical currents and the electrical voltage, using the following relations:

$$THDI = \frac{\sqrt{\sum_{k=2}^{n} I_k^2}}{I_1} \cdot 100, [\%], \tag{5}$$

$$THDU = \frac{\sqrt{\sum_{k=2}^{n} U_k^2}}{U_1} \cdot 100, [\%]. \tag{6}$$

Generally, in electrical networks it is found that the electrical voltage is less distorted than the electrical currents.

3 Example of Harmonic Analysis

It is considered a transformer station equipped with a 20/0.4 kV, 1600 kVA transformer, which supplies all 0.4 kV installations, including the deforming receivers in a consumer's premises, through a general TGD distribution board.

At the 0.4 kV bars of the general switchboard, there is no compensating equipment and the consumer absorbs from the system, the fundamental electric current, and the spectrum of harmonic electric currents circulates to the transformer, $\sum_{k=2}^{n} I_k^2$, produced by all non-linear receivers, downstream of that consumer [6].

The nonlinear receivers cannot be connected in a balanced way to each of the three phases and the current spectra produced by them, during operation have variable structures on each phase of the electric circuits [5, 6]. Thus, the emergence of imbalances and non-symmetries is possible for each three-phase harmonic current system present in the spectrum, corresponding to any rank, regardless of whether it is rank three (3), multiple of three (3), or three (3) if it is unsymmetrical and unbalanced, it breaks down into three system components: positive (+) sequence system, negative sequence system (−), and zero (0) or homopolar sequence system.

At the neutral point of the star, the results of the three zero components are not zero, they are summed up regardless of frequency and enter the neutral conductor, having the value: $3 \cdot \sum_{k=2}^{n} I_k^{(0)}$ [6]. These components, which do not pass to medium voltage, overlap in the neutral conductor over the zero components of the fundamental current, because it is also non symmetric and unbalanced [5].

The additional charge level of the neutral conductor [2, 6], is specified by the deforming residual current, calculated with the relation:

$$I_{rezid\,N} = 3 \cdot \sqrt{\sum_{k=2}^{n} \left(I_k^{(0)}\right)^2}. \tag{7}$$

The effective value of the non-sinusoidal current distorted from the neutral conductor is calculated by:

$$I_{N(RMS)} = 3 \cdot \sqrt{I_{01}^2 + \sum_{k=2}^{n} \left(I_{0k}^{(0)}\right)^2}. \tag{8}$$

The distorted current $I_{N(RMS)}$, which contains the zero components of all fundamental and harmonic electric currents generated by all the nonlinear receivers of the consumer [3], is the real value flowing through the neutral conductors of the transformer (star-connected windings) and continuing throughout the consumer's premises [6].

Simultaneously with this situation present in the 0.4 kV transformer, the phenomenon also takes place on the part of 20 kV (windings connected in a triangle) [6].

The voltages recorded on the three phases as well as the recorded currents are shown in Fig. 1.

The variation of the THDI total harmonic distortion factor (%) and the change of the 3, 5, 7, 11, 13 (3, 5, 7, 11, 13) harmonic currents on the neutral conductor are shown in Fig. 2.

The harmonic measurement method complies with the actual regulations (IEC 61000-4-30) and the measurements were made with Power Analyzer (software Metrel Power View, v.3.0).

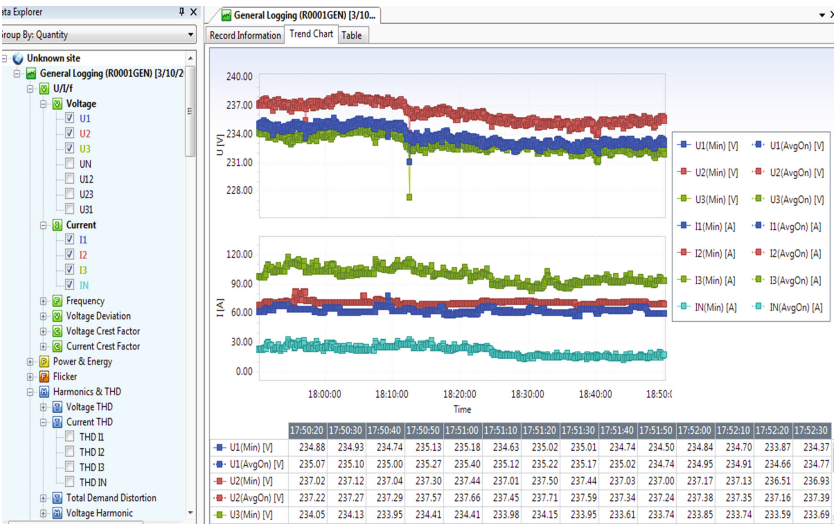

Fig. 1. Variation of the supply voltage on the three phases (V) and the phase currents and the neutral conductor (A), within the time considered.

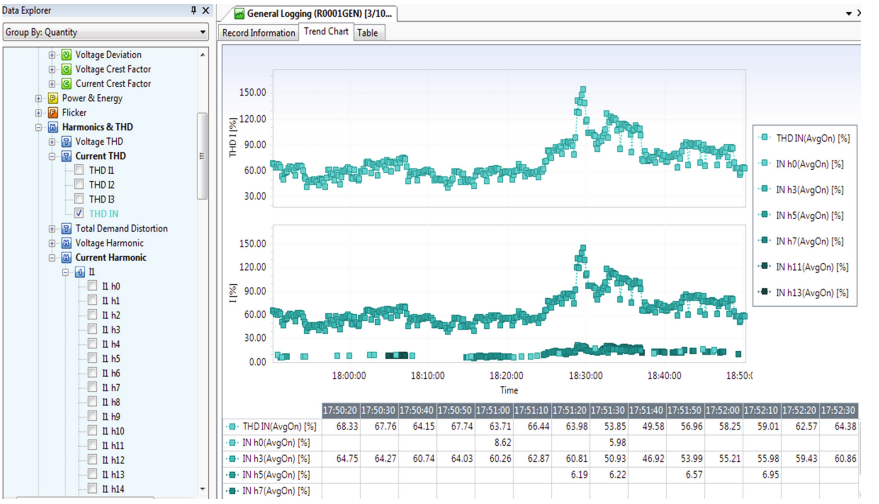

Fig. 2. Variation of current harmonics [%] of order 3, 5, 7, 11, 13 and of the total harmonic distortion factor [%], on the neutral conductor, within the time interval considered.

4 Conclusions

The additional charging of the neutral conductor is certainly not an overloading, i.e. the exceeding of the permissible value of the electric current corresponding to the section of the neutral conductor, is a situation which would be a danger to it due to excessive heating.

In the conditions of the non-symmetrical and unbalanced deformation regime, in the neutral conductor [6], apart from the harmonics of three (3) and multiple three (3) harmonics, the zero sequence components of the other harmonics are present in the spectrum, whose ranks are: 5, 7, 11, 13 and so on.

The presence and generalization of non-symmetrical and unbalanced distortions in low voltage networks due to single-phase nonlinear receivers create new complex situations in the sense that in the unbalanced and unbalanced distortion regime, depending on the degree of unbalance and load, there are circulating harmonic currents and in facilities where their presence was not expected [5, 6].

For the application of various compensation measures (consisting of the installation of active or passive filters for different harmonic ranges present) in an electrical network node, regardless of the rated voltage stage, it is necessary to know the existing situation by making electrical measurements.

From the analysis of the measurements made (and not all of them are presented in this paper), it is observed that the limits of the values of the individual voltage harmonics in the low voltage electrical networks, at the supply terminals, for ranges up to 25 (in percent) against the fundamental voltage U_1 (standard: EN 50160; CEI 61000-2-2) and the harmonic current limit values emitted in low-voltage equipment of three-phase equipment (CEI 61000-2-4 standard).

References

1. Golovanov, C., Albu M, ș.a.: Probleme moderne de măsurare în electroenergetică, In: Editura tehnică, București (2001)
2. Toader, C., Scutariu M., Postolache, P.: Neutral loading effect of low-voltage network nonsinusoidal regime. Bull. UPB, Ser. C **63**(1–4), 97–105 (2003)
3. Cicco, G., Postolache, P., Toader, C.: Analysis of three-phase systems with neutral under distorted and und unbalanced conditions in the symmetrical component-based framework. IEEE Trans. Power Deliv. **22**(1), 674–683 (2007)
4. Golovanov, N., Postolache, P., Toader, C.: Eficiența și calitatea energiei electrice. In: AGIR, București (2007)
5. Cicco, G., Postolache, P., Toader, C.: Triple harmonics: myths and reality. Electr. Power Syst. Res. **81**, 1541–1549 (2011)
6. Iordănescu, I., Postolache, P., Toader, C., Jișa, M.: Fenomenul deformant în instalațiile electrice și eficiența măsurilor de atenuare. In: Ed. AGIR, București (2012)

Human Upper Limb Motions Video Analysis Used for Rehabilitation Robotics

Dorin Popescu(✉), Cristian Petre Copilusi, Horatiu Roibu, Ligia Rusu, and Mihnea Ion Marin

University of Craiova, A.I. Cuza 13, Craiova, Romania
dorinp@robotics.ucv.ro

Abstract. This paper presents ongoing research activities for development of an upper limb rehabilitation robotic system needed to a rehabilitation clinic. The medical and technical requirements analysis for an upper limb rehabilitation robotic system were established, the upper limb motion video analysis were done. The video analysis aim was to evaluate the joint trajectories and range of motion of a human upper limb. An experimental motion analysis was performed using a modern equipment and the interest joints were elbow and wrist. The experimental activity was developed on a human subject when performs motions. The obtained results will be useful for the rehabilitation robotics, in order to implement the rehabilitation exercises with an upper limb rehabilitation robotic system.

Keywords: Video analysis · Human motion · Biomechanics · Kinematics Rehabilitation robotics

1 Introduction

Different types of injuries (with traumatic or non-traumatic causes) dramatically change the life of the patients due to their consequences. The role of rehabilitation for upper limb is the return to activities of daily living. Prokinetic Clinic carry on rehabilitation of human limbs. They identified the need to use a passive rehabilitation robotic system (RRS) with 3 degrees of freedom for upper limb according to their own requirements. Our partnership project has to design and develop a robotic system for the passive rehabilitation of the upper limb.

Monitoring and assessing body kinematics and dynamics of the upper limb joints could improve the quality of rehabilitation robotic therapy. The study of upper limb movement and motion analysis is composed of three serial joints analysis, the shoulder, the elbow, and the wrist, that could have mechanical analysis and obtain information about the kinematics, forces, and moments generated at all three joints. In present the research activity is focused on development the best model to simulate upper limb mechanical properties and it has used various techniques and analytic methods.

Nowadays the complex motions evaluation can be performed with high-end equipment based on sensors applied on the body (for example, the system consists of wearable inertial measurement unit (IMU) sensors attached to the patient's limbs) or by using motion analysis equipment such as VICON, SIMIMotion, CONTEMPLAS

K. Ntalianis and A. Croitoru (Eds.): APSAC 2017, LNEE 489, pp. 264–273, 2019.
https://doi.org/10.1007/978-3-319-75605-9_37

[1, 2]. Analyses of upper limb movements are generally performed by measuring kinematic variables of the links and joints with accelerometers, electrogoniometers, or cameras.

The optical systems with high resolution in space and time could be used to record 3D kinematics of the upper limb and the detection of upper limb segments postures and movements. Thus, the 3D biomechanical models of the whole or partial upper limb have been developed. These models have used optimization methods to compute muscle forces and limb postures.

Another aspect is the one that these methods and equipment can be used on the human recovery after injuries, by creating a database with motions performed by humans when they are in a good health conditions and have these information as reference ones for physical recovery after injuries [3].

Yang and colleagues proposed a decision support system for optical motion analysis, using a single camera, detecting and tracking markers attached to subject's joints, data analytics for calculating relevant rehabilitation parameters and robust classification based on graph-based signal processing [4].

Perez et al. presented an inertial sensor-based monitoring system for measuring and analyzing upper limb movements. Their aim was the integration of this motion-tracking device within a portable rehabilitation system for brain injury patients [5].

Richards presented a comparison of commercially optical motion analysis systems [6]. There are some systems with high accuracy and real-time tracking features. These systems using multiple infrared cameras capture human motion, by tracking reflective markers fixed to the skin (anatomical landmarks of the subject) [7, 8]. The disadvantages of these systems are the cost, space, and portability.

The measurement and analysis of upper limb human movement can be used to:

- design an upper limb rehabilitation robotic system;
- implement control algorithms for an upper limb rehabilitation robotic system;
- provide feedback to clinicians during the performance of rehabilitation exercises.

Current upper limb motion assessments are focused on single-joint kinematics. Multi-joint biomechanical evaluations is required, particularly for goal oriented reaching movements.

The paper is organized as follows: in the next Sect. 2 we discuss about medical and technical requirements analysis; in Sect. 3 we present our video motion analysis system and the upper limb motion analysis with the experimental results; then we present our work done for designing of an upper limb rehabilitation robotic system; Sect. 5 presents the conclusions of this paper.

2 Medical and Technical Analysis

The main focus of first step of our research was to create specifications for hardware and mechanical system design of a rehabilitation robotic system (RRS) for upper limb.

Within the project we used several tools such as participant observation, interviews and questionnaires to understand people in their natural work environment. We used these methods for future phases of design, to provide a perspective on the work of

therapists, as therapist interacts with the patient and what tools used. Observation sessions and interviews were limited to observing therapists' interactions with their patients at Prokinetic Rehabilitation Clinic.

Based on the above information, it was developed a questionnaire with 48 questions, measuring the level of agreement or sense of importance of an item. For example, the first question concerned about description of a successful kinesiotherapy treatment. Social and professional reintegration of patients achieved the highest percentage (85.3%), closely followed by functional rehabilitation (76.5%; Fig. 1).

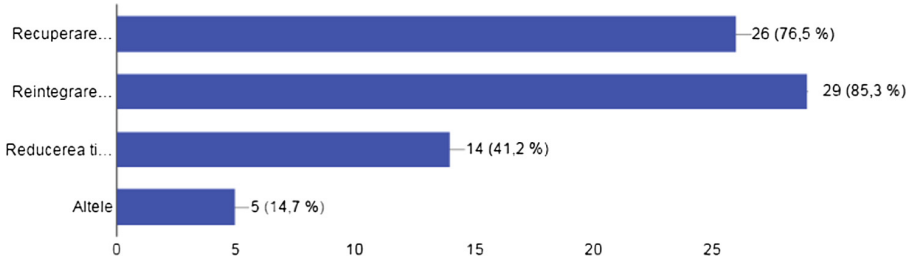

Fig. 1. Rehabilitation purpose/objectives.

Responses to the survey were used for a medical and technical analysis, including statistical analysis and will be used in the design of a RRS. The results of the statistical analysis are presented in [9].

3 Upper Limb Motion Analysis

3.1 Experimental Setup

Upper limb motion analysis has been done using Vicon system (14 Vicon T10 video cameras and Vicon Nexus software; Fig. 2) commonly used in clinical rehabilitation practice. We will use this analysis in order to implement the control algorithms for an upper limb rehabilitation robotic system (an exoskeleton with 3 DoF).

An experimental motion analysis was performed using a modern equipment (that is recognised as the state of the art) and the interest joints were: elbow and wrist.

Impairment of the upper limb following injuries can be assessed in a number of ways (for example, for stroke it is presented in [10]). It can be done through:

- measuring physical attributes, for example range of motion, motion speed, strength and coordination;
- quantitatively assessing the ability to carry out a functional task such as the RTG movement.

To calculate the relevant joint angles, the video system tracks, through the captured frames, the reflexive markers adhered to the skin (or special black suit) overlying specific anthropometric points of the shoulder, elbow, and wrist of the human subject,

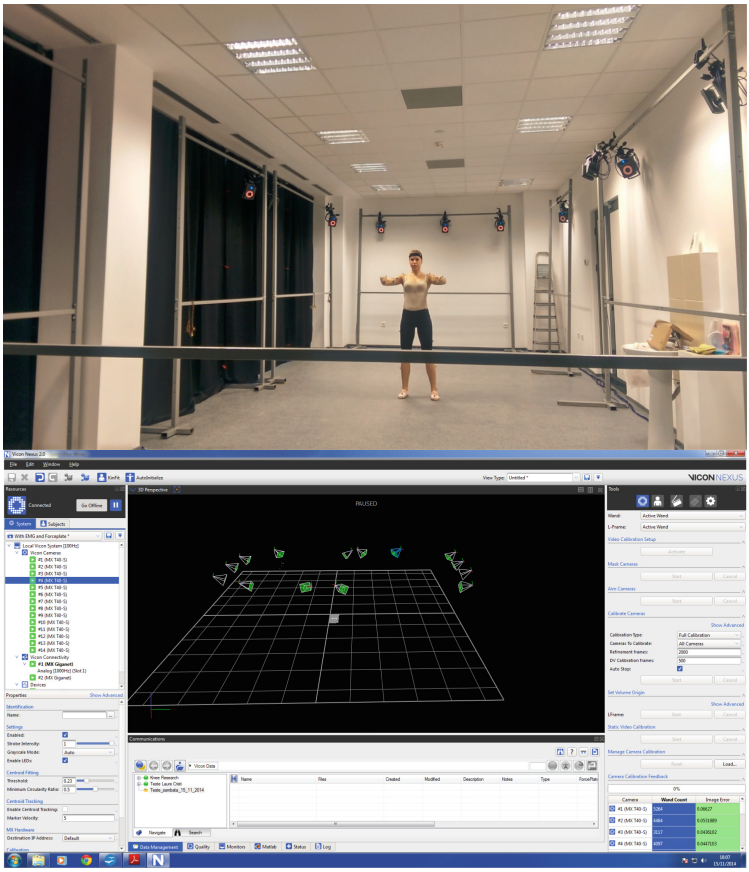

Fig. 2. Vicon system (hardware and software).

presented in Fig. 3. The tracked motion patterns are then used by the Vicon software to calculate the three angles in each frame.

Development of the new optical system with high resolution in space and time could be used to record 3D kinematics of the upper limb and the detection of upper limb segments postures and movements.

Based on the above arguments and by having the Vicon equipment for experimental human motion analysis, a motion will be analyzed by performing some types of movements. With this equipment the human upper limb joints angular variations, and trajectories will be evaluated in a 3D space. This could be used in rehabilitation robotics for programming a human upper limb exoskeleton in terms of complex motions (at high speeds and combined motions for elbow and wrist joints).

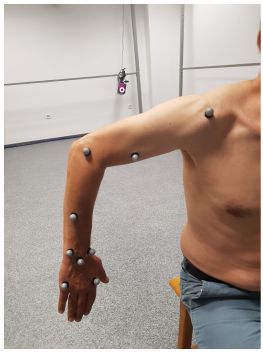

Fig. 3. The reflexive markers adhered to the skin.

3.2 Experimental Analysis

As regarding the experiment this was conducted by a physician, two scientists in mechanical engineering and two scientists in mechatronics engineering. The chosen healthy human subjects have the anthropometric data known and these will serve as input data for equipment calibration. The human subject were men and women, age 22 to 55, 50 to 95 kg, 1.50 to 1.85 m height and their dimensional parameters known.

The analysed motions were the following, both designed by therapists from the Prokinetic Clinic:

- Pure movements (trying not to move the rest of the joints): elbow flexion/extension, elbow pronation/supination and wrist flexion/extension.
- Functional tasks as RTG movement [11] (eating or drinking): the subject picks up a glass or fork from the desk, carries it towards the mouth and puts it back on the desk.

According to the equipment setup, the movements of the markers with reflective properties were analyzed. Those markers represents the joint centers of the human upper limb. The collected data were acquired for both types of motions and these consist in joint center trajectories expressed in meters and angular amplitudes. Namely a motion was recorded for the person between 0 to 10 s, repetitive. The acquired data were processed in real-time. Also, using Vicon Nexus software a virtual upper limb skeleton was elaborated in accordance with the person anthropometric parameters (Fig. 4).

The frame acquisition was done at a value of 100 frames/second.

A kinematic model is built to estimate 3D upper limb motion. The upper limb is represented as a kinematic chain of rigid bodies with three joints (shoulder, elbow, and wrist) and six degrees of freedom.

The obtained results are shown in Figs. 5, 6, 7 and 8 and represents angular amplitudes, velocity and upper limb trajectory for the acquired motion of the subject.

The flexion/extension angular velocity for elbow calculated by Vicon ProCalc is presented in the Fig. 6.

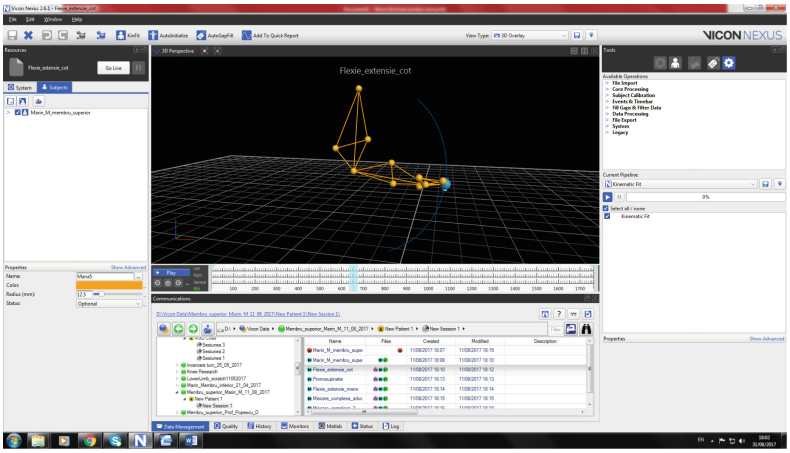

Fig. 4. Upper limb skeleton definition.

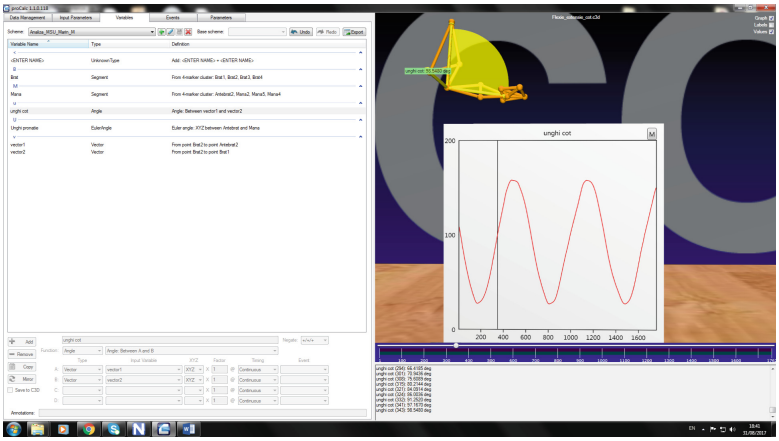

Fig. 5. Flexion/extension elbow (Vicon ProCalc).

The VICON equipment records on an infrared environment which needs special attention to the reflexive objects existent during analysis [12].

If it will have a look to the diagram from Fig. 5 the extension elbow angular amplitude has an appropriate maximum value of 157.6°. If it will discuss about the wrist angular amplitude from diagram of Fig. 8, it can be observed that the values are around of 55.3°. It can be remarked that the elbow amplitude decrease at a value of 27.3° and in case of the hand wrist, the lower value is −29.2°. The pronation/supination elbow angle varies between −69.3 and 57.4°. Also the obtained results correspond with the existent values on database from specialized literature in biomechanics domain [13, 14].

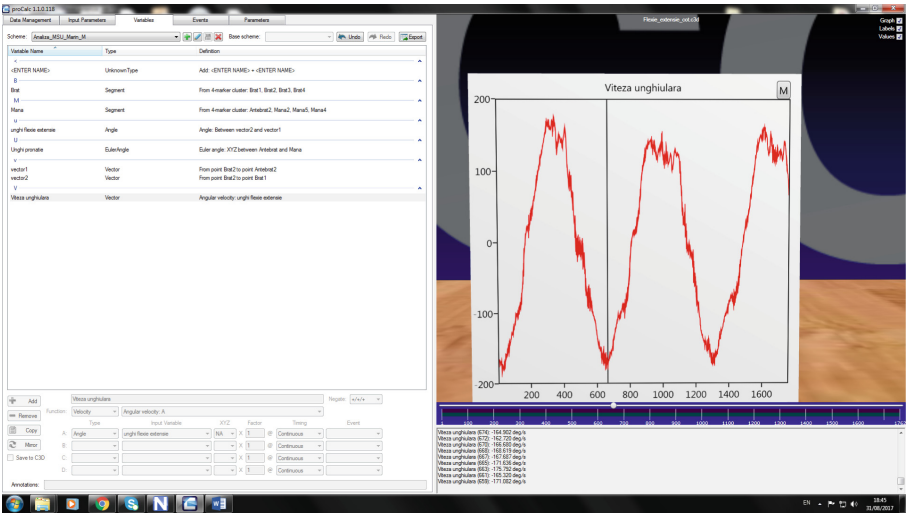

Fig. 6. Flexion/extension angular velocity for elbow, calculated by Vicon ProCalc.

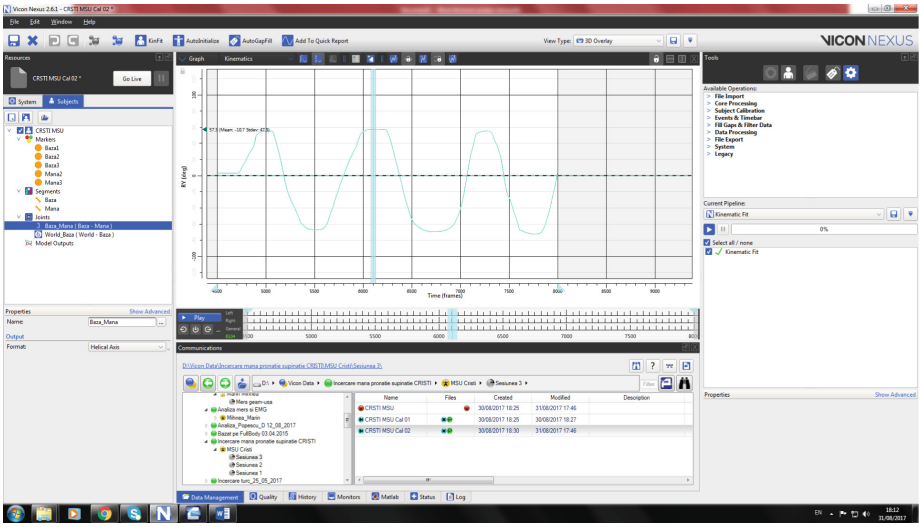

Fig. 7. Pronation/supination elbow angle (Vicon Nexus).

4 The Rehabilitation Robotic System

In this period we work to design the mechanical (by SolidWorks; Fig. 9), actuation and control systems for a RRS. After considering the deficiencies and problems found in existing control systems, we propose a hybrid architecture, two-level structure for the robotic control system.

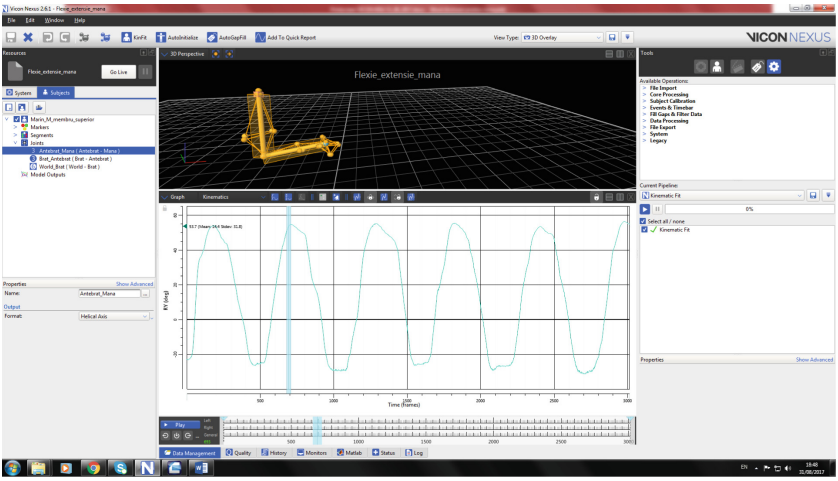

Fig. 8. Flexion/extension angle for wrist (Vicon Nexus).

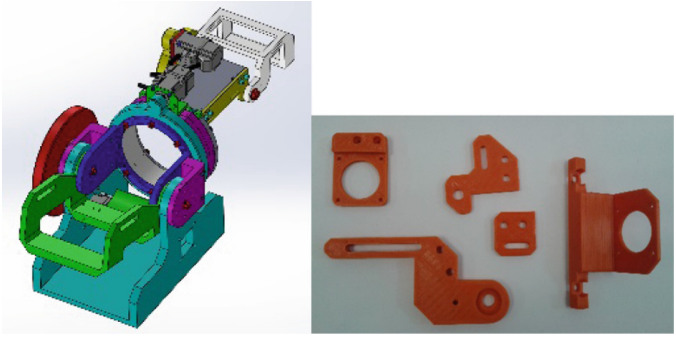

Fig. 9. The rehabilitation robotic system (under design) and some 3D printed components

The RRS will allow flexion/extension of elbow, supination/pronation for elbow and flexion/extension for wrist. Some components (Fig. 9) of our RRS will be fabricated using a 3D printer (designed and developed in our laboratory).

Based on the experimental analysis, the obtained results will be implemented on programming of the control system of the 3 actuators for human upper arm complex motions and rehabilitation. Basically this robotic system will have to perform similar motions at its high-end capacity.

5 Conclusions

The specifications required by Prokinetic users for a robotic system for the rehabilitation of upper limb resulting from first phase of research were established. Understanding of the treatment methods and of the rehabilitation targets used by therapists to

treat upper limb is important to guide the design and integration of robotic systems in clinical practice.

This paper describes a procedure for evaluating the behavior of a person during an upper limb motion (pure movements and functional tasks as eating or drinking). Through this experimental analysis, remarks were obtained regarding the behavior of the human subject analysis on movements. In particular a high-speed motion analysis equipment has been used for measuring motion ranges of significant points for the human upper limb. With these it can be established the motion laws for programming a human upper limb recovery robotic exoskeleton.

This project aims to use a user-centered design process to create an upper limb RRS for patients and therapists from Prokinetic. The end-users will be involved actively, continuously throughout the RRS design and development. Designing a usable upper limb rehabilitation robotic system must address the needs of its users.

Monitoring and assessing body kinematics and dynamics about the upper limb joints could improve the quality of rehabilitation robotic therapy.

Experimental results show that the Vicon system can capture upper limb motion patterns accurately. Currently available optical motion analysis systems are expensive and require multiple infrared cameras, large laboratory space.

Acknowledgments. This work was supported by 109BG/2016 grant of the Romanian National Authority for Scientific Research and Innovation, CNCS/CCCDI – UEFISCDI, project number PN-III-P2-2.1-BG-2016-0139, within PNCDI III.

References

1. Ceseracciu, E., Sawacha, Z., Cobelli, C.: Comparison of markerless and marker-based motion capture technologies through simultaneous data collection during gait: proof of concept. PLoS ONE **9**(3), e87640 (2014). https://doi.org/10.1371/journal.pone.0087640
2. Vicon Motion Analysis Equipment User Manual (2014)
3. Koger, R.: 101 Great Youth Soccer Drills. Mc Graw Hill, New York (2005)
4. Yang, C., Kerr, A., Stankovic, V., Stankovic, L., Rowe, P., Cheng, S.: Human upper limb motion analysis for post-stroke impairment assessment using video analytics. IEEE Access **4**, 650–659 (2016)
5. Pérez, R., Costa, U., Torrent, M., Solana, J., Opisso, E., Cáceres, C., Tormos, J.M., Medina, J., Gómez, E.J.: Upper limb portable motion analysis system based on inertial technology for neurorehabilitation purposes. Sensors **10**, 10733–10751 (2010)
6. Richards, J.G.: The measurement of human motion: a comparison of commercially available systems. Hum. Mov. Sci. **18**, 589–602 (1999)
7. Aggarwal, J.K., Cai, Q.: Human motion analysis: a review. Comput. Vis. Image Understand. **73**(3), 428–440 (1999)
8. Poppe, R.: Vision-based human motion analysis: an overview. Comput. Vis. Image Understand **108**(1–2), 4–18 (2007)
9. Popescu, D., Manta, F., Rusu, L., Avramescu, T.E., Zavaleanu, M., Petrisor, A.: Medical and technical requirements analysis for upper limb rehabilitation system. In: Proceedings of the 18th International Carpathian Control Conference (ICCC), pp. 539–544 (2017)

10. Kelly-Hayes, M., Robertson, J.T., Broderick, J.P., Duncan, P.W., Hershey, L.A., Roth, E.J., Thies, W.H., Trombly, C.A.: The American Heart Association stroke outcome classification: Executive summary. Circulation **97**, 2474–2478 (1998)
11. Turton, A.J., Cunningham, P., Heron, E., van Wijck, F., Sackley, C., Rogers, C., Wheatley, K., Jowett, S., Wolf, S.L., van Vliet, P.: Home-based reach-to-grasp training for people after stroke: Study protocol for a feasibility randomized controlled trial. Trials **14**(1), 109 (2013)
12. Vicon. https://www.vicon.com/products/
13. Copilusi, C.: Researches regarding applicable mechanical systems in medicine. Ph.D. thesis (2009)
14. Williams, M.: Biomechanics of human motion. W.B. Saunders Co., Philadelphia (1996)

Interactive Control System Proposal for High Switching Frequency Resonant Converters

Pavol Spanik[1(✉)], Michal Frivaldsky[1], Ondrej Hock[1], and Andrej Kanovsky[2]

[1] Faculty of Electrical Engineering, Department of Mechatronics and Electronics, University of Zilina, 010 26 Zilina, Slovakia
{pavol.spanik, michal.frivaldsky}@fel.uniza.sk
[2] Delta Electronics Slovakia, Priemyselna 4600/1, 01841 Dubnica nad Vahom, Slovakia
andrej.kanovsky@deltaww.com

Abstract. The paper deals with a possibility of computer control of DC/DC converters. This control approach has been developed for the laboratory testing of resonant converters. The control system is implemented within DSP. The communication between control system and user is implemented by a control panel running on host computer (i.e. PC). The interleaved two channel LLC resonant converter has been used as the physical model.

Keywords: Computer control system · Interleaved converter · LLC converter Launchpad TMS320F2802x

1 Introduction

Nowadays, the energy efficiency and power density are the main quality indicators in the SMPS. For the reasons of ensuring high power density, the trend is to increase the operating frequency of power converter. The higher the switching frequency is, the more visible reduction of weight and dimensions of accumulation elements (inductors, capacitors, transformers) is possible. Until the beginning of 80 years, the maximum switching frequency range was around several tens of kilohertz (20–50 kHz), now there are converters with switching frequency operating at several megahertz. It should also be noted, that the use of higher switching frequencies however brings also some negatives. One of such negative impacts of high switching frequency operation is linear increase of switching losses of semiconductor devices, which consequently will negatively affect the efficiency of the entire power system. Therefore, high demands are placed on the dynamic characteristics of semiconductor devices, while it is also necessary to use special commutation techniques in order to reduce the switching losses. The above mentioned facts have resulted in the development of new perspective resonant topologies. One of the best known and nowadays the most widely used topology of resonant converter is LLC converter [1–6]. Resonant converters are special types of power supplies and in order to secure reliable operation, it is very important to investigate operational characteristics of such topologies [7–11].

K. Ntalianis and A. Croitoru (Eds.): APSAC 2017, LNEE 489, pp. 274–279, 2019.
https://doi.org/10.1007/978-3-319-75605-9_38

In this paper the possibility of computer control of perspective resonant converters is being described. Proposed control strategy enables in simple way to discover each operational characteristic of any power resonant converter. The proposal is verified on the dual-interleaved LLC converter.

2 LLC Converter

The LLC converter today represents well-known topology, which is characterized by many advantages compared to other standard resonant converters. First analysis of this topology was realized since 1990. The problem was that power electronic designers had been operating it just as series resonant converter. Later, couple of scientists realized new analysis of its behavior, which uncovered remarkable abilities of LLC resonant converter [3]. In particular in its half-bridge implementation the LLC resonant half-bridge with its many benefits and very few drawbacks is an excellent solution (Fig. 1). One of the major difficulties that engineers are facing with this topology is the lack of information concerning the way it operates [4].

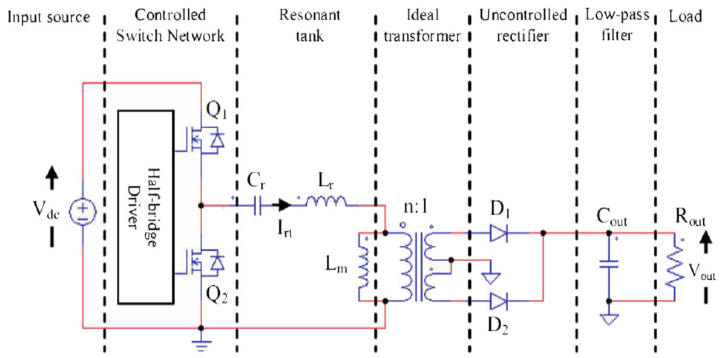

Fig. 1. The block scheme of LLC resonant half-bridge DC/DC converter.

The principal waveforms of the converter during various operational states are shown on Fig. 2. It is well known, that LLC converter can be operated within wide range of its voltage – gain characteristic, while the selection of the operational region is dependent on the input – output conditions of the converter (i.e. input voltage, output power etc.). Thus mostly used regions are above main resonant frequency, and below main resonant frequency. Main difference is in the voltage gain of the resonant circuit and also in the shape of the current flowing through the main circuit (transistors – high frequency transformer – diodes). Each operational region is therefore characterized with different system behavior from power losses point of view as well as from dynamic behavior. Therefore, the tool for investigation of these phenomenons is valuable. For that reason interactive user interface was developed in order to easily vary main operational characteristics.

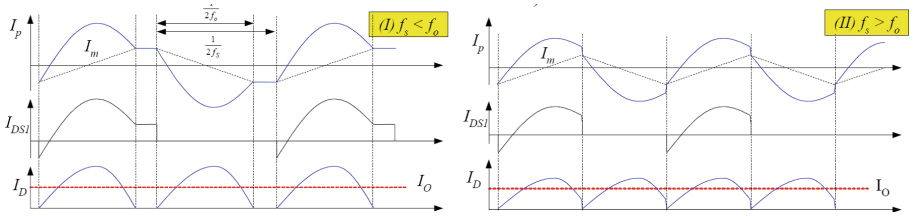

Fig. 2. Operational wavefors of LLC converter above (right) and below (left) resonant frequency (I_m – magnetizing current, I_p – transformer primary current, I_{DS} – transistor´s current, I_D – output diode current).

3 The Computer Control System Design

Purpose of the presented tool is on-line control of the high power density dual interleaved LLC converter. For that reason, the GUI for any kind of application with embedded DSP was designed. Digital control algorithm is running on the embedded DSP to control operation of LLC resonant converter. The control panel is running on the host computer (i.e. PC), which completes the entire solution by exposing and demonstrating parameters/capabilities of the DSP and target application (Fig. 3). This approach enables to interact with the target application and change the behavior of the power stage in real time. Beside that, all measured values can be displayed, what is done through the use of measuring cards. Utilizing of the described graphic user interface make it easy to demonstrate behavior of the LLC converter and can help to understand theory of operation for beginners or students.

By entering the switching frequency in the control panel the user can move with the operational point of the LLC converter within whole operation range and consequently observe the change of waveforms online (Fig. 5). Additionally with the change of the position of panel's control items the user can control auxiliary functions of the hardware like over voltage protection, over current protection, under voltage of the DC bus, etc.…(depends on the hardware implementation). Instead of that, proposed environment and control system enables to design PID controller and run converter in closed loop operation.

Embedding of the TI's launchpad XL TMS320F2802x into design of the LLC converter is the easiest way how to implement the digital control capabilities to the design and enables designer to connect it to the computer by on-board JTAG emulator. Described Control Panel was designed with the use of GUI Composer Designer. The GUI Composer Designer is the design tool used for development of various industrial applications. GUI Composer is integrated into Code Composer Studio providing an integrated environment for development of target application and custom GUI within the same environment. GUI Composer apps can be designed and verified using full debug capabilities of Code Composer Studio.

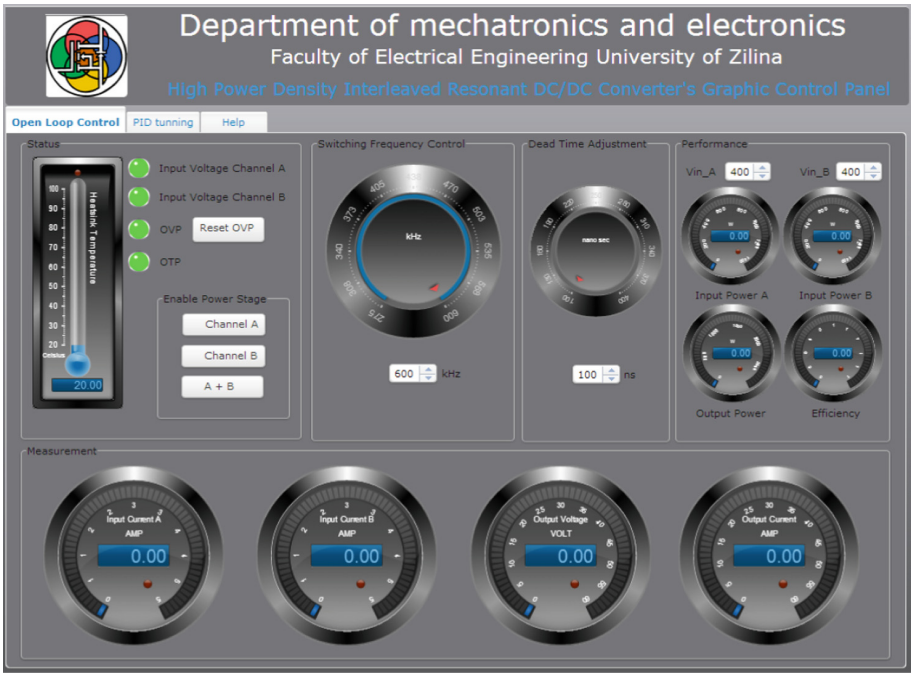

Fig. 3. Main window of the control panel.

4 Experimental Verification

The experimental verification was done on the experimental prototype (Fig. 4) of dual interleaved LLC converter. The main input output parameters of this converter are:

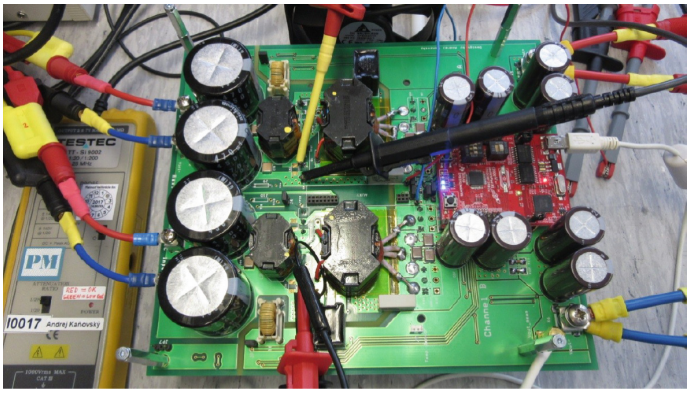

Fig. 4. Experimental prototype of high power density dual interleaved LLC resonant converter

– input voltage range: 200–400 Vdc
– output voltage range: 40–60 Vdc
– switching frequency: 200–600 kHz
– output power: 500–2500 W

This experimental prototype was interconnected with proposed control system and consequently regulation and control in real – time was verified. It might be seen (Fig. 5) that interactive control enables to investigate whole regulation and operational range of the LLC converter, and also it is possible to investigate in detail each waveform of the main circuit. Among other things it is also possible to determine switching losses and overall efficiency of the converter during any operational condition.

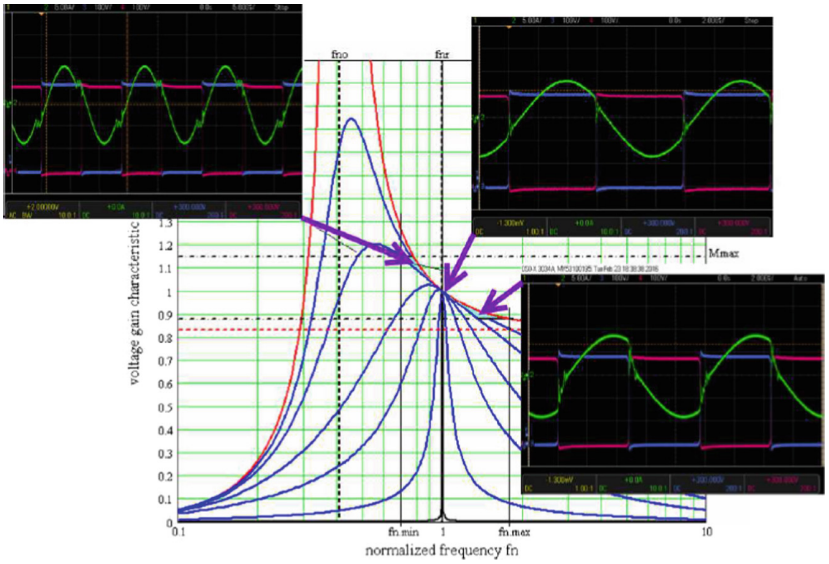

Fig. 5. Example of the interpretation of voltage gain characteristics and relevant operational waveforms of LLC converter during various conditions

5 Conclusion

The paper has dealt whit the computer control system for the DC/DC converters. The system was applied on the interleaved two channel LLC converter (Fig. 4). The user can analyze the behavior of converter using the control panel, running on host PC. For example operation modes below or above resonant frequency can be investigated together with possibility of investigation within open or closed loop of control system. The system is suitable mainly for beginners or students, who are not familiar with operation of high frequency resonant converter.

Acknowledgement. The autors wish to thank for the support of this work within the project APVV – 0314 – 12 – The development of new generation of power supplies with low circulating energy, high efficiency and with multifunctional output, which is granted by Slovak national grant agency APVV.

References

1. Frivaldsky, M., Dobrucky, B., Prazenica, M., Koscelnik, J.: Multi-tank resonant topologies as key design factors for reliability improvement of power converter for power energy applications. Electr. Eng. **97**(4), 287–302 (2015). https://doi.org/10.1007/s00202-015-0336-3. ISSN 0948-7921, ISSN(online)1432-0487
2. Jovanovic, M.: Technology drivers and trends in power supplies for computer/telecom. APEC, Plenary session presentation (2006)
3. Mazgut, R., Galad, M., Kascak, S., Spanik, P.: Analysis of multi-resonant LLCLC converter. In: 2016 ELEKTRO (2016)
4. www.datasheetarchive.com
5. Lee, F.C., Barbosa, P., Xu, P., Zhang, J., Yang, B., Canales, F.: Topologies and design considerations for distributed power system applications. Proc. IEEE **89**(6), 939–950 (2001)
6. Frivaldsky, M., Koscelnik, J., Prazenica, M.: Multiresonant LCL2C2 tank converter, In: IECON 2014: 40th Annual Conference of the IEEE Industrial Electronics Society, Dallas, TX, U.S.A., 30 October–01 November, 2014, pp. 5047–5052. IEEE (2014) ISSN 1553-572X, ISBN 978-1-4799-4033- 2
7. Yang, B.: Topology investigation for front end DC/DC power conversion for distributed power system, Ph.D. dissertation (2003)
8. Kandrac, J., Frivaldsky, M., Prazenica, M., Simonova, A.: Design and verification of proposed operation modes of LLC converter. Electr. Electr. Eng. Kaunas **18**(8), 27–30 (2012). ISSN 13921215
9. Fu, D.: Topology Investigation and System Optimization of Resonant Converters, Ph.D. thesis, Blacksburg, Virginia, 4 February 2010
10. Dubrucky, B., Frivaldsky, M., Koscelnik, J.: Analysis of non-linear inverter circuitry of LCTLC topologie. COMPEL Int. J. Comput. Math. Electr. Electr. Eng. **34**(3), 824–839 (2015). ISSN 0332-1649
11. Jensen, S., Corradini, L., Rodriguez, M., Maksimovic, D.: Modeling and digital control of LCLC resonant inverter with varying load, In: Energy Conversion Congress and Exposition (ECCE), 17–22 September 2011, vol. 1, pp. 3823–3829 (2011)

Integral Assessment of Power Network Equipment Operational Risks: Special Aspects

Alexandra Khalyasmaa(✉)

Ural Federal University named after the first President of Russia B. N. Yeltsin, Mira Street 19, 620002 Ekaterinburg, Russia
lkhalyasmaa@mail.ru

Abstract. One of the main problems, facing power system utilities today, is the problem of optimizing their own limited technical and economic resources and creating such an assets management system, that will provide comprehensive assessment and prediction of the technological risks of power network equipment operation. Risk-based approach is generally subdivided into three stages: risk analysis, risk assessment and risk management, description of which is provided at the introductory part of the paper. The research mainly addresses the problems of power network equipment operational risks assessment, based on the analysis of the influence of various technical parameters and indicators on the accuracy and quality of risks' estimations. Within the framework of the research, a novel scenario-based probabilistic approach to risks assessment as a part of power network assets management problem is provided. Power equipment risks are calculated according to estimated technical state of the units under consideration, which significantly improves the quality of risk-management. The effectiveness of the proposed approach is demonstrated on the basis of power transformer operational risks assessment problem.

Keywords: Risk assessment · State assessment · Power equipment
Energy utility

1 Introduction

Today, the management of production assets for power enterprises (grid companies, large industrial enterprises, owning electrical equipment) becomes not only a priority issue of the economic nature in terms of investment programs, but also, among other things, the issue of maintenance and repair programs improvement, which is aimed at optimizing the life cycle of substation equipment.

Such a duality of tasks does not allow one to solve them one-sided, excluding one or the other component. Therefore, it is only possible to get an effective system for production assets management of the power system utilities, when the blocks of power equipment technical state assessment and risks management are operated simultaneously. It should be noted, that this interconnection should not be consistent, as it is implemented in most of the existing systems, such as [1–3], but parallel with the possibility of the feedback link implementation. In other words, the asset management

K. Ntalianis and A. Croitoru (Eds.): APSAC 2017, LNEE 489, pp. 280–286, 2019.
https://doi.org/10.1007/978-3-319-75605-9_39

system should be sensitive not only to the changes in technical state assessment block, but also to the changes in economic indicators and the risks.

Therefore, the main problem facing power system utilities today is the problem of optimizing their own limited technical and economic resources and creating such a mathematical model for assets management system implementation, that will allow a comprehensive assessment and prediction of the state and corresponding risks of power network equipment, while providing on its' basis precise and qualitative solutions, both in the case of technical parameters of power equipment unit, and economic internal and external indicators and parameters.

2 The Main Aspects of Power Equipment Risks Assessment

Production assets management of any enterprise, according to [4], is management in conditions of uncertainty, which means that it requires special attention to risks accounting. When taking into account risks, it is necessary to consider a risk as a complex value, consisting of risk analysis, risk assessment and management. Each of the components has its own problems in term of identification and analysis.

2.1 Risk Analysis Problem

In most modern power systems, the first stage of risk analysis is the formulation of power equipment technical state estimation, and then, on its basis, the analysis of its operational risks. It is obvious that the analysis of the risks depends on the accuracy and quality of technical state identification of the power network equipment. Thus, no matter how qualitatively the risk identification process has been done, if the evaluation of the technical state of the power equipment is not accurate enough, then the analysis, and, subsequently, the risk assessment will only worsen the quality of the forecast, increasing the identification error by several times. This is due to the fact, that in real operational conditions of the power equipment it is practically impossible to obtain a definite estimation of the technical state. This is only possible if the state is close to a normal one and all the parameters are within the permissible values. But, obviously, the normally operated equipment unit has minimal risks.

It is much more difficult to predict the risks, when technical state assessment of the power equipment unit does not meet technical requirements, or cannot be correctly identified. The main problem is the lack of statistical data, on the basis of which it would be possible to identify and assess the possible risks.

Within the framework of this study, the analysis was carried out for the main substation equipment of a large grid company, owning 106 substations of 35–500 kV. One of the main tasks of the research was to identify on the basis of the results of technical diagnostics and testing, the equipment units, that do not comply with technical documentation requirements.

It can be seen from Table 1, that the total number of equipment units, that do not comply with standard and technical requirements ranges from about 10% to 20%. Within the present research work there is no division by voltage ratings of power equipment, or by type - this is generalized data. The annual statistics of substation

equipment technical state confirms that typically no more than 2–5% of the total number of power equipment units of different types do not comply with standard and technical documentation. Such small sample can hardly be used for risk identification.

Table 1. Power equipment units, that do not meet technical documentation requirements

Equipment	Total 2015, units	Total 2016, units
Power transformers	103	145
Current transformers	10	18
Voltage transformers	40	28
Circuit breakers	100	86

Within the framework of other studies [5, 6] the author proved, that in order to build a reliable forecast, the sample size should not be less than 75 values for each type of power equipment units, otherwise the forecast is considered to be unreliable.

It follows from all of the above, that in order to avoid the problem of inaccurate assessment and forecasting of risks, it is necessary to begin the development of risk assessment system with the adjustment of the technical state identification system.

2.2 Risk Assessment Issues

First of all, the problem of risk assessment is connected with the technical state assessment sub-system. The fact is that modern systems for technical state assessment are based on the principle of unambiguous conclusion formulation, which briefly describes current technical state of the power equipment unit, for example, “normal” or “faulty, but operable”.

According to the author’s vision, such an approach - obtaining a single solution is not the optimal one, since in this case the level of conformance of technical state assessment and real technical state of the object it is not clear. From the point of view of operation experience, the same equipment unit can be referred to different technical states, having the same characteristic values, especially if these are boundary values between one and the other state. Thus, the inaccuracy in risk assessment of risks comes precisely from the inaccuracy of technical state assessment.

The possible solution to the problem is the application of membership functions. Depending on the type of the object under consideration, the type of limiting values (one-sided or two-sided range), the diagnostic method, etc., the type and number of membership functions can be different. Determination of the optimal type and number of membership functions is a separate task for technical state assessment of electrical equipment. Selection of a number and type of membership functions for the power transformer technical state assessment problem is presented in the case study in [7].

When the result is obtained as a numerical characteristic of belonging to each of the specified states, it will be possible to increase the accuracy of risk assessment and, in addition, to make the risk assessment procedure a probabilistic one, which will also give the possibility to consider all additional factors, that can affect the result.

2.3 Risk Management Issues

The problem of risk management in the same way depends on technical state assessment of the object under consideration. Risk management is practically the second stage of the system for technical state assessment of the power network equipment. It can be classified as a fuzzy multi-criteria problem for analyzing a set of particular solutions $Y = \{y_1, y_2, \ldots, y_n\}$, containing n elements (groups of parameters), obtained in the first stage.

Thus, in this case, the implementation of the decision-support system can be treated as determining the optimal solution (taking into account the ranking of possible solutions) for the further operation of the power network equipment, based on the assessment of its technical state, calculated on the basis of available aggregate information about the object.

The estimation of the probability of each decision, based on the assessment of the technical state of the system, is carried out by quantitative analysis of the significance and contributions of the final event into the total risk (probability). The decision regarding the necessity of the most significant events' probabilities adjustment and allocation of the resources, required to change the probabilities of this events, is made on the basis of the calculation results, obtained at the previous stage.

3 Power Network Equipment Risk Assessment System

3.1 Technical State Assessment

In this paper, the author presents an approach for power network equipment risk assessment and describes the basic principles of construction and functioning of the system within the framework of energy enterprises' assets management. Nowadays such reversibility (bi-directionality) of the processes in production assets management systems can be achieved by using artificial intelligence methods.

A computational example of the risk assessment was carried out for the oil-filled power transformer TDTN-110/35/10 kV, using retrospective operation dataset in April–May 2011. The analysis of power transformer technical state was carried out using available diagnostic data, presented in Table 2.

The results of calculations for a power transformer TDTN-110/35/10 kV according to the proposed methodology of technical state assessment are presented in Table 3. The software package MATLAB was used as a modeling tool. The state of the transformer TDTN-110/35/10 can be characterized as "faulty, but operable" with a probability of 74.4%, and as "emergency" - with a probability of 26.6%. Based on the results of the technical state assessment of the power transformer TDTN-110/35/10 kV, the following decisions can be made on the basis of the membership functions:

- carry out repairs (the probability of making this decision is 88.3%);
- decommissioning (the probability of making this decision is 11.7%).

Table 2. Power transformer initial dataset

Chromatographic gas analysis						
Gas	H_2	CH_4	C_2H_4	C_2H_6	C_2H_2	Date
% vol.	0,000304	0,000395	0,00167	0,0000548	0,00391	12.04
% vol.	0,000376	0,00044	0,00183	0,0000574	0,00454	27.04
% vol.	0,000546	0,000501	0,00193	0,0000566	0,00498	03.05

Open-circuit losses							
Phase	Commissioning			Last measurements			
	AB	BC	CA	AB	BC	CA	Date
ΔP_{xx}, W	9,2	9,3	11,4	10,5	11,0	15,5	27.04

Insulation resistance							
Circuit	Commissioning			Last measurement			
	HV-MV +LV+C	MW-LV +HV+C	LV-HV +MV+C	HV-MV +LV+C	MW-LV +HV+C	LV-HV +MV+C	Date
R_{60}, Ohm	3000	2500	3000	4600	4100	3900	27.04
R_{60}, Ohm	3000	2500	3000	2400	2100	3300	03.05
Commissioning Date	1993						
Capital repair Date	2008						

Table 3. Power transformer technical state assessment

№	Transformer element	Data	Tech. state	Rank
1	Transformer oil and general technical state assessment	CADG (electric defect)	0,83	5
		CADG (thermal defect)	0,0	1
2	Magnetic core	Open-circuit losses	0,0	1
3	Solid insulation	Insulation resistance	0,79	5
4	Windings technical state	Ohmic resistance	0,3	3
		Comis. date and capital repair date	0,0	1
Transformer technical state assessment			**0,628**	
Quantitative characteristic of the decision			**0,706**	

3.2 Risk Assessment

In this case, based on the obtained evaluation of the technical state of the power transformer under consideration, the following risks can be identified, depending on various decisions, according to the flowchart in Fig. 1. Figure 1 shows a block diagram of the risk assessment sub-system implementation, based on the assessment of power equipment technical state.

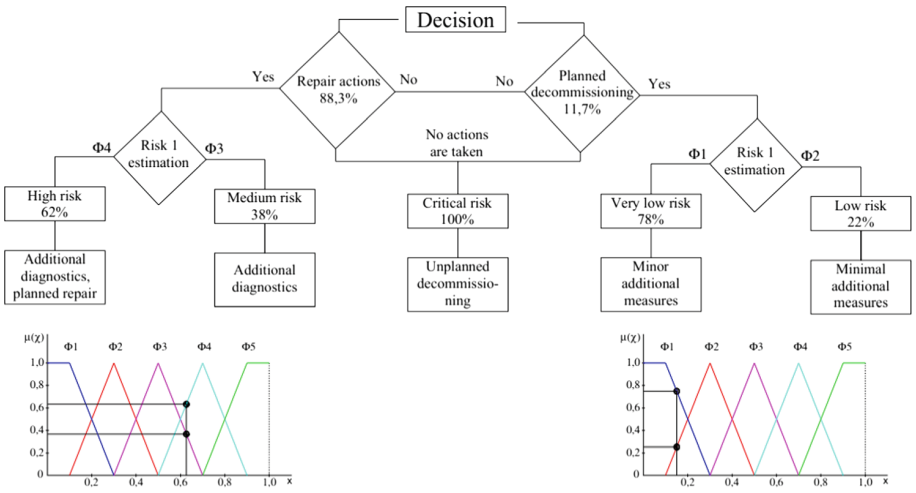

Fig. 1. Risk assessment flowchart

4 Conclusion

Today, the problem of technical and economic resources optimization forces energy companies to develop mathematical models for the production assets management system, which will give the possibility to comprehensively evaluate and predict the state and risks of power network equipment, while forming precise and qualitative solutions either for technical or economic criteria.

In the developed system, it is suggested to use a scenario-based approach, that takes into account the best (optimistic) and worst (pessimistic) scenario of the system dynamics when making a decision, which is carried out for the purpose of power equipment life cycle optimization. The problems of analysis, evaluation and risk management are also associated primarily with the sub-system power equipment technical state assessment. It is obvious, that before developing a risk management system, it is necessary to improve the system of power equipment technical state assessment. A probabilistic approach will favor the improvement of the accuracy and quality of risk management.

References

1. Pritkin, B.V.: Technical and Economic Analysis of the Production Cycle, p. 398. UNITI (2000). (in Russian)
2. Dubrov, A.M., Lagosha, B.A., Hrustalev, E.Y.: Risk Modeling in Economy and Business. Finance and Statistics (2000). (in Russian)
3. Hampton, J.J.: Fundamentals of Enterprise Risk Management: How Top Companies Assess Risk, Manage Exposure, and Seize Opportunity, 320 p. AMACOM (2009). (in Russian)
4. Pugach, O.V., Orlov, A.I.: Approaches to general theory of risk. System Analysis, pp. 49–82. Bauman Moscow State Technical University (in Russian)

5. Khalyasmaa, A.I., Dmitriev, S.A.: Expert system for engineering assets' management of utility companies. In: Proceedings of the 10th IEEE International Symposium on Diagnostics for Electric Machines, Power Electronics and Drives (SDEMPED 2015), pp. 421–427 (2015)
6. Khalyasmaa, A.I., Eroshenko, S.A.: Training samples construction for energy utilities operational assets management. Lecture Notes in Electrical Engineering, pp. 229–236 (2018)
7. Khalyasmaa, A.I., Dmitriev, S.A., Kokin, S.E., Glushkov, D.A.: Defining membership functions in power equipment state assessment problem. In: 5th International Conference Power Engineering, Energy and Electrical Drives, Riga, Latvia, pp. 229–233

Author Index

K. Ntalianis and A. Croitoru (Eds.): APSAC 2017, LNEE 489, pp. 287–288, 2019.
https://doi.org/10.1007/978-3-319-75605-9